Doctoral theses at NTNU, 2016:350

Francisco Javier Macias

Hard Rock Tunnel Boring

Performance Predictions and Cutter Life Assessments

Doctoral thesis

Francisco Javier Macias

NTNU
Norwegian University of
Science and Technology
Thesis for the degree of
Philosophiae Doctor
Faculty of Engineering Science and Technology
Department of Civil and Transport Engineering

ISBN 978-82-326-2042-5 (printed ver.)
ISBN 978-82-326-2043-2 (electronic ver.)
ISSN 1503-8181

Doctoral theses at NTNU, 2016:350

NTNU
Norwegian University of
Science and Technology

Francisco Javier Macias

Hard Rock Tunnel Boring

Performance Predictions and Cutter Life Assessments

Thesis for the degree of Philosophiae Doctor

Trondheim, December 2016

Norwegian University of Science and Technology
Faculty of Engineering Science and Technology
Department of Civil and Transport Engineering

NTNU
Norwegian University of
Science and Technology

NTNU
Norwegian University of Science and Technology

Thesis for the degree of Philosophiae Doctor

Faculty of Engineering Science and Technology
Department of Civil and Transport Engineering

ISBN 978-82-326-2042-5 (printed ver.)
ISBN 978-82-326-2043-2 (electronic ver.)
ISSN 1503-8181

Doctoral theses at NTNU, 2016:350

Printed by NTNU Grafisk senter

Abstract

The use of hard rock tunnel boring machines (TBMs) has become widely and generally used with success but in too many cases, due to unanticipated situations and/or inappropriate assessments, with catastrophic consequences. Hard rock tunnel boring involves major investments and high levels of geological risk, which require reliable performance predictions and cutter life assessments.

Hard rock tunnel boring leads the interaction between the rock mass and the machine, which is a process of great complexity. The tunnelling system around the excavation process has a great relevance in the final goal of performance predictions for hard rock TBMs, which is the estimation of time and cost.

The overall aim of this thesis is to build on the existing knowledge of tunnel boring and wear processes, technology and capacity, thus enhancing performance prediction and cutter life assessments in hard rock tunnel boring projects.

The prediction model for hard rock TBMs developed by the Norwegian University of Science and Technology (NTNU) is based on a combination of field performance data, engineering geological back-mapping, and laboratory testing. The development of TBM technology during recent decades, and the possible influence of parameters not considered in previous versions, has made revision of the model to improve prediction accuracy an essential requirement.

TBM specifications, the penetration rate and cutter life models have been revised and extended to adapt to the current technology. In addition, it has been incorporated a new definition of the rock mass fracturing, the influence of the cutterhead velocity (rpm) on penetration rate on the in response to the results of in-situ trials 'RPM tests' and cutter thrust on cutter life. The tunnel length effect on time consumption for the tunnelling activities has been introduced for the estimation of the machine utilization and therefore in the advance rate model. A revised and extended version of the current version of the NTNU prediction model for TBM performance and cutter life has been published included in this thesis.

Cutter consumption and parameters such as cutter ring wear play a significant role in performance and cost predictions, especially in hard rock conditions. Cutter wear involves a complex tribological system in interaction with the geological properties of the rock mass. Existing laboratory test methods fail to reproduce wear behaviour encountered during tunnel boring. Because of this, and the importance of cutter wear, it was considered of interest to develop a new rock abrasivity test method for tool life assessments in hard rock tunnel boring: The Rolling Indentation Abrasion Test (RIAT).

Understanding the processes and failure mechanisms during cutter wear enabled new knowledge to be applied as part of the development of the new rock abrasivity test method for laboratory use. In addition, cutter wear mechanisms affecting cutter rings during tunnel boring might lead to better cutter consumption predictions and future improvements in cutter ring development.

Preface and acknowledgments

This thesis is submitted to the Norwegian University of Science and Technology (NTNU) as partial fulfilment of the requirements for the degree of *philosophiae doctor* (PhD).

The work reported in this thesis has been performed at the Department of Civil and Transport Engineering, NTNU from September 2012 to June 2016, with Professor Amund Bruland as main supervisor and Eivind Grøv of SINTEF as co-supervisor.

The PhD was linked to a joint research project named “Future Advanced Steel Technology for Tunnelling” (FAST-Tunn), which involves collaboration between Robbins, BASF CGC, the Norwegian National Rail Administration, Scana Steel Stavanger, BMS Steel, LNS Group, Banbendererde Engineers and SINTEF/NTNU.

This PhD study combining academia, research and industrial partners, from clients to contractors and from manufacturers to consultants, has been an exceptional opportunity to gain knowledge and experience in the amazing world of hard rock TBM tunnelling. In addition, it has been a great 'excuse' to make proper research, to be involved in grateful technical discussions, to perform scientific writing and to be actively participating in conferences around the world.

The mixture of relevant projects, tunnelling experts and challenging goals has been essential to achieve the ambitious objectives initially proposed.

After almost four years enjoying, I could definitely expand the text on different directions. However, at some point, I just needed to stop the writing process trying to keep it reasonably comprehensive, constricted and precise. I will definitely keep my interest in research within the field.

I want to express his sincere gratitude to all the people who, in one way or another, has been involved, collaborating and/or supporting me during my PhD studies.

Firstly, I would like to thank Professor Amund Bruland for being my mentor; I am very pleased for that. I came here because of him and it was worth it. His guidance, support and feedback, was of great importance. I will never forget the interesting and enjoyable discussions plenty of professional feedback. I am highly grateful for how much I have learned at his side.

My work is a part of a long-term commitment by the department in research and development in the tunnel-boring field. My sincere gratitude to all the previous researches involved on the development of the NTNU prediction model from early 1970's. I have placed myself on their shoulders.

Furthermore, I would like to extent my thanks to the support made by the research project named “Future Advanced Steel Technology for Tunnelling” (FAST-Tunn) to which the PhD was linked. Thanks to the partners involved: Robbins, BASF CGC, the Norwegian National Rail Administration, Scana Steel Stavanger, BMS Steel, LNS Group, Banbendererde Engineers, SINTEF and NTNU, for supporting my expenses and their representatives for

listening and following my achieves. Special thanks to my co-supervisor Eivind Grøv for his helpful during the research process and for the final detailed review of my dissemination, especially in the last stages of the writing process.

I want to thank Pål Drevland Jakobsen who gave me a warm welcome to Norway and supported me dealing with the PhD and university world. He was always available to review my writings from the early stages, giving me useful advice. Sharing office and having fieldwork together made the teamwork beyond professional.

Special thanks to Filip Dahl (SINTEF), a colleague and a friend. His expertise, together with his interest in laboratory research and interesting discussions, have helped to solve the difficulties during the development of the new test method (RIAT). He was always positive leading with the research progress, 'two steps ahead, one back',

Nuria Espallargas has introduced me and guided through the tribology world. She has successfully led the analysis of wear mechanisms in cutter rings and she was very helpful when trying to understand the wear mechanism on cutter steels. I appreciate her disposition to help me providing useful advices and invaluable friendship.

Sindre Log (Robbins) for supporting this PhD work with valuable field data, arranging site visits and any requirements with related to TBMs that I needed.

Several students at NTNU have carried out interesting works on relevant topics within this PhD work. I am grateful to Wojtek Smolen and Marek Multan for their contributions on testing with the SGAT in crushed rock and giving support during the preliminary stages of the RIAT development. Also to André Svendsvoll Langnes and Anders Jørgensen Valestrand who were following up an ongoing TBM project in India during their master thesis; in addition, André Svendsvoll Langnes performed interesting work in field-testing on a TBM site at Southeast Asia. Special gratitude to Leon Eide, I am very pleased to his thorough work in the middle of USA and his great friendship. I want to extent to Jarand Nærland who carried out his master thesis dealing with the understanding of the basic cutter wear mechanisms. His collaboration and interest resulted in a final work of great value.

I would like to thank Steve Smading (Robbins) for his technical support during the PhD and carefully review of the thesis. His contributions have definitely improved it.

I extent my thanks to all my colleagues at FAST-Tunn research project and NTNU. Specially to my office colleague Yongbeom Seo, for being a pleasant office and research mate, with entertainment talks, Solveig Vassenden for enjoyable travelling and discussions and Yangkyun Kim for his advices and enjoyable talks.

Thanks to my honest friend, Sonia Santor who spent many hours in carefully reading my initial writing and drafts.

Research in tunnel boring requires fieldwork and TBM data from tunnel sites. Without that collaboration, reliable research would have not been possible. I am very grateful to the industrial partners, which have collaborate, during my PhD work: The Robbins Company (several sites), MT Höjgaard (Jacob Clemensen), LNS Group, Starkraft and Stillwater Mining

Company. Special thanks to Tobias Andersson (TBM site manager) who was always ready to support me. His collaboration, providing data, field testing, gathering samples and technical feedback was of great importance. It was a pleasure to work close.

Collaborating with colleagues is also of great importance for proper research. I am very grateful for the joint work carried out with former PhD student Lisa Wilfing (TUM).

I want to thank the laboratory team at SINTEF, technicians Joaquim Eggen, Niklas Haugen and Simon Alexander Hagen for his interest and availability to assist me. Special thanks to Kjartan Følke for the invaluable time together during the SBU testing and his patience with my Norwegian skills. In addition to my current employer SINTEF and colleagues to be so comprehensive with my "special" situation.

Thanks to all the reviewers of my manuscripts in international journals and conferences, their corrections and critics definitely improved my publications.

Especial gratitude to my parents, Felicidad and Teodoro, who have been always supporting me. Without their support and love, I would never have gotten this far!

I cannot forget my dog and faithful friend Chuby, who has pushed me every day to take fresh air with long walks helping the rationale to flow.

Last, but not least, my lovely wife and best friend Elsa. She has always been supporting and enduring me, helping me to defeat all the obstacles. I am grateful for believing me and following me in this adventure to Norway, leaving her family and life, so that I could fulfil this dream. A few words will not be enough for expressing my gratitude!

Table of contents

Abstract ..... **i**
Preface and acknowledgments ..... **iii**
List of figures ..... **xi**
List of tables ..... **xix**
Part I ..... **xxv**
1 Introduction **1**
1.1 General remarks 1
1.2 Objective of the thesis and research design 2
1.3 Research scope and limitations 4
1.4 Structure of the thesis 5
1.5 Scientific dissemination 6
2 Background and theoretical framework **11**
2.1 General 11
2.2 Hard rock tunnel boring 11
2.2.1 Introduction 11
2.2.2 Tunnel boring 12
2.2.3 Cutter discs 14
2.2.4 Real-time monitoring 15
2.3 Rock mass boreability 16
2.3.1 General remarks 16
2.3.2 Intact rock boreability 18
2.3.3 Comparison of drillability assessments 23
2.3.4 Rock mass assessments 27
2.3.5 Planes of weakness/discontinuities 30
2.4 Rock abrasivity and cutter wear 31
2.4.1 State-of-the-art rock abrasivity testing in hard rock tunnelling 31
2.4.2 Cutter wear in hard rock tunnel boring 35
2.5 Performance prediction and cutter life models in hard rock tunnel boring 36
2.5.1 General remarks 36
2.5.2 Performance prediction models in hard rock tunnel boring 39
2.5.3 Cutter life assessments in hard rock tunnel boring 41
2.6 The NTNU prediction model for hard rock TBMs 43

2.6.1 Introduction 43
2.6.2 Model parameters 44
3 Research methodology and procedures 47
3.1 General approach 47
3.2 Literature review 48
3.3 Field research 48
3.3.1 General remarks 48
3.3.2 Description of the projects 49
3.3.3 Engineering geological back-mapping 52
3.3.4 TBM data logging and processing 56
3.3.5 Cutter consumption 61
3.3.6 Cutter life 67
3.4 Field Trials 72
3.4.1 General remarks 72
3.4.2 Penetration tests 73
3.4.3 RPM tests 75
3.5 Laboratory research 79
3.5.1 General remarks 79
3.5.2 Soft Ground Abrasion Tester using crushed rock samples (SGAT-CR) 80
3.5.3 Development of a new rock abrasivity test method – the Rolling Indentation Abrasion Test (RIAT) 83
3.5.4 Experiments to investigate cutter wear mechanisms 87
4 Results and discussion 97
4.1 Revision of the NTNU prediction model for hard rock TBMs 97
4.1.1 Introduction 97
4.1.2 Machine parameters 101
4.1.3 Category intervals for drillability indices 107
4.1.4 Rock mass fracturing 108
4.1.5 Penetration rate model 120
4.1.6 Influence of cutterhead velocity on penetration rate 127
4.1.7 Cutter life model 138
4.1.8 Machine utilization and gross advance rate 150
4.1.9 Sensitivity analysis of the NTNU model 158
4.1.10 Limitations of the NTNU model 161

4.2 Development of a new rock abrasivity test method 163
4.2.1 Introduction 163
4.2.2 Development of the Rolling Indentation Abrasion Test (RIAT) 167
4.3 Cutter wear mechanisms in hard rock tunnel boring 176
4.3.1 Introduction 176
4.3.2 Hardness profiles of worn cutters 177
4.3.3 Influence of temperature - Tempering experiment 179
4.3.4 Influence of corrosion on the abrasion of cutter steels 181
4.3.5 Failure mechanisms 181
4.3.6 Concluding remarks 187
5 Conclusions and recommendations 189
5.1 Research questions 189
5.2 Main findings 190
5.3 Recommendations and further work 192
5.3.1 General recommendations 192
5.3.2 Further work 193
References 195
Part II 205
Appendix 345

List of figures

Figure 1. Diagram illustrating the research design. Literature review is involved during all the research work. 4

Figure 2. Basic sketch of an open hard rock TBM (Log, 2016). 12

Figure 3. The principle of chip formation under a disc cutter (Modified from NTH, 1983). .. 13

Figure 4. Consecutive stages of chip formation, chip loosening and stress release for multiple passes using one cutter disc (Lislerud, 1997)..... 13

Figure 5. Four approaches used to analyse rock breaking in tunnel boring: a) an LCM (Gertsch et al., 2007), b) an indentation test using a TBM tool (Innaurato et al., 2007), c) a scaled rock cutting test (Entacher et al., 2014) and d) a punch test (Yagiz, 2009)..... 20

Figure 6. Summary diagrams showing a) Brittleness Value (S_{20}) and b) Sievers' J-Value (SJ) (Dahl et al., 2012)..... 21

Figure 7. Recorded Drilling Rate Index (DRI) ranges for some rock types (Bruland, 2000bd) 21

Figure 8. Recorded Cutter Life Index (CLI) ranges for some rock types (Bruland, 2000bd).. 22

Figure 9. Correlation between UCS and S_{20}. The coloured boxes refer to UCS classification ranges given by ISRM and corresponding ranges in the suggested S_{20} classification (Dahl et al, 2012)..... 23

Figure 10. Correlation between the DRI and UCS (NTNU/SINTEF database, 2016). 24

Figure 11. Correlation between the DRI and UCS (MPa), grouped according to rock type (NTNU, 1983). 25

Figure 12. Schematic representation of the brittleness value (S_{20}) and Sievers J-value (SJ) in the breaking process under a cutter disc in hard rock. 26

Figure 13. Correlation between the CAI and the AVS. The coloured boxes refer to CAI classification ranges given by Cerchar Institute, 1986 and corresponding ranges in the suggested AVS classification. (Dahl et al., 2012)..... 26

Figure 14. Correlation between the CLI and the CAI_s (NTNU/SINTEF database, 2016). Shaded area represents the correlation introduced by Bruland (2000 d) 27

Figure 15. The main types of rock mass discontinuities classified according to length. The length range for joints is modified after Palmström (1995). 30

Figure 16. Two main types of CERCHAR test apparatus commonly in use. Type 1 (left) represents the original design. Type 2 (right) is the modified CERCHAR apparatus as reported by West (1989). 1 = mass, 2 = pin chuck/guide, 3 = stylus, 4 = specimen, 5 = vice and 6 = lever/hand crank (ISRM, 2014)..... 32

Figure 17. The LCPC abrasivity testing device (Thuro et al., 2007). 1 = motor, 2 = metal impeller, 3 = sample container (diameter = 93 mm, height = 100 mm) and 4 = funnel tube..... 34

Figure 18. Outline of the Abrasion Value Cutter Steel (AVS) test (Dahl et al., 2012)..... 35

Figure 19. The relationship between relative excavation costs and degree of rock fracturing. 37

Figure 20. Result of analyses of large number of TBM tunnels where the best performances (WR, World Record) are represented by the uppermost lines showing best shift, day, week and month. (Barton, 2000) 38
Figure 21. Timeline of the common prediction models developed during the last 40 years. .. 39
Figure 22. Geographical distribution of the hard rock TBM projects. 50
Figure 23. Summary of rock property variations encountered at the project sites. 51
Figure 24. Template for engineering geological back-mapping in bored tunnels (recommended for TBM diameters greater than approximately 5 m). 53
Figure 25. Basic terms linked to the stereographic projection and stereonet illustrating the angles used in equation 1 (Article V). 54
Figure 26. Graph used to calculate the fracturing factor (k_s) on the basis of fracture class and the angle between the tunnel axis and the planes of weakness. From Bruland (2000f). 54
Figure 27. Influence of systematically occurring fissures or joints at various angles to the tunnel axis. From Bruland (2000f). 55
Figure 28. Chipping pattern for boring in fractured rock with regular, short spacing between planes of weakness (e.g. class IV) and at an angle of 90 degrees. From Bruland (2000f). 55
Figure 29. An example of logged TBM data showing net penetration rate (m/h) versus cutter thrust (kN/cutter) for a 50-metre tunnel section. 57
Figure 30. An example of logged TBM data showing net penetration rate (m/h) versus cutter thrust (kN/cutter) for a 50-metre tunnel section. The data have been sorted to display values above the 50 kN/cutter. 58
Figure 31. An example of logged TBM data showing net penetration rate (m/h) versus cutter thrust (kN/cutter) of a 50-metre tunnel section. The data have been sorted to display values above 150 kN/cutter. 59
Figure 32. Average cutter thrust (right) values for the defined cutter thrust levels used for sorting logged TBM data. 60
Figure 33. Average net penetration rate values for the defined cutter thrust levels used for sorting logged TBM data. 60
Figure 34. Template used to record cutter wear data used to calculate cutter life, wear patterns and ring wear along a tunnel section. 62
Figure 35. The calculation of cutter consumption (in cutter/m) for a theoretical cutterhead installed with three cutters (Bruland, 2000e). 63
Figure 36. An example of cutter consumption per cutter position for Project D. 64
Figure 37. Total data distribution for a) the reasons of cutter replacement and b) cutter consumption/repositioning. 64
Figure 38. Cumulative wear recorded for Project D. 65
Figure 39. Cutter ring wear and recommended wear limits for Project B. Average ring wear for changes related total cutter changes, and changes due to abrasive wear and other factors related to the bearing set. 66

Figure 40. Cutter wear height and recommended wear limits for Project D. Average wear height for changes related to total cutter changes, and changes due to abrasive wear and other factors related to the bearing set. 66
Figure 41. The causes of cutter change/replacement according to the prediction model. 67
Figure 42. Correction factor for abrasive minerals (k_Q) modified from Bruland (2000b) 70
Figure 43. Methodology for estimating levels of uncertainty in connection with cutter life... 71
Figure 44. Plot of the penetration curve for two penetration tests. 74
Figure 45. Plot of $\log_{10}$ values for M_1 and i_0 for two penetration tests. 75
Figure 46. An example of a graph resulting from an 'RPM test' included in this thesis. 77
Figure 47. An example of 'RPM test' results. Vertical lines (from right to left) denote the start of the test, the cutterhead rpm reference and the cutterhead rpm optimal. 78
Figure 48. An example of normalized 'RPM test'. 78
Figure 49. Diagram (left) showing the Soft Ground Abrasion Tester (SGAT) and photo (right) of the test rig (from Jakobsen et al., 2013). 80
Figure 50. The drilling tool used for testing the SGAT using crushed rock samples. The test piece is 8 centimetres long with a 1 x 1 cm cross-section. 81
Figure 51. The Iddefjord granite. A crushed rock sample (left) and intact rock (right). 82
Figure 52. Proposed trends of the curves for samples A, B, C and D during SGAT-CR testing. 83
Figure 53. Outputs from the RIAT method 84
Figure 54. Versions of tools used during development of the Rolling Indentation Abrasion Test (RIAT) method. From left (initial) to right (current). 85
Figure 55. Relationship between cutter diameter and diameter/tip width ratio for real TBM cases (a mini-TBM with a 0.6 m diameter cutter has been included). Extrapolation to test scale shows that the diameter/tip width ratio of miniature cutters is in accordance with real TBM performance. 86
Figure 56. Rock samples after testing using the RIAT. (a) limestone, (b) basalt, (c) Basalt Xiamen, (d) Trondhjemite (tonalite), (e) Rosa Porriño granite (RP granite), (f) Iddefjord granite, (g) Gris Mondariz granite (GM granite) and (h) quartzite. 87
Figure 57. Cutter ring samples 01 (left) and 02 (right), taken from Project D. 88
Figure 58. Mini-cutter ring samples. 89
Figure 59. A Leica MEF4 optical microscope (right) and an FEI Helios NanoLab Dual Bean FIB microscope (left). 91
Figure 60. Image showing hardness indentations on a TBM cutter ring sample. 93
Figure 61. The Matsuzawa macro-hardness indenter (left) and the Leica VMHT MOT micro-hardness indenter (right). 94
Figure 62. A tribocorrosion test rig (see paper IX). 95
Figure 63. Performance prediction flowchart generated by the latest version of the NTNU model. 100

Figure 64. Standard number of cutters on a cutterhead (N_0). Data from the projects used in this thesis. 102
Figure 65. Installed cutterhead power (kW). Data from the projects used in this thesis. 103
Figure 66. Recommended gross average thrust per cutter disc. The upper limit applies to boring in rock masses with a low degree of fracturing, while the lower limit refers to boring in medium to highly fractured rock masses. 104
Figure 67. A correlation of rock mass fracturing factor (k_s) with cutter thrust. The recommended range of cutter thrust values (taken from Figure 66) is indicated by the shaded area. 105
Figure 68. Cutterhead velocity (rpm) as a function of TBM diameter and cutter diameter. The graph shows the applied and optimal cutterhead velocities, as well as values taken from tests, and the maximum installed velocity for each of the projects analysed. 106
Figure 69. Mapping subjectivity. Frequency distribution of fracture classes for the mapped sections in Project A. The reader is also referred to Paper V (currently under review). 109
Figure 70. The main types of intact rock and rock mass discontinuities encountered during back-mapping in hard rock TBM tunnelling. Types are categorised according to length based on the NTNU methodology. The shaded area indicates where data have been derived from laboratory tests carried out on intact rock. 111
Figure 71. Schistose fabric and cross-fractures in a schistose rock (modified after NTH, 1983). 111
Figure 72. Average fracture spacing used to define fracture classes. Both previous and new fracture class terminologies are included. 112
Figure 73. A typical Marked Single Joint in a rather non-fractured rock mass. The MSJ has some filling material, it carries some water and there is clear overbreak along parts of the MSJ. 114
Figure 74. Schematic outlining different approaches to the understanding of rock mass boreability in connection with hard rock TBM tunnelling. 115
Figure 75. A photograph taken during a tunnel face inspection showing void areas generated after tunnelling in a fractured rock mass. The tunnel axis orientation is 160 degrees. (Photo courtesy of Tobias Andersson). 116
Figure 76. Illustration of the varying influence of the relative angle (α) between the fracture sets and tunnel direction. 117
Figure 77. Crack analysis of a rock chip sample (Photo courtesy of Solveig Vassenden). ... 117
Figure 78. Significance of the TBM cutterhead diameter when boring in rock masses with low degree of fracturing (modified from NTH, 1984). 118
Figure 79. Critical cutter thrust (M_1) as a function of the equivalent fracturing factor. The plotted values are taken from the results of penetration tests included in this thesis. 121

Figure 80. Penetration coefficient (b) as a function of the equivalent fracturing factor. The plotted values are taken from the results of penetration tests included in this thesis. 122
Figure 81. Predicted effect of the increment of cutter thrust on the penetration rate according to the NTNU penetration rate model. 123
Figure 82. Rock mass fracturing factor (k_s) plotted against the angle between the tunnel axis (α) and the fracture sets for different fracture classes. 124
Figure 83. Rock mass fracturing factor (k_s) plotted against the angle between the tunnel axis (α) and the fractures sets for fracture classes exhibiting low degrees of fracturing. The lowest value is 0.36. 125
Figure 84. Plot of DRI correction factor values (k_{DRI}). The plotted values are those obtained as part of this PhD research work. 126
Figure 85. Basic net penetration rate where d_c = 483 mm, a_c = 70 mm and recommended rpm. 126
Figure 86. A Summary of the normalised RPM tests conducted as part of this thesis. Maximum and optimal relative rpm and relative penetration rate values are included. 129
Figure 87. Values obtained from 'RPM tests' conducted as part of this thesis. The trend line shows the relative influence of RPM on relative penetration rates. 129
Figure 88. A histogram and normal distribution curve illustrating the relationship between optimal RPM and machine diameter values. 130
Figure 89. Penetration rate and net penetration rate values obtained from the 'RPM test' C-2. 131
Figure 90. Average values of size of largest chip (left) and cubic chip size (right) obtained from the 'RPM test' C-2 (Eide, 2014). 133
Figure 91. Relationship between gross average cutter thrust and relative 'optimal' cutterhead rpm based on the tests conducted as part of this thesis. A maximum correlation level fit has been selected. 134
Figure 92. Relationship between gross average cutter thrust and relative optimal PR based on the tests conducted as part of this thesis. A maximum correlation level fit has been selected. 135
Figure 93. Relationship between the equivalent fracturing factor (k_{ekv}) and relative cutterhead rpm based on the tests conducted as part of this thesis. A maximum correlation level fit has been selected. 135
Figure 94. Relationship between the slope generated from all test results and the relative cutterhead rpm value based on the tests conducted as part of this thesis. A maximum correlation level fit has been selected. 136
Figure 95. Summary of results of 'RPM tests' carried out at below optimal cutterhead rpm values. The data included are optimal and minimum relative rpm, together with relative penetration rate. 137

Figure 96. A correction factor for cutterhead velocity that differs from the recommended value as a function of relative rpm. 137
Figure 97. A plot showing penetration rate data obtained from projects A, C and D. The data shows actual versus predicted PR values measured along 50-metre tunnel sections. 138
Figure 98. Normalised cutter replacement curves for different TBM diameters (Bruland, 2000e). The plotted points (dots and triangles) represent an example of data from the projects used in this thesis. 139
Figure 99. Correction factor for TBM diameter. The plotted points represent data from the projects used in this thesis. 140
Figure 100. Correction factor for abrasive minerals (k_Q). 141
Figure 101. The influence of cutter thrust levels on cutter life for highly abrasive rocks (4.5<CLI<5.9). The 20-in. cutter diameter value is deliberately excluded from the data used to construct the trend line. 143
Figure 102. Correction factor applied to the influence of cutter thrust on cutter life for highly abrasive rocks (4.5<CLI<5.9). 144
Figure 103. A plot showing basic cutter ring life obtained using the 2016 version of the NTNU model for 483 mm and 508 mm diameter cutters. For comparison, the plot also shows basic cutter ring life of the NTNU 2000 version of the model. Results from the uncertainty analysis are also plotted. 145
Figure 104. Plots showing basic cutter ring life (h) for 432 and 483 mm cutter diameters obtained from the updated (2016) version of the NTNU model. 146
Figure 105. Basic cutter ring life (H_o) as a function of the Sievers' J value (SJ) corresponding to CLI values between 5.2 and 9.9 (from very low to medium, according to Dahl et al., 2012). The minimum SJ value is limited to 1.5. 147
Figure 106. Relationship between CLI and bearing-related or other reasons for cutter replacement. 148
Figure 107. Relationship between basic cutter ring life (h) and bearing-related or other reasons for cutter replacement. 148
Figure 108. Principal cutter life fracturing factor. 149
Figure 109. Cutter life data and wear patterns from several tunnel sections. 150
Figure 110. Time spent to replace a cutter, including inspection time (min.). From Projects D and C. 152
Figure 111. Actual time consumption compared with model predictions for Project D (left) and for a tunnel section from Project E (right). 153
Figure 112. Time consumption per kilometre (h/km) for repair and service of the TBM (T_{TBM}), for miscellaneous factors (T_m), and for repair and service of the backup (T_{back}). Data from Projects D and E. 154
Figure 113. Effective working hours per week. From Projects D and E. 155
Figure 114. Analysis of the influence of the tunnel length. 156
Figure 115. Additional time (h/km) plotted against tunnel length. 156

Figure 116. Cumulative additional time for the length of the tunnel (h/km). 157
Figure 117. Variation in predicted NPR (m/h) in response to variation in input parameters. 159
Figure 118. Variation in predicted cutter life (in h/c) in response to variation in input parameters. 160
Figure 119. Variation in predicted cutter life (in sm^3/c) in response to variation in input parameters. 161
Figure 120. Average weight loss results following SGAT tests using crushed rock for three fraction sizes of the Iddefjord granite (0-5 mm, 0-10 mm and 4-6 mm) and three rotational speeds (30, 50 and 70 rpm). The standard deviation is also shown. 165
Figure 121. Sieve curves for the samples A, B, C and D before and after testing. Weight loss data obtained from the SGAT-CR tests are also included. 166
Figure 122. Outline and photograph illustrating the components of the Rolling Indentation Abrasion Test (RIAT) method (reproduced from paper VIII). 167
Figure 123. Results from RIAT tests for eight rock types. The $RIAT_i$ parameter is shown on the x-axis left (red stippled line) and the $RIAT_a$ parameter on the x-axis right (blue columns). The error bars indicate the standard deviation (reproduced from Paper VIII). 169
Figure 124. The relationship between the $RIAT_a$ and $RIAT_i$ indices based on data obtained from testing eight rock types. A best-fit maximum correlation level has been selected (reproduced from Paper VIII). 170
Figure 125. Cumulative weight loss for a miniature cutter as a function of elapsed RIAT test time using a sample of Trondhjemite (reproduced from Paper VIII). 170
Figure 126. Diagrams showing the relationships between the $RIAT_a$ index and the AVS following the testing of eight rock types (Reproduced from Paper VIII). 172
Figure 127. Plots illustrating correlations between the $RIAT_a$ (a) and (b), and $RIAT_i$ (c) and (d) indices and the CLI for the eight rock types tested. Plots (b) and (d) are the corresponding correlations in which the limestone values are excluded (Reproduced from Paper VIII). 173
Figure 128. Correlations between the $RIAT_a$ and $RIAT_i$ indices and quartz content (a) and (c) and equivalent quartz content (b) and (d), for the eight rock types used in the RIAT tests (Reproduced from Paper VIII). 175
Figure 129. Correlations between VHNR and the (a) $RIAT_a$ and (b) $RIAT_i$ indices for the eight rock types used in the RIAT tests (Reproduced from Paper VIII). 175
Figure 130. Microstructure of the cutter disc steel (H 13 tool steel) tested as part of this study (Reproduced from Paper IX). 177
Figure 131. Hardness profiles for TBM cutter ring sample no. 02. 178
Figure 132. Hardness profiles for TBM cutter ring sample no 04. 179
Figure 133. Hardness profiles resulting from tempering experiments performed after 1, 2 and 4 hours on TBM cutter ring sample no. 05 (unused cutter ring). The rectangles represent hardness values at the wear surface of TBM cutter ring samples 01 and 04. 180

Figure 134. Hardness profile resulting from a tempering experiment performed for 1 hour on TBM cutter ring sample no. 04. Points and horizontal lines indicate hardness values at known distances from the wear surface of the sample. 180
Figure 135. An optical image of a cross-section cut parallel to the rolling direction of a TBM cutter ring (sample no. 03). Reproduced from Nærland (2015). 182
Figure 136. Optical images of cross-sections cut parallel to the rolling direction of RIAT mini-cutter ring sample 15 (left) and 16 (right). Reproduced from Nærland (2015). 182
Figure 137. Optical images of cross-sections taken from TBM cutter ring sample no 02. The cross-sections are cut parallel (left) and at right angles (right) to the rolling orientation. Reproduced from Nærland (2015). 183
Figure 138. An optical image of a parallel cross-section of TBM cutter ring sample no. 02. Reproduced from Nærland (2015). 184
Figure 139. An SEM surface image of the RIAT mini-cutter ring sample no. 13. Reproduced from Nærland (2015). 185
Figure 140. An FIB image of a cross-section (transverse) from TBM cutter ring sample no. 02 (Reproduced from Nærland, 2015). 186
Figure 141. FIB images of cross-sections (transverse) from TBM cutter ring samples no. 01 (left) and no. 04 (right). Reproduced from Nærland (2015). 186
Figure 142. FIB images of cross-sections (transverse) from RIAT mini-cutter ring sample no. 07 (left) and no. 16 (right). Reproduced from Nærland (2015). 187

List of tables

Table 1. Summary of the articles included as part of this PhD thesis. 6
Table 2. Classification of rock based on uniaxial compressive strength (ISRM, 1978) 18
Table 3. Category intervals for drillability indices 22
Table 4. Common rock mass classification systems used in connection with tunnelling projects. 28
Table 5. The most common laboratory testing methods for measuring rock abrasivity in connection with hard rock tunnel boring. 31
Table 6. CAI abrasivity classification (ASTM, 2010; ISRM, 2014). 33
Table 7. Classification of LAC (Thuro et al., 2007). 34
Table 8. Classification of rock abrasion on cutter steel (Dahl et al., 2012). 35
Table 9. Commonly used performance prediction models including their input and output parameters. 40
Table 10. Common cutter life models including their input and output parameters. 42
Table 11. History of the NTNU prediction model for hard rock TBMs 44
Table 12. Machine parameters and rock properties influencing net penetration rate. 45
Table 13. Machine parameters and rock properties influencing cutter wear. 45
Table 14. The main characteristics of the TBM project sites. 49
Table 15. Summary of the main rock properties encountered at the project sites. 50
Table 16. Summary of the principal machine characteristics used at the project sites. 51
Table 17. Average values of cutterhead velocity, cutter thrust and net penetration rate of the sorted data as defined by cutter thrust levels. 59
Table 18. Cutter thrust and basic penetration data for a penetration test example. 74
Table 19. Laboratory test methods used in this study. 79
Table 20. Main properties of the Iddefjord granite. 81
Table 21. Fraction sizes used for testing of the SGAT with crushed rock samples. Testing was performed at three different rotation speeds (30, 50 and 70 rpm) and at a constant advance rate of 10 mm/min. 82
Table 22. Proposed fraction size distributions for the samples (A, B, C and D) of Iddefjord granite prior to testing using the SGAT-CR method. The rotation speed was 50 rpm. 82
Table 23. Main parameters for the RIAT method 84
Table 24. Overviews of the cutter ring wear analysis tests. The symbol "◯" indicates that a test has been performed, while the symbol "-" indicates that the test has not been performed. 88
Table 25. Metallographic etchants used in preparation for optical imaging (Nærland, 2015). 89
Table 26. Steps involved in the FIB microscopy milling process (Nærland, 2015). 92
Table 27. Summary of the main parameters used for the tribocorrosion test. 95

Table 28. Summary of materials used during the tribocorrosion tests (see paper XI). 96
Table 29. Rock properties and machine parameters that influence net penetration rate. 98
Table 30. Rock properties and machine parameters that influence cutter wear. 99
Table 31. The most common cutter disc specifications currently used in hard rock tunnel boring. 101
Table 32. Cumulative percentage for category intervals of drillability indices (Bruland, 2000g). 107
Table 33. Category intervals for drillability indices. 107
Table 34. Fracture class terminology as defined by the average spacing between fractures. 113
Table 35. Summary of the penetration test results included in this thesis. 121
Table 36. Summary of the 'RPM tests' included in this thesis. Rock property values such as DRI, CLI and k_{ekv} are also included, as well as values for thrust, relative cutterhead rpm (initial and optimal) and relative PR (initial and optimal). 128
Table 37. Summary of the values of rpm, gross cutter thrust, penetration rate, net penetration rate and torque for the 'RPM test' C-2. 131
Table 38. Summary of outcomes for the RPM test C-2. 132
Table 39. Summary of average chip size measurements, chipping frequency, cubic chip size and chip shape factor values applied during the RPM test C-2 (Eide, 2014). 132
Table 40. The time taken to replace a cutter. 152
Table 41. Example of application of the calculation of additional time resulting from tunnel length. 157
Table 42. Standard values used in the sensitivity analysis. 158
Table 43. Variation in parameter values used in the sensitive analysis. 158
Table 44. The results of SGAT-CR tests using crushed rock for three fraction sizes of Iddefjord granite, carried out at three rotational speeds. 164
Table 45. Distribution of fraction sizes from four samples (A, B, C and D) of Iddefjord granite before and after testing using the SGAT-CR method. Weight loss data for all the samples are also included. 165
Table 46. Results of RIAT tests on eight rock types (reproduced from Paper VIII). 168
Table 47. Laboratory test results for eight rock types (limestone, basalt, Basalt Xiamen, Trondhjemite, RP granite, Iddefjord granite, GM granite and quartzite). Tests include NTNU drillability tests (S20, SJ, AVS, DRI^{TM} and CLI^{TM}), the Cerchar test (CAI_s), uniaxial compressive strength tests (UCS) and density measurements (Reproduced from Paper VIII). 171
Table 48. Essential mineral compositions for limestone, basalt, basalt Xiamen, Trondhjemite, RP granite, Iddefjord granite, GM granite and quartzite (Reproduced from Paper VIII). 174
Table 49. Quartz content, equivalent quartz content and Vickers hardness number for rock (VHNR) values for the eight rock types used in the RIAT tests (Reproduced from Paper VIII). 174

Table 50. Composition of a standard TBM cutter ring and RIAT mini-cutter samples. 176

List of acronyms and abbreviations

ASTM	American Society for Testing and Materials
AVS	Abrasion value cutter steel
BTS	Brazilian tensile strength
CAI	Cerchar abrasivity index
CLI	Cutter life index
CSM	Colorado School of Mines
DRI	Drilling rate index
FIB	Focused ion beam
HV	Hardness Vickers
ISRM	International Society for Rock Mechanics
LAC	LCPC abrasivity coefficient
LCM	Linear cutting machine test
LCPC	Laboratorie Central des Ponts et Chaussées (French Public Scientific and Technical Research Establishment).
MSJ	Marked single joint
NPR	Net penetration rate (m/h)
NTNU/NTH	Norwegian University of Science and Technology
PLT	Point load test
PR	Penetration rate (mm/rev)
Q	Rock quality designation number
RIAT	Rolling indentation abrasion test
RMi	Rock mass index
RMR	Rock mass rating
rpm/RPM	Cutterhead velocity in revolutions per minute
RQD	Rock quality designation
SEM	Scanning electron microscope
SGAT	Soft ground abrasion tester
SGAT-CR	Soft ground abrasion tester with crushed rock
SINTEF	Foundation for Scientific and Industrial Research
TBM	Tunnel boring machine
UCS	Uniaxial compressive strength
VHNR	Vickers hardness number of the rock

List of main symbols

a_f	Average spacing between fractures
b	Penetration coefficient
d_c	Cutter diameter
d_{tbm}	TBM diameter
f_D	Cutterhead factor
H_h	Instantaneous tool life in hours per cutter
H_m	Instantaneous tool life in metres per cutter
H_f	Instantaneous tool life in solid (in situ) cubic metres per cutter
i_0	Basic net penetration rate
k_{ekv}	Equivalent rock mass fracturing factor
k_s	Rock mass fracturing factor
$k_{s\text{-}tot}$	Total rock mass fracturing factor
$k_{s\text{-}avg}$	Average of the total rock mass fracturing factor
M_B	Gross average cutter thrust
M_{ekv}	Equivalent cutter thrust
M_1	Critical cutter thrust
N_0	Standard number of cutters
N_{tbm}	Number of cutters
$RIAT_a$	RIAT abrasivity index
$RIAT_i$	RIAT indentation index
Q	Abrasive minerals content
r_i	Relative radius of cutterhead position i
SJ	Sievers' J-value
S_t	Fissure class
S_f	Fracture class
S_{20}	Brittleness value
U	Machine utilization
W_m	Instantaneous tool life in cutters per metre
α	Smallest angle between a fracture set and the tunnel axis
σ_c	Uniaxial compressive strength

Part I

1 Introduction

1.1 General remarks

During recent decades, there has been a significant increase in the development of underground infrastructure worldwide due to the great demands placed on civil and mining infrastructure projects. These demands are expected to increase in the future, combined with a growing need to excavate deeper leading to increasing tunnel lengths (ITA, 2012).

Tunnelling using the Tunnel Boring Machine (TBM) approach has become widely used and is currently an important method employed by the tunnelling industry. The development of TBM technology has made the approach applicable in an increasingly wider range of rock mass conditions. Technically speaking, excavations can now be carried out in almost all rock conditions using this method, given certain economic constraints. The use of TBMs involves major investments and high levels of geological risk. Performance and cutter consumption have a great influence on the successful execution of mechanised tunnelling, especially in hard rock conditions. Furthermore, the method requires accurate predictions of TBM performance and costs, which in turn facilitate the control of risk and enable projects to avoid delays and budget overruns.

The interaction between the rock mass and the machine is a process of great complexity. Performance predictions and cutter life assessments are not straightforward issues and involve major risk assessments, especially in hard rock conditions.

The prediction model for hard rock TBMs developed by the Norwegian University of Science and Technology (NTNU) is based on a combination of field performance data, engineering geological back-mapping, and the laboratory testing of rock samples. The model has been updated continuously since descriptions of the first version were published in the 1970s (NTH, 1976). The last version was published in 2000 by Bruland (2000b).

The NTNU prediction model for performance predictions and cutter life assessments is widely used in hard rock tunnelling applications. The development of TBM technology during recent decades, and the possible influence of parameters not considered in previous versions, has made revision of the model to improve prediction accuracy an essential requirement.

Cutter consumption and parameters such as cutter ring wear play a significant role in performance and cost predictions, especially in hard rock conditions. Cutter wear involves a complex tribological system in interaction with the geological properties of the rock mass. Existing laboratory test methods fail to reproduce wear behaviour encountered during tunnel boring. Because of this and the importance of cutter wear, it was considered of interest to

develop a new rock abrasivity test method as a means of obtaining more realistic measures of cutter wear during hard rock tunnelling.

Understanding the processes and failure mechanisms during cutter wear enabled new knowledge to be applied as part of the development of a new rock abrasivity test method for laboratory use. In addition, cutter wear mechanisms affecting cutter rings during tunnel boring might lead to better cutter consumption predictions and future improvements in cutter ring development.

This PhD thesis was linked to a joint research project named "Future Advanced Steel Technology for Tunnelling" (FAST- Tunn), involving a collaboration between The Robbins Company, BASF CGC, the Norwegian National Rail Administration, Scana Steel Stavanger, BMS Steel, LNS Group, Banbendererde Engineers and SINTEF/NTNU.

The two main objectives of the FAST-Tunn project were to increase the efficiency of TBM hard rock excavation performance using improved cutter rings, and to improve the ability of the NTNU model to predict performance during tunnelling operations in Norway (Grøv et al., 2013).

1.2 Objective of the thesis and research design

The overall aim of this thesis is to build on our existing knowledge of tunnel boring and wear processes, technology and capacity, thus enhancing performance prediction and cutter life assessments in hard rock tunnel boring projects.

In order to achieve this aim, three main research objectives were formulated:

- ✓ To revise and extend the current version of the NTNU prediction model for TBM performance and cutter life.
- ✓ To develop a new rock abrasivity laboratory test method for tool life assessments in hard rock tunnel boring.
- ✓ To analyse the wear process and identify failure mechanisms in cutter tools during tunnel boring.

The aim and research objectives were proposed as a part of the PhD research plan (Macias, 2013). Initially, the second objective was formulated to enable recognition of the need and opportunity to develop a new abrasivity test method for laboratory use to improve cutter ring wear prediction.

As a result, a number of additional research issues emerged with the aim of addressing the proposed objectives:

<u>To revise and extend the NTNU performance and cutter life prediction model for hard rock tunnel boring</u>

- To decide if a revision of the current version is required and appropriate.
- To revise and extend TBM specifications and operational parameters.

- To establish a classification of the rock mass.
- To find out if it possible and required to address the influence of new parameters such as:
    - Cutterhead velocity (rpm) influence on penetration.
    - Cutter thrust influence on cutter consumption.
    - Tunnel length influence on machine utilization.

To develop a new rock abrasivity laboratory test method for tool life assessments in hard rock tunnel boring

- To establish if a new rock abrasivity test method is required.
- To find out if the development of a new rock abrasivity test method is appropriate.
- To establish if the results are of interest when compared with existing laboratory test methods.

To analyse the wear process and failure mechanisms in cutter rings used for tunnel boring

- To establish if the identification of wear mechanisms in TBM cutter rings is appropriate.
- To establish if the identification of the influence of other possible wear factors such as temperature and tribocorrosion are relevant.
- To investigate if the wear process for the new laboratory test method is representative.

Figure 1 is an illustration of the research design for this study.

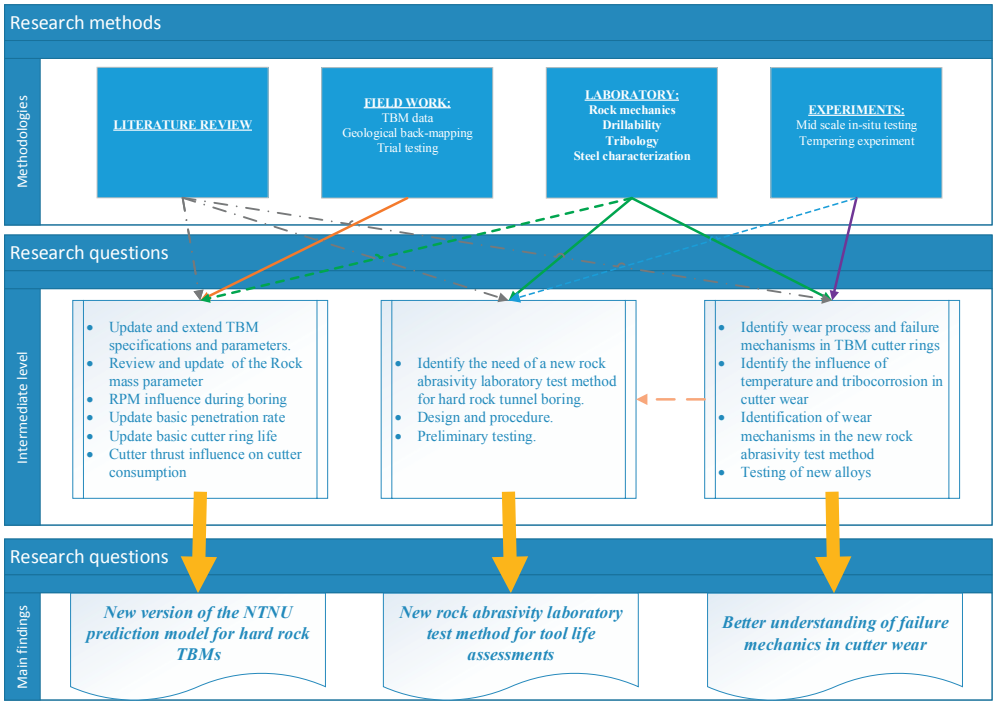

Figure 1. Diagram illustrating the research design. Literature review is involved during all the research work.

1.3 Research scope and limitations

This PhD study focuses on hard rock tunnelling. The tunnelling of soft ground is beyond the scope of the study. A definition of the term "hard rock" is given in chapter 2.3.2.

The NTNU model has been revised based on current TBM technologies as applied in project documents made available to this study.

The main limitations encountered during the study were as follows:

- The relevance of current TBM technologies applied in the projects studied may be limited due to the high level of variation among machine designs and their operation. Variation in geology is also a factor here.
- The limited extrapolation of engineering geological back-mapping in the case of large diameter TBM tunnels. This is a common issue for tunnels which are ultimately lined with concrete because geological mapping is limited to the tunnel face. This reduces the amount of data available in comparison with open TBM tunnelling projects.
- An evaluation of other methods used to assess rock mass and accompanying predictive models is beyond the scope of the present thesis.
- The level of risk associated with performance prediction and cutter life assessments increases with increased abrasivity and decreases as the degree of fracturing increases.

A large number of tunnel sections exhibiting high levels of rock quality and lithologies of high abrasivity have been included in this study.

- Cutter alloy quality is not recorded in the data used for cutter life assessments in this study, and the influence of different steel alloys and their design has not been specifically incorporated. It is assumed that where possible, the tunnelling project selects the tool steel quality required for excavation of the rock in question. In addition, there is a great reluctance in the tool manufacturing industry to share information related to process and quality.
- Difficulties in obtaining representative cutter ring samples, the availability of laboratory equipment, and time constraints linked to the completion of this PhD have restricted the scope of cutter wear mechanics analysis in this study.
- The introduced influence of parameters on penetration rate and cutter life have limited data and they will need further validation.

1.4 Structure of the thesis

This thesis is presented in the form of a "monograph" divided on two parts and one appendix. Part I includes important research methodologies and results presented in a total of five chapters. Part II of the thesis comprises three published scientific articles, five published conference papers and one completed manuscript draft for a scientific article. The papers are appended to the thesis itself. Much of the research has not been published prior to preparation of this thesis document, and this material is discussed in more detail here. There are plans to disseminate the main results in the near future. The appendix includes a new edition of the NTNU model for performance predictions and cutter life assessments.

The aim of assembling the material in this way is to give readers a systematic understanding of the studies included in the thesis. Readers may be directed to specific papers included in the thesis (part II), and the new version of the NTNU prediction model (Appendix).

Chapter 1 presents an overview of the research context and objectives of the PhD study. The limitations on the scope of the research are also included.

Chapter 2 discusses the background and state-of-the-art of hard rock tunnel boring. Topics such as rock boreability, boring process and cutter wear are discussed, and the chapter also provides an introduction to performance prediction and tool life assessments in connection with hard rock tunnel boring.

Chapter 3 presents and discusses the major research methodologies used during the investigation process to achieve the defined objectives. There is a discussion of the detailed analysis of the testing procedures and techniques used.

Chapter 4 presents and discusses a selection of the major research results, including an analysis of what the study has achieved.

Chapter 5 addresses the main findings of the present PhD thesis and offers recommendations for further work.

1.5 Scientific dissemination

The output regarding to dissemination in term of dissemination from the research work is summarised in Table 1.

Table 1. Summary of the articles included as part of this PhD thesis.

Objective	Dissemination
RQ 1: Revise and extension of the NTNU model	Paper **I**
	Paper **II**
	Paper **III**
	Paper **IV**
	Paper **V**
	Paper **VI**
RQ 2: Development of new rock abrasivity test method	Paper **VII**
	Paper **VIII**
RQ 3:Wear mechanisms	Paper **IX**

I. Macias, F.J., Jakobsen, P.D., Seo, Y. and Bruland, A. (2014). *Influence of the rock mass fracturing on the net penetration rates of hard rock TBMs.* Tunnelling and Underground Space Technology Vol. 44 (2014), pp 108-120.

II. Macias, F.J., Jakobsen, P.D., Bruland, A., Log, S., Grøv, E. (2014). *The NTNU Prediction Model: A Tool for Planning and Risk Management in Hard Rock TBM Tunnelling*. Proceedings of the World Tunnel Congress 2014 - Tunnels for a better Life, Foz do Iguazu, Brazil (2014).

III. Macias, F.J., Jakobsen, P.D. and Bruland, A. (2014). *Rock mass variability and TBM prediction*. The 2014 ISRM European Rock Mechanics Symposium (Eurock 2014), Vigo, Spain (2014).

IV. Macias, F.J., Eide, L.N.R., Jakobsen, P.D., Jacobs, C. and Bruland, A. (2015). *Performance prediction of a hard rock TBM used in mining development*. RETC 2015, New Orleans, USA (2015).

V. Seo, Y., Macias, F.J., Jakobsen, P.D., and Bruland, A. (Submitted February 2016). *Influence of subjectivity in geological mapping on the prediction of hard rock TBM performance*. Rock Mechanics and Rock Engineering.

VI. Macias, F.J., Wilfing, L., Andersson, T., Thuro, K. and Bruland, A. (2015). *Performance and cutter life assessments in hard rock tunnelling.* EUROCK 2015 & 64th Geomechanics Colloquium. Schubert (ed.). Salzburg, Austria (2015).

VII. Macias, F.J., Dahl, F.E. and Bruland, A. (2015). *New rock abrasivity test method by rolling disc*. International Congress of Rock Mechanics 2015. Montréal, Québec, Canada, paper 634 (2015).

VIII. Macias, F.J., Dahl, F.E. and Bruland, A. (2016). *New rock abrasivity test method for tool life assessments on hard rock tunnel boring: The Rolling Indentation Abrasion Test (RIAT)*. Rock Mechanics and Rock Engineering, Vol. 49, no. 5 (2016), pp 1679-1693.

IX. Espallargas, N., Jakobsen, P.D., Langmaack, L., Macias, F.J. (2015). *Influence of corrosion on the abrasion of cutter steels used in TBM tunnelling*. Rock Mechanics and Rock Engineering, Vol. 48, no. 1 (2015), pp 261–275.

The following relevant publications are not included in this thesis:

Macias, F.J. and Bruland, A. (2014). D&B versus TBM: Review of the parameters for a right choice of the excavation method. The 2014 ISRM European Rock Mechanics Symposium (Eurock 2014), Vigo, Spain (2014).

Macias, F.J., Jakobsen, P.D., Seo, Y, Bruland, A. and Grøv, E. (2014). Rock Mass influence on Hard Rock TBM Performance Prediction. Proceedings of the World Tunnel Congress 2014 - Tunnels for a better Life, Foz do Iguazu, Brazil (2014).

Paper I:

Macias, F.J., Jakobsen, P.D., Seo, Y. and Bruland, A. (2014). **Influence of the rock mass fracturing on the net penetration rates of hard rock TBMs**. Tunnelling and Underground Space Technology, Vol. 44 (2014), pp 108-120.

This paper addresses the relationship between the degree of fracturing and the net penetration rate of hard rock TBMs. It is based on fieldwork consisting of geological back-mapping and analysis of performance data from a tunnel excavated by a TBM. Different correlations between net penetration rate and the fracturing factor (k_s) have been identified for a variety of k_s values.

Paper II:

Macias, F.J., Jakobsen, P.D., Bruland, A., Log, S. and Grøv, E. (2014). **The NTNU Prediction Model: A Tool for Planning and Risk Management in Hard Rock TBM Tunnelling.** Proceedings of the World Tunnel Congress 2014 - Tunnels for a better Life, Foz do Iguazu, Brazil (2014).

This paper presents an evaluation of the NTNU prediction model based on a case involving a 3.4 metre-diameter open hard rock tunnel excavated using a TBM. The model is validated for

the present project as an effective tool for project planning, risk management and claims assessment.

Paper III:

Macias F.J., Jakobsen P.D., Bruland A. (2014). **Rock mass variability and TBM prediction.** The 2014 ISRM European Rock Mechanics Symposium (Eurock 2014), Vigo, Spain.

This paper evaluates the influence of rock mass variability on the prediction of performance and cost of hard rock TBM projects. A risk analysis of rock mass variability for a complete intact rock boreability scenario is carried out for a hard rock TBM project using the NTNU prediction model for hard rock TBMs.

Paper IV:

Macias, F.J., Eide, L.N.R., Jakobsen, P.D., Jacobs, C. and Bruland, A. (2015). **Performance prediction of a hard rock TBM used in mining development.** Rapid Excavation tunneling Conference (RETC 2015), New Orleans, USA (2015).

This paper is a part of the review of the NTNU prediction model. It includes assessments and comparisons between model performance predictions and actual results in the case of a hard rock TBM tunnelling project used in mining development.

Paper V:

Seo, Y., **Macias, F.J.,** Jakobsen, P.D., and Bruland, A. (Under review). **Subjectivity influence of geological mapping on the NTNU model.** Rock mechanics and rock engineering.

This paper attempts to assess the influence of geological mapping for TBM performance prediction purposes. Predicted net penetration rates based on the rock mass fracturing factor (k_s) are compared with actual values taken from field data. The results indicate that the comparisons between predicted and actual net penetration rates are in good agreement with the mapping-based predictions. This paper is under review and an outline of the manuscript is included in this thesis in the appendix dedicated to the compilation of articles.

Paper VI:

Macias, F.J., Wilfing, L., Andersson, T., Thuro, K. and Bruland, A. (2015). **Performance and cutter life assessments in hard rock tunnelling.** EUROCK 2015 & 64th Geomechanics Colloquium. Schubert (ed.). Salzburg, Austria (2015).

This paper presents an evaluation of performance predictions and cutter life assessments based on a TBM project involving particularly hard rock conditions. Extensive geological back-mapping, complete rock laboratory testing and TBM data gathering were carried out in

order to analyse and assess performance and cutter life using the CSM, Gehring and NTNU prediction models for hard rock TBMs.

Paper VII:

Macias, F.J., Dahl, F.E. and Bruland, A. (2015). **New rock abrasivity test method by rolling disc.** International Congress of Rock Mechanics 2015. Montréal, Québec, Canada, paper 634 (2015).

This paper describes initial testing of the new rock abrasivity test method – the Rolling Indentation Abrasion Test (RIAT), developed as a part of the work carried out in this PhD study. The paper presents a brief description of the procedure and preliminary results.

Paper VIII:

Macias, F.J., Dahl, F.E. and Bruland, A. (2016). **New rock abrasivity test method for tool life assessments on hard rock tunnel boring: The Rolling Indentation Abrasion Test (RIAT).** Rock mechanics and rock engineering, Vol 49, no. 5 (2016), pp 1679 – 1693.

This paper summarises the development of the new abrasivity test method by rolling disc – the Rolling Indentation Abrasion Test (RIAT), previously introduced in Paper VII. Several rock types, exhibiting a wide range of abrasiveness, were tested by the RIAT as part of this study. The new test is evaluated by a comprehensive laboratory testing programme that includes the most commonly used abrasivity test methods, and takes mineral composition into account.

Paper IX:

Espallargas N., Jakobsen P.D., Langmaack L., **Macias F.J.** (2015). **Influence of corrosion on the abrasion of cutter steels used in TBM tunnelling**. Rock mechanics and rock engineering (2015), Vol. 48, no.1 (2015), pp 261 - 275.

This paper examines the effect of corrosion on the abrasion wear of cutter tools. It demonstrates that the presence of conditioning additives minimises wear rates, but fails to suppress corrosion of the cutting tools.

2 Background and theoretical framework

2.1 General

Hard rock Tunnelling plays an important role within the substantial increase in the development of underground infrastructure during the last decades. A large number of underground constructions excavated in hard rock employ the Drill and Blast excavation (D&B) and Tunnel Boring Machine (TBM) methods. Both methods are widely and successfully used.

The use of hard rock TBMs has become widely and generally used with extraordinary success but in more cases than would be desirable, with catastrophic consequences. The use of TBMs involves major investments and high levels of geological risk and the applicability and viability of TBM projects need to be carefully and realistically considered which in turn facilitate the control of risk and enable projects to avoid delays and budget overruns. These facts indicate a need of reliable TBM prediction models and better understanding of the TBM tunnelling.

The interaction between the rock mass and the machine is a process of great complexity in TBM tunnelling. Rock mass is of great importance during tunnel boring and suitable assessments of rock mass boreability are of great importance. Boreability can be defined as the resistance (in terms of ease or difficulty) encountered by a TBM as it penetrates a rock mass composed of intact rock containing planes of weakness.

Furthermore, cutter consumption may strongly influence performance and cost, especially in hard and abrasive rock conditions. Cutter consumption combined with penetration rate and machine utilization will result in the estimation of the excavation time and cost.

2.2 Hard rock tunnel boring

2.2.1 Introduction

A TBM is a machine used for the full face excavation of tunnels in hard rock. The basic elements of a TBM are the cutterhead, the cutterhead carrier (installed with cutterhead drive motors), the machine frame and the clamping and driving equipment (Figure 2). The boring system is essentially made up of the cutterhead embedded with disc cutters. Boring is achieved when the rotating cutterhead is pressed against the rock. Cracks propagate radially from the cutter ring at the contact zone between the cutter edge and the rock surface. This breaks the rock into coarse chips along the cracks between the cutter kerfs.

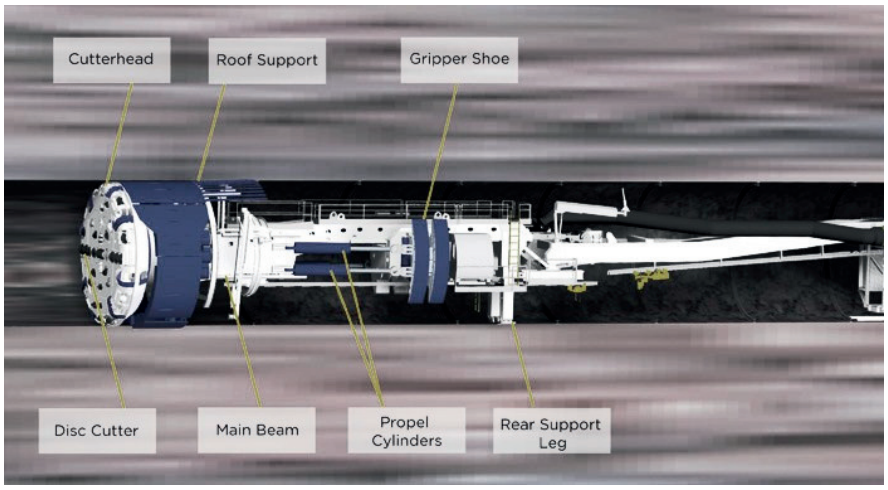

Figure 2. Basic sketch of an open hard rock TBM (Log, 2016).

The development of hard rock TBMs for full face excavation purposes started in the early 1880s. The development of TBM technology was significantly accelerated by the introduction of the rolling disc cutter, which was first used at the beginning of the 1950s by James S. Robbins based on ideas developed in 1850 by Charles Wilson.

2.2.2 Tunnel boring

Tunnelling is achieved by pressing the rotating cutterhead and its discs against the rock with great force. As the cutterhead rotates, it penetrates further into the rock.

This 'indentation' process is the result of a combination of the following failure modes:

- Initial cutter indentation of the rock surface. The cutter tip causes compaction and crushing of the rock material. The rock is crushed to powder due to the high stresses generated in the contact zone between the cutter edge and the rock surface.
- Cracks propagate radially from the cutter ring at the contact zone between the cutter edge and the rock surface. This breaks the rock into coarse chips along the fractures between the cutter kerfs. Lateral chipping from the kerf is the result of fracture formation in the rock along the principal stress trajectories.

Figure 3 shows the principle of chip formation under a disc cutter.

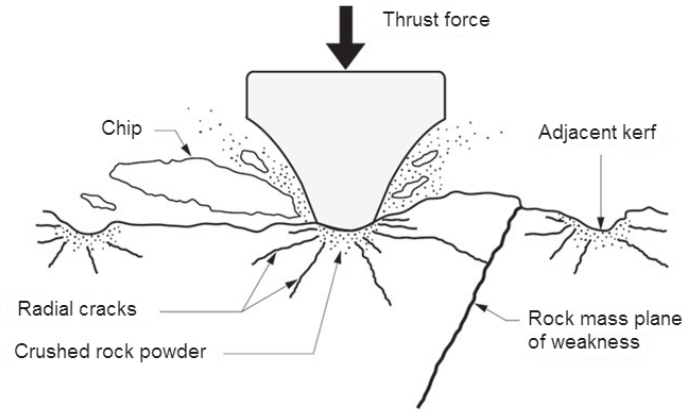

Figure 3. The principle of chip formation under a disc cutter (Modified from NTH, 1983).

Multiple pass cutting will be needed if chip loosening does not occur with the first tool pass (Figure 4).

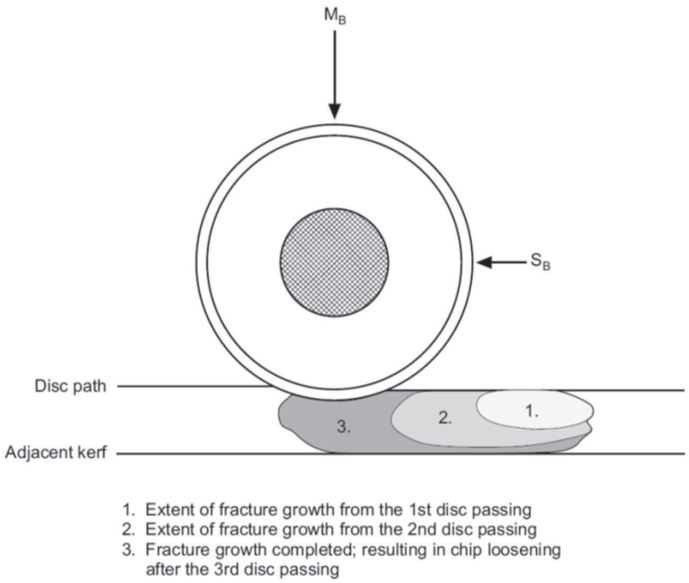

Figure 4. Consecutive stages of chip formation, chip loosening and stress release for multiple passes using one cutter disc (Lislerud, 1997)

The resistance of the rock under excavation by a cutter disc has been commonly termed 'rock cuttability' (Lislerud, 1997). The cuttability parameter depends not only on the rock but also on aspects of the cutting process (indentations, cutter diameter, cutter speed, cutter thrust, the presence of water, etc., (Lislerud, 1997).

Various apparatus and procedures have been developed to assess mechanical rock properties in relation to cuttability. These properties can be categorised as follows:

- Strength and deformability
- Surface hardness
- Brittleness
- Toughness
- Abrasivity

The influence of rock mass discontinuities on cuttability acts at a large scale, typically affecting several individual cutters simultaneously as well as the overall performance of the cutterhead (Lislerud, 1997).

The NTNU/SINTEF methodology for hard rock tunnel boring employs a different definition of the relationship between intact rock and the rock mass involved. The term 'rock drillability' is defined as the resistance of the intact rock under excavation by a cutter disc, while the term 'rock boreability' is used when the influence of the rock mass is taken into account (Bruland, 2000d; Dahl et al., 2012).

2.2.3 Cutter discs

Cutter technology has experienced continuous development resulting in the reliable cutters in use today (Roby et al., 2009). The technical range in tunnel diameters bored by TBMs in massive, hard and abrasive rock conditions has been increased from less than 3 metres to more than 14 metres. Major economic limitations must be expected in the face of technical challenges.

However, limitations resulting from the quality of cutter ring steel are yet to be overcome nowadays. Current cutter ring steel technology does not permit use of the full thrust capacity of current machines, but limits the long-term average cutter thrust per cutter for a 483 or 508 mm cutter diameter to 312 kN. A new generation of cutter material, allowing a higher thrust in hard rock conditions, will increase TBM penetration rates and cutter life. An increase of 15% in the thrust applied may result in as much as a 50% increase in penetration. This in turn may reduce excavation costs and thus extend the scope of application of the TBM method (Bruland, 2000a). Improvements in cutter ring capacity will require corresponding improvements in rolling bearing capacity.

The radial rating of bearing sets, according to bearing manufacturer, is around 432 kN (216 kN each). This rating assumes no additional axial force component, and results in a fatigue life of 90 million revolutions – equivalent to 3,000 hours at 500 rpm. Given a recommended maximum cutter thrust of 312 kN per cutter, the ratio for the bearing sets is around 70% (Smading, 2016). However, cutter bearings are not steadily or smoothly loaded during boring. They are exposed to peak loads from about 3.5 times higher than a nominal cutter load in fractured rock (Entacher et al, 2013). Thus, it appears that bearings normally do not fail due to pure fatigue. Factors such as overload, lubrication film breakdown or contamination are the

most likely explanations for cutters exhibiting dramatically shorter lifetimes than 90 million revolutions.

Improvements of cutter ring quality will allow the use of reduced tip width. A reduced tip width increases the contact stress and, therefore, influences the radial cracks propagation and chip formation. At the present, the cutter profile with constant cross section (CCS) discs are generally used (Rostami, 2008).

Spacing between cutters is linked with crack propagation under a cutter discs and subsequent chip formation between two adjacent cutters. Rostami (2008) showed the variation of normal force as a function of penetration for various spacing values. Cho et al (2010) simulated three-dimensional rock cutting behaviour by disc cutters using numerical modelling. According to Bruland (2000f), the thrust level and the cutter spacing must be adapted to the rock mass properties.

The thrust is one of the main machine parameters affecting rock breaking and therefore penetration rate. Average thrust is commonly used and it is measured over a period of time, and is thus not indicative of peak loads measured over short time intervals during the rock-breaking process. The NTNU model uses 'gross average cutter thrust per cutter', which is obtained by dividing total gross thrust by the number of cutters in the cutterhead.

Other methodologies use a 'friction force' reducing the total thrust applied (Gong et al., 2007; Frenzel et al., 2012; Wilfing et al., 2015b). The 'friction force' reflects the contact area between the shield and the rock mass and it might be measured pushing or retracting the cutterhead when rotating without contact with the tunnel face.

During boring, several aspects might reduce the friction. The cutterhead is pushed against the tunnel face reducing the friction on the shield and/or the vibration on the cutterhead during continuous boring. According to Bruland (2000f), the losses due to friction of the cutterhead, loss of hydraulic pressure, etc. during boring is approximately 10% or less of the gross thrust. The friction effect during boring is not well understood yet and it is still no agreement within the TBM tunnelling industry.

2.2.4 Real-time monitoring

Real-time monitoring of individual cutter thrust, cutter rolling, cutter wear and temperature would greatly improve TBM efficiency and provide a better understanding of the rock breaking and cutter wear processes. A measure of instantaneous cutter wear status for all cutters would be a relevant improvement, reducing the need for inspections and thus improving TBM efficiency. Slurry and EPB machines, which will be used more frequently in future hard rock boring projects, such cutter wear instrumentation would be even more beneficial due to cutter change complexity.

The use of remote instrumentation and monitoring of specific cutter positions are currently under development, but are as yet not fully applicable. Shanahan (2010) and Entacher et al.

(2013) have documented some attempts, and such processes are planned for use in ongoing projects (Bruland, 2015; Log, 2016).

2.3 Rock mass boreability

2.3.1 General remarks

'Rock mass boreability' is a comprehensive parameter of rocks under excavation, and expresses the result of the interaction between a given rock mass and a TBM. Boreability can be defined as the resistance (in terms of ease or difficulty) encountered by a TBM as it penetrates a rock mass composed of intact rock containing planes of weakness.

Penetration rate and cutter wear are influenced by intact rock and the rock mass properties. Intact rock properties are typically defined in terms of strength, abrasivity, porosity, schistosity and rock petrography.

The planes of weakness or discontinuities in a given rock mass, and the orientation of the fracture system(s) may be the main parameters influencing penetration and cutter wear. Penetration rate may also be influenced by in situ rock stress, groundwater and other factors.

Many studies have examined the influence of geological parameters on the performance of tunnel boring machines. These include Wanner and Aeberli (1979), Howarth (1981), Lindqvist and Lai (1983), Sanio (1985), Bruland (2000), Barton (2000, 2012,2013a), Ribacchi and Lembo-Fazio (2005), Gong et al. (2005, 2006), Zhao et al. (2007),Yagiz (2009), Yagiz et al. (2011), Hassanpour et al. (2011), Bejari and Khademi (2013), Farrokh et al. (2012) and Macias et al. (2014).

Wanner and Aeberli (1979) considered the property of joint frequency which is determined by the total joint area per unit volume of excavated rock. Field observation indicated that only joints produced by shear stresses exert a significant influence on specific TBM penetration. Howarth (1981) performed experimental work and concluded that moderately fractured rock can improve TBM performance. Lindqvist and Lai (1983) demonstrated the influence of intact rock properties in laboratory experiments. Sanyo et al. (1985) considered and studied the importance of rock mass anisotropy as well as discontinuities.

Zhao et al. (2007) developed an ensemble neural network as a means of establishing a relationship between the specific rock mass boreability index (SRMBI) and four influential rock mass properties: compressive strength, brittleness, joint spacing and joint orientation. Ribachi and Lembo-Fazio (2005) analysed excavation data from a TBM project in a gneiss formation and documented the influence of rock quality on TBM performance. They indicated that, for a given type of rock, fracture spacing has a predominant influence. Gong et al. (2005, 2006) ran numerical models of joint spacing and orientation and achieved good agreement with data from field investigations at NTNU methodology.

Zhao et al. (2007) developed an ensemble neural network as a means of establishing a relationship between the specific rock mass boreability index (SRMBI) and four influential rock mass properties: compressive strength, brittleness, joint spacing and joint orientation.

The influence of both intact rock properties and rock mass parameters have major significance for the TBM prediction models developed by Gehring (1995), Bruland (2000), Barton (2000), Bieniawski et al. (2006) and Delisio et al. (2013). Hassanpour et al. (2010, 2011) and Farrokh et al. (2012) analysed the influence of geology on performance predictions produced by TBM prediction models for several TBM projects considering the rock geological influence on the performance predictions.

Rock mass fracturing is found to be the geological factor that exerts the greatest influence on net penetration rate, and which consequently also has a major impact on tunnelling costs in hard rock (Bruland, 2000). A high rock mass fracturing parameter means greater rock mass boreability during hard rock TBM excavation.

Several researchers have reported the influence of in situ rock stresses on TBM performance. According to observations in rocks exhibiting high stress anisotropy and the major principal stress aligned parallel to the tunnel face, Bruland (2000d) indicated that rock stress had a positive influence on net penetration rate. According to Barton (2000), higher horizontal stresses will result in lower boreability due to the increased strength of the rock mass highly confined. Yin et al. (2014) employed sets of penetration tests to demonstrate the influence of in situ rock mass conditions on the rock fragmentation process during TBM boring indicating a reduced of the rock boreability with high rock mass stresses. For rock masses with layers closely parallel to the principle stress, the breaking process is facilitated.

Wilfing (2016) investigated two parameters, the toughness of rocks and the discontinuity pattern in rock mass in order to illustrate the improvement of the Gehring (1995) penetration prediction model.

Vassenden (2016) has two main scopes of her PhD is to find an economical and time efficient method to detect and map the effects of the disc cutters and investigate how the rock mass is effected by the disc cutters of a full size TBM in hard rock. The second scope is to investigate if the rotation speed of the cutterhead affects the rock breaking, and to document any effects.

Seo (2016) analyses numerical modelling of rock breaking in hard rock TBM tunnelling during his PhD research. Mid-scale testing by using Linear Cutting Machine (LCM) tests is used to study rock breaking process.

Geng et al. (2016a) simulated the rock breaking process of TBM normal cutters using ABAQUS based VUMAT strategy, and verified the models using a full-scale rotary cutting machine (RCM). Geng et al (2016b) carried out simulations of the mechanical performance of TBM cutterhead in mixed rock ground conditions by using a ray intersection algorithm and verified the models using a full-scale experimental cutterhead system.

2.3.2 Intact rock boreability

The term 'rock' is not always precisely defined. Table 2 shows the classification of rock types in terms of rock strength presented by the International Society of Rock Mechanics (ISRM). The specific parameter used is Uniaxial Compressive Strength, UCS (ISRM, 1978).

Table 2. Classification of rock based on uniaxial compressive strength (ISRM, 1978)

Definition	UCS (MPa)
Soil	< 0.25
Extremely low strength	0.25 - 1
Very low strength	1 - 5
Low strength	5 - 25
Medium strength	25 - 50
High strength	50 - 100
Very high strength	100 - 250
Extremely high strength	> 250

The research presented in this thesis focuses on 'hard rock' conditions which, according to the classification above, fall within the categories high, very high and extremely high strength (UCS > 50 MPa).

There are several methodologies available to assess the influence of intact rock properties in hard rock tunnel boring. Following, the main intact rock properties and commonly used test methodology are listed:

- Strength testing: Uniaxial Compressive Strength (UCS), Brazilian Tensile Strength (BTS), Point Load Test (PLT).
- Surface hardness: Sievers' J miniature drill test (SJ), Vickers hardness (VH).
- Brittleness: brittleness tests (S_{20}), several definitions including: strain, UCS and tensile strengths, stress-strain relations.
- Abrasivity: Cerchar test (CAI), LCPC test, Abrasion Value Steel test (AVS), abrasive minerals content, Vickers hardness number of rock (VHNR).
- Rock petrography (rock texture, mineral composition).

According to Gehring (1995), rock 'toughness', as well as UCS, also influences TBM penetration performance. The term rock 'toughness' describes the deformation behaviour at which the rock responds to the applied load by high plastic deformation and distinct post-failure range (Wilfing, 2016). Wilfing (2015b, 2016) analysed rock toughness using a wide range of laboratory testing including UCS, BTS, LCPC-breakability coefficient (Thuro et al,

2007) and PLT. The aim is to develop a common and appropriate method for rock toughness characterisation that could be applied in TBM performance prediction.

Howarth and Rowlands (1987) developed a quantitative measure of rock texture described as grain: shape, orientation, degree of grain interlocking and relative proportions of grains and matrix. The texture coefficient shows highly statistically significant correlations with rock strength and drillability data.

Other approaches have been developed in order to evaluate rock cutting and breaking during tunnel boring. Many researchers (Rostami and Ozdemir, 1993; Chang et al., 2006; Gertsch et al., 2007; Cho et al., 2010, 2013) have actively used the Linear Cutting Machine (LCM), initially developed by the Colorado School of Mines (CSM). The LCM employed full-scale cutter discs (17 or 19 inch cutter diameter) and large rock samples.

Innaurato et al., (2007) performed a specific indentation laboratory test simulating the action of cutter discs on rock breaking. The indentation test uses a TBM cutter ring over a rock sample with variable lateral confinement. The results indicated different breaking efficiency when the lateral pressure varies.

Entacher et al. (2014) developed and evaluated a scaled rock-cutting test, involving a steel cutter with a carbonitrided surface, representing a 1:8 scale model of a typical 432 mm (17-inch) constant cross-section mounted as an attachment in a hydraulic press. Load is transferred to the test rig to produce a pure rolling force, which is measured on the frame of the press. The rock specimen is a 10-centimetre diameter half core with a height of approximately 9 cm. Results from full mid-scale linear cutting tests (using an LCM) in three different lithologies were used as reference values for the scaled rock test carried out by the authors.

The punch test, developed by Handewith (1970), has been used by many researchers to evaluate parameters such as rock drillability, cutting force estimates and TBM penetration rate (Cook, 2009; Dollinger et al., 1998; Yagiz, 2002, 2009). Jeong et al. (2015) performed a series of punch tests to investigate the dependency of results on the size of the rock specimen. Their results led to suggestions for an ideal specimen size and a testing procedure, and new punch test indices were proposed. A prediction model, limited to 17-inch cutters, was introduced based on the proposed indices. Good agreement was observed when the predicted forces were compared with the results of the LCM tests.

Figure 5 shows a summary of four approaches used to evaluate rock breaking during tunnel boring: a) an LCM, b) and indentation test using a TBM tool, c) a scaled rock-cutting test and d) a punch test.

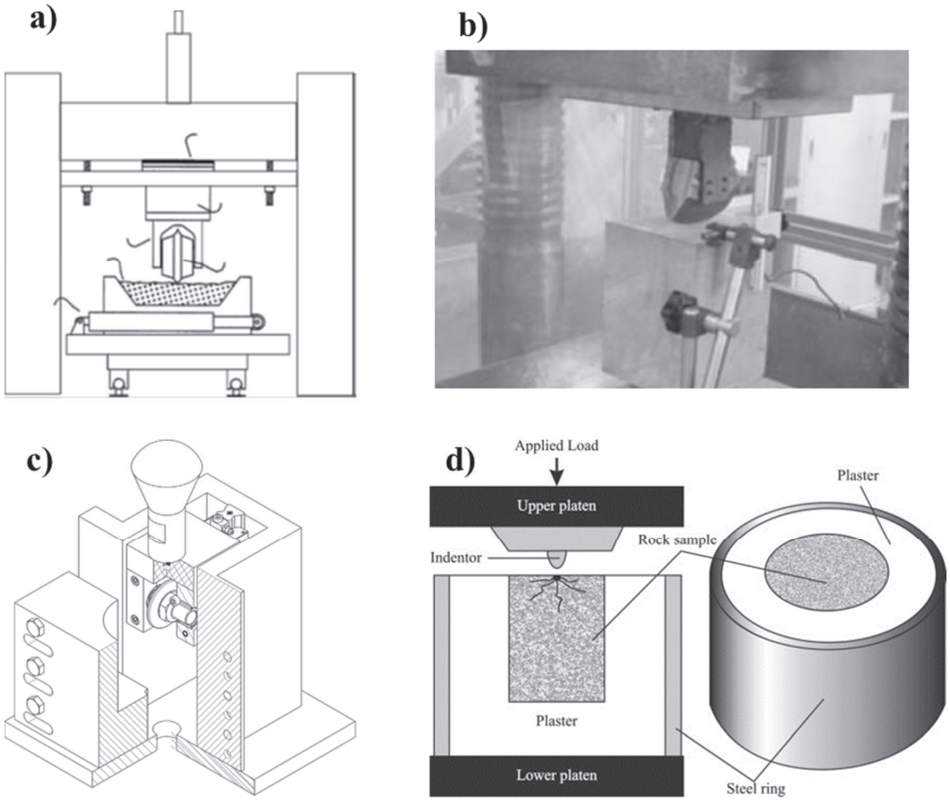

Figure 5. Four approaches used to analyse rock breaking in tunnel boring: a) an LCM (Gertsch et al., 2007), b) an indentation test using a TBM tool (Innaurato et al., 2007), c) a scaled rock cutting test (Entacher et al., 2014) and d) a punch test (Yagiz, 2009).

NTNU/SINTEF drillability testing

The Drilling Rate Index (DRI) and Cutter Life Index (CLI) have been selected as the drillability parameter for intact rock. DRI is a laboratory index for the indirect measurement of intact rock boreability (drillability). The higher the DRI, the higher the drillability. It is an indirect measure of the breaking work required and an effective gauge of the rock-breaking process under a cutter disc and is defined as the brittleness value adjusted for surface hardness. CLI expresses life in boring hours for cutter disc rings of steel for tunnel boring machines.

The brittleness test method used by NTNU/SINTEF combines brittleness (S_{20}) and surface hardness measured using the Sievers' J test. S_{20} indicates the amount of energy required to initiate cracks prior to crushing the rock (Figure 6a). The Sievers' J-Value (SJ) represents rock surface hardness in terms of the rock's resistance to indentation (Figure 6b).

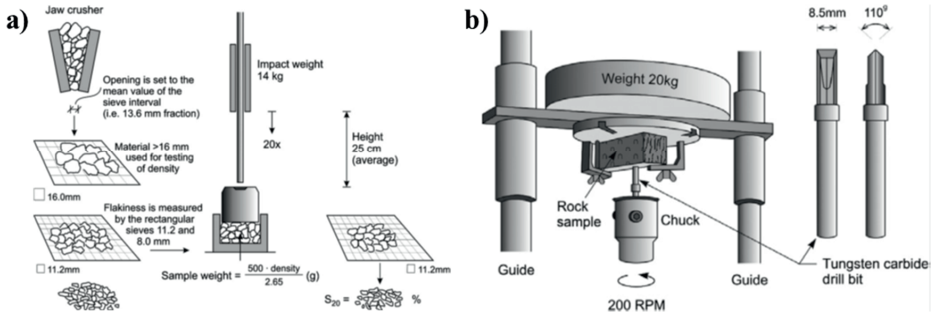

Figure 6. Summary diagrams showing a) Brittleness Value (S_{20}) and b) Sievers' J-Value (SJ) (Dahl et al., 2012).

Variation in DRI values for some common rock types are shown in Figure 7.

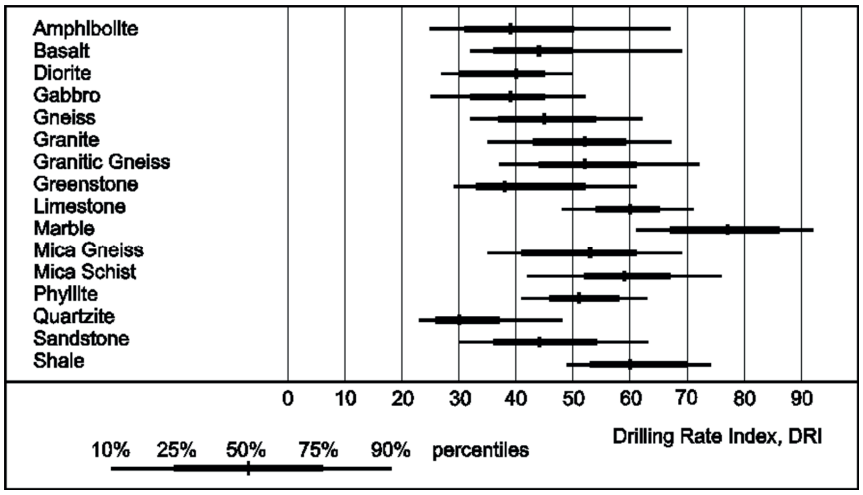

Figure 7. Recorded Drilling Rate Index (DRI) ranges for some rock types (Bruland, 2000bd)

The Abrasion Value Cutter Steel (AVS) index was developed and presented by NTNU at the beginning of the 1980s and is often referred to as the "Norwegian abrasion test method". The AVS index represents a measure of rock abrasion or the ability of a rock to induce wear on cutter ring steel. Following this chapter is detailed explained.

The Cutter Life Index (CLI) is assessed based on the SJ and the AVS values. The higher the CLI, the higher the cutter life in boring hours.

Variation in CLI values for some common rock types are shown in Figure 8.

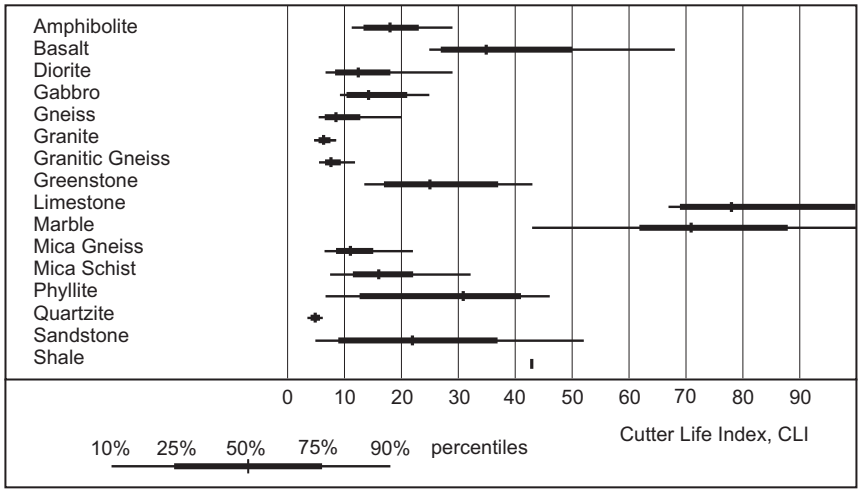

Figure 8. Recorded Cutter Life Index (CLI) ranges for some rock types (Bruland, 2000bd)

A classification related to the distribution of the results in the database, updated within this thesis, is proposed (Table 3).

Table 3. Category intervals for drillability indices

Category	DRI	CLI
Extremely low	< 26	< 4.8
Very low	26 - 32	4.8 – 5.8
Low	33 - 41	5.9 – 8.2
Medium	42 - 52	8.3 – 15.6
High	53 - 62	15.7 – 35
Very high	63 - 73	36 – 72
Extremely high	> 73	> 72

The NTNU/SINTEF drillability test method has gained international recognition. Nonetheless, there are a few laboratory facilities in the world that are able to reproduce these tests as opposed to other more commonly used test methodologies such as UCS and BTS. There are however, besides located in Norway, some other laboratories worldwide, in Australia, South Korea, Spain, South Africa, Turkey and USA, which possesses the necessary equipment. The trademark acronyms and terms relating to the indices DRI™ (Drilling Rate Index™) and CLI™ (Cutter Life Index™) are however unique to test results originating from the NTNU/SINTEF laboratory in Trondheim (Norway).

2.3.3 Comparison of drillability assessments

Rock strength

Parameters such as UCS, PLT, BTS or DRI are frequently used to describe the intact rock properties in connection with TBM tunnelling.

As previously discussed, the DRI combines brittleness (S_{20}) and surface hardness measured using the Sievers' J test. It is logical to analyse the relation between brittleness and DRI with rock strength. Figure 9 shows the correlation between UCS and S_{20}.

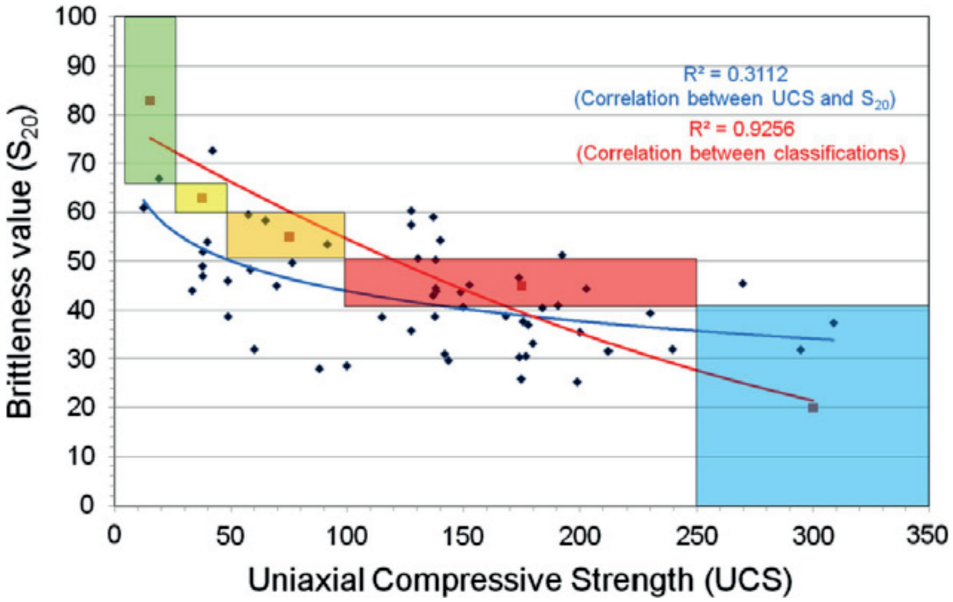

Figure 9. Correlation between UCS and S_{20}. The coloured boxes refer to UCS classification ranges given by ISRM and corresponding ranges in the suggested S_{20} classification (Dahl et al, 2012).

Figure 9 shows a relatively poor relation between S_{20} and UCS. This might be explained by the fact that S_{20} is performed by applying repeated impacts on the sample material, causing crushing of the sample material, while UCS is performed by applying load on the sample, at a relatively slow constant rate, until failure occurs

Figure 10 shows the correlation between the UCS and DRI. The same level of poor relation is shown.

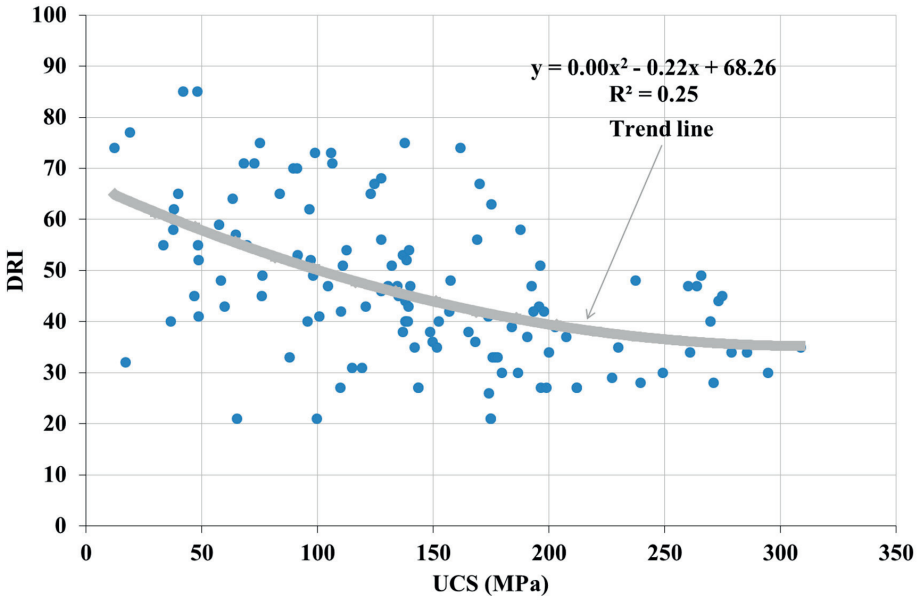

Figure 10. Correlation between the DRI and UCS (NTNU/SINTEF database, 2016).

Figure 11 shows the variation between the DRI and UCS in relation to rock type. The results indicate that UCS exhibits less variation than DRI in foliated or schistose rocks such as phyllite, mica gneiss, mica schist, shale and green schist, as well as to calcitic rocks such as limestone and marble. However, amphibolitic gneiss seems to exhibit greater variation in UCS than in the DRI.

Sedimentary rocks such as siltstone and sandstone, and igneous rocks such as granite, appear to exhibit a good correlation.

The measured compressive or tensile strengths of anisotropic rocks depend on the testing direction, whereas the DRI is not influenced by the testing direction.

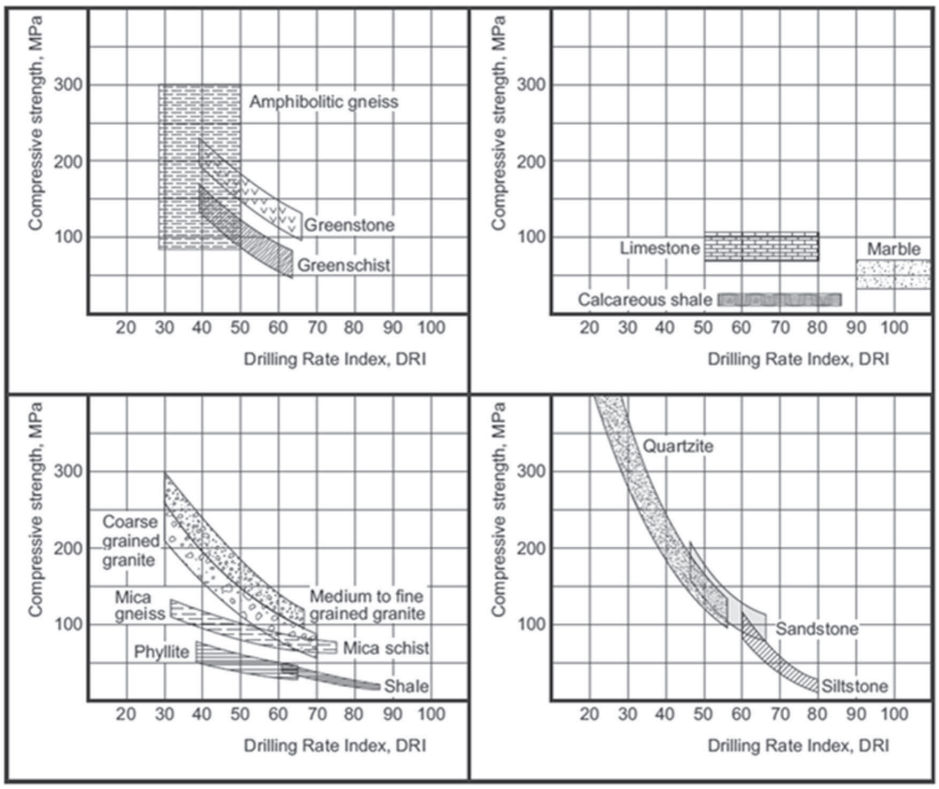

Figure 11. Correlation between the DRI and UCS (MPa), grouped according to rock type (NTNU, 1983).

Yarali and Soyer (2013) examined the relationships between the DRI and strength properties (UCS, BTS, PLS, Schmidt rebound hardness, SRH and Shore scleroscope hardness, SSH). The results indicated a clear correlation between DRI and strength indexes.

As previously stated, the NTNU methodology and hence, the NTNU prediction model for hard rock TBMs, have selected the DRI as a laboratory index for the indirect measurement of intact rock boreability. The rock under a cutter disc breaks by tensile stress in a dynamic effect which occur in a very short period (estimated to be less than 0.1 second according to Bruland, 2000f) resulting in great loading rates (MPa/s). Compared to the load rate recommended by ISRM for testing of the rock compressive strength, which is 0.5 - 1.0 MPa/s, the estimated load rate indicates that the rock strength rather should be tested by a dynamic or impact test than by compressive strength. The DRI is considered an effective gauge of the rock-breaking process under a cutter disc due to the combination of brittleness value adjusted to the rock surface The brittleness test, is believed to crush the rock mostly by induced tension in an 'instant' process due to impact loading). The brittleness value (S_{20}) expresses the amount of energy required to initiate and crush the rock. Finally, the DRI is obtained from the S_{20} adjusted for rock surface hardness (SJ).

Figure 12 is a schematic representation of the brittleness value (S_{20}) and Sievers J-value (SJ) in the breaking process under a cutter disc in hard rock.

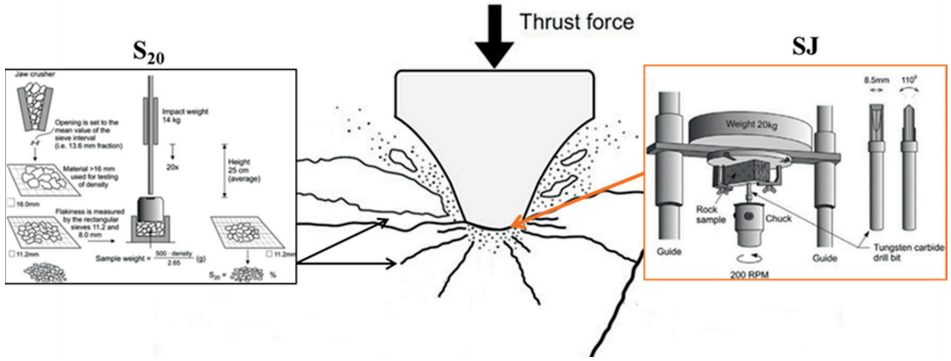

Figure 12. Schematic representation of the brittleness value (S_{20}) and Sievers J-value (SJ) in the breaking process under a cutter disc in hard rock.

Rock abrasivity

The CAI and CLI indexes are commonly used to assess rock abrasivity and cutter wear in hard rock TBM projects.

The AVS, like the CAI, is a test method used to determine the abrasiveness of rock and one of the tests forming part of the CLI. Figure 13 shows correlation between the CAI and the AVS (Dahl et al., 2012).

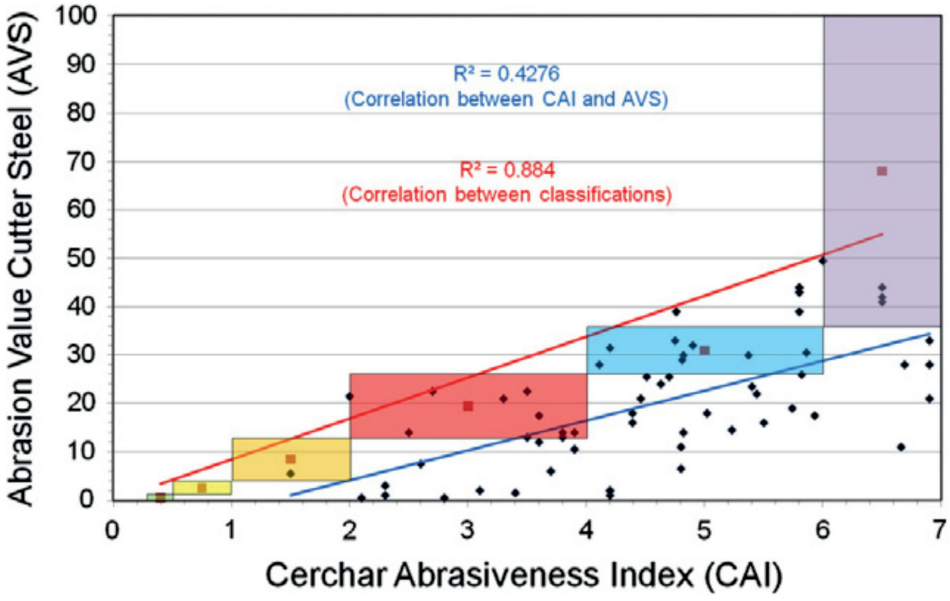

Figure 13. Correlation between the CAI and the AVS. The coloured boxes refer to CAI classification ranges given by Cerchar Institute, 1986 and corresponding ranges in the suggested AVS classification. (Dahl et al., 2012)

The correlation between the two test methods, CAI and AVS, (Figure 13) shows a relatively clear trend although with scattered values. This relation can be regarded as logical since the AVS and the CAI are affected by the same rock properties and characteristics.

Figure 14 shows the correlation between the CLI and CAI. The best fitting is used for comparison.

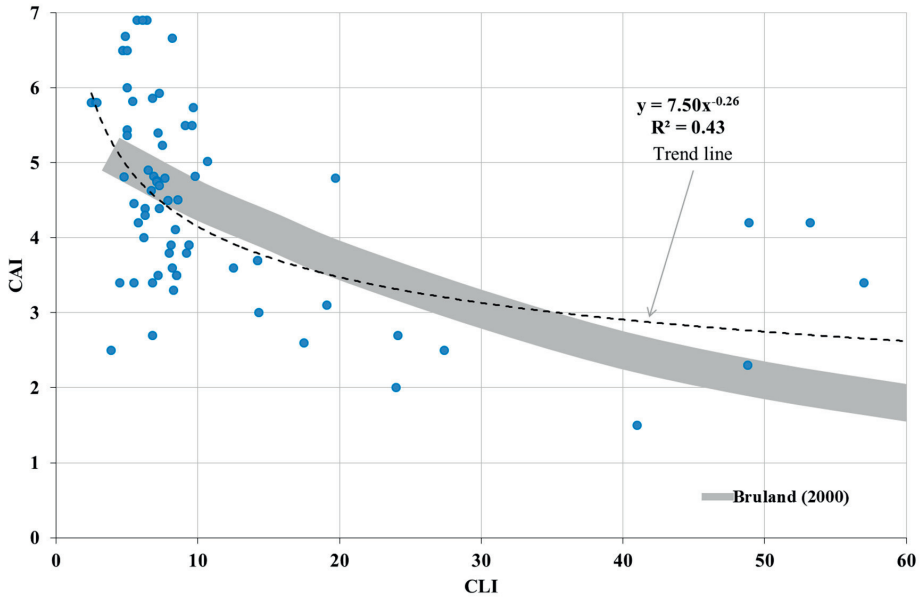

Figure 14. Correlation between the CLI and the CAI_s (NTNU/SINTEF database, 2016). Shaded area represents the correlation introduced by Bruland (2000 d)

The figure shows a good agreement with the correlation introduced by Bruland (2000d). The relation shows a relatively clear trend but an uncertainty of the given equations should be considered, due to the limited number of observations. The correlation should only be used for rough estimates.

2.3.4 Rock mass assessments

There is no single parameter that can fully represent the properties of jointed rock masses. Different parameters have different emphases, and can only provide a satisfactory description of a rock mass in an integrated form (Singh and Goel, 2011).

Several rock mass classification systems have been developed to characterise rock masses under excavation during tunnelling projects. Table 4 provides a summary of the most commonly used systems.

Table 4. Common rock mass classification systems used in connection with tunnelling projects.

Rock mass classification	Author	Year
Rock Quality Designation (RQD)	D.U. Deere	1964
Rock Mass Rating (RMR)	Z.T. Bieniawki	1973
Rock Tunnelling Quality Index (Q)	N. Barton, R. Lien and J. Lunde	1974
Degree of fracturing (k_s factor)	NTNU (NTH)	1981
Rock Mass Index (RMi)	A. Palmström	1995
Geological Strength Index (GSI)	E. Hoek and E.T. Brown	1997

The RQD (Rock Quality Designation) method was the first attempt to classify rock quality. It measures the percentage of intact rock fragments greater than 100 mm (4 inches) in length recovered from a core.

The Rock Mass Rating (RMR, Bieniawski, 1973) ranks rock masses according to a points system (from 0 to 100) using ratings of five parameters assessed according to standard criteria. The five parameters are as follows:

- Uniaxial compressive strength of intact rock material
- Rock quality designation (RQD)
- Spacing of discontinuities
- Condition of discontinuities given as
    - Length, persistence
    - Separation
    - Smoothness
    - Infilling
    - Alteration/weathering
- Groundwater conditions

These parameters provide a basic RMR value, which may then be adjusted for the method of excavation and the orientation of discontinuities relative to the excavation direction. Since initial development of the RMR classification system, it has undergone several significant modifications (Bieniawski, 1989).

N. Barton, R. Lien and J. Lunde at the Norwegian Geotechnical Institute first proposed the Q-system for rock mass classification in 1974 (Barton et al., 1974).

Their definition of rock mass quality (Q) is given by combining six rock mass parameters in the following equation (1):

$$Q = \left[\frac{RQD}{J_n}\right] \cdot \left[\frac{J_r}{J_a}\right] \cdot \left[\frac{J_w}{SRF}\right] \quad (1)$$

where

RQD = Rock Quality Designation. For RQD ≥ 10 = 115 – 3.3 Jv ≤ 100
J_n = Joint Set Number
J_r = Joint Roughness Number for a critically-oriented joint set
J_a = Joint Alteration Number for a critically-oriented joint set
J_w = Joint Water Reduction Factor
SRF = Stress Reduction Factor that takes into account in situ stresses and observed tunnelling conditions
J_v = Volumetric Joint Count

The value of Q is measured on a logarithmic scale and varies from 0.001 (for exceptionally poor rock quality) to 1,000 (for exceptionally good rock quality).

The Q-system has been updated on several occasions in recent years. The original parameters have not been changed, but some of the ratings for the SRF have been modified by Grimstad and Barton (1993).

The goals of the Q-system are to characterise the rock mass and generate a preliminary empirical design for the support system.

The RMi system was developed in order to characterise the strength of a given rock mass for construction purposes. It is based principally on reduced rock strength caused by jointing (Palmström, 1995) and is expressed as equation (2):

$$Q = \sigma_c \cdot JP \tag{2}$$

where

σ_c = uniaxial compressive strength of intact rock measured on 50 mm samples
JP = jointing parameter

JP is a reduction factor representing the size and condition of the faces of the block in question. The condition of the faces is represented by their friction properties (joint roughness and alteration) and the size of the joints (joint size).

The Geological Strength Index (GSI) was first presented in preliminary form by Hoek et al. (1992) and subsequently further developed by Marinos and Hoek (2000, 2001). The GSI can be used for both hard and weak rock masses and is based on an essentially qualitative geological description of the rock mass. The only function of this system is to provide an estimate of the properties of the rock mass in question (Marinos et al., 2005).

More recently, the RMR system (Bieniawski et al., 2006) and the Q system (Barton, 2000) have been used to predict TBM performance during hard rock tunnelling (Rock Mass Excavability, RME and Q_{TBM}) In addition, Palmström (1995) made an attempt to use the RMi factor based on the NTNU prediction model.

Discontinuities or planes of weakness in a rock mass contribute considerably to net penetration rate and cutter wear in hard rock TBM tunnelling. The rock mass fracturing factor (k_s), introduced by NTH (1981), was developed to assess the influence of the rock mass on TBM performance predictions in connection with hard rock tunnelling. More recently, a three dimensional representation of fracturing was included (NTH, 1994). The k_s factor considers the simultaneous influence of the degree of fracturing and the orientation of the planes of weakness (Bruland, 2000 bde).

2.3.5 Planes of weakness/discontinuities

The collective term "discontinuity" (often interchangeable with the term "fracture") is used in rock mechanics to describe all planes of weakness along which the coherence of intact rock is interrupted (Wittke, 2014).

The literature contains many classifications of discontinuities based on magnitude of shear and, length Figure 15 shows the classification used by the Norwegian Rock Mechanics Group (NBG).

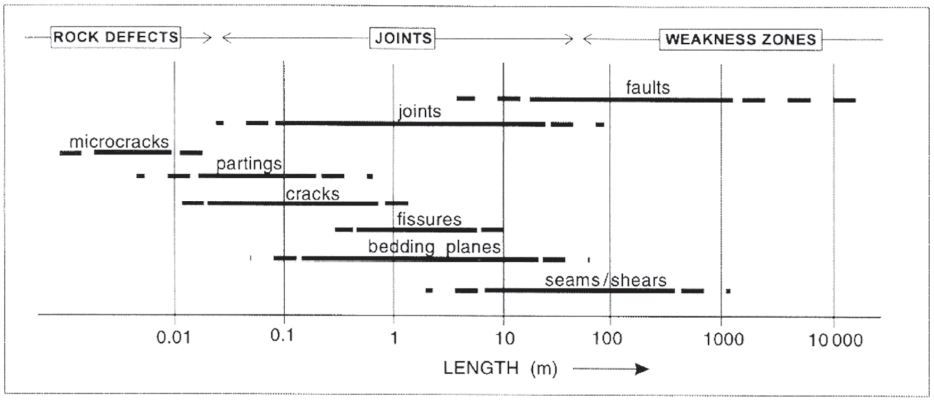

Figure 15. The main types of rock mass discontinuities classified according to length. The length range for joints is modified after Palmström (1995).

The term 'joint' has been defined as a plane of discontinuity of natural origin along which no visible displacement is observed (NGB, 2000).

A 'crack' is defined as a small, partial or incomplete discontinuity (ISRM, 1975; NBG, 2000).

Bedding planes are normally the most significant discontinuities observed in sedimentary rocks. Foliation planes are the most common discontinuities developed in metamorphic rocks.

The rock mass classification systems use various terms to express planes of weakness. The Q- and RMi systems use the term 'joint', while the RMR system uses 'discontinuity'. The GSI system employs both terms interchangeably.

The term ‘fracture’ is a general term used in geology for all kinds of discontinuities in a rock mass caused by mechanical stresses. The NTNU methodology for rock mass assessment for TBM performance prediction defines two types of fractures: joints and fissures. “Joints” as continuous fractures that can be followed all around the tunnel profile and ”fissures” as non-continuous joints or fractures that can only partly be followed around the tunnel profile such as filled joints exhibiting low strength, foliation and bedding plane fissures.

In addition, the NTNU methodology includes highly distinctive discontinuities as Marked Single Joints (MSJ): These may be entirely open, may conduct water or may be filled with clay. Minor faults filled with gouge may be classified as MSJ.

Since the NTNU classification system was developed, experience from the back-mapping of bored tunnels for TBM performance prediction in hard rock tunnelling has shown that the majority of rock mass fracturing can be classified by the terms ‘Fissures’ or ‘Marked Single Joints’. ‘Systematic jointing’ is observed only in short tunnel sections (Bruland, 2000b).

2.4 Rock abrasivity and cutter wear

2.4.1 State-of-the-art rock abrasivity testing in hard rock tunnelling

During recent decades, many test methods have been employed to measure rock abrasivity. Table 5 provides a list of the most commonly used methods in connection with tunnel boring.

Table 5. The most common laboratory testing methods for measuring rock abrasivity in connection with hard rock tunnel boring.

Test method	Index	Principle	Rock sample	Testing tool
CERCHAR test (1986)	CERCHAR Abrasivity Index (CAI)	Indenter (hard steel) moves over a rock surface	Intact rock	Steel stylus
LCPC test (1990)	LCPC abrasivity Index (ABR)	Impeller (medium hard steel) rotating in a vessel containing crushed rock	Crushed rock (4-6.3 mm)	Metal impeller
NTNU/SINTEF abrasivity (1983)	Abrasion Value cutter Steel (AVS)	Cutter ring steel piece sliding over crushed rock	Crushed rock (<1mm)	Cutter ring steel piece

Rock abrasiveness is normally influenced by the content of quartz and other hard and abrasive minerals that the rock contains. The measurement of mineralogical parameters such as quartz content, ‘Equivalent Quartz Content’ or the ‘Vickers Hardness Number Rock (VHNR)’ involve methods that adopt approaches that are different from model testing, and are thus

commonly used for the characterisation of rock abrasivity and applied to several cutter life estimation models.

The 'Equivalent Quartz Content' parameter encompasses the influence of the entire mineral content of the rock on abrasiveness relative to quartz, while the 'Vickers Hardness Number' is used as a measure of the abrasiveness of each individual component mineral. Individual Vickers hardness values, combined with the percentage of each mineral found in a rock, can be used to calculate the so-called Vickers Hardness Number Rock, or VHNR (Salminen and Viitala, 1985).

The CERCHAR abrasivity test is used to determine the CERCHAR Abrasivity Index (CAI) and was originally developed and presented by the Centre d'Études et Recherches des Charbonnages de France in the 1970s (Valantin, 1974).

The test measures the wear on the tip of a steel stylus having a Rockwell Hardness of HRC 55 (ISRM, 2014) or HRC 40 (ASTM, 2010). Firstly, a rock specimen is held firmly in the test apparatus (Figure 16). A normal force of 70 N is applied while the stylus is moved a total distance of 10.0 mm across the specimen surface. The movement of the stylus should be completed within 1 ± 0.5 s using 'Type 1' apparatus, and within 10 ± 2 s using 'Type 2' apparatus.

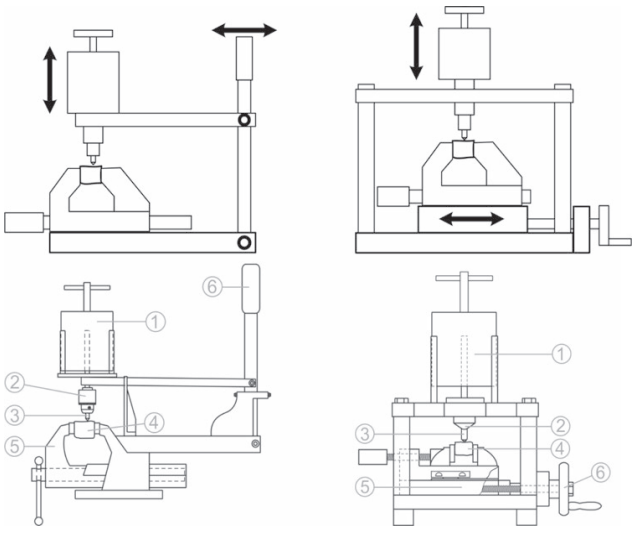

Figure 16. Two main types of CERCHAR test apparatus commonly in use. Type 1 (left) represents the original design. Type 2 (right) is the modified CERCHAR apparatus as reported by West (1989). 1 = mass, 2 = pin chuck/guide, 3 = stylus, 4 = specimen, 5 = vice and 6 = lever/hand crank (ISRM, 2014).

The CAI is a dimensionless unit and is calculated by multiplying the wear on the specimen surface in units of 0.01 mm by 10. Table 6 shows the CAI abrasivity classification system suggested by the ISRM (2014).

Table 6. CAI abrasivity classification (ASTM, 2010; ISRM, 2014).

Classification of abrasiveness	CAI	
	ASTM 2010	ISRM, 2014
Extremely low	ND	0.1–0.4
Very low	0.3-0.5	0.5–0.9
Low	0.5-1.0	1.0–1.9
Medium	1.0-2.0	2.0–2.9
High	2.0-4.0	3.0–3.9
Extreme/Very high	4.0-6.0	4.0–4.9
Quarzitic/Extremely high	6.0-7.0	≥5

The LCPC test is used to determine an index called the 'LCPC Abrasivity Coefficient' (LAC) for classifying the abrasivity of the rock. The testing principle was originally developed and presented by the Laboratorie Central des Ponts et Chaussées in the 1980s (Normalisation Française P18-579, 1990).

An outline of the test apparatus is given in Figure 17. The impeller is a rectangular metal plate of dimensions 50 × 25 × 5 mm made of standardised steel with a Rockwell hardness of B 60–75. It rotates for 5 minutes at a speed of 4,500 rpm inside a cylindrical container filled with the rock sample material, which consists of 500 ± 2 grams of a crushed, sieved (fraction 4–6.3 mm) and air-dried rock specimen. The impeller is weighed before and after testing and its weight loss constitutes a measure of rock abrasivity.

The LAC is expressed as the weight loss of the impeller divided by the sample mass (500 g) as determined by the equation (3):

$$LAC = (m_0 - m)/ M \quad (3)$$

where

m_0 = weight in grams of the steel impeller prior to the test
m = its weight following the test
M = weight of the sample material (0.0005 t)

The LAC value is the same as the 'ABR' defined by Normalisation Française P18-579 (1990).

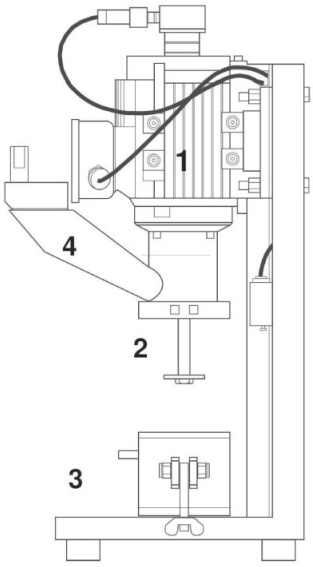

Figure 17. The LCPC abrasivity testing device (Thuro et al., 2007). 1 = motor, 2 = metal impeller, 3 = sample container (diameter = 93 mm, height = 100 mm) and 4 = funnel tube.

The LAC varies from between 0 and 2,000 g/t for natural rocks and soil samples, and a good linear relationship between LAC and CAI was reported by Thuro and Käsling (2009). A classification for the LAC is shown in Table 7.

Table 7. Classification of LAC (Thuro et al., 2007).

LAC (g/t)	Classification
0–50	Not abrasive
50–100	Not very abrasive
100–250	Slightly abrasive
250–500	Medium abrasive
500–1,250	Very abrasive
1,250–2,000	Extremely abrasive

The Abrasion Value Cutter Steel (AVS) index was developed and presented by NTNU at the beginning of the 1980s and is often referred to as the "Norwegian abrasion test method". The AVS index represents a measure of rock abrasion or the ability of a rock to induce wear on cutter ring steel. It is a time-dependent parameter determined by measuring the abrasion of cutter steel caused by crushed and sieved (< 1.0 mm) rock powder. Figure 18 is an illustration of the method (Dahl et al., 2012).

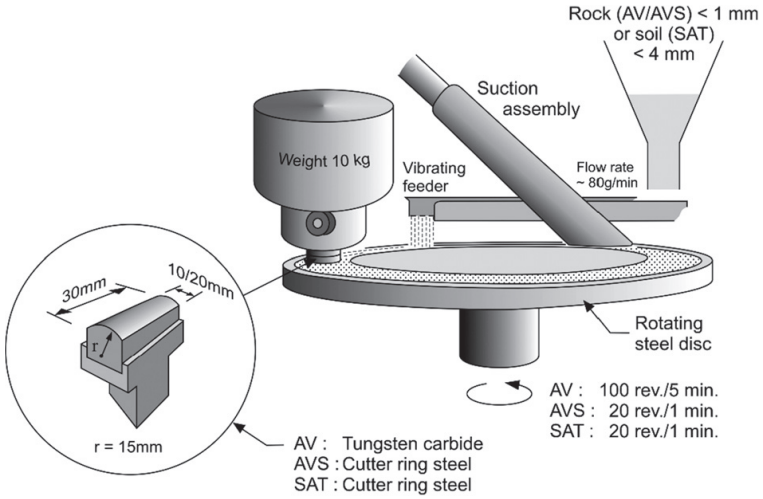

Figure 18. Outline of the Abrasion Value Cutter Steel (AVS) test (Dahl et al., 2012).

The AVS index is defined as the measured weight loss of the test piece in milligrams after 1 minute (20 revolutions) of testing. According to Dahl et al. (2012), AVS values currently in the NTNU/SINTEF database following 2,621 recorded tests range from 0.0 (not measurable, recorded for limestone) to 68.5 (quartzite). An AVS classification is presented in Table 8.

Table 8. Classification of rock abrasion on cutter steel (Dahl et al., 2012).

AVS (mg)	Abrasion on cutter steel
≥44.0	Extremely high
36.0–44.0	Very high
26.0–35.9	High
13.0–25.9	Medium
4.0–12.9	Low
1.1–3.9	Very low
≤1.0	Extremely low

2.4.2 Cutter wear in hard rock tunnel boring

Disc cutter wear has been analysed by several researchers. Bruland (2000e) describes a variety of wear behaviours depending on whether the cutter wear process is defined as ‘abrasive’ or ‘destructive’. Abrasive wear is the most common, and is proportional to cutter rolling distance. The relationship between cutter wear and rolling distance has since been verified. Frenzel et al. (2008) define two main groups of factors that influence disc cutter wear – geological and operational.

Hassanpour et al. (2014) analysed the relationship between geological parameters and cutter consumption in a recently completed hard rock TBM tunnel project that excavated pyroclastic and mafic igneous rocks. The results indicated that the best correlations with cutter life were exhibited with the intact rock parameters VHNR and UCS.

In recent years, abrasive wear and its relationships with rock and cutter steel properties and other tribological system parameters have been analysed by several researchers (Petrica et al. 2013; Ratia et al. 2014, Espallargas et al. 2014 and Ellecosta et al., 2015). Petrica et al. (2013) studied the relationship between wear behaviour and physical and mechanical rock properties. Ratia et al. (2014) analysed the effect of abrasive properties on steels and hard metals, concluding that it is essential during wear assessments to consider both contact conditions and the entire wear environment. Espallargas et al. (2014) employed several laboratory tests to evaluate the influence of corrosion on abrasive wear on TBM cutter steel as it interacts with excavation fluids. Ellecosta et al. (2015) performed the Vickers hardness test using loads of up to HV 30. Several rock types and relevant disc cutters were tested in order to evaluate the method's relevance for the characterisation of rock abrasivity and wear.

2.5 Performance prediction and cutter life models in hard rock tunnel boring

2.5.1 General remarks

Performance predictions and costs estimates are often decisive in the selection of excavation methods, and have a major influence on the planning and risk management of TBM excavation projects. Reliable prediction facilitates the control of risk and enables delays and budget overruns to be avoided.

The main factor used for predictions of parameters such as advance rate, cutter consumption and the costs of hard rock TBM tunnelling projects is the net penetration rate (m/h). Penetration rate is determined from both rock mass properties and machine parameters.

The final goal of performance prediction for hard rock TBMs is the estimation of time and cost. Advance rate determines the total boring advance achieved over a period (e.g. days, weeks, months…). Advance rate is given from the net penetration rate (m/h) and considering the machine utilization. The machine utilization is net boring time of the total available time expressed in percentage. Much of the available time is used for other activities than boring (e.g. re-gripping, cutter change and inspection, repair and service of the TBM and back-up, rock support, transport system installation and delays, tunnel service installation and delays, surveying and others).

Estimations should in addition consider assembly and disassembly of the TBM and the back-up, permanent rock support and lining, excavation of niches or branching, boring through and stabilizing zones of poor rock quality, probe drilling and pre-injection works, major machine breakdowns, dismantling of installations, additional time for unexpected rock mass conditions.

Excavation costs predictions for hard rock TBM projects incorporate a geological risk, which becomes of major importance, from a cost point of view, when degrees of fracturing are low.

Low values of degree of fracturing (e.g. St 0, 0-I and St I-) have a dramatic influence on excavation cost estimates. However, if the rock mass is highly fractured, then variations in degree of fracturing do not significantly influence excavation costs.

Figure 19 illustrates relative excavation costs as determined by the degree of fracturing for a 7 m diameter TBM with standard machine specifications and rock properties (medium drillability and abrasivity) by using the NTNU model (Bruland, 2000b). The reference excavation cost value applied is for fracture class St I.

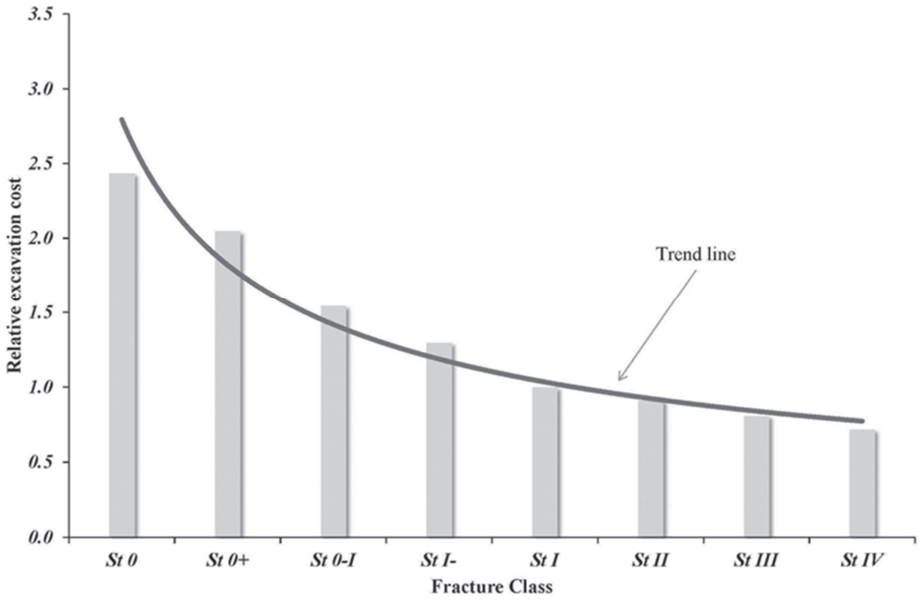

Figure 19. The relationship between relative excavation costs and degree of rock fracturing.

At lower degrees of fracturing, results indicate increments in predicted excavation costs of 20 to 70 per cent between individual classes, amounting to an increase in approx. 150 per cent relative to the reference standard, class St I. However, variation within highly fractured rock masses results in a reduction of the predicted excavation cost of 10 to 30 per cent between individual classes (amounting to a reduction of approx. 40 per cent relative to the reference). Important to bear in mind that additional time and cost associated with ground stability in highly fractured and faulted zones is not included.

It is also important to bear in mind that the fracture classes St 0, St I and St IV shown in Figure 13 represent fracture factors (k_s) of 0.36, approx. 1.0 and over 4.0 respectively. This emphasises the degree of risk involved when moving from class St 0 to St I.

Special care should thus be taken when predicting TBM performance and excavation costs in rock masses exhibiting low levels of fracturing.

The length of the tunnel has great influence on the performances due to problems with the tunnelling system (transport system, supply delays, ventilation and/or water). In addition, longer tunnels have greater likerhood to have end rock mass qualities and, normally, a more deficient geology investigation.

It has been emphasized by Barton (1999, 2000, 2012, 2013) that the utilization is time-dependent with, in reality, a deceleration gradient. The machine utilization, and thus advance rate, is not a constant in tunnel length and therefore time.

Barton (2000) shows the importance to consider tunnel length and therefore time. Trends more than 1000 km of TBM cases shows a successive decline advance rate with the time (Figure 20).

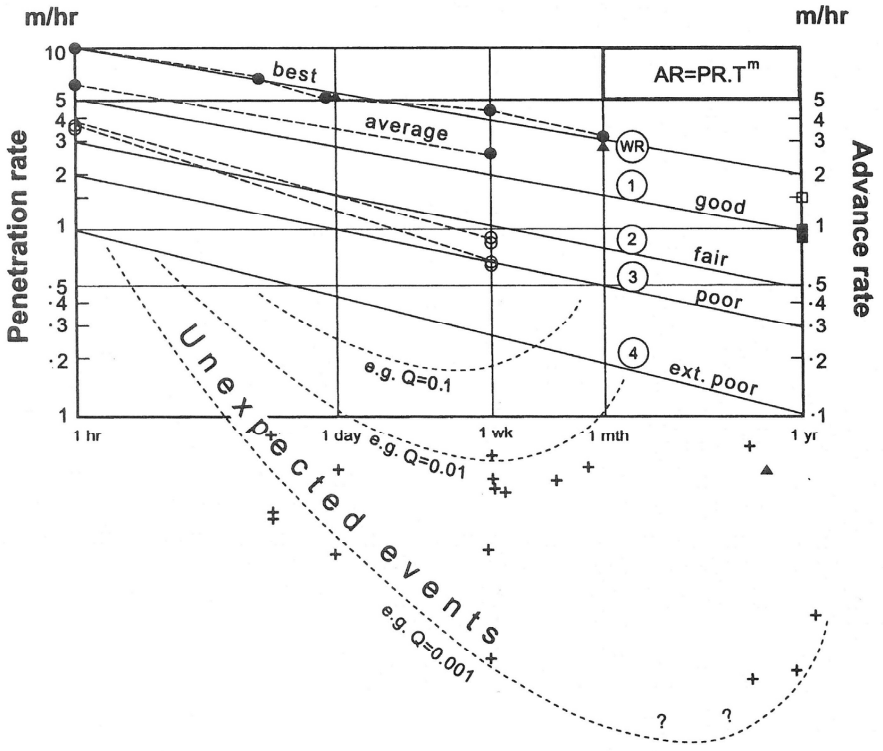

Figure 20. Result of analyses of large number of TBM tunnels where the best performances (WR, World Record) are represented by the uppermost lines showing best shift, day, week and month. (Barton, 2000)

In the last decades, only the Q_{TBM} model (Barton, 2000, 2013) has considered the decline of the advance rate due to the tunnel length, and therefore time dependence. The NTNU prediction model has introduced in the revised edition, included within this thesis (see section

4.1.7 and appendix), extra time consumption in the tunnelling activities due to the tunnel length, for the 'learning curve' and for long headings.

The RME model (Bieniawski et al., 2006) considers an 'adaptation factor' which reduces the advance rate during the 'learning curve' effect. Surprisingly, the 'adaptation factor' becomes positive with increasing tunnel length not including other reasons of deceleration which is not what has been reported by other researches (Barton, 2000; Bruland, 2000b) and within this thesis.

2.5.2 Performance prediction models in hard rock tunnel boring

Several prediction models for estimates of performance and cutter wear in hard rock tunnel boring have been developed in recent decades. Models used to estimate penetration rates include those of Graham (1976), Farmer and Glossop (1980), Büchi (1984), CSM model (Rostami and Ozdemir, 1993; Rostami, 1997), the Gehring model (1995), the Luleå University of Technology method (Nelson et al., 1994), the NTNU model (Bruland, 2000), the Q_{TBM} (Barton, 2000), RME (Bieniawski et al., 2006), Gong and Zhao (2009), Hassanpour et al. (2011) and Farrokh et al. (2012).

Figure 21 shows a timeline of common developed performance prediction models the last 40 years. The revision of the NTNU model, outcome of this thesis, has been already included.

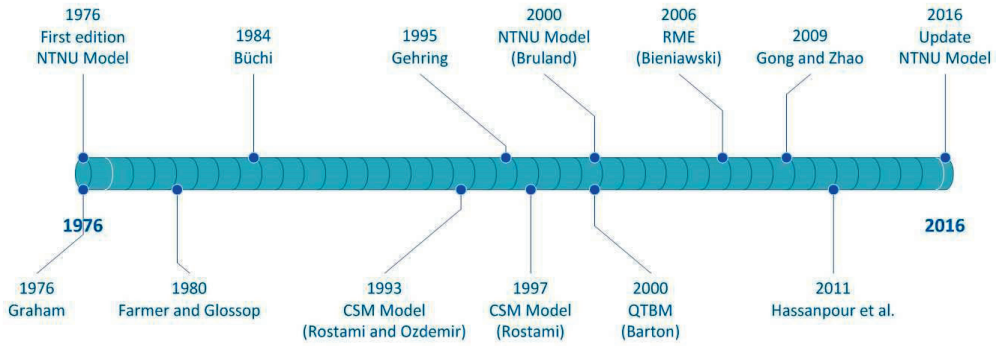

Figure 21. Timeline of the common prediction models developed during the last 40 years.

There are several current research projects focusing either on developing new prediction models for hard rock TBM excavation, or improving existing ones. One example is the ABROCK project which involves an analysis of penetration and cutter wear. This project is a collaboration between six university institutes – the University of Innsbruck (Austria), TU Munich (Germany), MU Leoben (Austria), CSM Golden (USA), and ETH Zürich and EPF Lausanne (both from Switzerland), clients and contractors (Schneider et al. 2012). The aim of this project is develop a forecasting model for penetration and wear based on the Alpine geology. The first outcome of this project is the developed modified Gehring model, called 'Alpine Model', for penetration rate predictions (Wilfing, 2016).

Commonly used prediction models have been the subject of comparison – Rostami et al. (1996), Grandori et al. (2011), Farrokh et al. (2012), Macias et al. (2014b, 2015bc), Paltrinieri et al. (2016) and Hassanpour et al. (2016).

These models adopt very different approaches and their input parameters, especially in terms of rock mass properties, exhibit substantial variation. This makes balanced comparisons problematic. However, under ordinary conditions, the results of the models may exhibit satisfactory agreement. A further issue for consideration is the scope of applicability of the different models.

Table 9 summarises the main basic input and output parameters of the common performance prediction models.

Table 9. Commonly used performance prediction models including their input and output parameters.

Penetration rate model	Basic input parameters		Output parameters	Reference
	Rock parameters	Machine parameters		
Gehring model	UCS, rock mass fabric	Cutter thtust, cutter diameter and spacing	Penetration rate	Gehring (1995)
CSM Model	UCS, BTS	Cutter diameter, cutter tip width, average cutter spacing, number of cutters, cutterhead rpm, thrust force	Penetration rate	Rostami (1997)
NTNU model	DRI, porosity, degree of fracturing, orientation, CLI, quartz content	TBM diameter, Cutter diameter, number of cutters, gross average cutter thrust, rpm	Penetration rate, advance rate	Bruland (2000)
Q_{TBM}	Q-value (with RQD_o), rock strength (UCS, PLT), density, porosity CLI, quartz content, induced biaxial stress on tunnel face	Average cutter load, TBM diameter	Penetration rate, advance rate	Barton (2000)
RME	RMR parameters, DRI	TBM diameter, type of machine	Penetration rate, advance rate	Bieniawski et al. (2006)

Other prediction models have been developed in last years. Yagiz (2008) identified five rock mass properties as independent variables for penetration rate predictions from data collected

one TBM project in New York City, USA. Statistical approach resulted in a prediction equation.

Gong and Zhao (2009) introduced a rock mass conceptual model for TBM penetration rate prediction. The relevant rock mass properties identified for the model were rock strength, rock brittleness, joint spacing and joint orientation. The model is based on data collected from during the construction of the Deep Tunnel Sewerage System (DTSS) in Singapore.

Hassanpour et al. (2011) proposed a new prediction model for machine performances or net penetration rate (m/h). Two main rock properties were selected for the new model, uniaxial compressive strength (UCS) and Rock Quality Designation (RQD) and operational parameters, average cutterhead thrust and cutterhead velocity. The model is based on empirical data from four tunnelling projects with a total length of 55 km and TBM diameters of 4.5-10 metres.

Farrokh et al. (2012) generated a model on the basis of the analysis of data from more than 300 international TBM projects. The data records, including rock mass properties and machine parameters, were analysed by multivariate regression resulting in regression equations to calculate the penetration rate.

Delisio and Zhao (2014) introduced a new model for TBM performance prediction specifically in blocky rock conditions. The model was developed from TBM data and geological/geotechnical parameters collected in two tunnels excavated in a ground with blocky conditions.

Yagiz (2014) developed the modified CSM model by including the effect of rock mass fracture and brittleness to the existing version of the model (Rostami, 1997). Rock mass fracture is a combination of fracture spacing and angle based on the NTNU methodology (Bruland, 2000bd). Assessment of brittleness is determined using the punch penetration test.

Wilfing (2016) has recently introduced the modified Gehring model, called 'Alpine Model' for penetration rate predictions. The new approach introduces a new parameter named 'y-intercept BTS or LBC approach' in the original equation (Gehring, 1995) in order to assess the relation between the applied force and resulting penetration in hard rock tunnel boring. The new parameter depends on the LCPC breakability and the Brazilian tensile strength.

2.5.3 Cutter life assessments in hard rock tunnel boring

Tunnelling performance and costs may be strongly influenced by the level of consumption of cutter discs, especially in hard and abrasive rock conditions. Thus, in order to achieve reliable planning and risk control, reliable methods for predicting cutter consumption are needed.

Many factors influence the number of cutters consumed during a hard rock TBM tunnelling project. Abrasive wear has been confirmed to be the major factor during normal operations (Rostami, 1997; Bruland, 2000b; Frenzel et al., 2008), combined with the influence of rolling distance.

Recent methods and models developed to make cutter life assessments include those of Gehring (1995), the CSM model (Rostami 1997), the NTNU model (Bruland, 2000b), Maidl et al. (2008), the Rock Mass Excavability Index, RME (Bieniawski et al. 2009), Frenzel (2011) and Hassanpour et al. (2014).

Currently, the cutter life models developed at the CSM (Rostami, 1997) and the NTNU (Bruland, 2000b) are the most commonly used approaches to predicting cutter consumption for hard rock TBMs, although several other approaches have been proposed in recent years.

The CERCHAR Abrasivity Index (CAI), as defined by the ASTM (2010) and/or the ISRM (2014) is used by the CSM model. The CAI can be used to estimate the average rolling distance of a given cutter. Factors such as the total number of cutters, cutter costs and change times, as well as probable operational delays, can be predicted.

Table 10 shows the test methods applied in assessing rock abrasivity in the most commonly used cutter life models.

Table 10. Common cutter life models including their input and output parameters.

Cutter life model	Basic input parameters		Output parameters	Reference
	Rock parameters	Machine parameters		
Gehring	CAI, UCS		Wear rate, cutter life	Gehring (1995)
CSM	CAI	Cutterhead rpm	Cutter life, delays, total cost	Rostami (1997)
NTNU	CLI, quartz content (%)	Cutterhead diameter (m), cutter diameter (mm), number of cutters, cutterhead rpm	Cutter life, delays, total cost	Bruland (2000)
Maidl	CAI, UCS		Average cutter ring life	Maidl et al. (2008)
RME	CAI, UCS		Cutter life	Bieniawski et al. (2009)
Frenzel	CAI	Cutterhead diameter (m)	Cutter life, delays, total cost	Frenzel (2011)

The NTNU model is based on the time-dependent abrasion of the cutter rings (see section 2.6). The parameters that influence cutter wear in this model are the Cutter Life Index (CLI), rock quartz content (%), the TBM diameter, cutter diameter, the number of cutters and cutterhead velocity (rpm). The Cutter Life Index (CLI) is evaluated based on the Sievers' J-

value and the Abrasion Value Cutter Steel (AVS) as defined by Bruland (2000g). Cutter life, measured in hours, is combined with the net penetration rate (m/h) and the TBM diameter to calculate cutter life in terms of 'metres per cutter' and 'solid cubic metres per cutter'. Factors such as the total number of cutters, cutter costs, cutter change time, the influence of cutters on advance rate (m/week), and total costs are also included.

The Gehring model (Gehring, 1995) also used the CERCHAR test method, and established a relationship between CAI and cutter ring weight loss (mg of steel) per metre rolling distance.

Maidl et al. (2008) proposed an empirical relationship between the mean rolling distance life (in metres) of 17-inch diameter cutter discs and the unconfined compressive strength and CAI index for different rock types. Cutter wear is expressed in terms of 'g/km of rolling distance'.

The Rock Mass Excavability Index (RME, Bieniawski et al., 2009) is also based on the CAI. The authors examined empirical correlations between the RME and cutter consumption, and presented three levels of variation for the CAI. They also established different correlations for values of Uniaxial Compressive Strength (UCS, expressed in MPa) of intact rock for values both above and below 45 MPa.

Frenzel (2011) proposed a cutter consumption prediction model, valid for 17-inch disc cutters, based on an analysis of a large number of tunnelling projects. The CAI index is used to assess rock drillability and direct empirical relations with cutter consumption are derived. Relative costs for refurbishment are also discussed.

Hassanpour et al. (2014) have proposed a new empirical TBM cutter wear prediction model based on data collected from a long tunnel project carried out in Iran in pyroclastic and mafic igneous rocks. The relationship between cutter life and average mineral hardness (quantified using the VHNR) and UCS is established.

2.6 The NTNU prediction model for hard rock TBMs

2.6.1 Introduction

The philosophy of the NTNU model is to achieve reliable predictions by combining relevant rock properties and machine parameters. The model involves several steps are involved in the NTNU prediction model for hard rock TBMs in order to estimate time and costs involved in tunnel excavation using factors such as : net penetration rate, cutter life as well as advance rate and excavation costs. The NTNU models used to estimate hard rock tunnelling, penetration rate and cutter life provide reliable and practical tools for:

- estimating net penetration rate and cutter wear
- estimating time consumption and excavation costs, including risk
- assessing risk linked to variation in rock mass boreability and machine parameters
- establishing and managing contract price regulation
- verifying machine performance
- verifying variation in geological conditions

The models can be used at various stages of a given project:

- ✓ Preliminary and feasibility studies
- ✓ Evaluation of the excavation method
- ✓ Project design and optimisation
- ✓ During tendering and contract processes
- ✓ Documentation during construction
- ✓ Possible disputes and claims

The models are based on project site studies and statistics derived from more than 40 tunnelling projects carried out in Norway and abroad, involving more than 300 kilometres of tunnel. The data have been systematised and normalised and the results are regarded as being representative of well-organised tunnelling projects.

The model has had been the subject of continuous development a successive development since the first version was published in 1976 by the NTNU (formerly NTH). Bruland (2000a) gives a brief description of the model development with some comparisons.

Table 11 shows the successive editions of the NTNU prediction model to date.

Table 11. History of the NTNU prediction model for hard rock TBMs

EDITION	YEAR
1st edition	1976
2nd edition	1979 (published in 1981)
3rd edition	1983
4th edition	1988
5th edition	1994
6th edition	2000

2.6.2 Model parameters

Net penetration rate and cutter life are dependent on both rock properties and machine parameters. Rock properties consist of both intact rock and rock mass parameters. The model combines rock properties to derive in a rock mass boreability parameter called the 'equivalent fracturing factor' (k_{ekv}) while the machine parameters are combined into a single parameter called 'equivalent thrust' (M_{ekv}).

Cutter life (in hours) is equivalent to the cutter life in relation to rolled distance (km/cutter) for a given cutterhead rpm. Cutter life is combined with the penetration rate (m/h) and the TBM diameter to calculate the cutter life in the terms 'tunnel metres excavated per cutter' (m/cutter) and 'solid or in situ cubic metres excavated per cutter' (sm^3/cutter).

As noted above, net penetration rate is dependent on both rock properties and machine parameters. These are summarised in Table 10 below.

Table 12. Machine parameters and rock properties influencing net penetration rate.

ROCK PROPERTIES		MACHINE
Intact Rock	**Rock Mass**	**PARAMETERS**
Drilling Rate Index, DRI	Rock Mass Fracturing Factor (k_s)	TBM diameter
		Cutter diameter
Porosity		Number of cutters
		Gross average cutter thrust
		Average cutter spacing
		Cutterhead rpm

Cutter wear is dependent on the rock properties and machine parameters summarised in Table 11 below.

Table 13. Machine parameters and rock properties influencing cutter wear.

ROCK PROPERTIES	MACHINE PARAMETERS
Cutter Life Index, CLI	TBM diameter
	Cutter diameter
Content of abrasive minerals	Number of cutters
	Cutterhead rpm
	Gross average cutter thrust

The gross advance rate is estimated on the basis of three input parameters:

- Net penetration rate
- Machine utilisation
- Number of working hours during the period in question (e.g. a week)

The machine utilisation parameter is in turn based on the time spent in completing the various operations required to excavate the tunnel.

3 Research methodology and procedures

3.1 General approach

The research carried out as part of this PhD is a multidisciplinary process involving several different methodological approaches.

A number of sub-goals, derived from different research areas and methods, have to be achieved in order to complete the overall objectives described in chapter 1. These are listed below:

- The acquisition of hard rock TBM field data, geological back-mapping, and rock samples for testing
- Laboratory testing for drillability, rock strength, abrasivity and analysis of mineral composition
- The performance of sufficient TBM trials to generate reliable statistical correlations between field and laboratory data
- The revision of the NTNU TBM prediction model by broadening the range of factors included as dictated by current needs, including factors and conditions that have not been considered until now:
    - To advance the state-of-the-art by including data from current projects
    - To transfer the potential impact of the greater understanding of the boring process to the prediction model. This includes:
        - The influence of cutterhead velocity during hard rock boring
        - The influence of cutter thrust on cutter consumption
    - To increase the scope of application of the NTNU TBM prediction model by adapting it to current needs
- The investigation of the potential and need to develop a new abrasivity test method under conditions closer to real tunnelling situations in order to promote good laboratory reproducibility and prediction of cutter ring wear
- The collection of TBM cutter rings
    - To analyse wear processes and failure mechanisms by means of current laboratory methods, and to identify these phenomena in used TBM cutter rings
    - To validate the wear process as part of the new laboratory test method

The overall research methodology strategy has been a combination of the following:

- Continuous literature review
- Field research/trials
- Laboratory research
- Field and laboratory experiments
- Data processing and discussion

3.2 Literature review

An initial comprehensive literature review was carried out with the aim of establishing a research background and an understanding of the state-of-the-art regarding hard rock tunnel boring. Literature review has been a continuous process throughout the PhD work, with the aim of maintaining close contact with developments in the scientific community.

The review has been based on articles published in international journals and scientific monographs for which quality is assured by the work of journal editors and peer review.

International conference and congress proceedings provide supplementary sources, subject to critical review, and the conferences themselves provide fora where knowledge can be shared.

Finally, magazines and websites provide useful sources of additional information on current developments and the state-of-the-art in the industry.

3.3 Field research

3.3.1 General remarks

Geological data has been collected along selected tunnel sections. Data have been derived from continuous engineering geological back-mapping and drillability testing, machine specifications and TBM data, and the analysis of performance and operational parameters.

The quality of information and analyses has been given precedence over quantity. Projects have been selected on the basis of the following factors:

- ✓ Diameter variability across the standard TBM cutterhead diameter range
- ✓ Rock mass variability – hard rock boreability and abrasivity
- ✓ Availability of quality data
- ✓ Access to enable engineering geological back-mapping

Field research has consisted of the following:

- Engineering geological back-mapping
- TBM data logging and processing
- Recording of tool and cutter consumption data
- Trials – penetration and 'RPM tests'
- Sample gathering for laboratory testing and mineralogical analysis
- Cutter ring specimen gathering for wear mechanism analysis

Performance and tool consumption data represent sensitive information in the TBM tunnelling industry, requiring that confidentiality agreements be entered into between contractors, clients, consultants and other institutions involved in this PhD study.

3.3.2 Description of the projects

A total of five hard rock TBM project sites, involving 7 machines, are included in this PhD study. Table 14 provides a summary of the project sites and the information obtained during field research. Figure 22 shows the geographical distribution of the project sites.

Table 14. The main characteristics of the TBM project sites.

Parameters	Project				
	A	**B**	**C**	**D**	**E**
Project type	Hydropower	Water transfer	Mining development	Hydropower	Irrigation
Region	Europe	Southeast Asia	North America	Europe	Asia
Tunnel diameter (m)	3.4	5.2	5.5	7.2	10.0
Lining	-	-	-	-	Concrete segments
Approximate tunnel length (km)	8.2	17.0	6.2*	7.0	42.0*
Geological back mapping	◯	***	◯**	◯	****
Cutter consumption	◯	◯	-	◯	◯
Rock samples	◯	◯	◯	◯	◯

◯ Included
* Project not finished
** Core logging
*** Limited mapping
**** Limited tunnel face mapping

Figure 22. Geographical distribution of the hard rock TBM projects.

High rock strength and abrasivity introduce high risk to the processes of performance prediction and cutter life assessment. The geological conditions encountered in these projects are highly variable, but for the most part involve high levels of low drillability/rock strength and abrasivity.

Table 15 summarises the properties of the lithologies encountered in each of the projects included in this study.

Table 15. Summary of the main rock properties encountered at the project sites.

Parameters	Project				
	A	B	C	D	E
Lithology	Sill/Basalt	Granite	Norite	*Several	Granite
Density (g/m^3)	2.7 – 3.0	2.6 – 2.7	2.7 – 2.9	2.6 – 2.7	2.6
UCS (MPa)	198**	94 – 192	80 – 82	76 – 264	324**
	Very high	High-very high	High	Medium-Extremely high	Extremely high
DRI	21 – 69	34 – 58	49 – 60	38 – 75	43 – 45
	Ext. low-High	Low-High	Medium-High	Low-Very high	Medium
CLI	8.8 – 47.0	4.2 – 6.0	11.6 – 24.1	4.5 – 99.6	5.4 – 5.5
	Medium-very high	Extremely low-Low	Medium-High	Extremely low-Extremely high	Very low
Abrasive mineral content	3 – 4 %	32 – 40 %	<1 %	5 – 61 %	34 – 36 %

*Mica schist/mica gneiss/granodiorite/quarzitic gneiss/marble
**Limited testing

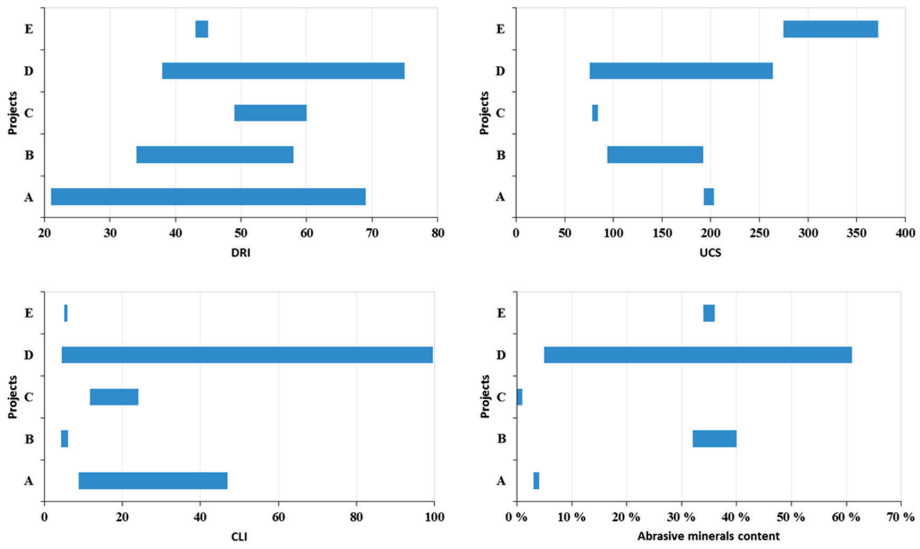

Figure 23. Summary of rock property variations encountered at the project sites.

Most of the seven machines used in these projects are of the open gripper type. The exception is Project E, where a double shield machine was used. Cutter diameters ranged from 432 to 508 millimetres. Table 16 shows the main characteristics of the machines used in the projects.

Table 16. Summary of the principal machine characteristics used at the project sites.

Parameters	Project				
	A	B	C	D	E
TBM diameter	3.4 m	5.2 m	5.5 m	7.2 m	10.0 m
TBM type	Open gripper	Open gripper	Open gripper	Open gripper	Double shield
Cutter diameter	432 mm	483 mm	483 mm	483 mm	483/508
Number of cutters	27	35	33	46	67
Average cutter spacing	63.0 mm	74.7 mm	83.33 mm	78.6 mm	74.8 mm
Maximum recommended cutterhead thrust	237 kN/c	312 kN/c	312 kN/c	312 kN/c	312 kN/c
Cutterhead velocity	12.8 rpm	0 - 11.2 rpm	0 – 10 rpm	0 - 8.7 rpm	0 – 8.0 rpm
Boring stroke	1.55 m	1.80	1.83 m	1.87 m	1.70 m

3.3.3 Engineering geological back-mapping

Continuous engineering geological back-mapping was carried out where possible in order to evaluate rock mass properties in the tunnel in question. For Project C, rock mass assessment was performed by core logging parallel to the tunnel alignment.

The process of tunnel back-mapping consists of the continuous and detailed mapping of rock mass fracturing and rock type distribution, rock sampling, and the subsequent laboratory testing of rock properties. The purpose is to establish a geological model of the tunnel that can then be used for the evaluation of machine performance, machine utilisation, trials, cutter life and other factors.

Mapping in terms of measuring factors such as type and degree of fracturing, fracture sets and orientation, and identifying rock type, is a highly subjective process. An analysis of the influence of subjectivity on the prediction process was carried out as part of this PhD study (paper V).

The engineering geological back-mapping procedure employed during this study is based on the NTNU approach (Bruland, 2000d), and consists of the following steps:

- Determination of rock type
- Identification of the strike and dip of Marked Single Joints
- Notes on other singular phenomena such as intrusions, mixed face, water, rock support, etc.
- Determination of the number of fracture systems and type of fracturing (joints or fissures) for each system
- Measurement of the strike (α_s) and dip (α_f) of the fracture system(s)
- Measurement of the strike (azimuth) of the tunnel (α_t)

Rock samples are taken for the laboratory investigation of drillability properties and mineral composition.

According to Bruland (2000d), the measurements recorded should represent the average of the tunnel sections in question. Sections may be subdivided for measurement purposes if changes in rock type or other factors so dictate.

Section volume may be evaluated in order to obtain a representative view. However, in order to ensure that the rock mass being measured is universally representative, the degree of fracturing should be measured using a scanline along one of the tunnel walls.

The individual re-mapping of selected, shorter, sections (20-30 metres in length, at 150-200 metre intervals) should be carried out once mapping of the entire tunnel section is completed.

Prior to mapping a new tunnel section, it is important to check and evaluate the map of the previous 30-50 metre section. This will ensure that individual mapping exercises are adapted to on-site geology.

Mapping measurements should be recorded using standardised entries. Figure 24 shows a mapping sheet template for engineering geological back-mapping in bored tunnels.

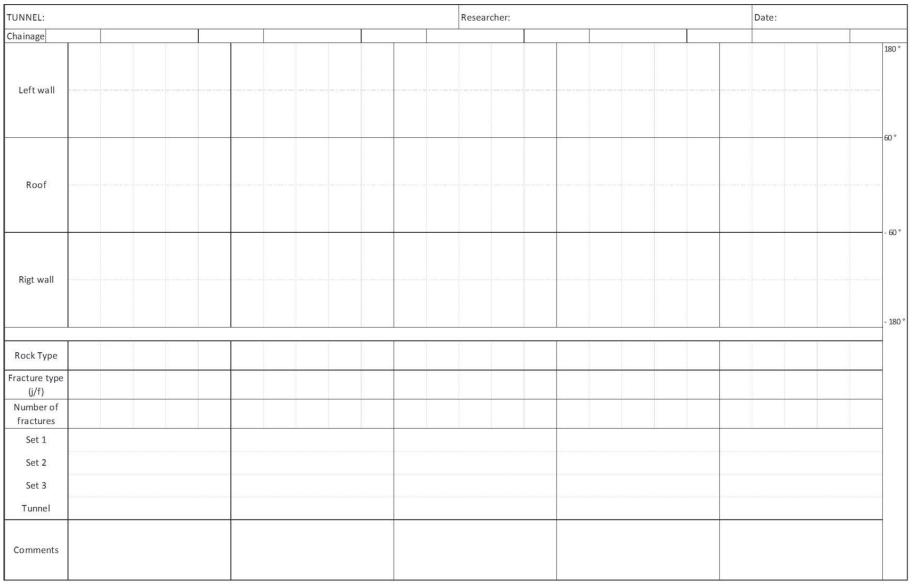

Figure 24. Template for engineering geological back-mapping in bored tunnels (recommended for TBM diameters greater than approximately 5 m).

In the NTNU prediction model, the angle between the tunnel axis and the planes of weakness is calculated using equation (4) (below):

$$\alpha = \arcsin \cdot (sin\alpha_f \cdot \sin(\alpha_t - \alpha_s)) \tag{4}$$

where

α_s = strike angle of the planes of weakness
α_f = dip angle of the planes of weakness
α_t = azimuth of the tunnel axis

Figure 25 shows the basic terms linked to the stereographic projection and stereonet illustrating the angles used in the previous equation.

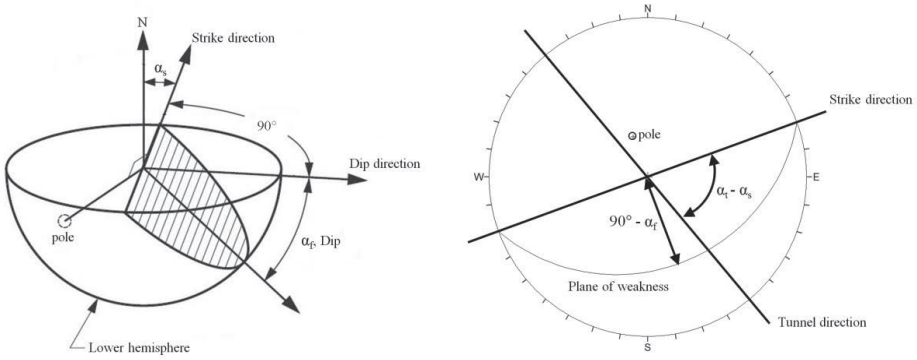

Figure 25. Basic terms linked to the stereographic projection and stereonet illustrating the angles used in equation 1 (Article V).

The fracturing factor (k_{si}) for each section is calculated using the plots shown in Figure 26 (Bruland, 2000).

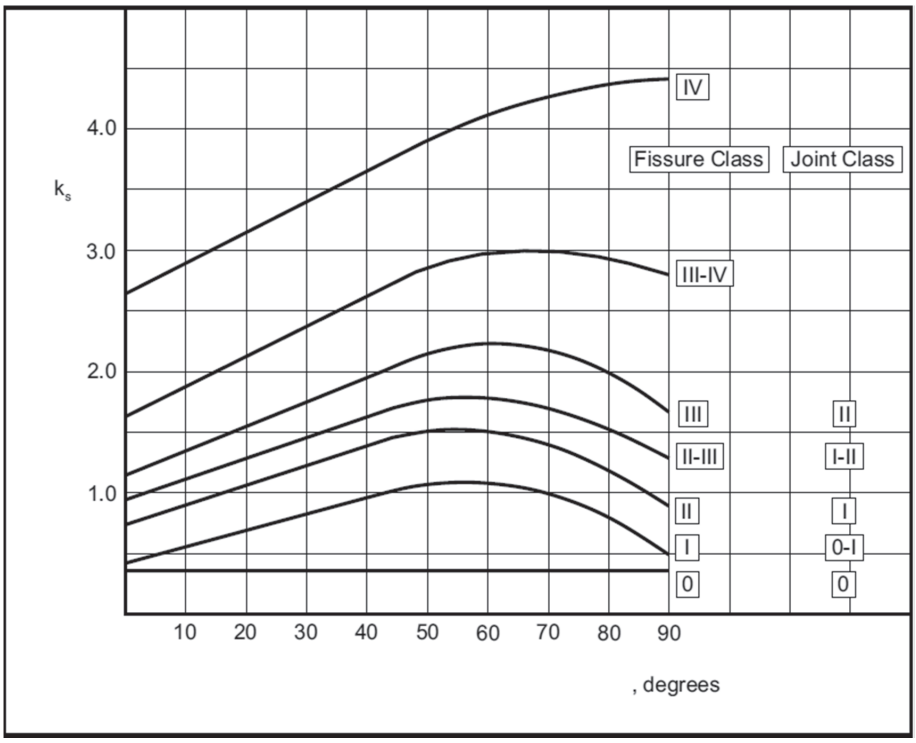

Figure 26. Graph used to calculate the fracturing factor (k_s) on the basis of fracture class and the angle between the tunnel axis and the planes of weakness. From Bruland (2000f).

The curves in Figure 26 suggest that with increased spacing between the joints or fissures, there will be an optimum angle between the tunnel axis and the planes of weakness. The angle

providing the highest fracturing factor is about 60 degrees. This is explained by the presence (or absence) of joints or fissures at the rock face, as illustrated in Figure 27.

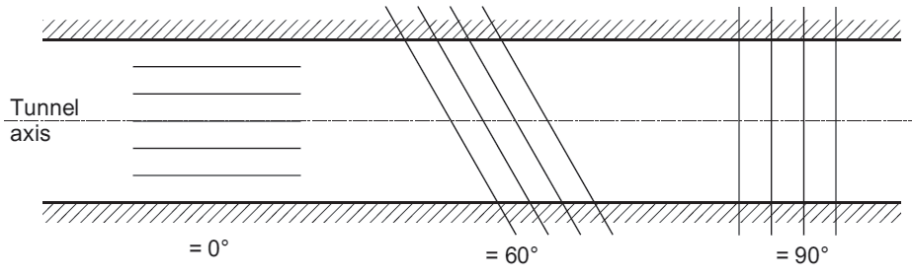

Figure 27. Influence of systematically occurring fissures or joints at various angles to the tunnel axis. From Bruland (2000f).

When the spacing between the planes of weakness is very short, such as in fissure class IV, the maximum fracturing factor occurs at 90 degrees. In this case, radial cracks from beneath the cutter will reach a plane of weakness (see Figure 28) and the fracturing factor will increase until the angle of 90 degrees is achieved.

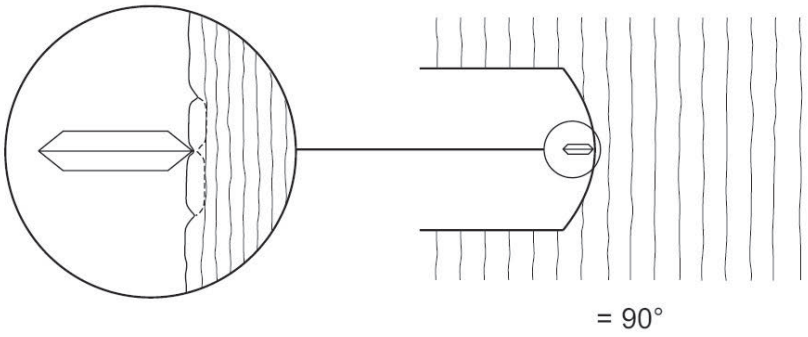

Figure 28. Chipping pattern for boring in fractured rock with regular, short spacing between planes of weakness (e.g. class IV) and at an angle of 90 degrees. From Bruland (2000f).

Excavation using TBMs involves a geological risk which requires careful analysis. In high quality rock masses containing few or no fractures, the risk involved in achieving accurate performance prediction takes on a greater importance. Thus, a detailed determination of fracture class is essential in rock masses exhibiting low fracture classes (0, I, II) and will enable us to determine if it is the intact rock or rock mass properties that control the boring process.

Once k_{si} has been obtained for each mapped section, a total (weighted) average is calculated using equation (5) below (Bruland, 2000e):

$$k_{s-avg} = \frac{\sum_{i=1}^{n} l_i}{\sum_{i=1}^{n} \frac{l_i}{k_{s-i}}} \quad (5)$$

where

l_i = tunnel length for fracturing class "i" along the mapped section
k_{s-i} = k_s factor for fracturing class "i" along the mapped section

It is essential to obtain k_{s-avg} in the form of a weighted average in order to provide a realistic and representative value for the entire length of the section in question.

In situations where more than one set of planes of weakness are recorded, the total fracturing factor is calculated using equation (6) below (Bruland, 2000e):

$$k_{s-avg} = \sum_{i=1}^{n} k_{si} - (n-1) \cdot 0.36 \quad (6)$$

where

k_{si} = k_s factor for fracturing class "i" along the mapped section
n = number of fracture sets

In situations where it is difficult to separate the observed rock mass fractures into sets, average values for fracture spacing and angle for the total rock mass fracture system should be calculated.

3.3.4 TBM data logging and processing

Modern TBMs are equipped with data logger systems which record machine parameters automatically. However, such automatic systems are not used universally, and handwritten bore reports are still common, especially in connection with older TBMs.

Large amounts of data are required to generate a reliable prognosis. However, appropriate processing is needed so that representative machine parameter values are applied.

The data obtained from logger systems includes:

- indications of when excavation (boring) is taking place, i.e. when the cutterhead is rotating with a thrust above a given threshold value
- the cutterhead's total gross thrust, excluding factors such as towing of the back-up system
- the cutterhead velocity (rpm)
- the cutterhead position, i.e. chainage

The NTNU model uses the term 'gross average thrust', which is defined as the total thrust force applied during boring, taking into account the friction or drag of the cutterhead and

cutterhead support system, as well as other factors causing loss of thrust. The gross average thrust per cutter is obtained by dividing the total gross thrust by the number of cutter discs.

Experience during the last decade has shown that, in general, thrust is the limiting factor under normal hard rock tunnelling operations. In case of highly fractured rock and soft ground machines can become torque limited (Bruland, 2000; Smading, 2016). This has been confirmed during this research. For this reason, torque is not included as one of the TBM parameters subject to analysis.

Raw data from tunnelling reports in the form of shift logs recorded by TBM crews, etc. are also useful.

The use of TBM data logger systems requires an initial analysis in order to safeguard correct interpretation of the data and define a data processing procedure. A description of the procedure used in this research is following included.

Figure 29 is a scatter plot of raw logged TBM data logged showing net penetration rate (m/h) versus cutter thrust (kN/cutter) for a 50-metre tunnel section.

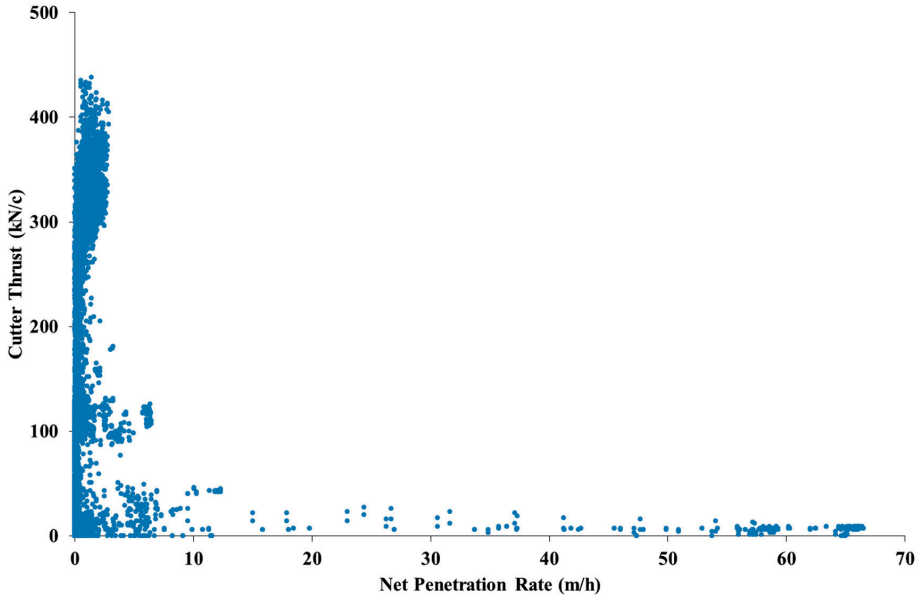

Figure 29. An example of logged TBM data showing net penetration rate (m/h) versus cutter thrust (kN/cutter) for a 50-metre tunnel section.

The data set shown in Figure 29 shows a number of exceptionally high values of net penetration rate at very low values of applied cutter thrust. Clearly this cannot be achieved during TBM boring. Some of these values originate from situations when the cutterhead is moved forwards towards the tunnel face without excavation actually taking place.

The sorting of cutter thrust values above 50 kN/c (Figure 30) identifies atypical values of net penetration rate for relatively low values of applied cutter thrust. Some of these values may have been recorded when the cutterhead, as mentioned above, is moved forwards towards the tunnel face without excavation taking place. However, such values could also arise during drilling through zones containing concentrations of planes of weakness or faults. For this reason, it is important to bear in mind the consistency of the geology and rock mass linked to the section in question. This will reveal whether or not such atypical values have been obtained as a result of excavation.

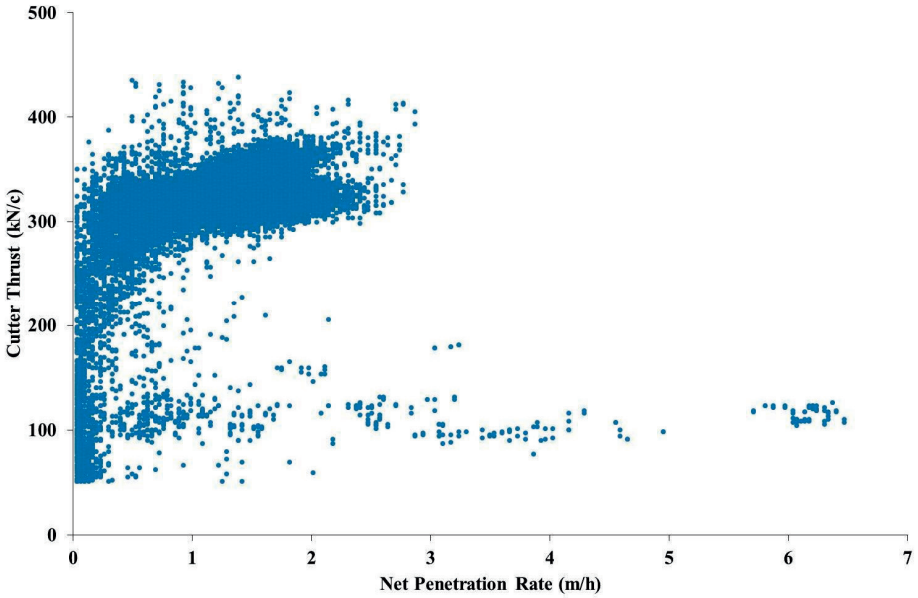

Figure 30. An example of logged TBM data showing net penetration rate (m/h) versus cutter thrust (kN/cutter) for a 50-metre tunnel section. The data have been sorted to display values above the 50 kN/cutter.

Figure 31 shows an example of logged TBM data for which data above 150 kN/cutter values have been sorted.

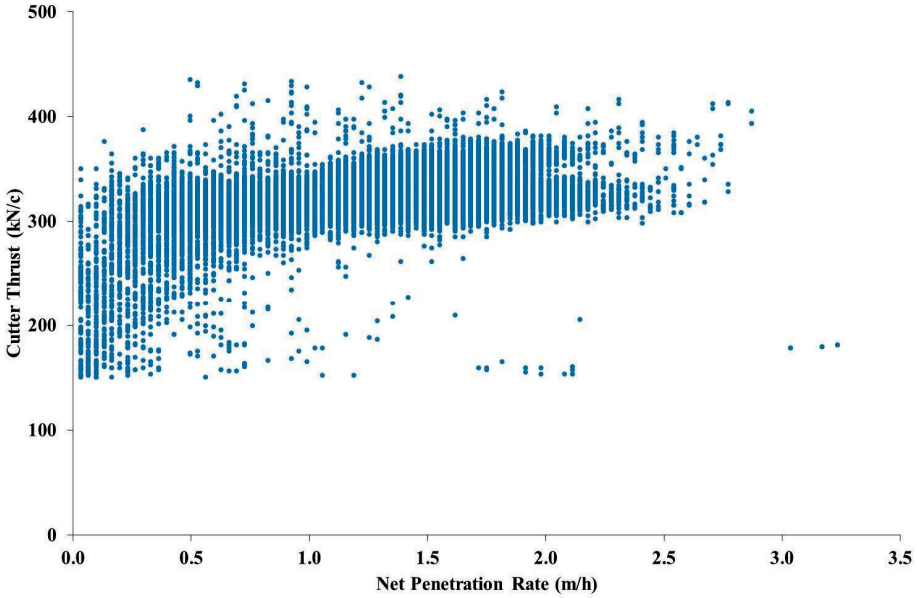

Figure 31. An example of logged TBM data showing net penetration rate (m/h) versus cutter thrust (kN/cutter) of a 50-metre tunnel section. The data have been sorted to display values above 150 kN/cutter.

A representative value of cutter thrust used to sort the data is obtained by continuing with data processing and analysing average values of cutterhead velocity (rpm), gross cutter thrust and net penetration rate.

After selecting a reasonable threshold gross cutter thrust value for processing, values below 1 rpm can be discarded.

Table 17 lists the average values of cutterhead velocity (rpm), cutter thrust and net penetration rate.

Table 17. Average values of cutterhead velocity, cutter thrust and net penetration rate of the sorted data as defined by cutter thrust levels.

	Average cutterhead speed (rpm)	Average cutter thrust (kN/cutter)	Average net penetration rate (m/h)
>0 kN/c	6.08	299.48	1.21
>50 kN/c	6.14	311.87	1.22
>100 kN/c	6.18	315.96	1.23
>150 kN/c	6.23	319.96	1.23
>200 kN/c	6.25	321.28	1.24
>250 kN/c	6.26	322.49	1.25

Figure 32 and Figure 33 show average cutter thrust and net penetration rate for a selection of cutter thrust levels used for sorting the data.

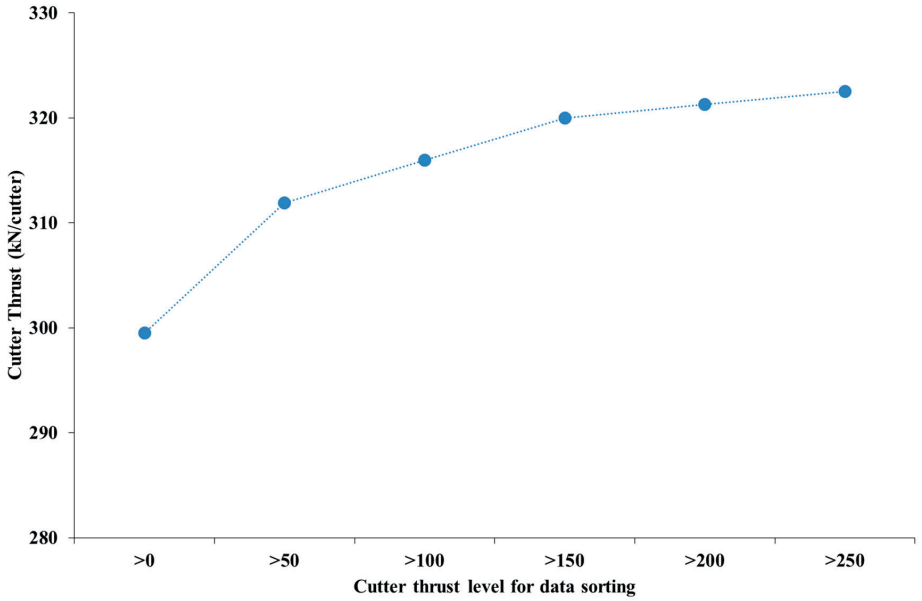

Figure 32. Average cutter thrust (right) values for the defined cutter thrust levels used for sorting logged TBM data.

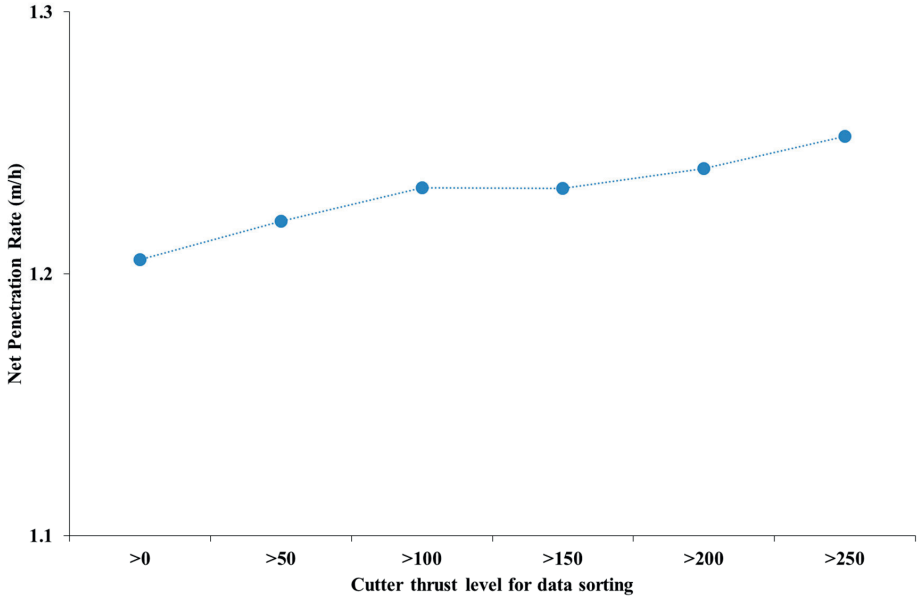

Figure 33. Average net penetration rate values for the defined cutter thrust levels used for sorting logged TBM data.

After the sorting process summarised in Table 17 and Figure 32 and Figure 33, the cutter thrust value exhibiting the most consistent averages is shown to be 150 kN/cutter. In this case, as shown in Table 17, there is a tendency for the most consistent values to occur above the 150 kN/cutter level. The results may vary for different machines, rock mass properties and, therefore, for different tunnel sections.

3.3.5 Cutter consumption

Introduction

Tool consumption is documented at the TBM sites as part of cutter changes and inspection procedures, combined with cutter repair logs recorded at the cutter shop. At a minimum, such data usually include the following:

- Consumption for each cutter position
- Chainage and machine hours at each change
- The reason for changing each cutter
- Repositioned cutters
- Wear height of each ring
- Spare parts consumption

The quality of recorded cutter data is of great significance to obtain reliable interpretations of detailed instantaneous cutter consumption and average cutter life.

It is a common procedure to swap partly-used cutters from the outer to the inner gauge. Such re-positioning is noted in the cutter change log and is used in cutter consumption calculations.

The following definitions are introduced to avoid confusion:

The term ‘cutter change’ is defined as the operation involved in replacing one or more worn or damaged cutters at a given time. Cutter change no. 1 is defined as the start of the boring process.

The term ‘cutter replacement’ is defined as the replacement of a worn cutter with a new or rebuilt cutter (installation of a new ring as a minimum requirement here) at a single position as part of a cutter change.

The term 'cutter reposition' is defined as the movement of cutters between positions during a cutter change or cutter inspection.

The following alphabetic codes are used in this study to denote the reasons for carrying out cutter changes:

- Abrasive wear (W) – cutter replaced due to maximum cutter ring wear
- Blocked (B) – cutter replaced due to blocked bearing
- Chipping (C) – cutter replaced due to chipping in the cutter ring
- Mushrooming (M) – cutter replaced d due to excessive mushrooming in the cutter ring
- Damaged Hub (H) – cutter replaced due to damaged hub

- Oil leakage (L) – cutter replaced due to oil leakage in the bearing
- Ring crack (F) – cutter replaced due to crack(s) in the cutter ring
- Others (X) – cutter replaced for reasons other than the above. The reason(s) should be noted

The levels of skills and experience of cutter personnel are important in order to ensure high quality cutter reports. Such reports are subject to measurement subjectivity and errors during the recording of the reasons for cutter replacement.

Figure 34 shows a template that can be used to record cutter consumption data. The data are used to calculate cutter consumption and cutter change patterns (distributions of reasons for cutter change) and to analyse the parameter 'ring wear per cutter'.

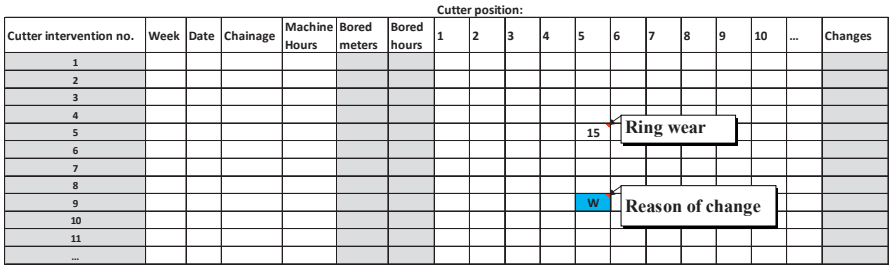

Figure 34. Template used to record cutter wear data used to calculate cutter life, wear patterns and ring wear along a tunnel section.

Instantaneous cutter consumption

The parameter 'instantaneous cutter consumption' is calculated between cutter change and inspection log in the tunnel and cutter repair log at the cutter shop.

Figure 35 illustrates the basic concept behind the calculation model for cutter wear (expressed in cutter/m). The same model is used to calculate the cutter consumption term (cutter/h) by substituting the chainage (in metres) for each cutter change with the corresponding machine hours. A description of the detailed model is beyond the scope of this thesis. A database Excel application developed at NTNU (Frostad, 2013) is used to make the calculations.

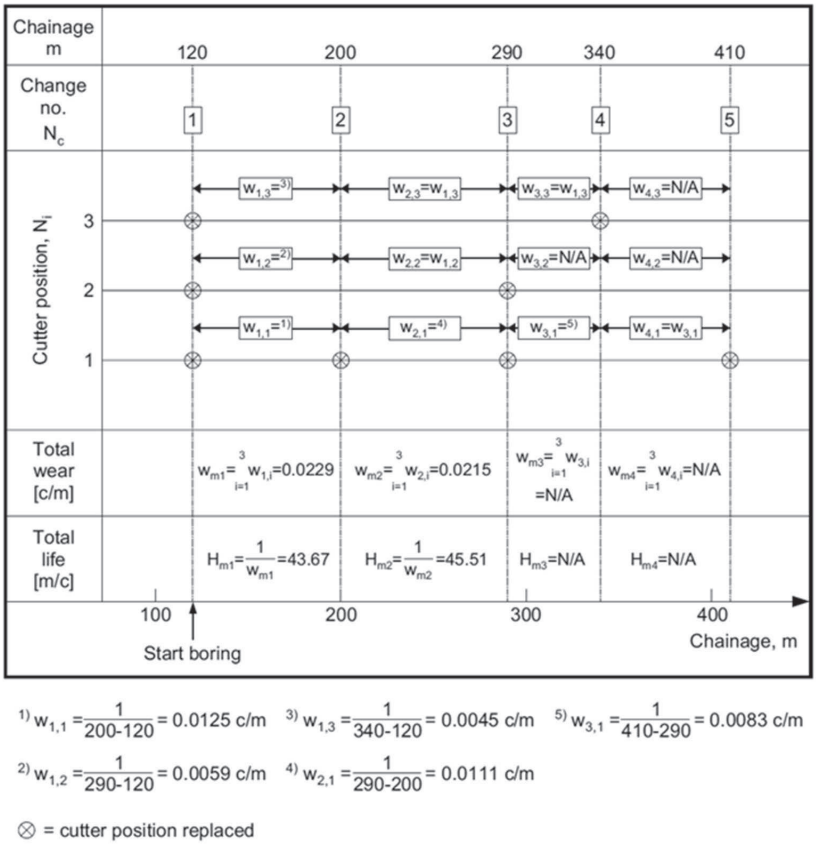

Figure 35. The calculation of cutter consumption (in cutter/m) for a theoretical cutterhead installed with three cutters (Bruland, 2000e).

The instantaneous tool life can be expressed in terms of average cutter ring life in hours per cutter (H_h, h/cutter), in meters per cutter (H_m, m/ cutter) or in cutters per meter (W_m, cutter/m) and in solid cubic metres per cutter (H_f, m^3/cutter). It should be noted that these parameters refer only to cutter consumption in cutter rings.

Special focus was directed on the selection of tunnel sections used for cutter life assessments. Care was taken to avoid incorrect cutter life assessments resulting from the influence of preliminary defined and short sections.

The term 'cutter consumption per (cutter) position' is used to calculate both the cutterhead factor (f_D) and the TBM diameter correction factor used in the calculation of cutter consumption (Bruland, 2000e). This is also valuable information for use when evaluating cutterhead design.

Figure 36 presents an example of cutter consumption per cutter position.

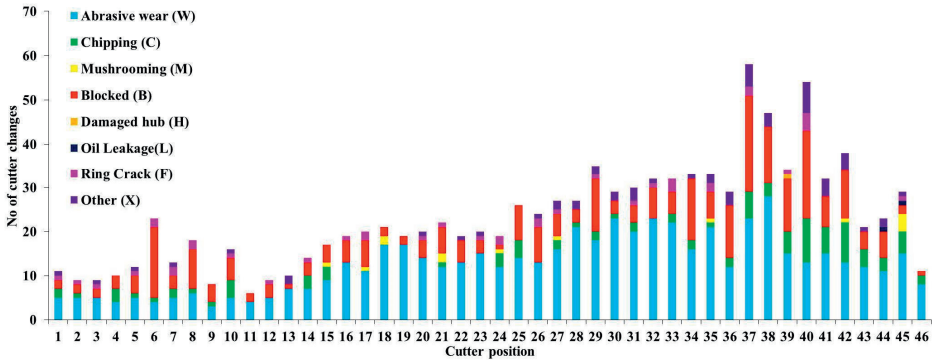

Figure 36. An example of cutter consumption per cutter position for Project D.

When analysing instantaneous cutter consumption, it is important to evaluate cutter replacement pattern distribution as a means of validating the cutter life data. Figure 37 shows the distribution (in per cent) of the reasons for cutter replacements that form the basis of cutter consumption data used in this study.

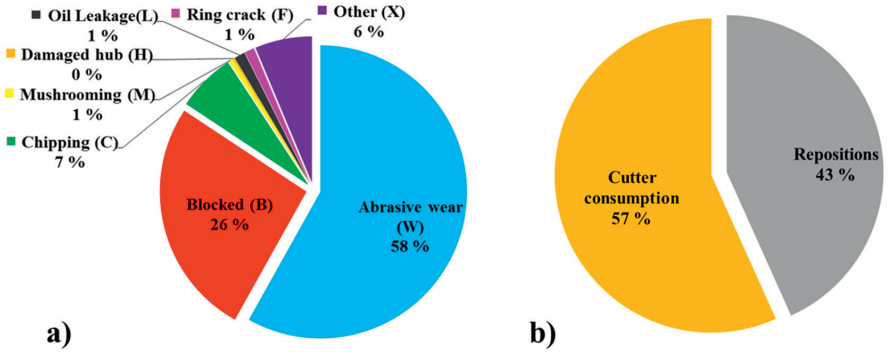

Figure 37. Total data distribution for a) the reasons of cutter replacement and b) cutter consumption/repositioning.

Figure 37 shows the results for the entire database used in this study, while representative sections were selected for processing of the results.

It is important to note that a large amount of cutter replacement due to bearing-related factors may have several causes, such as machine operation, lithologies exhibiting low abrasivity, highly fractured rock mass or a combination of these.

Tool wear management (e.g. cutter inspection and reposition) with control of wear height limits in order to follow the recommended limits according to the positions as well as the wear height difference between neighbour cutters play an important role.

Cutter ring wear

The wear rate of an individual cutter ring is measured in terms of loss of ring height. Cutter ring life should be measured during every cutter inspection and after replacement at the cutter repair shop.

An analysis of the total wear (expressed in millimetres of cutter ring consumed) is presented in Figure 38.

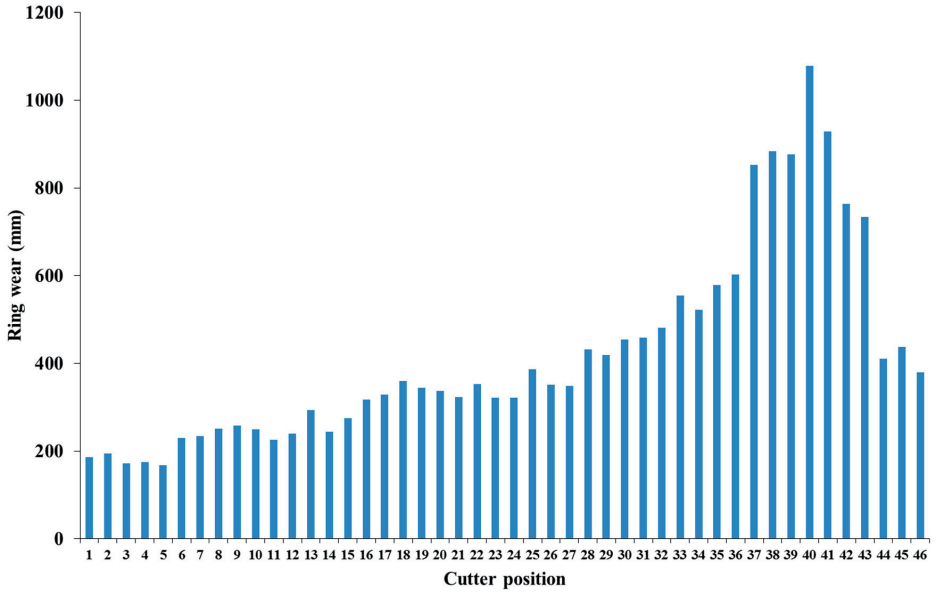

Figure 38. Cumulative wear recorded for Project D.

Pre-defined wear limits are recommended for every cutter position in order to avoid excessive wear height differences between neighbouring cutters. This avoids the occurrence of undesirable unbalanced cutter load peaks. The cutter wear profile will depend on cutterhead design and will vary with the position of the cutters.

As previously described, cutters may need to be changed as a result of damage due to other factors such as blockage, hub damage, oil leakage, ring cracks, etc.

Figure 40 shows cutter wear profiles for Projects B and D respectively. The plots display the average wear for total cutter changes, and changes due to wear and other factors related to the bearing set.

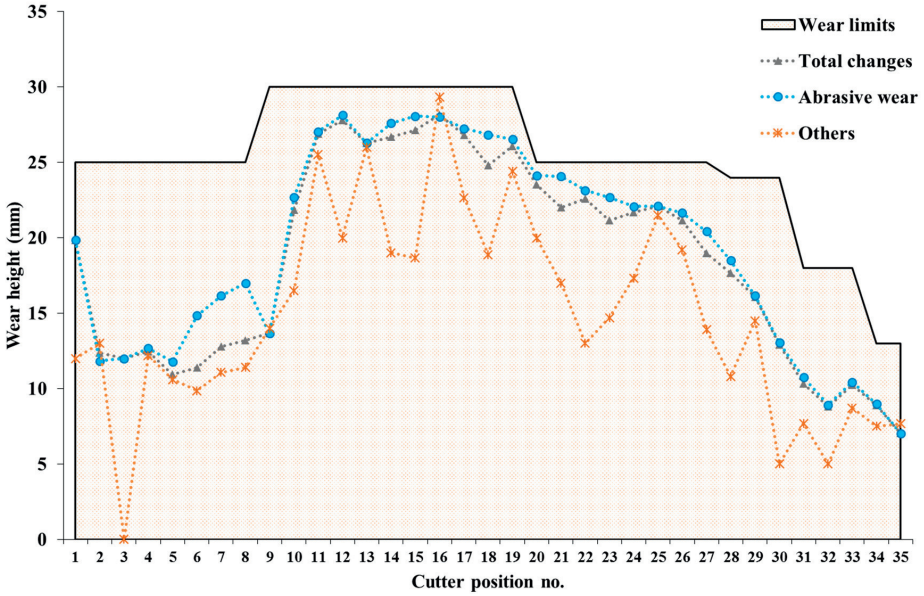

Figure 39. Cutter ring wear and recommended wear limits for Project B. Average ring wear for changes related total cutter changes, and changes due to abrasive wear and other factors related to the bearing set.

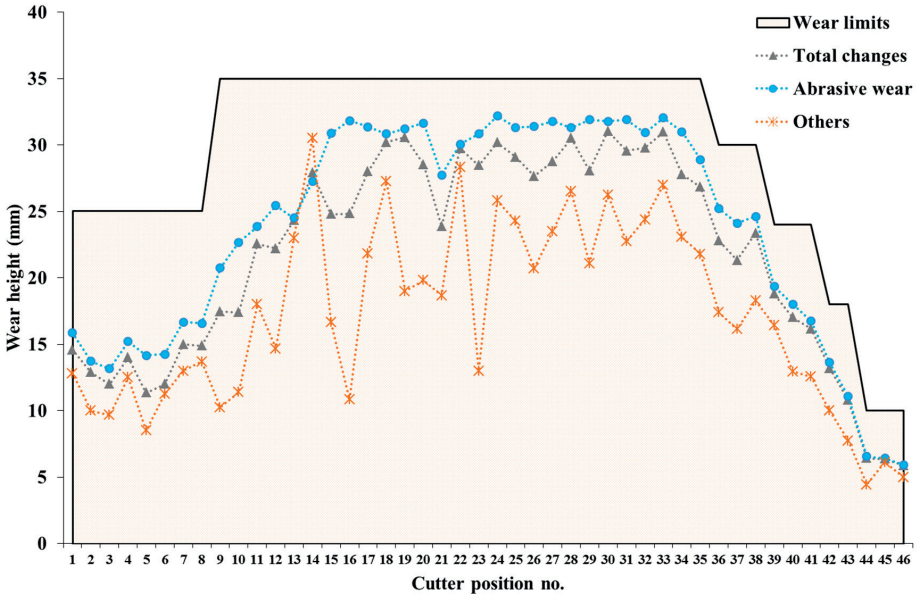

Figure 40. Cutter wear height and recommended wear limits for Project D. Average wear height for changes related to total cutter changes, and changes due to abrasive wear and other factors related to the bearing set.

It is noted that even when a cutter is replaced due to reasons other than those related to the bearing set, the proportion of abrasive wear in the cutter rings is considerable, indicating how predominant this wear mechanism is.

Positions 15, 16 and 23 illustrated in Figure 40 exhibit unexpected low average wear height for cutters replaced due to reasons other than abrasive wear (e.g. bearing set) when compared with the overall average due to wear. This behaviour may be due to poor cutter replacement or cutterhead design issues.

3.3.6 Cutter life

The cutter life model has been reviewed based on detailed information about geology, rock mass, drillability testing and instantaneous cutter life analysed and derived from selected tunnel sections for Projects A, C, D and E.

The estimation model presupposes that a TBM operates at a thrust level that result mainly in abrasive wear to the cutter rings. The amount of cutters changed due to cutter ring wear processes (abrasive, mushrooming and chipping) should amount to somewhat greater than 70% of total changes, of which chipping and/or mushrooming alone constitute the cause of less than between 5 and 10% of the total number of changes (Figure 41).

Cutters changes due to bearing set damage (blockage, leakage, hub damage, etc.) should comprise the cause of less than between 20 and 30% of the total number of changes.

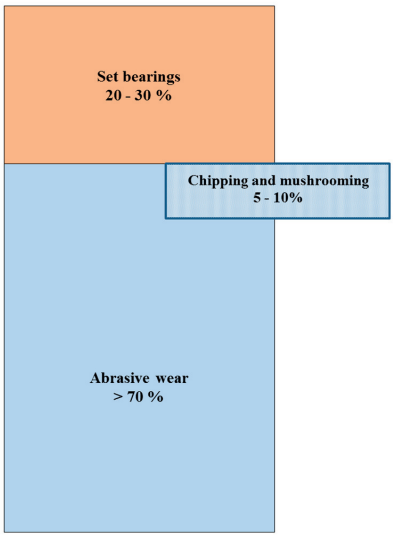

Figure 41. The causes of cutter change/replacement according to the prediction model.

Basic cutter ring life is back-calculated from instantaneous cutter life values for every tunnel section. Correction factors are taken into account.

Cutter ring life

This section provides detailed information about the methodology used to calculate cutter ring life.

The value of 'basic cutter ring life' (expressed in boring hours), is proportional to the Cutter Life Index CLI. Correction factors required for TBM diameter, cutterhead velocity (rpm), the number of cutters and abrasive minerals are discussed below.

Correction for TBM Diameter

Centre and gauge cutters have shorter lifetimes than face cutters. As TBM diameter increases, the ratio of centre and gauge cutters to face cutters decreases, causing the lifetime of the average cutter to increase.

The cutterhead factor is calculated by analysing the cutter ring consumption per position to a cutterhead with radius 1 and average cutter position of 1 ring per position (Bruland, 2000f).

$$r_{ri} = \frac{N_i}{N_{tbm}} \tag{7}$$

where

r_i = relative radius of cutterhead position no. i
N_i = cutter position no. i
N_{tbm} = number of cutter positions on the cutterhead

$$H_{ri} = \frac{\sum H_{ni}}{N_{tbm} \cdot H_{ni}} \tag{8}$$

where

H_{ri} = relative cutter ring life of position no. i
H_{ni} = number of cutter rings used at position no. i

$$f_D = \frac{\sum H_{ri}}{N_{tbm}} \tag{9}$$

where

f_D = cutterhead factor

$$k_D = \frac{f_D}{f_{D0}} \tag{10}$$

where

k_D = correction factor for TBM diameter with regard to cutter ring life

f_{D0} = cutterhead factor of the reference cutterhead

The correction factor for TBM diameter has been analysed. For detailed discussion, see section 4.1.7-cutter life.

Correction for cutterhead velocity (rpm)

Cutter ring life is inversely proportional to cutterhead velocity, based on the assumption that for a given set of lithological conditions, lifetime is proportional to rolling distance and independent of rolling velocity. The correction factor for varying cutterhead velocity is shown in equation (11).

$$k_{rpm} = \frac{42 / d_{tbm}}{rpm} \tag{11}$$

where

d_{tbm} = TBM cutterhead diameter (m)
rpm = cutterhead velocity (updated as part of this thesis)

The influence of cutterhead velocity on hard rock tunnelling has been analysed as part of this study, resulting in a new recommendation for applied cutterhead velocities (rpm). This has already been included in the velocity correction factor (new constant value is 42).

Correction for the number of cutters

When the actual number of cutters on a cutterhead differs from the model, the average lifetime of an individual cutter will change. The correction factor is expressed by equation (12):

$$k_N = \frac{N_{tbm}}{N_0} \tag{12}$$

where

N_{tbm} = actual number of cutters
N_0 = standard number of cutters (updated as part of this thesis)

Correction for abrasive minerals

Cutter ring life varies with the relative proportions of quartz and other hard and abrasive minerals, such as garnet, epidote, olivine, pyrite, etc., contained in the rock under excavation. Figure 42 shows a correction factor applied as a function of quartz content only (Bruland, 2000b). Experience at NTNU has shown that the content of minerals such as garnet, epidote, olivine, pyrite, etc., can be incorporated with quartz content when estimating cutter ring life from the plot in Figure 42. Other abrasive minerals are going to be considered in the

calculations and the shape of the curve for rock types of group I to be analysed in this research work.

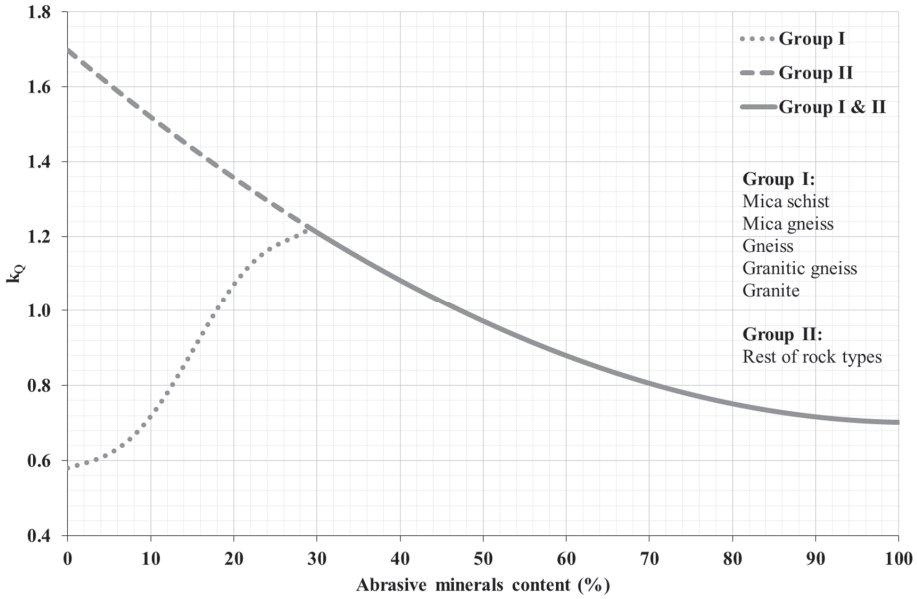

Figure 42. Correction factor for abrasive minerals (k_Q) modified from Bruland (2000b)

The average life of cutter rings is given by Equations (13), (14) and (15) below according to Bruland (2000b).

$$H_h = (H_0 \cdot k_D \cdot k_Q \cdot k_{rpm} \cdot k_N) / N_{tbm} \quad \text{(h/ c)} \tag{13}$$

$$H_m = H_h \cdot I_n \quad \text{(m/c)} \tag{14}$$

$$H_f = H_h \cdot I_n \cdot \pi \cdot d_{tbm}^2 / 4 \quad \text{(sm}^3\text{/c)} \tag{15}$$

where

H_0 = basic average cutter ring life (hours)
H_h = average cutter ring life (hours)
H_m = average cutter ring life (metres).
H_f = average cutter ring life (solid cubic metres)
I_n = net penetration rate
d_{tbm} = TBM diameter

H_0 expresses the lifetime of an individual cutter ring located at the average cutter position (≈ $0.59 \cdot r_{tbm}$) in machine hours. For example, for a CLI value of 8 and a quartz content of 35%,

an individual 483 mm diameter cutter ring in position 29 on a 7-metre diameter TBM with standard machine parameters will have a basic cutter ring life of approximately 135 hours.

Uncertainty analysis for basic cutter ring life

As previously discussed, basic cutter ring life depends on several parameters. Calculations of basic cutter ring life related to the CLI require an uncertainty analysis to be carried out if useful predictions are to be made.

For a given TBM and geology, the following parameters may be expected to exhibit some uncertainty:

CLI
Abrasive minerals content
Uncertainty

Evaluating uncertainty of rock properties should be based on using percentiles. Variation of 15 % of the cumulative distribution of CLI and quartz content (Bruland, 2000i) is used. For uncertainty due to ring steel quality, set bearing capacity and others, variation of 10 % is applied. Figure 43 illustrates the levels of uncertainty for these parameters.

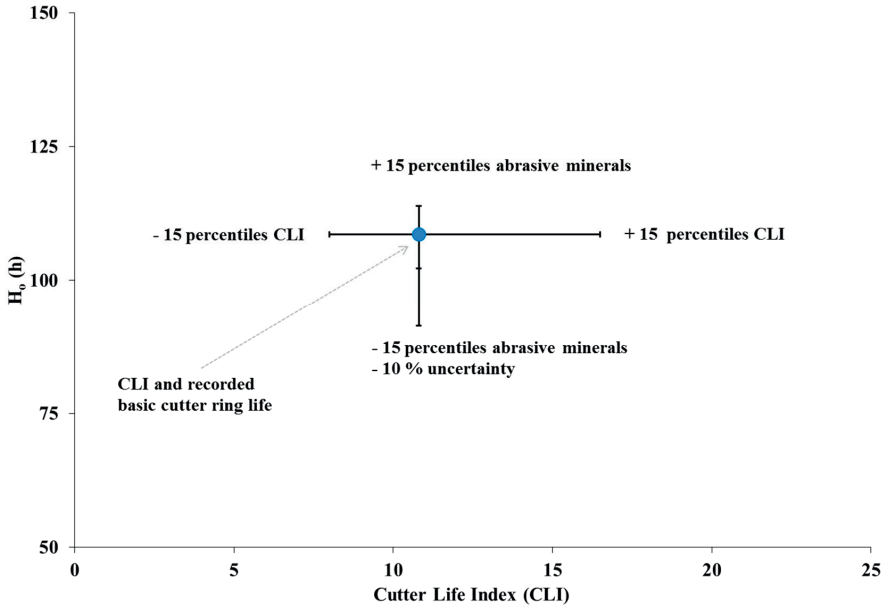

Figure 43. Methodology for estimating levels of uncertainty in connection with cutter life.

3.4 Field Trials

3.4.1 General remarks

Field trials conducted in connection with this study have involved two types of test; (1) the commonly used penetration test and (2) the so-called 'RPM test' introduced in this thesis.

The main purpose of performing field trials and tests is to evaluate machine performance under a given set of geological conditions. Field trials should be followed by detailed engineering geological mapping and rock sampling for drillability testing.

The test procedures and processing of data from the penetration and 'RPM tests' are described in the following. Examples of trial tests are included. Chip analyses methodology has been performed according to the recommendations of Bruland (2000e).

Penetration curve

The penetration rate estimation model is based on normalised penetration curves obtained from penetration tests carried out under a variety of rock mass conditions. A power function, equation (16) below, has been shown to provide the best fit to the data (Bruland, 2000e).

$$i_0 = \left(\frac{M_t}{M_1} \right)^b \quad \text{(mm/ rev)} \tag{16}$$

where

i_0 = basic penetration rate (mm/rev)
M_t = gross average cutter thrust at each thrust level (kN/cutter)
M_1 = critical cutter thrust (kN/cutter) required to achieve 1 mm/rev
b = penetration coefficient

The values of M_1 and b are found by linear regression of the $\log_{10}$ values of thrust and penetration. These values should fit to a straight line providing a linear regression expressed in equation (10):

$$\log_{10}(i_0) = A_R \cdot \log_{10}(M_t) + B_R \tag{17}$$

where A_R and B_R are the regression constants.

The $\log_{10}$ value of the equation for the basic net penetration rate results in equation (15):

$$\log_{10}(i_0) = b \cdot \left(\log_{10}(M_t) - \log_{10}(M_1) \right) \tag{18}$$

Since M_1 is the critical cutter thrust required to achieve 1 mm/rev, then by solving equation (12):

$$M_1 = 10^{-\frac{B_R}{A_R}} \tag{19}$$

the value of b is found by setting equation (17) = equation (18) and substituting M_1 with equation (19):

$$b = A_R \tag{20}$$

3.4.2 Penetration tests

A penetration test consists of a measurement of cutterhead penetration over a given time at a variety of logged thrust levels carried out at constant cutterhead velocity (Bruland, 2000e). The cutterhead torque for each cutter load level is also noted. Logging includes the measurement or recording of net penetration rate, cutter thrust level and cutterhead torque for the preceding and subsequent strokes. Other relevant data such as cutter wear state and cutterhead vibration level are also recorded, together with a note as to whether the test is performed at the start, middle or end of the stroke.

Chip samples are taken when possible for the stroke linked to the penetration test itself, and for the preceding and subsequent strokes.

A penetration test should include at least four thrust levels, including the maximum applied on site (M_{B100}). Rounded thrust level values, expressed in kN/cutter, are selected as follows:

- M_{t1} 0.70 ⇄ M_{B100}
- M_{t2} 0.80 ⇄ M_{B100}
- M_{t3} 0.90 ⇄ M_{B100}
- M_{t4} 1.00 ⇄ M_{B100}
- M_{t5} 1.05 ⇄ M_{B100}

A fifth thrust level is recommended if parameters such as cutter life and available torque so dictate.

For each thrust level, penetration is measured over a period corresponding to approximately 30 revolutions of the cutterhead. Thrust levels must be stabilised before measurement commences.

To ensure the quality of the test, the operator must maintain a constant thrust level during each step. The thrust level applied must be recorded for each step of the test and averaged over time.

As an illustration, the data and a plot from two of the penetration tests included in this thesis are presented below. Table 18 summarises the data for one of the penetration test example.

Table 18. Cutter thrust and basic penetration data for a penetration test example.

Cutter thrust M_t (kN/cutter)	Basic penetration i_0 (mm/rev)	Log_{10} M_t	Log_{10} i_0
303	8.2	2.48	0.91
263	6.6	2.42	0.82
229	4.5	2.36	0.65
214	4.3	2.33	0.63
200	3.7	2.30	0.57

Figure 44 shows the penetration curves for two penetration tests.

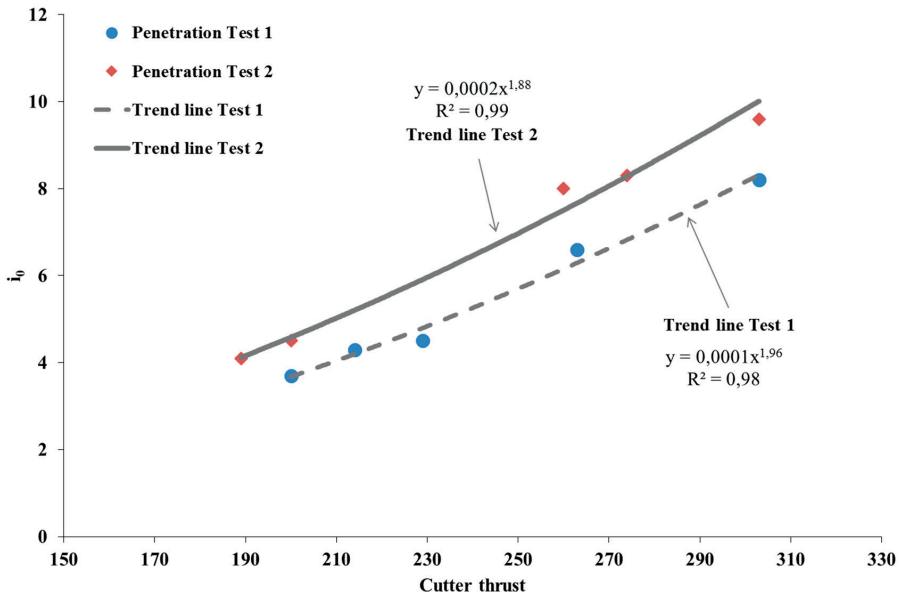

Figure 44. Plot of the penetration curve for two penetration tests.

When data from a penetration test is plotted in a log-log diagram, it is possible to get a quick evaluation of the test and to get a rough estimate of the parameters M_1 and b. Figure 45 displays a plot of the log_{10} values.

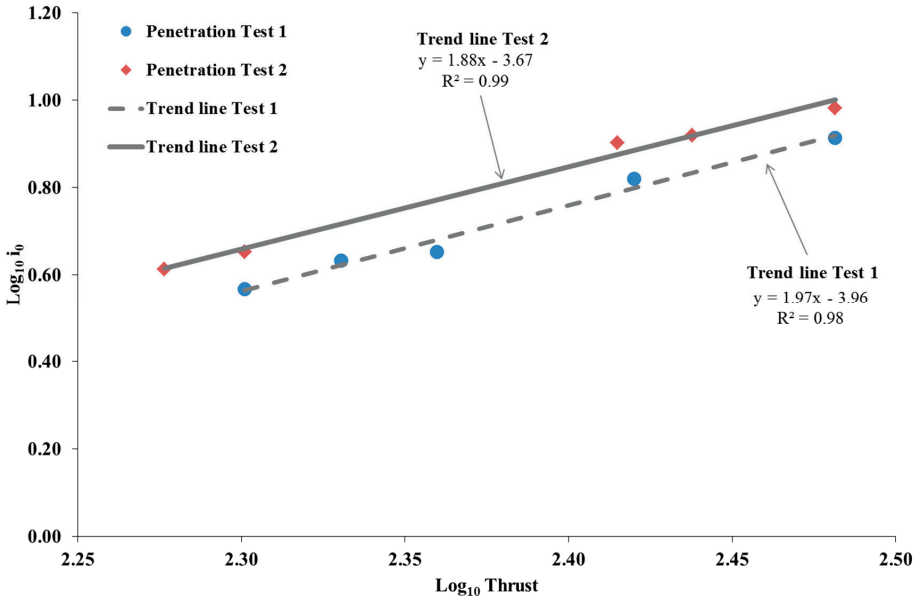

Figure 45. Plot of $\log_{10}$ values for M_1 and i_0 for two penetration tests.

The M_1 and b values for test 1 are 89 kN/cutter and 1.88 respectively, and for test 2, 103 kN/cutter and 1.97.

3.4.3 RPM tests

In order to evaluate the possible influence of cutterhead velocity (rpm) on penetration rate (PR, expressed in mm/rev) and net penetration rate (NPR, expressed in m/h), a full-scale trial test called the 'RPM test' has been introduced for this purpose.

An 'RPM test' measures cutterhead penetration over a given period at a variety of cutterhead velocities under constant cutterhead thrust. The aim of the test is to evaluate the influence of cutterhead velocity (rpm) on penetration rate (mm/rev) for maximum net penetration rates (m/h) for a given machine, geology and thrust level.

The proposed 'RPM test' procedure consists of the following steps:

1) Measurement of cutterhead penetration, penetration rate (mm/rev) and net penetration rate (m/h) at various velocities and constant thrust.

2) Rock mass assessment for the geology in question by means of (a) collecting rock samples for drillability testing and (b) chip sample analysis.

3) Recording of relevant data such as state of cutter wear, test time with respect to stroke torque, cutterhead vibration level, etc.

Parameters such as average net penetration rate, penetration rate and thrust must be averaged over the time taken for the tests. Machines equipped with continuous data logging permit better post-analysis of trial tests.

Several cutterhead velocity levels should be included in the tests. A minimum of four is recommended and this has been used as a guide during this study. The maximum and minimum cutterhead velocity value must be determined from tunnelling experience under similar conditions. Initially, the range of the four cutterhead rpms values selected should be as large as possible.

For each velocity selected, adequate boring time is required in order to achieve representative penetration values that are not influenced by previous cutterhead rpm levels. It has been experienced a clearer influence when testing over long or even complete strokes for each rpm level, which is in good agreement with Bruland (2000e).

The duration maintained for each cutterhead rpm level should be at least 3 minutes for small (e.g. 3 - 4-metre diameter), and 10 minutes for larger (e.g. 7 to 12-metre diameter) TBMs. Both cutterhead velocity and thrust must to be stabilised for each cutterhead rpm level. An analysis of net penetration rate, cutterhead velocity and cutter thrust must be carried out for the preceding and subsequent strokes.

The resulting values are penetration rate and net penetration rate for each ‘RPM test’ at constant thrust. These values are correlated using a trend line. The resulting equations are used to calculate the initial point of the ‘RPM test’, the optimal cutterhead velocity and the corresponding penetration rate for the final recommended cutterhead velocity.

‘RPM tests’ provide a cutterhead velocity value that results in a maximum NPR for a given machine, thrust and set of geological conditions. A range of NPR values lying within 5% of the maximum NPR can be defined. Once the maximum NPR is defined, the corresponding cutterhead rpm and penetration rate (mm/rev) can be set.

For rpm values greater and less than the maximum, the NPR is reduced. The penetration rate is reduced at higher cutterhead velocities. At lower rpms, PR increases up to one rpm level, after which it decreases dramatically, resulting in a corresponding reduction in the NPR. Figure 46 shows an example of an ‘RPM test’ included in this thesis.

The 'optimal' rpm is selected as the lower rpm with 5% less net penetration rate than the maximum. Figure 46 shows an example of an ‘RPM test’ included in this thesis.

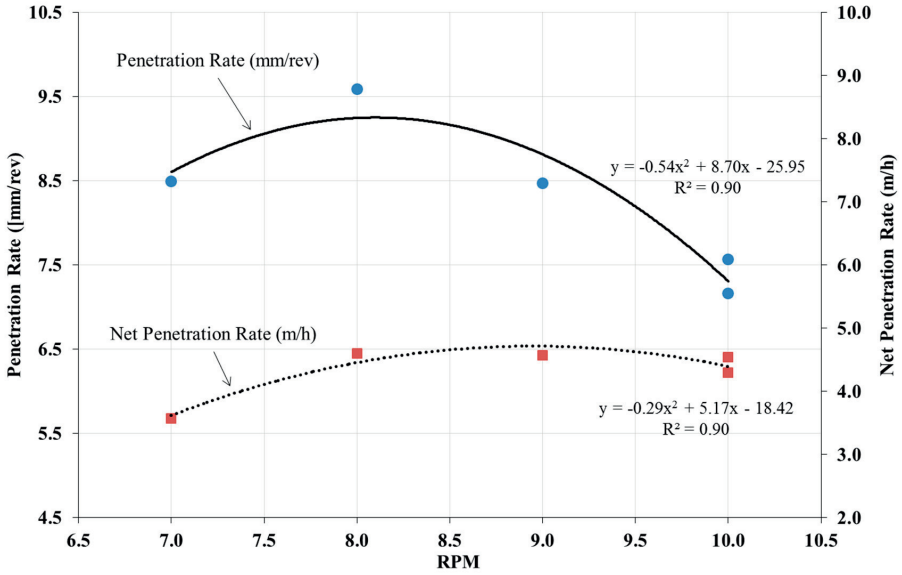

Figure 46. An example of a graph resulting from an 'RPM test' included in this thesis (reproduced from Eide, 2014).

For the initial, and for lower values, the penetration rate (mm/rev) remains increasing, whereas net penetration rate values (m/h) exhibit slight decreases. This behaviour indicates an efficiency increment during boring.

The results are normalised based on the recommended cutterhead velocity for each TBM diameter included in this thesis (see Section 4.1.2). Relative cutterhead rpm and PR values are used as shown in equations (21) and (22) below.

$$Relative_{rpm} = \frac{rpm}{Recommended\_rpm} \tag{21}$$

$$Relative_{PR} = \frac{PR}{Recommended\_PR} \tag{22}$$

The PR values correspond to those from the relevant 'RPM tests'.

The main results are presented in a graph plotted on the basis of 'RPM test' data from the previous example (Figure 47).

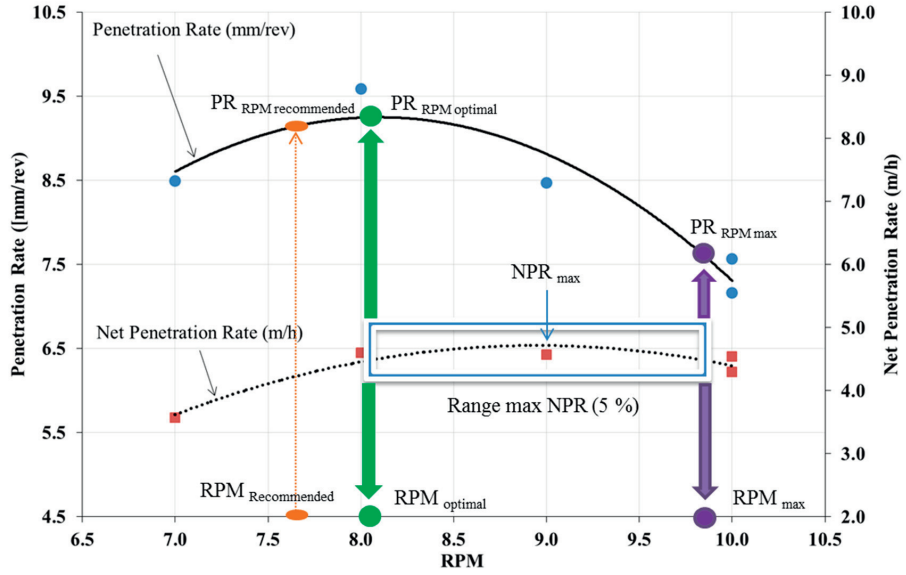

Figure 47. An example of 'RPM test' results. Vertical lines (from right to left) denote the start of the test, the cutterhead rpm reference and the cutterhead rpm optimal.

Figure 48 shows the results of a normalised 'RPM test' using data from the same example; maximum and optimal relative cutterhead rpm and penetration rate (PR) values are denoted by points.

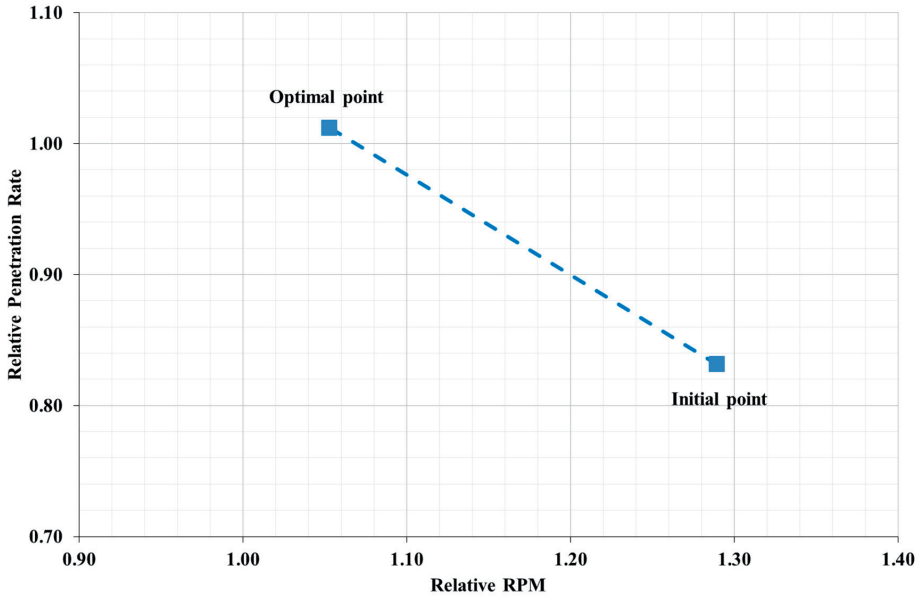

Figure 48. An example of normalized 'RPM test'.

The slope of the line in Figure 48 indicates the relative improvement in penetration rates resulting from application of the optimum cutterhead velocity. The greater the slope gradient, the greater the influence of cutterhead rpm on penetration rate.

3.5 Laboratory research

3.5.1 General remarks

Laboratory research linked to this thesis includes the use of established laboratory test methodologies, combined with the development of a new laboratory test method for rock abrasivity.

Several laboratory test methods have been used during this study in order to achieve its main objectives. Table 19 provides a summary of these methods and their corresponding references.

Table 19. Laboratory test methods used in this study.

	Test method	Reference
Rock Laboratory Tests	Density	ISRM (1978)
	Uniaxial Compressive Strength (UCS)	ISRM (1979)
	Point Load Test (PLT)	ISRM (1985)
	Brittleness Test Method (S_{20})	Dahl et al. (2012)
	Sievers'J miniature drill test (SJ)	Dahl et al. (2012)
	Abrasion Value Cutter Steel Test (AVS)	Dahl et al. (2012)
	Cerchar Test (CAI)	ASTM (2010), ISRM (2014)
	Soft Ground Abrasion Tester (SGAT)*	Jakobsen et al. (2013)
Tribocorrosion Tests	Reciprocating ball on plate test	Stachowiak and Batchelor (2005), Espallargas et al. (2015)
	Wet Rubber Wheel Test	Espallargas et al. (2015)
Hardness Tests	Vickers Hardness Test (VH)	ASTM E92-82(2003)
	Rockwell Hardness Test	ASTM E18 – 14a

* Modified for use with crushed rock

In addition, X-ray diffraction (XRD) method (Klug and Alexander, 1974) was employed to determine mineral compositions.

Drillability and strength tests (UCS, PLT) were performed in the NTNU/SINTEF laboratory in Trondheim in Norway. Some of the UCS tests were performed at the laboratory of the Chair of Engineering Geology at the Technical University of Munich in Germany, and at the Faculty of Geology at the University of Oviedo in Spain.

Tribocorrosion and hardness tests were performed at the NTNU/SINTEF Tribology Lab in Trondheim in Norway. Metallography and tempering experiments were carried out at the department of engineering design and materials.

Reliable results, combined with a representative selection of rock types, have been considered to be of key importance to this study.

3.5.2 Soft Ground Abrasion Tester using crushed rock samples (SGAT-CR)

The development of the Soft Ground Abrasion Tester (SGAT) was carried out by Jakobsen (2014) in order to assess the abrasion testing of similar in-situ soft ground conditions, and to increase the validity of tool life testing.

During the early stages of this study, tests were carried out to investigate the applicability of the SGAT in assessing rock abrasivity using samples of crushed rock. Several modifications of the tool design and testing parameters were introduced in order to adapt the testing procedure to the new sample conditions.

The current version of the SGAT apparatus includes a drive unit that provides both rotational and vertical movement (Figure 49).

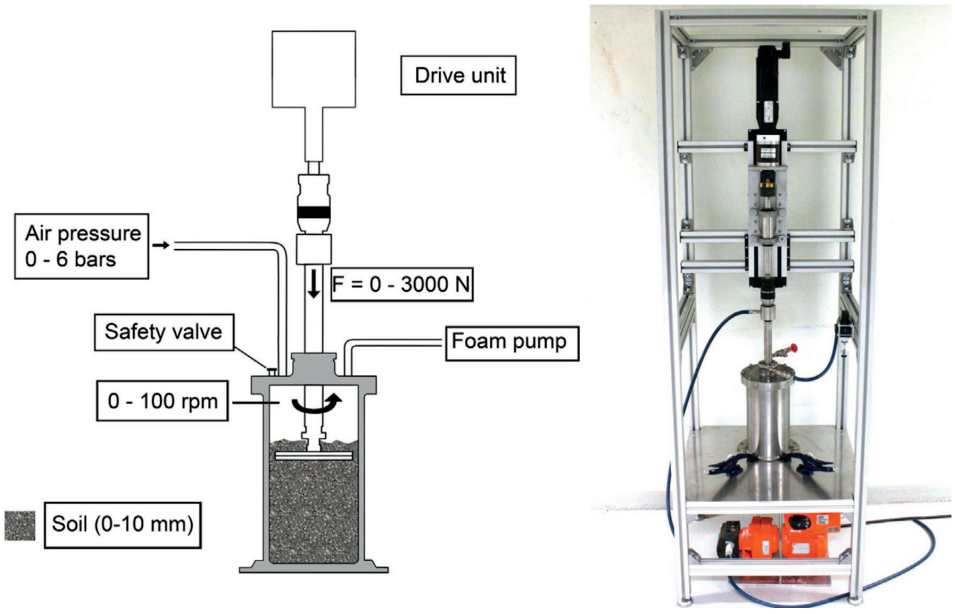

Figure 49. Diagram (left) showing the Soft Ground Abrasion Tester (SGAT) and photo (right) of the test rig (from Jakobsen et al., 2013).

After several attempts, the tool was eventually successfully adapted using a single 8-centimetre long steel bar. The bar was made of carbon steel with a Rockwell Hardness (HRC) of 20, and is thus similar to that introduced by Jakobsen et al. (2013). Figure 50 illustrates the new tool design.

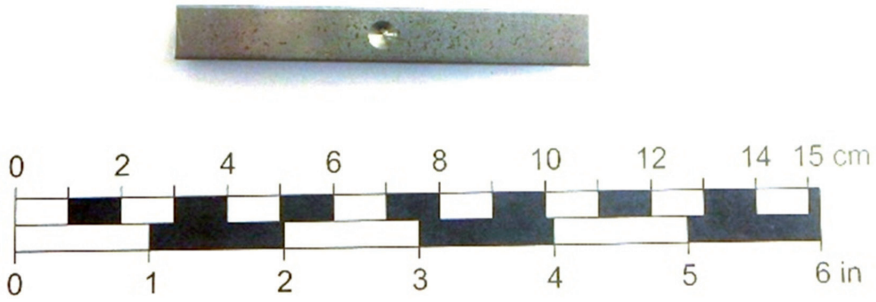

Figure 50. The drilling tool used for testing the SGAT using crushed rock samples. The test piece is 8 centimetres long with a 1 x 1 cm cross-section.

The tool was designed in order to have single use of new edges of the steel bar tools in the testing direction.

Previous experience at NTNU/SINTEF guided the study to use the rock type 'Iddefjord granite' for all the tests due its homogeneity and high abrasivity, as well as its ability to provide consistent results in other abrasivity tests. Several samples sizes were used during testing. Table 20 shows the relevant strength and abrasive rock properties of the Iddefjord granite.

Table 20. Main properties of the Iddefjord granite.

Property	Value
Density (g/cm^3)	2.6
UCS (MPa)	188.0
S_{20}	61.9
SJ	5.0
AVS	31.5
DRI	58.0
CLI	6.8
CAI_s	3.4

Figure 51. The Iddefjord granite. A crushed rock sample (left) and intact rock (right).

Two test methodologies were proposed, involving three fraction size samples and three rotation speeds (Table 21), combined with the testing of four grain size distributions at a constant rotation speed of 50 rpm (Table 23).

Three rotation speeds were employed during the tests (30, 50 and 70 rpm). Tool penetration was about 8 cm, with a penetration rate of 10 mm/min.

Table 21. Fraction sizes used for testing of the SGAT with crushed rock samples. Testing was performed at three different rotation speeds (30, 50 and 70 rpm) and at a constant advance rate of 10 mm/min.

Sample	Fraction size
A	0 – 5 mm
B	0 – 10 mm
C	4 – 6 mm

Table 22. Proposed fraction size distributions for the samples (A, B, C and D) of Iddefjord granite prior to testing using the SGAT-CR method. The rotation speed was 50 rpm.

Fraction size (mm)	Sample A (% pass)	Sample B (% pass)	Sample C (% pass)	Sample D (% pass)
9.5	100 %	100 %	100 %	100 %
8.0	98 %	84 %	74 %	50 %
6.3	90 %	71 %	50 %	25 %
4.0	75 %	53 %	30 %	10 %
2.0	50 %	34 %	16 %	3 %
0.01	0 %	0 %	0 %	0 %

The rock samples were crushed and sieved to obtain the different fraction sizes prior to filling the test bucket. Checks were made to ensure that the tool was properly embedded in the sample material prior to testing (Figure 52).

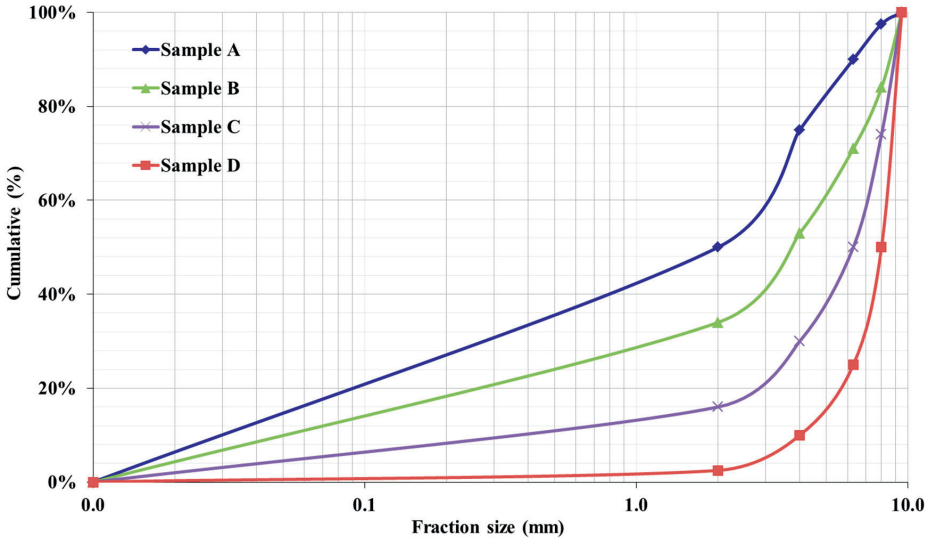

Figure 52. Proposed trends of the curves for samples A, B, C and D during SGAT-CR testing.

The results are expressed as the weight loss of the steel tool pieces (measured in mg) subsequent to testing. A minimum of three parallel tests were performed in order to obtain a representative average value.

3.5.3 Development of a new rock abrasivity test method – the Rolling Indentation Abrasion Test (RIAT)

This test procedure has been published previously (see papers VII and VIII). Paper VII describes preliminary testing procedures and paper VIII provides a detailed description of the final procedure using a greater variety of rock types than were used in the preliminary tests.

Testing procedure

The rolling velocity was set at 40 rpm with a standard thrust of 1,250 N. These values, discussed below, have been determined on the basis of real hard rock TBM cutter parameters and experience from previous evaluations. The tip width of the mini-cutters used in these tests is constant (4 mm) and the cutters are made of the AISI Type H13 Hot Work Tool Steel, which is the common basic alloy used for actual TBM cutter rings. The alloy has a Rockwell Hardness (HRC) of 50±1.

The main parameters used for the tests are given in Table 23.

Table 23. Main parameters for the RIAT method

Parameter	Value
Thrust (N)	1,250
Rolling velocity (rpm)	40
Testing time (min)	30

Figure 53 presents the outputs from the RIAT method.

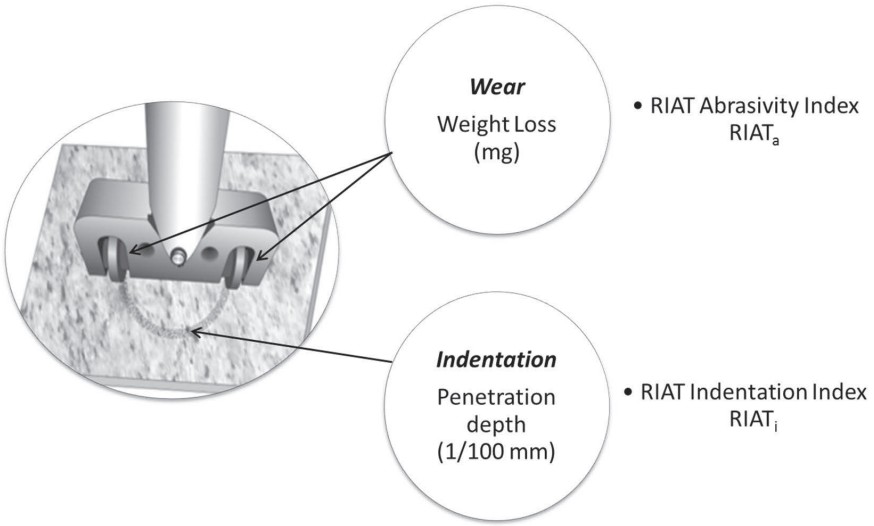

Figure 53. Outputs from the RIAT method

The RIAT Abrasivity Index ($RIAT_a$) is defined as the weight loss (in mg) incurred by a miniature cutter ring during a RIAT. A minimum of three tests are performed in order to obtain a representative average value. Dust and other debris should be removed from the track during testing using a combination of compressed air and suction. This also ensures that the tools are in constant contact with the intact rock.

In addition to cutter weight loss, a measurement is made of the penetration of the miniature cutters into the intact rock sample. The penetration value from a RIAT thus provides an indication of the indentation resistance or rock surface hardness. The RIAT Indentation Index ($RIAT_i$) is defined as the average value of ten evenly distributed measurements of cutter penetration depth (measured in 1/100 mm).

The tool dimensions were selected to accommodate testing on relatively small samples. The rolling diameter of the tool, or distance between cutters, is 60 mm. It is possible to use core samples, blocks, or any shape that complies with minimum size criteria.

Several different tool designs were tried out during the initial development of the RIAT. Figure 54 shows the various versions of tools used.

Figure 54. Versions of tools used during development of the Rolling Indentation Abrasion Test (RIAT) method. From left (initial) to right (current).

The RIAT miniature cutters have been developed according to actual TBM cutter ring standards.

In order to simulate as realistic conditions as possible during the tests, tool and other dimensions, and test parameters (rolling velocity and cutter thrust), have been determined on the basis of actual tunnelling conditions. To achieve this, an analysis of machine dimensions and main parameters covering the main range of diameters of hard rock TBMs has been carried out.

Mini-cutter diameters are restricted in order to produce rolling, but not torsion. Several tip widths were tried out with the intention of achieving as wide a tip as possible within the constraints of a reasonable diameter/tip width ratio. This ensures that a greater rate of wear is achieved and also facilitates additional wear analysis of the worn surface. Figure 55 shows the relationship between actual cutter diameters and the diameter/tip width ratio. Cutter diameters range from 381 to 508mm for hard rock TBMs, while 165 mm applies to the mini-TBM. The diameter/tip width ratio for the RIAT miniature cutters is in good accordance with actual TBM cutter performance.

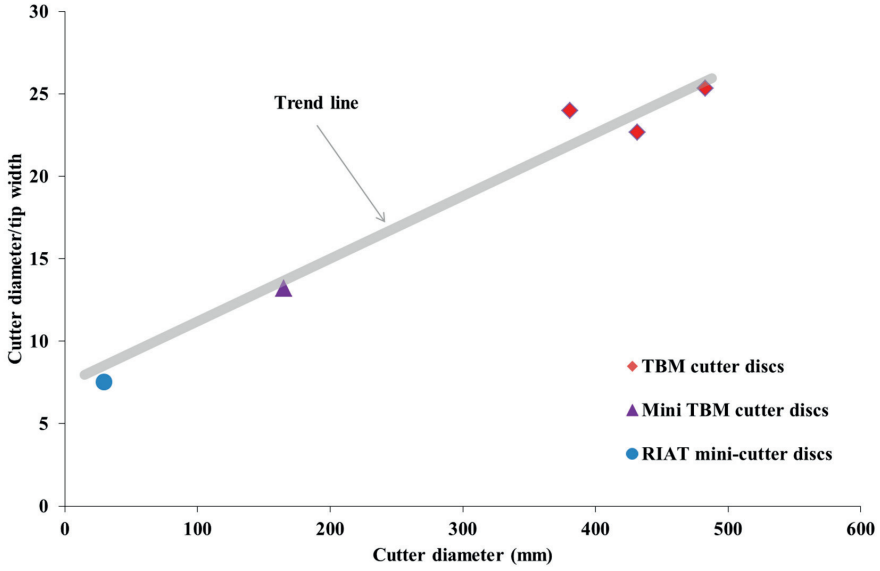

Figure 55. Relationship between cutter diameter and diameter/tip width ratio for real TBM cases (a mini-TBM with a 0.6 m diameter cutter has been included). Extrapolation to test scale shows that the diameter/tip width ratio of miniature cutters is in accordance with real TBM performance.

An attempt was made as part of the RIAT to simulate real TBM cutter rolling velocities. Cutter rolling velocities for real TBMs vary from 2.3 to 2.9 m/s for gauge cutters, and from 1.4 to 1.7 m/s for the average cutter position. In order to achieve the same rolling velocity using RIAT tool dimensions, the rotation speed of the RIAT tool would have to be in the range 30 to 57 rpm, so it was decided to perform the test at 40 rpm.

The estimated thrust required to produce the same average contact pressure is not easy to calculate because the indentation parameter is not measurable by any existing practical method (Bruland, 2000f). However, the approximate stress on the contact area for a simple roller disc cutter of uniform thickness, rolling along a rock surface under constant thrust and producing a constant depth of penetration, can be estimated using the approach outlined by Lislerud (1997).

Estimates of 300 MPa have been made as approximate theoretical stress levels in the contact area of actual TBM cutters producing typical penetration values. On the basis of the low penetration values (< 0.01 mm) achieved during a RIAT, and according to Lislerud (1997), the approximate thrust required to achieve stress levels equivalent to those produced by real TBMs was estimated to be 625 N. Considering the two cutters involved in the RIAT, the total thrust involved in the test is estimated to be 1,250 N. Initially, several thrust levels were tried out in order to avoid causing deformation ("mushrooming" effect) on the tips of the mini-cutter rings due to excess stress.

Samples

The RIAT is performed on an intact rock sample. The sample should be cut and ground in order to provide optimal leverage of the surface, and of a minimum size equivalent to a 100 mm-diameter core sample. However, the design of the tool enables minor deviations from these criteria to be accommodated.

Initial testing has been performed as part of the early development of the RIAT. Eight rock types, exhibiting a wide range of hard rock abrasivity (from low to high) were selected to test the method – limestone, basalt, Basalt Xiamen, Trondhjemite (tonalite), Rosa Porriño (RP) granite, Iddefjord granite, Gris Mondariz (GM) granite and quartzite. Figure 56 shows the appearance of some of the samples after the RIAT was carried out.

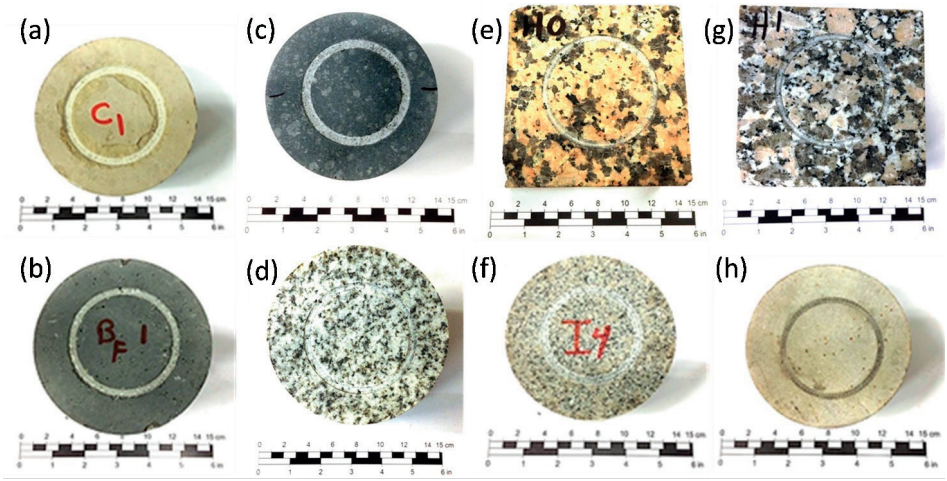

Figure 56. Rock samples after testing using the RIAT. (a) limestone, (b) basalt, (c) Basalt Xiamen, (d) Trondhjemite (tonalite), (e) Rosa Porriño granite (RP granite), (f) Iddefjord granite, (g) Gris Mondariz granite (GM granite) and (h) quartzite.

Rock samples were selected on the basis of initial test results (see Paper VII) and the fact that their abrasivity values cover much of the common rock abrasivity range.

3.5.4 Experiments to investigate cutter wear mechanisms

Worn TBM cutter ring samples from one of the TBM projects included in this thesis and worn mini-cutter rings from a RIAT have been investigated for cutter wear. For further details concerning the RIAT, the reader is referred to chapter 4.2.2 and papers VII and VIII included this thesis.

The experiments have been performed in collaboration with the Tribology group at the Department of Engineering Design and Materials at NTNU, headed by Professor Nuria Espallargas and some of her department's Master's degree students.

Samples

The cutter rings were replaced due to excessive wear, and the samples taken have an initial diameter of 483 mm. Data regarding their position on the cutterhead, instantaneous cutter life and rock mass properties were obtained.

The RIAT mini-cutter discs used in the test are 30 mm in diameter with tip widths of 4 mm. The test is performed on an intact rock sample.

Table 24 provides an overview of the analyses and tests performed on the TBM cutter ring and RIAT mini-cutter ring samples respectively.

Table 24. Overviews of the cutter ring wear analysis tests. The symbol "◯" indicates that a test has been performed, while the symbol "-" indicates that the test has not been performed.

Sample ID	Sample type	Rock Type	Composition	Hardness	Microstructure	FIB*	Tempering
01	TBM cutter	**-	-	◯	◯	◯	-
02	TBM cutter	**-	-	◯	◯	◯	-
03	TBM cutter	**-	-	◯	◯	◯	-
04	TBM cutter	**-	-	◯	◯	◯	-
05	TBM cutter	-	◯	◯	◯	-	◯
06, 07	RIAT cutter	Basalt	-	-	◯	◯	-
08, 09	RIAT cutter	Granite	-	-	◯	◯	-
10, 11, 12, 13	RIAT cutter	Granite	-	◯	◯	◯	-
14, 15, 16	RIAT cutter	Quartzite	-	-	◯	◯	-

*FIB = Focused Ion Beam
** Mica schist, mica gneiss, quarzitic gneiss

Figure 57 and Figure 58 show the worn TBM cutter ring and RIAT mini-cutter ring samples used during testing.

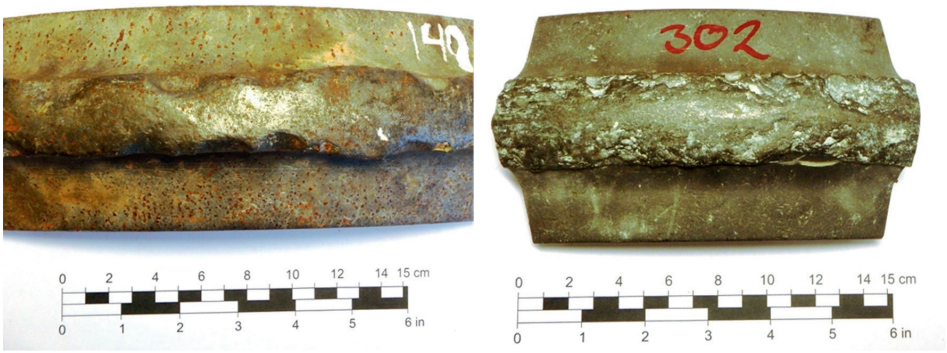

Figure 57. Cutter ring samples 01 (left) and 02 (right), taken from Project D.

Figure 58. Mini-cutter ring samples.

Metallography

Initial cutting of the sample slices from the cutter ring was performed using a large band saw with a WC grid blade. The saw was water-cooled to keep temperatures below 25°C. The slices were subsequently cut into smaller samples using a water-cooled Discotom-2 saw fitted with a circular blade.

The samples were then embedded in a two-component epoxy mixture "Epofix^{TM}" in a cylindrical mould for microscopic examination. These samples were 30 mm in diameter and 15 mm high. The circular surface of each cylindrical sample was ground with SiC paper and polished with a diamond suspension until a final roughness of less than 0.1 μm was achieved.

Sample preparation for optical microscopy also required an etching process in order to reveal the microstructure of the metallic samples as a prerequisite for investigating the phases present. Metallographic etchants have different functions depending on the components of the metal alloy. The following three etchants were used in the present study:

- Vilella's reagent
- Kalling's no. 2 reagent
- Marble's reagent

Table 25. Metallographic etchants used in preparation for optical imaging (Nærland, 2015).

Name	Content	Effect
Vilella's reagent	5 ml HCl (37%) 1 g picric acid 100 ml ethanol	Martensite is coloured. Ferrite, retained austenite and carbides unaffected.
Kalling's no. 2 reagent	50 ml HCl (37%) 50 ml ethanol 2 g $CuCl_2$	Martensite turns dark. Ferrite, retained austenite and carbides unaffected.
Marble's reagent	5 g $CuSO_4$ 50 ml HCl 50 ml water	Martensite turns dark. Ferrite, retained austenite and carbides unaffected.

Vilella's reagent provided a very favourable contrast between martensite and retained austenite. Unfortunately, its use at NTNU is restricted due to the risk of explosion, so most of the tests were performed under supervision at SINTEF. This etchant was used only as a datum against which to compare the quality and effect of other potential etchants.

The Kalling's no. 2 reagent provided results similar to those of the Vilella's reagent in areas removed from the very edges of the sample. During sample preparation, cracks readily formed at the interface between the metal and the epoxy. The high chloride concentration in this etchant resulted in crevice corrosion along these cracks, especially at the edges of the samples. For this reason, use of the Kalling's etchant was discontinued, but it is mentioned here as an option for possible future tests.

Marble's reagent also provided similar results to those of Vilella's etchant. This etchant is designed to reveal microstructure in Ni-alloys and super alloys. Some edge distortion was observed, but this can be explained by short etching times and modifications made to the concentrations of the etchant's active components. The etchant used in these tests had a lower $CuSO_4$ concentration than is recommended in original compositions.

A Leica MEF4M optical microscope (Figure 59) was used to obtain microstructure images. Lenses with 20X, 50X and 100X magnification were used. The magnification of the ocular lens on the camera is 10X, thus providing images of 200X, 500X and 1000X magnification respectively.

A Zeiss Ultra 55 Limited Edition scanning electron microscope (SEM) was used to obtain surface images at greater magnifications than those obtained by optical microscopy. Penetration of the sample by the electron beam excites electrons surrounding atoms on the surface of the rock. These are called secondary electrons and are used for surface imaging. An Everhart-Thornley detector was used to observe topography produced by the secondary electron signal. The setting 'low current mode' was used to provide better contrast, with an aperture of 20 mm was used to provide adequate depth of field.

A backscatter electron detector was used to detect elastically-reflected, backscattered electrons (BSE). These images reveal poor relief contrasts when compared to secondary electrons, but they do indicate which atoms are responsible for reflections resulting from atomic number (Z-contrast). Heavier atoms reflect more electrons than lighter ones, and thus appear as bright areas on the image.

Since an SEM was used for wear surface imaging, no surface grinding or polishing was needed. The samples were cut and cleaned prior to a five-minute period of ultrasonic bathing in acetone to remove dust, organic material and embedded rock debris from their surfaces.

When imaging microstructure, the microscope brightness was set at approximately 0%, and contrast at close to 100%. Large amounts of rock debris were still present on the surface after the ultrasonic bath. Non-conductive rock becomes charged during SEM imaging and the samples were therefore sputtered with gold to enhance conductivity and reduce image drift.

The microscope was also equipped with an Energy Dispersive Spectrometer (EDS). The EDS collects X-rays emitted from atoms in the sample and these are used to identify the elements present. Electrons in their ground state inhabit discrete energy levels in each atom. When struck by the electron beam, the electrons are excited from these levels leaving "electron-holes". Electrons further away from the nucleus will drop to lower energy levels in order to

fill the holes created, releasing excess energy in the form of X-rays. Each X-ray corresponds to a unique energy level and may therefore be used to identify the element in question. However, due to the large margins of error, the amount of each element present is difficult to measure precisely using this technique. In the present study, this approach was used only to identify the elements present in particles found in sample cross-sections.

In Focused Ion Beam (FIB) microscopy, ions are used to manipulate and image the sample. The use of ions enables surface manipulation of the sample by means of the deposition or sputtering away of material as imaging takes place. In this project, FIB microscopy was used to cut cross sections of the samples. These cross-sections were studied immediately after cutting without exposure to the air.

This study used an FEI Helios NanoLab DualBeam FIB microscope with a gallium source (Figure 59). The term 'DualBeam' indicates that in addition to a gallium source, the microscope is equipped with an electron source that enables standard SEM imaging.

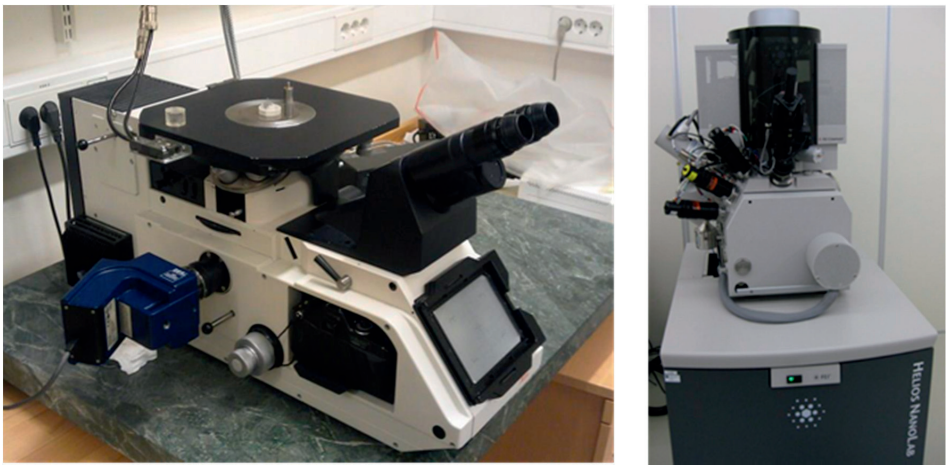

Figure 59. A Leica MEF4 optical microscope (right) and an FEI Helios NanoLab Dual Bean FIB microscope (left).

Cross-sectional cuts were made into the surfaces of the samples using Ga-ion milling. SEM imaging was used to study the nanocrystalline deformation layers in the samples by utilising secondary electrons. Samples prepared for FIB microscopy were cut using a Discotom-2 saw, followed by a five-minute ultrasonic bath in acetone. Table 26 provides an overview of the different milling parameters used.

The Ga-beam is cone-shaped with a radius proportional to the current output. A high current result in a wide cone while a low current provides a narrow one. To obtain meaningful results, the slope of the cross section should be as steep as possible. This is achieved by completing the cleaning process using a low current. Naturally, the efficiency of the milling is greater when higher currents are used, so a compromise is achieved by carrying out milling in a step-

wise fashion, using high currents at first, and then gradually decreasing the current as the milling area decreases. The final step results in a steep and even cross-sectional cut.

Table 26. Steps involved in the FIB microscopy milling process (Nærland, 2015).

Step	Description	Current
Carbon deposition	Creates a surface layer of carbon for smoother cross-sectional cuts.	21 nA
Rough cuts	Deep, coarse cuts made to expose cross-sections for further analysis. Deep trenches on either side of the carbon layer help to offload any removed atoms. Too shallow coarse cutting will result in shadowing.	21 nA
1st cleaning cut	Cuts into the carbon layer to straighten out the cross-section profile.	6.5 nA
2nd cleaning cut	Finalisation of the cross-section by additional straightening. Removal of surface stripes and cuts.	0.92 nA

Tempering experiment

A tempering experiment was performed to identify the evolution of hardness as a function of time and temperature, without including mechanical deformation. The samples were cut from an unused disc. Tempering was performed at 200, 300, 400, 500, 600 and 700°C.

Tempering is a process applied to hardened steels to achieve specific values of mechanical properties, as well as to relieve quenching stresses and ensure dimensional stability. The treatment requires heating the steel to temperatures between 250 and 650°C, depending on the properties required (Callister and Rethwisch, 2009). Hardness is reduced and ductility (negligible prior to tempering) is slightly increased.

Tempering is usually carried out following quenching from above the upper critical temperature. However, it is also used to relieve the stresses and reduce the hardness developed during welding, and to relieve stresses induced by forming and machining.

In the case of H13 and other tool steels, there will be retained austenite in the as quenched discs. Tempering, usually two times, transforms the austenite into tempered martensite. Retained austenite is undesirable because it can later transform under stress to martensite. The volume expansion associated with transformation from austenite to martensite can initiate brittle fracture. H13 discs are often tempered at the temperature corresponding with the peak of the secondary hardening curve. This secondary hardening peak is associated with the lowest ductility (Smading, 2016).

The effect of tempering is very time-dependant, and for it to be effective over short intervals of time, the starting temperature should be considerably higher than the upper critical temperature resulting in 'austenitization' process.

In this study, three samples were tested at each tempering temperature, using tempering periods of 1, 2 and 4 hours respectively. A Nabertherm N17 furnace was used for the tests (Nærland, 2015). No attempts were made to control the atmosphere inside the furnace. This will result in decarburization due to the presence of a lower carbon concentration in the air than in the steel. This phenomenon is consistent with normal TBM operations (during boring) and is therefore seen as a natural part of the experiment.

Each sample was cooled in air prior to examination. The effect of tempering was quantified by hardness measurements, which are described in the following section.

Hardness measurements

Macro-hardness measurements were carried out on TBM cutter ring samples and micro-hardness measurements on RIAT tested mini-cutter ring samples.

A Matsuzawa Seiki-DVK-1S hardness indenter (Figure 61) was used to perform the macro-hardness measurements. All measurements were carried out at 5 kgf, with the results expressed in HV5. Digital positioning of the optical microscope stage was used to measure the distance from the edge of the sample surface to the indentations, made along parallel lines extending from the edge of each sample. Three lines of indentations were measured for each sample in order to obtain an average (Figure 60).

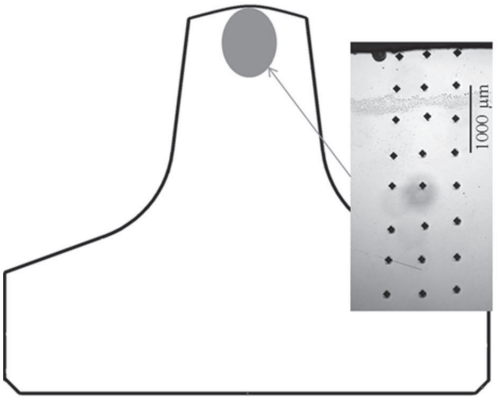

Figure 60. Image showing hardness indentations on a TBM cutter ring sample.

In the case of hardness measurements made after tempering, each sample was given ten indents, and an average value obtained. The Leica VMHT MOT micro-hardness indenter (Figure 61) was used to measure the hardness profiles of RIAT mini-cutter samples. The process was similar to that described above except for the distance from indentation to

surface. This was carried out manually by moving the sample stage by a pre-defined distance for each measurement. The measurements were performed at 0.025 kgf, with the results expressed in HV0.025.

Figure 61. The Matsuzawa macro-hardness indenter (left) and the Leica VMHT MOT micro-hardness indenter (right).

Tribocorrosion testing

A tribocorrosion test rig was used to evaluate the abrasion-corrosion performance of cutter steels on exposure to different chemical and geological media in hard rock systems. This consisted of a reciprocating ball-on-plate (sliding wear) test rig (Figure 62).

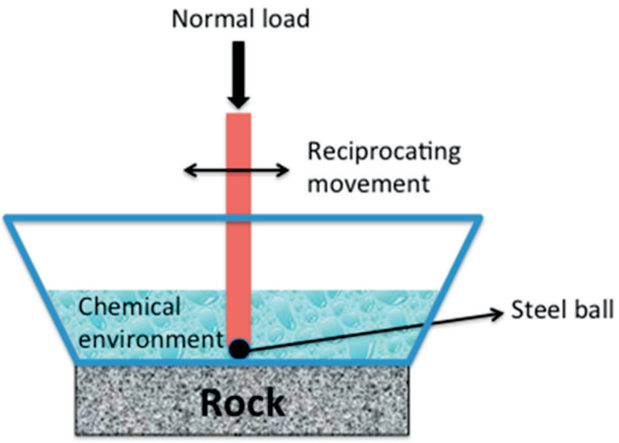

Figure 62. A tribocorrosion test rig (see paper IX).

Tests are performed by sliding a 6 mm-diameter steel ball (made from a steel disc taken from a TBM cutter ring) back and forth across the rock sample surface using a stroke length of 10 mm (Figure 62).

Table 27 summarises the main parameters used during the tribocorrosion test.

Table 27. Summary of the main parameters used for the tribocorrosion test.

Parameter	Value
Normal load (N)	5
Stroke length (mm)	10
Frequency (Hz)	1
Test period (min)	60

The normal load value was chosen on the basis of common stress indentation values using a cutter disc from a hard rock TBM under a thrust of 400 MPa. According to Hertz's theory of contact, and given the geometry proposed in this study, this corresponds to a normal load of 5 N (Stachowiak and Batchelor 2005). During the tests the rock material was exposed to a variety of ambient media; a) dry conditions, b) water obtained from the same site as the rock, c) distilled water, and d) a foam made using a 3% solution of conditioning additives in water (see paper IX for more details). The friction coefficient between the rock and steel ball was recorded for each test. All tests were performed at least twice in order to check their repeatability.

Samples

Samples obtained from field sites were tested using two tribocorrosion rigs, both adapted to accommodate geological materials.

The cutter tool steel used in the tests is defined as a hard rock tool steel – H13 (AISI 2013). The abrasive materials were derived from a hard rock sample from one of the projects included in this thesis. Table 28 presents a summary of all the field materials used and the corresponding tests and measurements performed.

Table 28. Summary of materials used during the tribocorrosion tests (see paper XI).

Material	**Steel**	**Rock**	**Water**	**Conditioning additives**
Nomenclature	**H13**	**Project A**	**Scandinavian site**	**ABR5 and SLF41**
Abrasiveness (AVS)	n/a	Yes	n/a	n/a
Hardness	Yes	Yes	n/a	n/a
Composition	Yes	Yes	Yes	Yes
pH	n/a	n/a	Yes	Yes
Tribocorrosion (sliding)	Yes	Yes	n/a	n/a

Individual water samples are expected to vary in their chemical content. Chloride content determines corrosion rates in metals (including cutter disc steels), so this factor is expected to have a major influence on tribocorrosion. The highest corrosion rates in air-saturated water are achieved at concentrations of 3.4 wt.% chloride, which is the same as that in seawater (Winston and Uhlig 2008). Real tunnelling projects occasionally use soil conditioners or anti-wear additives to prolong cutter tool life. Therefore, in this study tests have been performed using two different additive types manufactured by BASF Construction Chemicals; (1) ABR 5 – designed for hard rock (Anti-wear 2013) and (2) SLF41 – designed for soft ground/soils (Soil 2013). The concentrations of the additives used, and their physical state, have been selected to conform to real project situations, i.e., as foams comprising 3% concentrations in the liquid media (water or seawater) in question.

4 Results and discussion

This section presents the results that constitute the main findings of this PhD research study, from which the main contributions are:

- a revision and extension of the NTNU prediction model for performance and cutter life for hard rock TBMs.
- the development of a new rock abrasivity test method for tool life assessments on hard rock tunnel boring.
- an analysis of TBM cutter and RIAT mini-cutter ring wear mechanisms.

As yet unpublished results will be presented in more detail in this section.

4.1 Revision of the NTNU prediction model for hard rock TBMs

4.1.1 Introduction

Existing penetration rate and cutter life models have been revised and extended, and the entire revised NTNU prediction model for advance rate and cutter life assessments is included as an appendix to this thesis.

The revision and extension process has used detailed information from current projects, together with experience accumulated during the last decade. New information has been evaluated on the basis of its relative significance in the context of the total database now available.

This chapter includes discussions only of those aspects reviewed and their main outcomes. A final treatment of the results based on their quality and representativeness has been performed, and only aspects meeting pre-defined quality requirements have been included. Risk assessments of the variability of input parameters have been carried out in order to ensure that relevant uncertainties are included in the prediction model. The treatment methodology for these data is described in chapter 3 of this thesis.

The main aspects of the model subject to review, analysis, revision or extension are as follows:

- General machine specifications and operational parameters such as the standard number of cutters, cutter diameter, installed cutterhead power, recommended applied gross cutter thrust and cutterhead velocity
- The category intervals for DRI and CLI
- Fracture classes for systematically fractured rock masses. Inclusion of fracture classes for rock masses with low degree of fracturing
- The graph used to calculate the rock mass fracturing factor (k_s)

- The DRI correction factor
- The penetration coefficient (b) and basic penetration (i_0)
- Inclusion of the influence of cutterhead velocity on TBM penetration
- Inclusion of a correction factor for cutterhead velocity (k_{rpm})
- Basic cutter ring life (H_0)
- The correction factor for abrasive minerals (k_Q)
- Inclusion of a correction factor for cutter thrust level (k_T) for highly abrasive rocks
- Inclusion of a time consumption factor linked to the influence of tunnel length on operational activities

Net penetration rate and cutter life are dependent on both rock properties (intact rock and rock mass parameters) and machine parameters. In the NTNU model rock properties are combined to derive a rock mass boreability parameter called the 'equivalent fracturing factor' (k_{ekv}), while machine parameters are combined into a single parameter called 'equivalent thrust' (M_{ekv}).

Cutter life (in hours) is equivalent to the cutter life in relation to rolled distance for a given cutterhead velocity (rpm). Cutter life is combined in calculations with penetration rate (m/h) and TBM diameter to express cutter life also in terms of 'tunnel metres excavated per cutter' (m/cutter) and 'solid cubic metres excavated per cutter' (sm^3/cutter).

The rock properties and machine parameters that influence net penetration rate are summarised in Table 29 below.

Table 29. Rock properties and machine parameters that influence net penetration rate.

ROCK PROPERTIES		MACHINE
Intact Rock	**Rock Mass**	**PARAMETERS**
Drilling Rate Index (DRI)	Rock Mass Fracturing Factor (k_s)	TBM diameter
		Cutter diameter
Porosity		Number of cutters
		Gross average cutter thrust
		Average cutter spacing
		Cutterhead rpm

Cutter wear is influenced by the rock properties and machine parameters summarised in Table 30 below.

Table 30. Rock properties and machine parameters that influence cutter wear.

ROCK PROPERTIES	MACHINE PARAMETERS
Cutter Life Index (CLI)	TBM diameter
	Cutter diameter
Content of abrasive minerals	Number of cutters
	Cutterhead rpm
	Gross cutter thrust

Gross advance rate is estimated on the basis of the following four inputs:

- ✓ Net penetration rate
- ✓ Machine utilisation
- ✓ Number of working hours during the period under consideration (e.g. a week)
- ✓ Tunnel length

The machine utilisation parameter is in turn based on the time spent completing the various operations required to excavate the tunnel.

The NTNU prediction model does not account for the entire range of rock mass conditions that can be encountered under the 'hard rock' classification. However, the following list summarises the criteria applied within the scope of application of the model:

- Rock drillability, as expressed by the Drilling Rate Index (DRI), must be in the range 20 to 80. This corresponds roughly to the approximate UCS range 25 to 350 MPa. The strength parameter is equivalent to the ISRM classification 'medium to extreme' (Table 2).
- The rock type must exhibit medium to low porosity (less than approximately 10% by volume).
- The degree of fracturing of the rock mass must be such that the average spacing between planes of weakness is greater than approximately 50 mm.
- The rock breaking process during boring must be mainly by means of brittle failure (chipping) between the disc cutters.
- Rock mass quality must be such that the excavated tunnel will require only light-duty support mechanisms (rock bolts and/or shotcrete). Exceptions will occur in zones of weakness or as a result of other specified factors.
- Currently, the most common cutter diameter used in hard rock tunnelling is 483 mm (19 inches) and, for smaller TBMs, a diameter of 432 mm (17 inches) is used. The use of cutter ring diameters of 508 mm (20 inches) based on a 19 inches bearing set is starting to be commonly used in large TBMs
- The machine type will be a hard rock TBM open or shield type. The NTNU model is based on data derived from a wide variety of open TBM types used to perform tunnelling in rock mass conditions such as those summarised above.

- The machine utilisation (expressed as a percentage) does not include additional time spent on operations such as TBM and back-up assembly and disassembly, excavation work linked to niches, branching, etc., tunnelling through zones of poor quality, the occurrence of unexpected rock mass conditions, permanent rock support and lining operations, TBM downtime, etc.

Figure 63 shows a performance prediction flowchart generated by the latest version of the NTNU model.

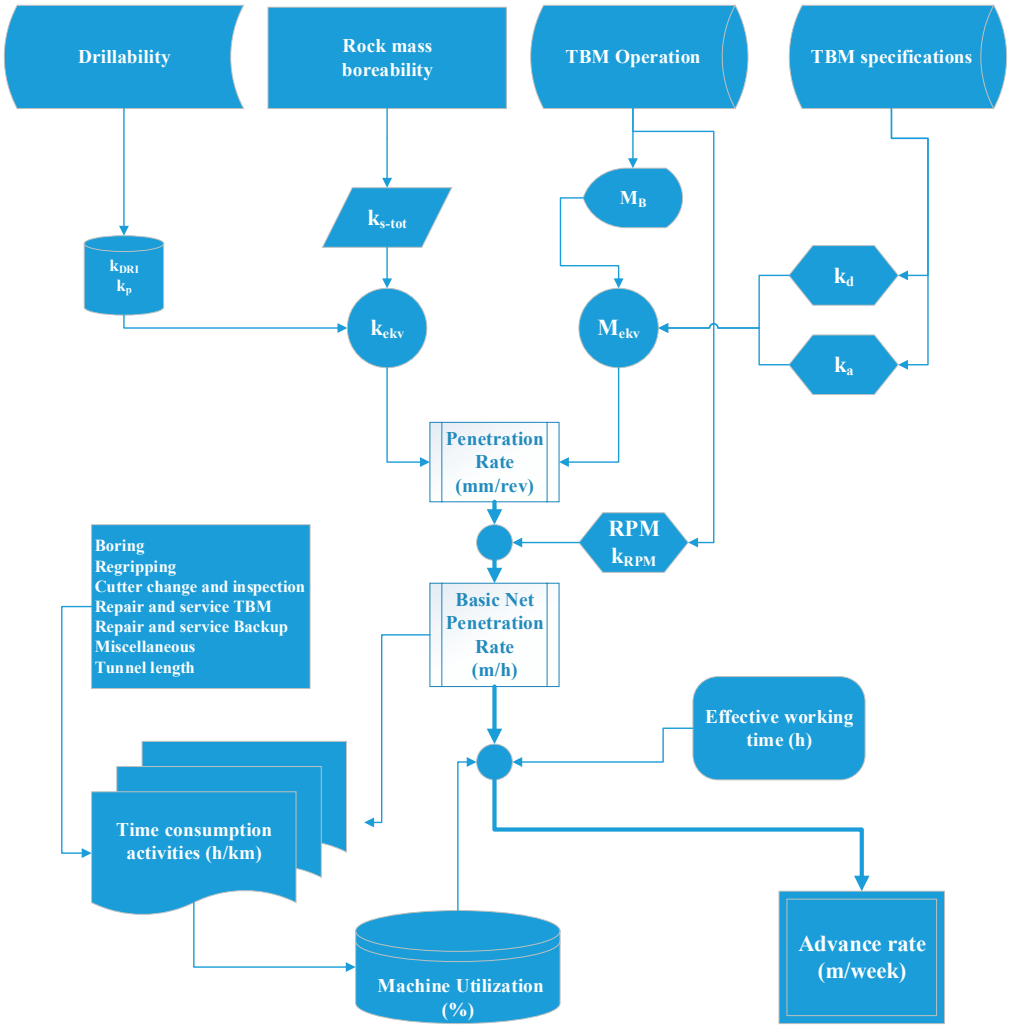

Figure 63. Performance prediction flowchart generated by the latest version of the NTNU model.

4.1.2 Machine parameters

Machine parameters are subdivided into two groups; 'machine specifications', such as machine and cutter diameters, the number of cutters or cutterhead power, and 'machine operation' parameters such as gross cutter thrust and applied rpm.

Machine specifications

The estimates of penetration rate and cutter life require inputs in the form of machine parameter. In the early planning stages of a tunnelling project such parameters must be assumed.

Machine specifications are subsequently revised as necessary to correspond with the TBM technology actually being used.

The data used in this thesis were derived from a combination of those linked to the projects specifically included in the thesis with other data derived from the early stages of other projects.

TBM diameter

Hard rock TBM diameters vary from 1.2 to 15 metres. However, based on background data inputs, NTNU models are applicable for diameters ranging from 3 to 12 metres.

Cutter diameter

As noted above, the most common cutter diameter currently used in hard rock tunnelling is 483 mm (19 inches). For smaller TBMs, a diameter of 432 mm (17 inches) is used (Table 31).

In recent years, cutter discs with diameters of 508 mm (20 inches) have been introduced. This increase in diameter is based on enlargement of a 483 mm diameter cutter disc.

Table 31 shows the most common cutter disc specifications currently used in hard rock tunnel boring.

Table 31. The most common cutter disc specifications currently used in hard rock tunnel boring.

Cutter Disc	Diameter		Tip width		Max. cutter load capacity
	in.	mm.	in.	mm.	kN
Cutter disc 17"	17	432	5/8	15.88	267
Cutter disc 19"	19	483	3/4	19.05	312
Cutter disc 20"	20	508	3/4	19.05	312

Standard number of cutters on the cutterhead

Figure 64 shows the standard number of cutters on a cutterhead as a function of disc cutter diameter and TBM cutterhead diameter. For smaller TBM diameters, space available on the cutterhead is limited, and the number of cutters indicated is the maximum.

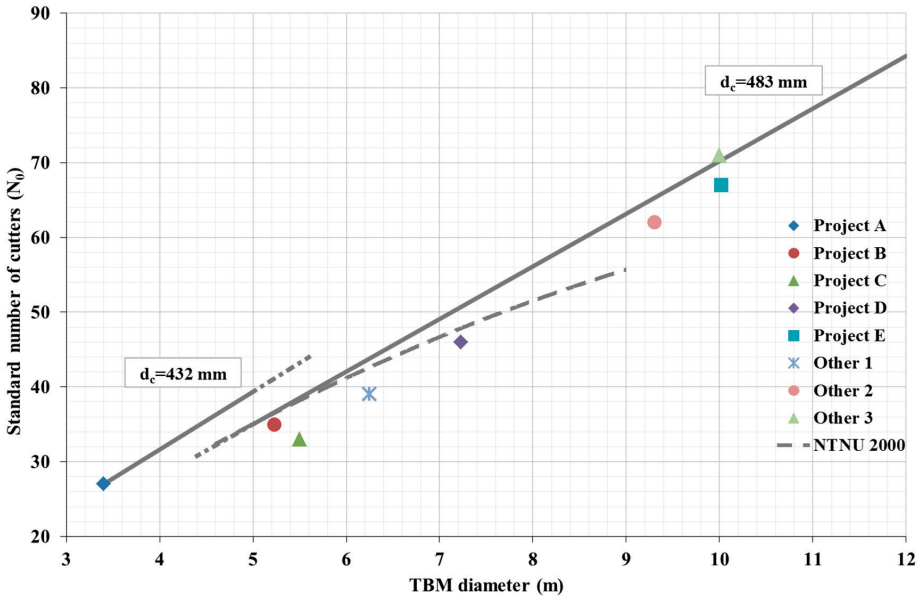

Figure 64. Standard number of cutters on a cutterhead (N_0). Data from the projects used in this thesis.

The number of cutters is related to the rock boreability. The lower the boreability, the greater the number of cutters that will be required. Previous versions of the NTNU model underestimated the number of cutters required for larger TBMs (Figure 64).

Cutterhead power

Installed cutterhead power is not considered to be a limiting factor for modern TBMs, if the machine has been adequately designed. However, to prevent cutterhead power imposing limitations on performance, installed power must provide sufficient torque to result in a penetration rate of approximately 14 mm/rev.

Figure 65 shows the installed power driving cutterhead rotation as a function of TBM and cutter diameter.

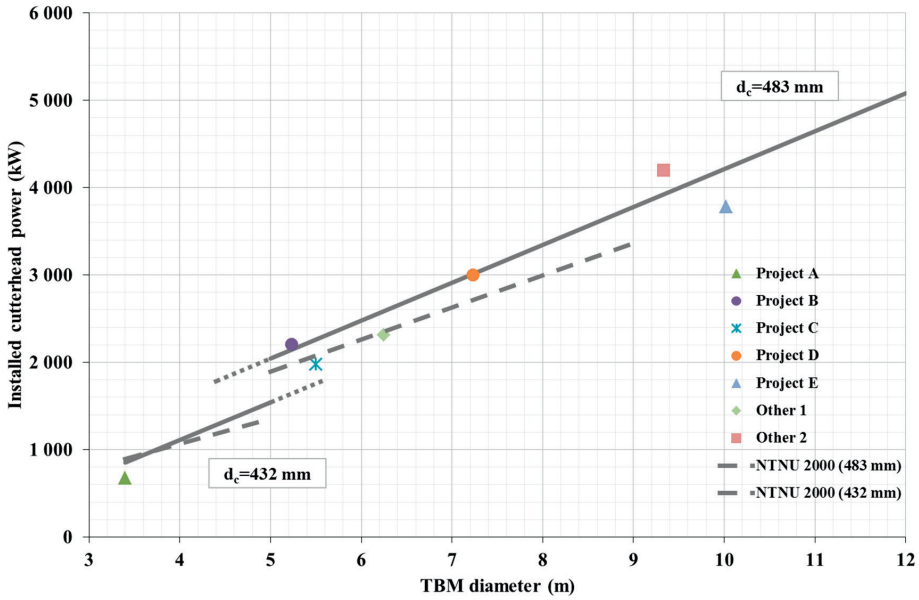

Figure 65. Installed cutterhead power (kW). Data from the projects used in this thesis.

Machine operation parameters

Cutter thrust

The NTNU model uses the term 'gross average thrust', which is a measure of the total thrust applied by the machine, taking into account friction or drag of the cutterhead and the cutterhead support system. Other factors that contribute to loss of thrust like pulling the back-up during boring will should be removed. The parameter 'gross average thrust per cutter' is obtained by dividing total gross thrust by the number of cutters. Gross average thrust is measured over a period of time, and is thus not indicative of peak loads measured over short time intervals during the rock-breaking process.

At present, the material quality of the steel ring continues to represent the limiting factor to cutter thrust, combined with the fatigue loading capacity. When estimating penetration rate etc., it is important to consider the thrust capacity of the cutter rings, as well as the capacity of the cutter bearings and the cutterhead main bearing.

Cutter thrust is the principal machine parameter influencing TBM performance in the NTNU model, and should thus be used with caution. Figure 66 provides a general outline of maximum gross average thrust per cutter disc as a function of cutter diameter and TBM diameter.

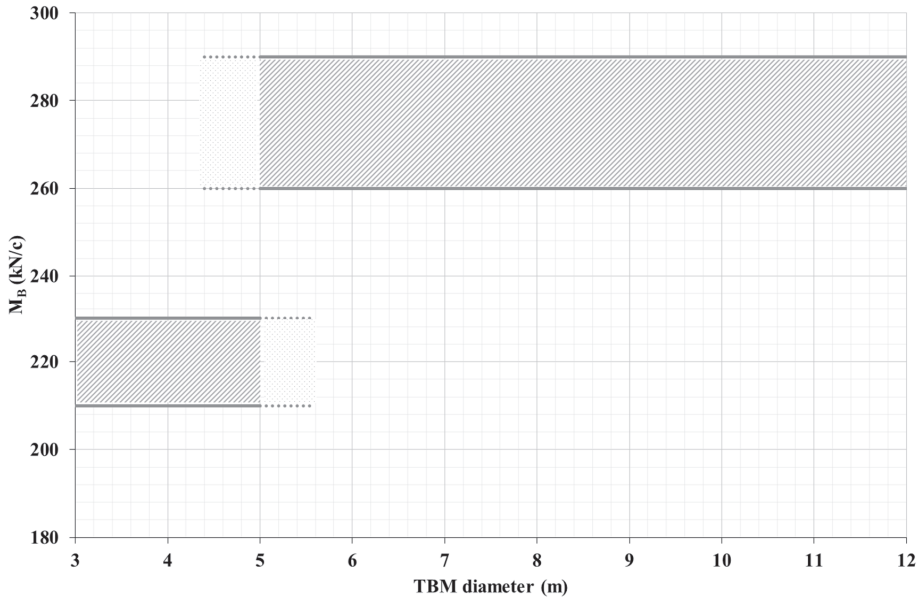

Figure 66. Recommended gross average thrust per cutter disc. The upper limit applies to boring in rock masses with a low degree of fracturing, while the lower limit refers to boring in medium to highly fractured rock masses.

Experience shows that thrust is reduced in more highly fractured rock masses (Figure 67 and Papers I and IV). This is in good agreement with NTH (1983) where the applied thrust capacity is expressed as a function of the degree of fracturing and the angle between the tunnel axis and the plane of weakness, which in fact is the rock mass fracturing factor (k_s).

Decisions to reduce thrust in response to increases in degree of fracturing are taken for operational reasons to avoid damage and excessive wear to the cutters resulting from vibrations and machine damage. Reductions in thrust reduce the influence of the rock mass fracturing factor (k_s) on penetration rate. However, penetration rate still increases with increases in the fracturing factor. This ‘‘indirect effect’’ of thrust reduces the real influence of k_s on penetration rate and thus also on net penetration rate (Paper I, Paper IV).

The data from Project C (Figure 67) show that gross cutter thrust (kN/cutter) varies from over 320 to around 220 kN/c from $k_s = 0.9$ (fracture class 4/St I)) to $k_s = 3.3$ (fracture class 7/St IV) respectively. The weighted average gross cutter thrust is 285 kN/c, with an average k_s value of 1.7, equivalent to fracture class 5/St II.

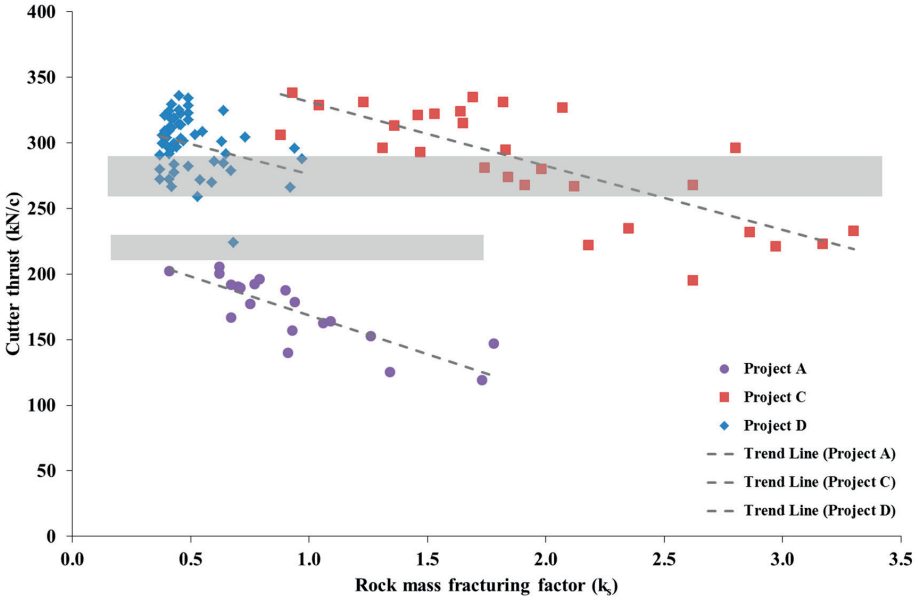

Figure 67. A correlation of rock mass fracturing factor (k_s) with cutter thrust. The recommended range of cutter thrust values (taken from Figure 66) is indicated by the shaded area.

In certain tunnelling situations, the applied thrust parameter should be treated with caution when it comes to performance prediction. For high rock mass fracturing values (resulting from a combination of degree of fracturing and fracture orientation), a lower applied thrust is recommended. When boring in hard rock with low levels of boreability, drillability and degree of fracturing, higher applied thrust values may be necessary, and the influence on cutter life should be taken into account (see section 4.1.6). Tunnelling along curves or on declines might require even lower thrust values.

The use of 'gross average thrust' might produce some uncertainties when using different types of machine (open or shield) and/or TBM diameters and thus different cutterhead weights and friction area.

Analysis of current TBM data have indicated a generalize increment of 'gross cutter thrust' regarding previous data in the database of the model. This might be explained due to the inclusion of larger TBM diameters and/or shield machines but also due to an improvement of the cutter technology allowing an increment of the applied cutter thrust.

During the research, it has been analysed the possible influence of TBM diameter, cutterhead weight and contact area, in the applied 'gross cutter thrust'. No conclusive outcomes were found due to limited variety of large TBMs.

Cutterhead velocity

Cutterhead velocity (expressed in rpm) is inversely proportional to the cutterhead diameter due to the need to limit the rolling velocity of the peripheral cutter.

In previous versions of the model, maximum cutterhead velocity was defined in relation to the maximum recommended rolling velocity of the gauge cutter. The reason for this was that some of the machines in our database were designed to operate at maximum cutterhead velocities in relation to the maximum recommended rolling velocity of the gauge cutter (Bruland, 2000f).

The idea that cutterhead velocity, seen in relation to the rolling velocity of the cutters, has a significant influence on penetration rate (mm/rev) was introduced by Bruland (2000f), and has been given due consideration in this thesis. A recommended applied cutterhead velocity has been defined based on experience and trial tests. The reader is referred to sections 3.4.3 and 4.1.5 for detailed information.

Figure 68 shows proposed maximum and recommended cutterhead velocities as a function of TBM diameter and cutter diameter.

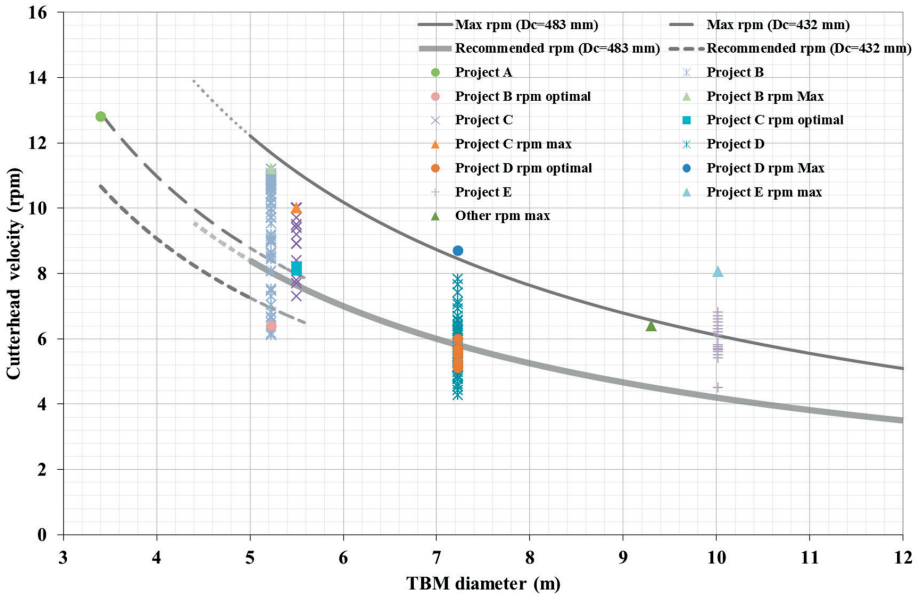

Figure 68. Cutterhead velocity (rpm) as a function of TBM diameter and cutter diameter. The graph shows the applied and optimal cutterhead velocities, as well as values taken from tests, and the maximum installed velocity for each of the projects analysed.

A range of available applied cutterhead velocities must be considered. In connection with the breaking process itself, a low optimal velocity is indicated for tunnelling in rock masses with low boreability and/or using low thrust values while the required optimal rpm is not necessarily as low in rock masses with good boreability. Tunnelling in highly fractured rock

may require a lower cutterhead velocity in order to avoid vibrations resulting in excessive wear to the cutters and possible machine damage. The capacity of the muck transport system (conveyor) is not always appropriate and might be exceeded. For this reason, a reduction of both cutterhead velocity and thrust will be necessary.

4.1.3 Category intervals for drillability indices

The current database includes a total of 3,068 DRI tests and 1,896 CLI tests. The category intervals are related to the distribution of the test results in the database (Bruland, 2000g). Table 32 shows the cumulative percentage for category intervals of drillability indices.

Table 32. Cumulative percentage for category intervals of drillability indices (Bruland, 2000g).

Category	Cumulative percentage of total number of samples
Extremely low	0 - 5
Very low	5 - 15
Low	15 - 35
Medium	35 - 65
High	65 - 85
Very high	85 - 95
Extremely high	95 - 100

Table 33 shows the category intervals for the drillability indices according to the current database.

Table 33. Category intervals for drillability indices.

Category	DRI	CLI
Extremely low	< 26	< 4.8
Very low	26 - 32	4.8 – 5.8
Low	33 - 41	5.9 – 8.2
Medium	42 - 52	8.3 – 15.6
High	53 - 62	15.7 – 35
Very high	63 - 73	36 – 72
Extremely high	> 73	> 72

The category intervals have slightly changed from the latest version (Bruland, 2000g) due to the incorporation of new data.

4.1.4 Rock mass fracturing

Rock mass fracturing is recognised as the geological factor that exerts the greatest influence on penetration rates. High rock mass fracturing results in greater rock mass boreability values in connection with hard rock tunnelling (Papers I, III, IV and VI).

This study has carried out analyses of geological issues by means of continuous engineering geological back-mapping and drillability testing, together with machine specifications and TBM data, TBM performance and operational parameters, along selected tunnel sections.

Rock mass fracturing in the NTNU model is defined using parameters such as the number of fracture sets, degree of fracturing, orientation of the fracture system(s) and tunnel alignment. The fracturing factor (k_s) is a single coefficient representing the simultaneous influence of the degree of fracturing and the angle between the tunnel axis and the planes of weakness in the rock mass. For detailed information, the reader is referred to Papers I and III, and section 3.3.3 of this thesis.

The definitions of the term ‘fracture’, and the plots used to calculate the ks parameter, have been revised as part of this research work.

Subjectivity of geological mapping on performance predictions

The subjectivity of geological mapping represents a major risk issue during evaluation of the rock mass fracturing factor (k_s). As previously discussed, the parameter k_s has a major influence on predictions of net penetration rate which in turn are used to forecast excavation durations and costs for TBM projects. In order to reduce the influence of subjectivity that mapping entails consideration should be given to the mapping criteria and the analysis of results (see Paper V, currently under review). Since geological mapping is a subjective matter, this study recommends utilising the simplest and most straightforward methods available.

For this research, subjectivity was tested by employing three different researchers, including the author, to perform separate engineering geological back-mapping in selected tunnel sections at project A. Their results were then compared. A description of this work and a detailed summary of the data can be found in Paper V appended to this thesis.

Distinctions between different types of fracture, including joints and fissures, were introduced by NTH (1981) and were adhered to up to and including the work of Bruland (2000bd). Experience from subsequent research work at NTNU has shown that fissures constitute the most common plane of weakness encountered during geological back-mapping, and it is these that are used as input to the NTNU TBM performance prediction model (Bruland, 2000b).

Subjectivity in engineering geological back-mapping as described above has an important influence on the expression of three key factors:

- Fracture type
- Fracture set orientations
- Degree of fracturing and fracture class

The main aims of this study are:

- to analyse how different engineers and/or researchers map and evaluate identical geological conditions according to the criteria set out in the NTNU prediction model.
- to assess the influence of risk related to mapping subjectivity on predicted net penetration rate values and project costs.
- to evaluate the influence of mapping section lengths and analysis of mapped section lengths on the predicted net penetration rate.

The results of degree of fracturing assessments and categorisation into fracture classes for tunnel sections mapped during Project A indicate that the coefficient of variation (CV) is relatively low – less than 20% for low degrees of fracturing. The CV for the classes "0" to "I" is approximately 19%, but is somewhat larger for fracture (fissure) classes "II", "III" and "IV". This can be explained by the narrower range of average fissure spacing values for the classes in question, and the relative lack of data available to this study.

Figure 69 presents the CV values generated by the three researchers for each fissure class.

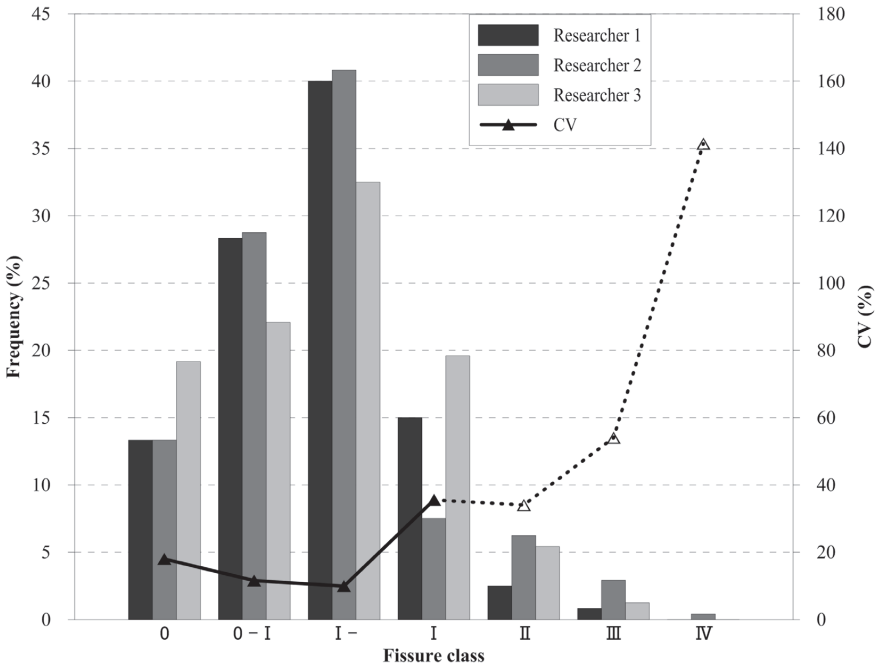

Figure 69. Mapping subjectivity. Frequency distribution of fracture classes for the mapped sections in Project A. The reader is also referred to Paper V (currently under review).

Variation in the orientation of the main fracture sets mapped by the three researchers lies within 6 degrees of the mean value. Variations in fracture orientation values derived from the three researchers result in corresponding variations of 12% and 7% when applied to calculate increments in predicted net penetration rate and reductions in predicted excavation costs respectively.

Fracture type mapping thus has a major influence on predicted net penetration rate and costs (Paper V). For this reason, it is important to establish clear criteria for fracture type assessment during geological mapping.

The results from this research clearly indicate that subjectivity linked to rock mass assessments, as input to the NTNU prediction model should be reduced. On the basis of the previous discussion and our experience of geological back-mapping in bored tunnels, we conclude that it is adequate for performance prediction purposes simply to use one term to describe the planes of weaknesses encountered in systematically fractured rock masses.

Fractures

In the light of the discussion above, the traditional distinction between 'fissure' and 'joint' has been removed and replaced by the single term 'fracture'. This term will be used in the remainder of this thesis.

In broader geological contexts, the term 'fracture' is commonly used to describe all kinds of discontinuities resulting from a mechanical break in a rock mass, and fractures occur in all rock types in virtually all structural domains (Davis, 1984). In engineering terms, the term encompasses all forms of discontinuity that are capable of inducing weakness under a cutter disc, and which thus may exert a major influence on tunnelling performance.

Fractures may be described as 'open', such as joints in granites, or 'filled'. Filling materials may include clays or low shear strength minerals such as calcite or chlorite. Low shear strength discontinuities produced by plastic deformation, sometimes called 'foliations', will also occur in mica-rich metamorphic rocks such as schists and gneisses.

The establishment of dimensional-related definitions for the wide variety of intact rock and rock mass discontinuities has proved to be problematic. Figure 70 presents a proposed length-based classification of the main types of discontinuities from an engineering geological perspective according to the NTNU back-mapping methodology.

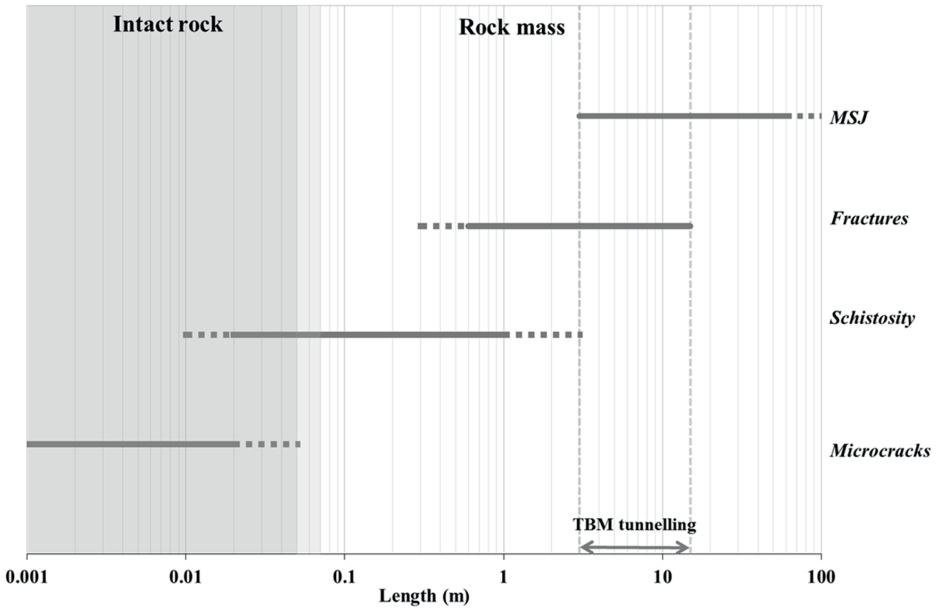

Figure 70. The main types of intact rock and rock mass discontinuities encountered during back-mapping in hard rock TBM tunnelling. Types are categorised according to length based on the NTNU methodology. The shaded area indicates where data have been derived from laboratory tests carried out on intact rock.

The lengths indicated in Figure 70 may vary depending on the geology.

In schistose rocks, such as mica schists, the distinction between the 'schistose fabric' (schistosity) of the rock and foliation fractures that develop along planes parallel to the schistose fabric can be problematic. In such cases, it is essential not include the effect of schistosity twice – both as a drillability parameter and an additional plane of weakness (Figure 71).

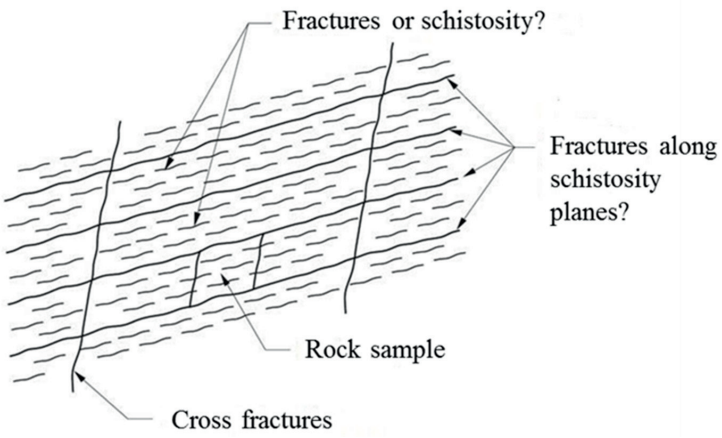

Figure 71. Schistose fabric and cross-fractures in a schistose rock (modified after NTH, 1983).

Non-fractured rock masses (Class 0) include massive, fracture-free, rocks such as can occur in the case of intrusive dykes, sills and batholiths. Rock masses that exhibit fractures infilled by minerals of a greater shear strength than the country rock, such as quartz or epidote, may also be categorised as Class 0.

As previously discussed, the influence of geology on the prediction performance of the NTNU model increases as the degree of fracturing in the rock mass decreases. Based on mapping analysis and experience, this thesis introduces the concept of a fracture class (s_f) "Class 1", which is intermediate between the formers fissure classes 0 and 0-I. Fracture classes are defined according to the logarithmic relationship with average fracturing spacing measured in centimetres (Figure 72).

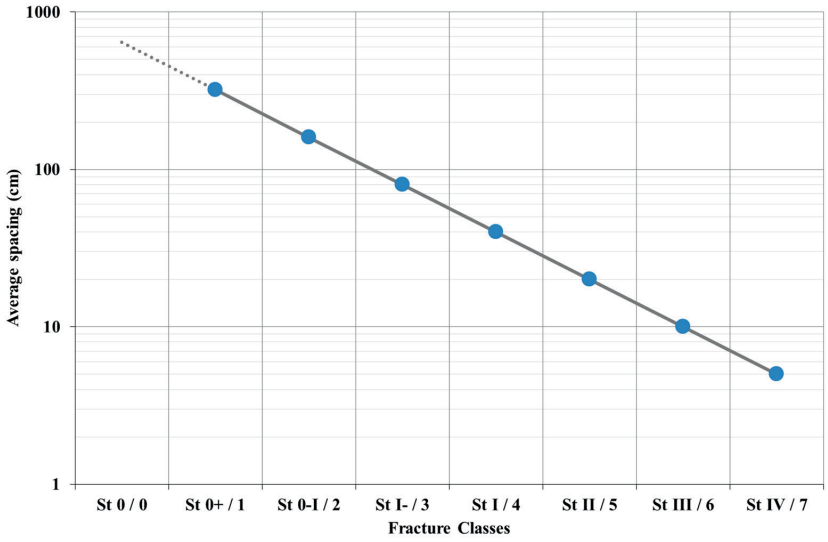

Figure 72. Average fracture spacing used to define fracture classes. Both previous and new fracture class terminologies are included.

A detailed definition of fracture classes exhibiting low degrees of fracturing has been included. Table 34 presents a summary of fracture class terminology as defined by the average spacing between fractures.

If the principal classes listed in Table 34 are inadequate for a detailed description of fracture spacing, intermediate classes could also be included for practical mapping purposes.

Table 34. Fracture class terminology as defined by the average spacing between fractures.

Fissure class (St) (Bruland, 2000)	Fracture Class (Sf)	Average spacing between fractures a_f (cm)	Range class (cm)	Degree of fracturing
0	0	∞	480 – ∞	Non-fractured
0	1	320	240 – 480	Extremely low
0 - I	2	160	120 – 240	Very low
I -	3	80	60 – 120	Low
I	4	40	30 – 60	Medium
II	5	20	15 – 30	High
III	6	10	7.5 – 15	Very high
IV	7	5	4 – 7.5	Extremely high

Marked Single Joints (MSJ)

No relevant information regarding to Marked Single Joints (MSJ) has been found during the study, and the approach of MSJ from the previous version has remained. However, due to the uncertainty attached to the interpretation and mapping of MSJ, some clarifications are given below.

Marked Single Joints (MSJ) includes highly distinctive discontinuities. These may be entirely open, may conduct water or may be filled with clay. Minor faults filled with gouge may be classified as MSJ.

Single joints are marked discontinuities in the rock mass and they are recorded individually. As the name indicates, they will appear as a singular phenomenon at the tunnel level, even if they belong to a systematically occurring joint set on a larger scale. Marked Single Joints may result in very high net penetration rates locally. Due to the risk of stability problems and damage to the cutters and the cutterhead, one should evaluate the effect carefully and consider possible delays if the Marked Single Joints may result in mixed face conditions, heavy rock support, water inflows, etc.

The theoretical penetration addition will increase with increasing angle between the tunnel axis and the plane of the Marked Single Joint (Bruland, 2000 and appendix within this thesis). Due to heavy machine vibrations and risk of excessive cutter wear or damage, it is not possible to fully utilise the penetration addition when the theoretical addition is more than approximately 40 %. In such cases, it is necessary to reduce the cutterhead thrust.

In rock mass with low boreability (e.g. DRI = 30 and a low degree of fracturing) the practical limit of penetration addition will be reached at an angle as low as 20° - 30°. When the angle between the tunnel axis and the plane of the Marked Single Joint is 80° - 90°, the influence of the joint will most likely be negative due to heavy vibrations and damage of the cutter rings. In any case, a Marked Single Joint at an angle of 80° - 90° will have influence over a very short distance and should therefore not be included in the penetration rate estimations (Bruland, 2000f).

Recommended guidelines for the interpretation and mapping of MSJ:

- MSJs are singular phenomena
- Spacing between MSJs must be on a level of several metres
- A MSJ must be a clearly visible plane of weakness, e.g.
    - having and aperture of at least some millimetres
    - being filled with clay or similar weak materials
    - being a thin (< 50 cm?) layer of a different rock type with relatively high degree of fracturing and/or significantly lower strength than the main rock type
    - contact/transition zones between the main rock and larger intrusions (thickness > 1 m?) with strong mineral alteration in the contact zone
    - contact/transition zones between rock types with strong mineral alteration in the contact zone
    - thin weakness zones (<20 cm thick?) causing only minor stability problems

The above is only a rough description; MSJs must be interpreted and identified separately.

Figure 73 shows a typical Marked Single Joint in a rather non-fractured rock mass. The MSJ has some filling material, it carries some water and there is clear overbreak along parts of the MSJ.

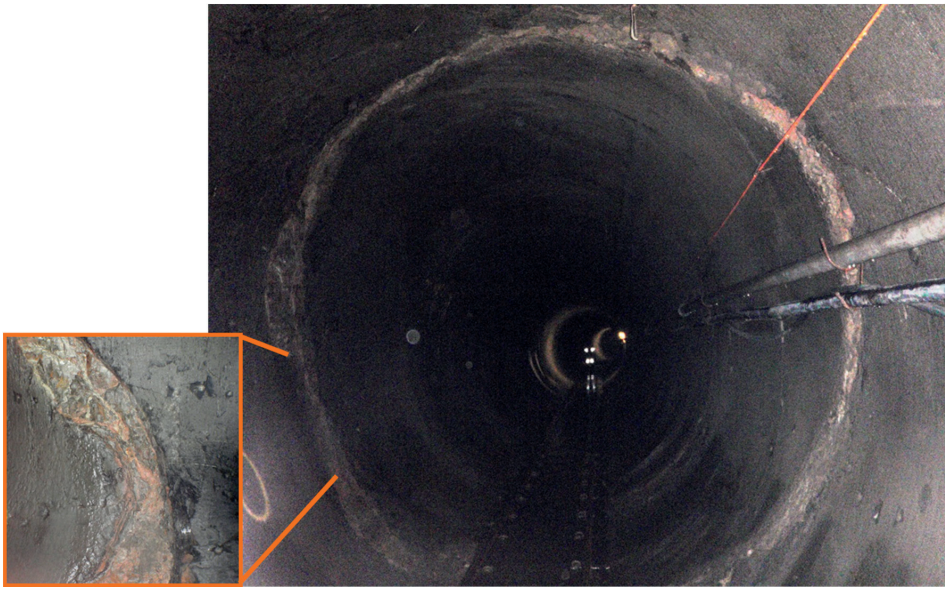

Figure 73. A typical Marked Single Joint in a rather non-fractured rock mass. The MSJ has some filling material, it carries some water and there is clear overbreak along parts of the MSJ.

Understanding rock mass boreability

An evaluation of the influence of rock mass on the TBM tunnelling process is not always easy or straightforward. A comprehensive understanding of the rock mass boreability requires different approaches to its evaluation. It is recommended here that both chip analysis and tunnel face inspection should be used to support engineering geological back-mapping (Figure 74).

Tunnel face inspection enables the identification of fractures that influence the rock breaking process, and the voids formed following the breaking process as determined by the presence of fractures. Continuous tunnel face inspection is a part of the geological back-mapping methodology.

The presence of voids implies that a few cutters have lost contact with the face during tunnelling, transferring the load to other cutters. This will result in a dynamic effect during the breaking process and therefore in an increase of the penetration rate. Moreover, the relative orientations of the fractures in relation to the tunnel direction result in different void sizes

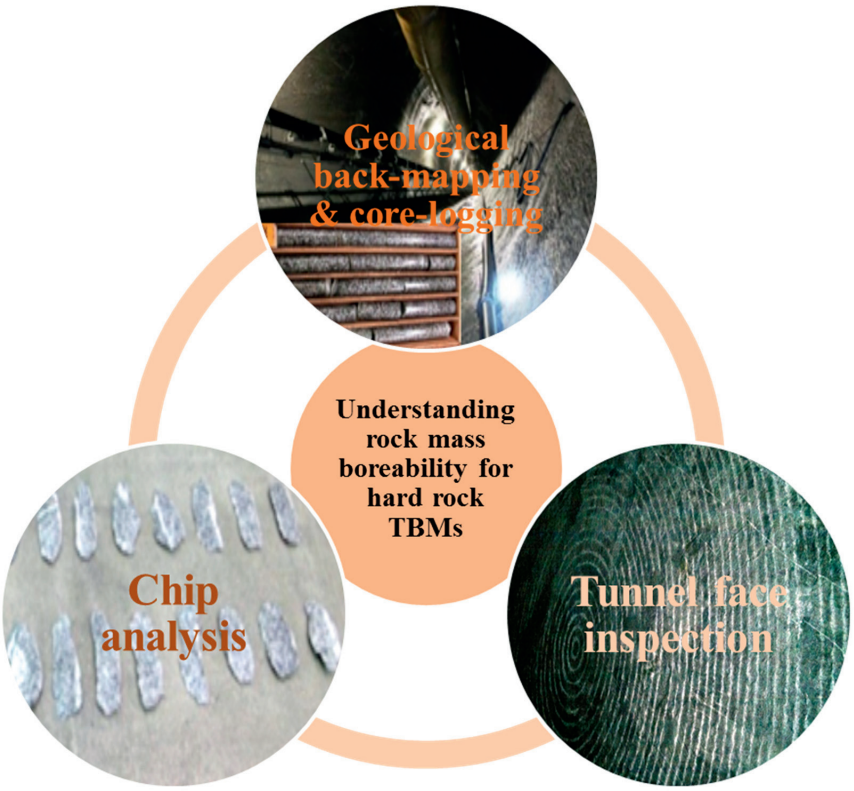

Figure 74. Schematic outlining different approaches to the understanding of rock mass boreability in connection with hard rock TBM tunnelling.

Figure 75 is a photograph taken during a tunnel face inspection showing two fractures that have different levels of influence on the rock breaking process due to their respective orientations. The fracture on the left exhibits a relatively high angle with the tunnel orientation (70°) and a dip of 70°. This results in a relative angle (α) of 62° that in turn results in a larger void area and thus a greater influence on the penetration rate.

The fracture on the right of the photograph exhibits an angle of 10° with the tunnel orientation and a dip of 50°, resulting in a relative angle (α-parameter) of 9°. This fracture has only a minimal influence on the rock breaking process, and only small areas of voids are observed.

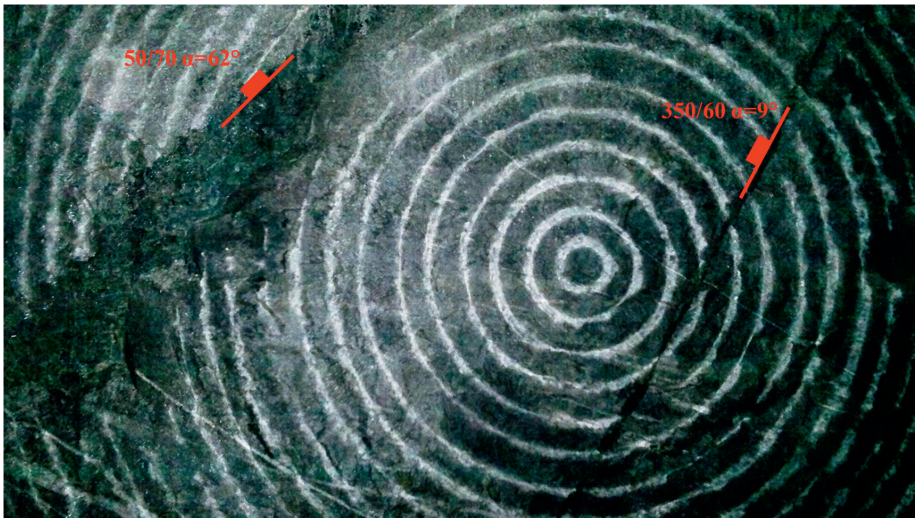

Figure 75. A photograph taken during a tunnel face inspection showing void areas generated after tunnelling in a fractured rock mass. The tunnel axis orientation is 160 degrees. (Photo courtesy of Tobias Andersson).

It is important to note the small veins shown in Figure 67 that do not influence the rock breaking process as rock mass. These veins, together with other small fractures, may have been considered during the geological back-mapping process, leading to overestimates of rock mass boreability and misleading performance predictions.

Figure 76 illustrates the varying influence of the relative angle between the fracture sets and tunnel direction on the rock mass fracturing factor (k_s) which is used in the NTNU model.

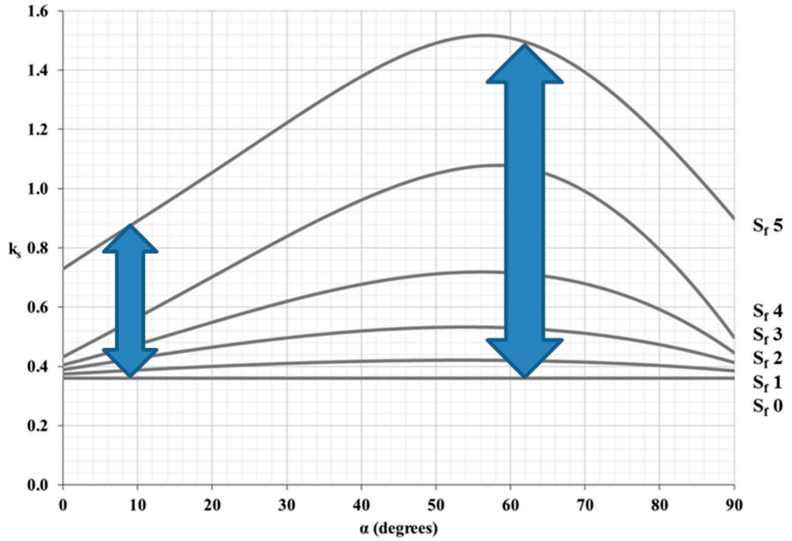

Figure 76. Illustration of the varying influence of the relative angle (α) between the fracture sets and tunnel direction.

In addition to tunnel face inspection, chip analysis provides information relevant to boring efficiency. It may also be a valuable tool that can contribute towards the understanding of the rock boreability of a given rock mass. Inspection of rock chips may enable us to identify and/or measure the variation in shear strength properties along a given plane of weakness and the possible influence on intact rock and the rock mass as a whole.

Figure 77 shows an analysis of crack propagation in a rock chip sample.

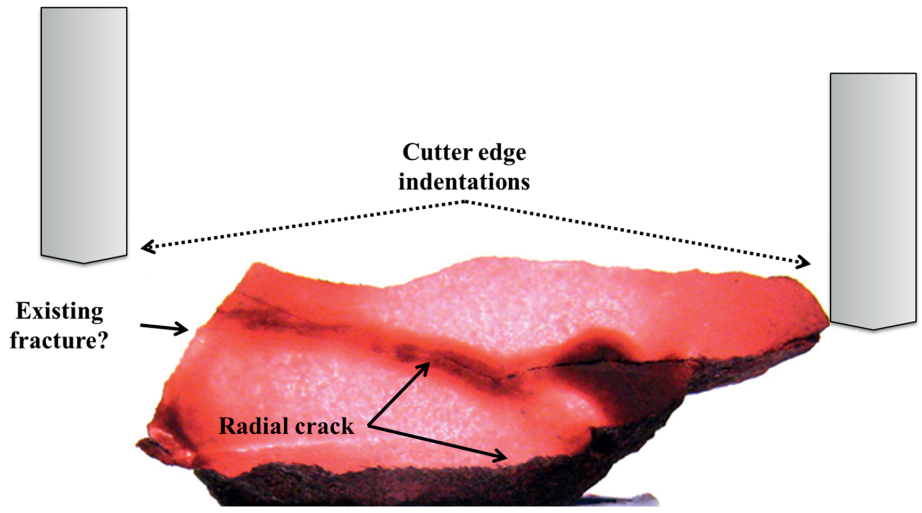

Figure 77. Crack analysis of a rock chip sample (Photo courtesy of Solveig Vassenden).

Mapping considerations

Fracture characteristics such as aperture, type of filling and persistence are also considered to have a major influence on the process of obtaining reliable rock mass parameters as input to tunnelling prediction models. For example, it is essential to assess the relative persistence (length) of fractures in relation to TBM diameter. A 5-metre fracture identified as persistent in a 5-metre diameter tunnel may be less persistent (discontinuous) in a wider tunnel, and will thus have a different influence on rock breaking performance in the two contexts.

Furthermore, the influence of fractures when boring in rock mass with low degree of fracturing depends on the TBM diameter (NTH, 1983). Figure 78 shows the significance of the TBM cutterhead diameter when boring in rock masses with low degree of fracturing.

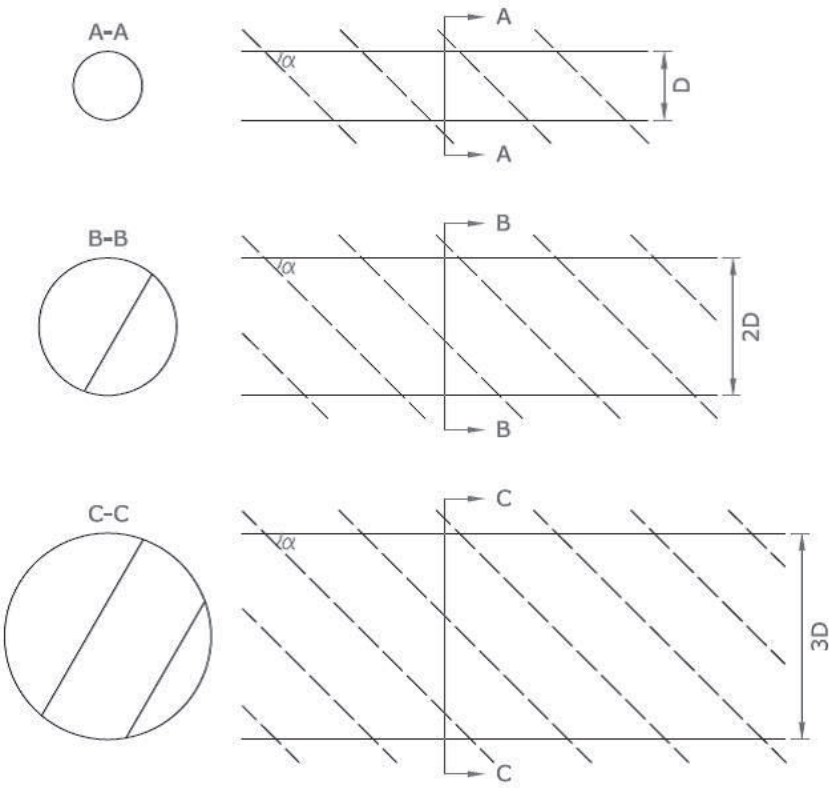

Figure 78. Significance of the TBM cutterhead diameter when boring in rock masses with low degree of fracturing (modified from NTH, 1984).

For larger TBM cutterhead diameters, greater average spacing of fractures and orientations could have greater influence on the penetration rate. At the same time, the influence of a fracture may be different depending on the TBM cutterhead diameter. This significance of the TBM cutterhead diameter is not well understood yet.

The profiles of TBM tunnels in hard rock are normally smooth and as such do not provide a clear view of fracture contacts. However, it seems that in any event a clear and simplified inclusion in the model of the principal fracture characteristics may result in an improvement in the definition of the rock mass fracturing parameter.

Unfortunately, there was insufficient back-mapping data available to the author of this thesis to enable the proper inclusion of these fracture characteristics in the revised rock mass model.

It is considered likely that geological mapping in bored tunnels may result in better assessments of rock quality properties than in drill-and-blasted tunnels. Barton (2000) discussed findings from the Svartisen tunnel (Løset, 1992), where Q-values mapped in the TBM tunnel section was 1.5 to 3.0 times higher than those from the drill-and-blasted section for Q-values in the middle range (from 4 to 30).

Mixed Face Conditions

The mixed face phenomenon describes a tunnel face exhibiting two or more rock materials with significantly different boreability properties.

Mixed face conditions are very difficult to categorise due to the wide range of lithologies and other factors that may be encountered, and no standard definition is currently available. According to Streingrimsson et al. (2002) and Toth et al. (2013), UCS ratios for the weakest and strongest materials at or below 1/10 generally constitute an accepted definition in the tunnelling industry. However, UCS alone may have shortcomings as a parameter used to characterise rock or soil boreability. Many mixed face situations that have been analysed have exhibited rock-soil combinations where the strength properties were very different.

As previously discussed in this thesis, hard rock conditions are equivalent to UCS values > 50 MPa. Mixed face conditions occur where two or more rock mass bodies with significantly different boreability parameters are encountered at the tunnel face, and where the contrast influences operational parameters, penetration rate, cutter consumption and advance rate.

The rock mass at the face exhibiting the highest strength properties will have the most influence on the operational parameters of the machine. This is because the strongest rock type will require a higher level of thrust per cutter than the weaker areas to achieve equal penetration. The main challenge of boring through mixed face conditions is to avoid overloading the cutters when they enter and bore through the strongest rock types at the tunnel face. Moreover, the distribution of strong and weak layers will change as the TBM advances, requiring the operator to continuously adjust the machine's operational parameters.

According to Bruland (2000f), by quantifying the rock mass boreability of both the stronger and weaker parts of the tunnel face, it may be possible to obtain an approximation of the force distribution between the different rock masses based on the achieved basic penetration rate, average cutter load for the face as a whole, and the percentage of strong and weak rock types encountered at the face.

Streingrimsson et al. (2002) proposed a universal mixed face correction factor that takes into account the relative occurrence of rock types of different mechanical properties, and the net penetration rate for each rock type.

Due to vibrations in the cutterhead and the extremely high cutter forces that are generated when a cutter rolls from the weak to the strong part and/or rock types in the tunnel face, it is unlikely that it will be possible to utilise a thrust level of more than 90 - 100% of the gross cutter thrust used when mixed face conditions are not present. In addition, lower rpm values should be expected.

4.1.5 Penetration rate model.

The penetration rate model is based on normalised penetration curves. The best fit to these data is established to be a power function. The model is based on the equation below (20) for basic net penetration rate:

$$i_0 = \left(\frac{M_{ekv}}{M_1} \right)^b \quad \text{(mm/rev)} \tag{23}$$

where

i_0 = basic penetration rate (mm/rev)
M_{ekv} = equivalent cutter thrust (kN/cutter)
M_1 = critical cutter thrust (kN/cutter, the thrust required to achieve 1 mm/rev)
b = penetration coefficient

Penetration curves are found by processing data recorded during penetration tests. A penetration test involves a full-scale trial during which thrust values are varied while cutterhead velocity for a given geology is kept constant. A description of the test procedure is given in section 3.4.2.

The critical cutter thrust (M_1) and the penetration coefficient (b) for a given geology are found by regression from the penetration tests.

Table 35 provides a summary of the penetration test results included in this thesis.

Table 35. Summary of the penetration test results included in this thesis.

k_{ekv}	M_1 (kN/cutter)	b
1.08	114.20	2.63
0.84	104.68	1.96
0.84	89.32	1.88
2.25	92.06	1.97
0.47	136.88	3.21
1.90	100.02	1.18
0.94	165.92	4.38
0.65	159.35	3.93
1.93	67.96	1.31
0.61	128.94	2.72
2.06	137.03	2.35
0.61	188.24	2.23
0.39	265.57	4.88

Figure 79 and Figure 80 show the relation between the equivalent fracturing factor (k_{ekv}) and the critical thrust (M_1), and the penetration coefficient (b), respectively. The values are taken from the results of penetration tests included in this thesis.

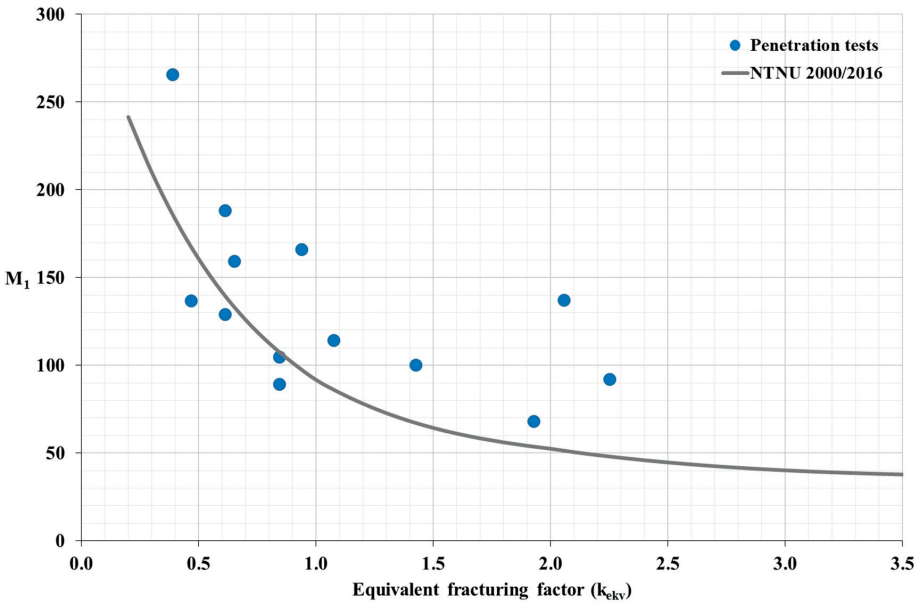

Figure 79. Critical cutter thrust (M_1) as a function of the equivalent fracturing factor. The plotted values are taken from the results of penetration tests included in this thesis.

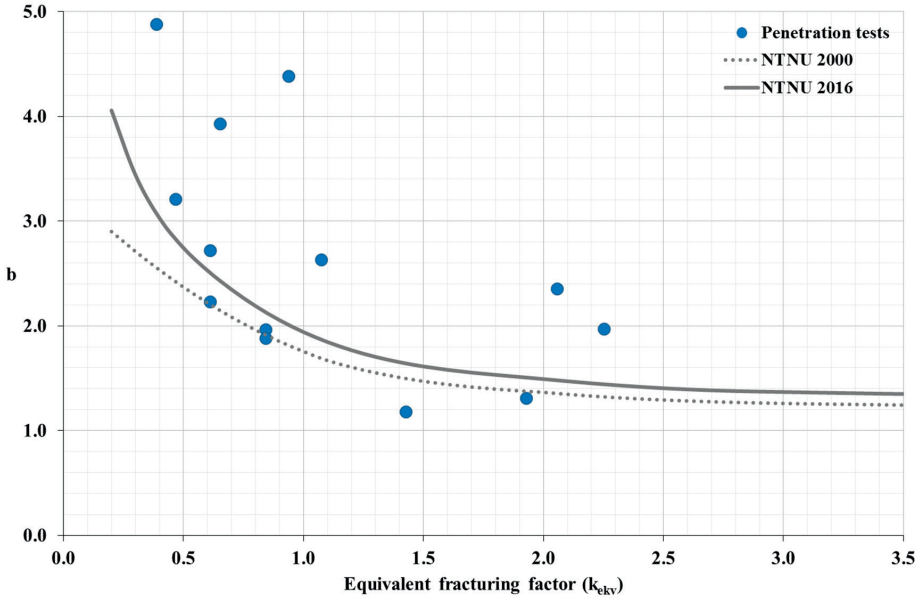

Figure 80. Penetration coefficient (b) as a function of the equivalent fracturing factor. The plotted values are taken from the results of penetration tests included in this thesis.

A complete overview of the data shows that the total amount of values is in good agreement with the previous version of the model (Bruland, 2000b). For this reason, no modifications have been considered. A slight increment in critical thrust values is detected from the previous database, which might be explained by changes in cutter ring design (constant cross section and tip width), (Bruland, 2015).

A modification of the M_1 value would be necessary. However, the current database is limited so this will become a topic for future investigation.

The penetration coefficient (b) values shown in Figure 80 are in relatively good agreement with the curve produced by Bruland (2000b), although they exhibit a conservative tendency.

The penetration coefficient curve (b) has been modified to take adjustments to the proposed cutterhead velocities and other observations into account.

Figure 81 illustrates the predicted effect of the increment of cutter thrust on the penetration rate according to the NTNU penetration rate model

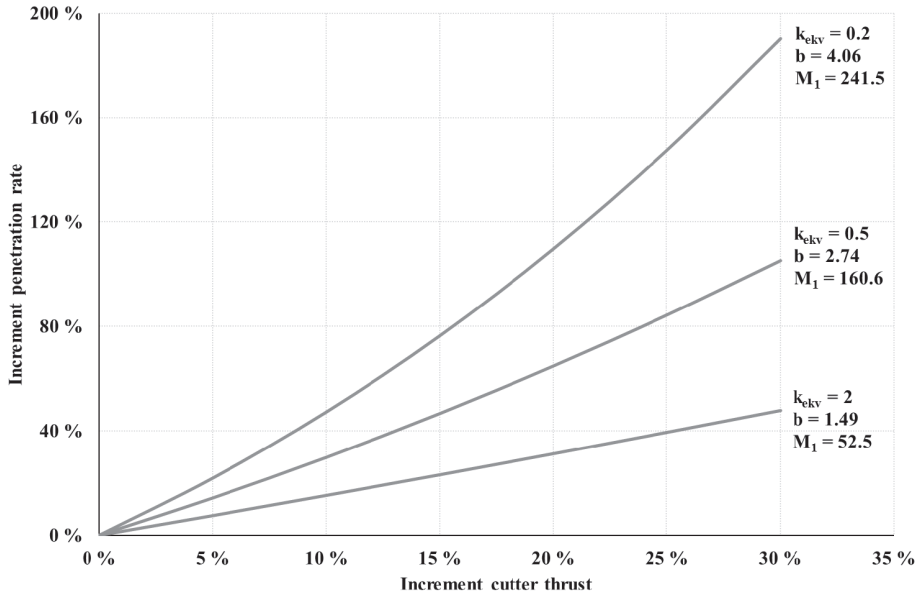

Figure 81. Predicted effect of the increment of cutter thrust on the penetration rate according to the NTNU penetration rate model.

Rock mass properties for TBM tunnelling are expressed by the equivalent fracturing factor (k_{ekv}).

$$k_{ekv} = k_{s-tot} \cdot k_{DRI} \cdot k_{por} \tag{24}$$

where

k_{ekv} = equivalent fracturing factor
$k_{s\text{-}tot}$ = total fracturing factor
k_{DRI} = correction factor for the DRI of the rock
k_{por} = correction factor for the porosity of the rock

Rock mass boreability is expressed by the fracturing factor (k_s), which is dependent on the degree of fracturing and the angle between the tunnel axis and the planes of weakness (α) in systematically fractured rock masses.

$$\alpha = \arcsin \cdot (sin\alpha_f \cdot \sin(\alpha_t - \alpha_s)) \tag{25}$$

where

α_s = strike angle of the planes of weakness
α_f = dip angle of the planes of weakness
α_t = azimuth of the tunnel axis

The fracturing factor is shown in Figure 82 as a function of fracture class and the angle between the tunnel axis and systematic fractures.

For more than one set of fractures, the total fracturing factor will be as follows:

$$k_{s-tot-avg} = \sum_{i=1}^{n} k_{si} - (n-1) \cdot 0.36 \tag{26}$$

where

$k_{s\text{-}tot}$ = total fracturing factor
k_{si} = fracturing factor for set no. i
n = number of fracture sets

A maximum of three fracture sets (n=3) is recommended, possibly with one or two main sets and one set including the random fractures. It is important to include all the fractures in the rock mass interpretation, i.e. random fractures (except marked single joints, MSJ).

The value of $k_{s\text{-}tot}$ should not exceed 4 since this will be outside the model range.

The fracturing factor (k_{si}) is calculated for each section of tunnel. Figure 82 shows the k_s parameter plotted against the angle between the tunnel axis (α) and the fractures sets for the different fracture classes.

A fracture class when low degree of fracturing has been included on the basis of the findings during the research work.

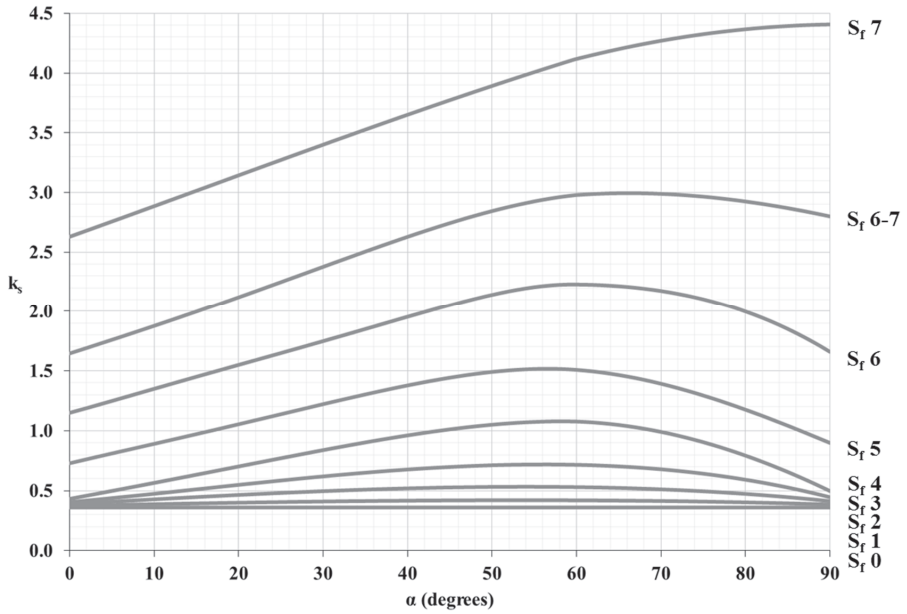

Figure 82. Rock mass fracturing factor (k_s) plotted against the angle between the tunnel axis (α) and the fracture sets for different fracture classes.

Figure 83 is a more detailed graph illustrating how the k_s parameter varies with α for fracture classes exhibiting low degrees of fracturing (between S_f 0 and S_f 5).

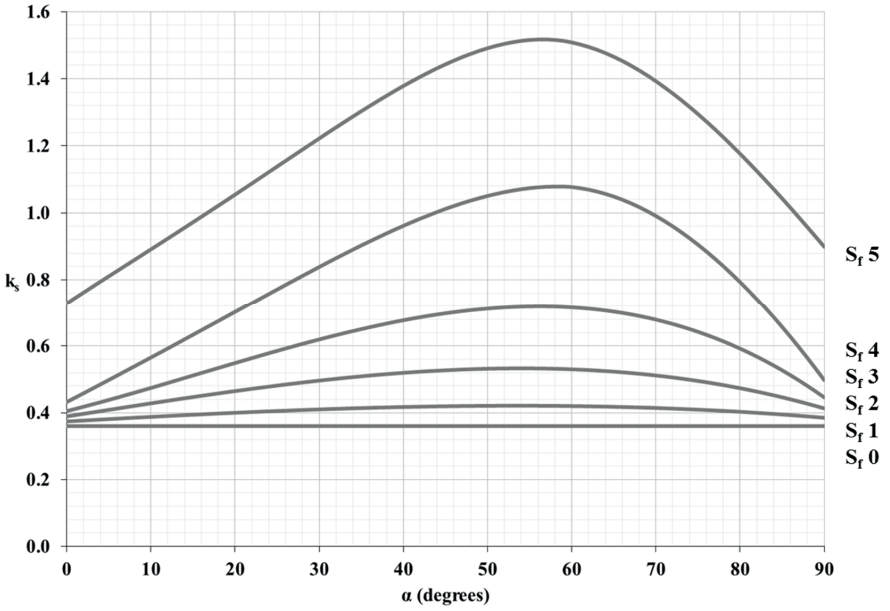

Figure 83. Rock mass fracturing factor (k_s) plotted against the angle between the tunnel axis (α) and the fractures sets for fracture classes exhibiting low degrees of fracturing. The lowest value is 0.36.

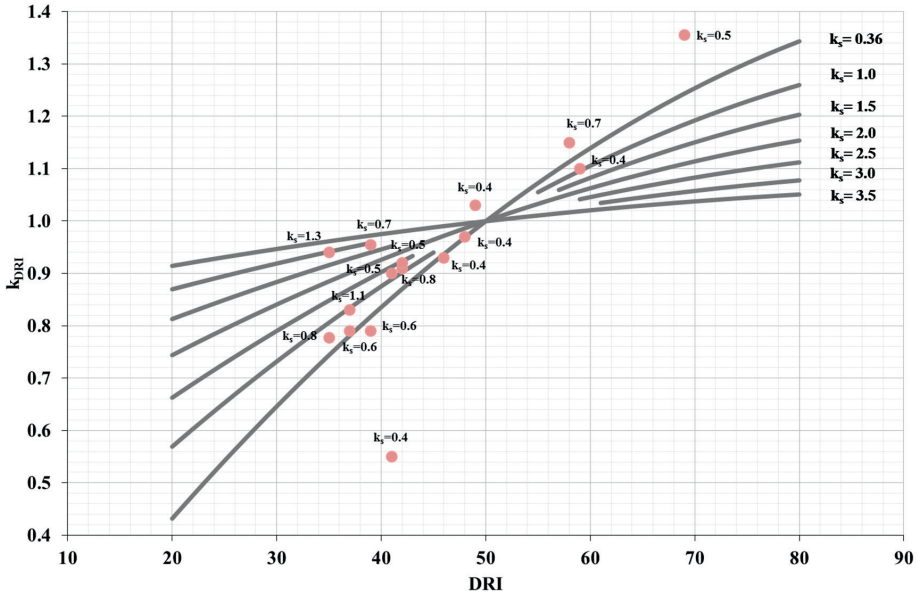

Figure 84. Plot of DRI correction factor values (k_{DRI}). The plotted values are those obtained as part of this PhD research work.

The DRI correction factor is presented in Figure 84. The plotted values are those obtained as part of this PhD research work.

No substantial modifications have been made to the DRI correction factor on the basis of general experience and the values obtained as part of this thesis work. Lines of interpolation have been included on the graph.

As shown in equation (23), the basic penetration (i_0) is a function of the equivalent thrust (M_{ekv}) and equivalent fracturing factor (k_{ekv}).

Equivalent thrust is given by Equation (27). Correction factors for cutter diameter (k_d) and the average cutter spacing (k_a) are provided in Bruland (2000b) and in the appendix to this thesis.

$$M_{ekv} = \mathrm{M}_B \cdot \mathrm{k}_d \cdot \mathrm{k}_a \qquad (\mathrm{kN/\,cutter}) \tag{27}$$

where

M_B = applied cutter thrust (kN/cutter)
k_d = correction factor for cutter diameter
k_a = correction factor for average cutter spacing

The correction factors for cutter diameter (d_c) and average cutter spacing (a_c) are used to normalise the database and have not been modified.

Figure 85 shows the basic net penetration rate (in mm/rev) for cutter of diameter 483 mm, average cutter spacing of 70 mm and a recommended RPM value.

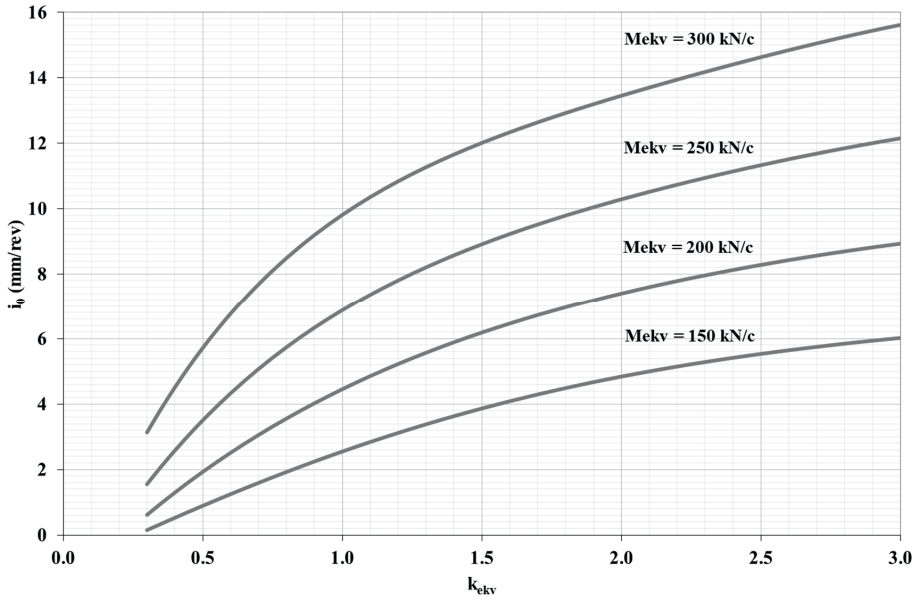

Figure 85. Basic net penetration rate where d_c = 483 mm, a_c = 70 mm and recommended rpm.

4.1.6 Influence of cutterhead velocity on penetration rate

Cutterhead velocity and the rolling velocity of the cutters have a significant influence on penetration rate.

A reduction in cutterhead velocity (rpm) values may improve boring efficiency and reduce excavation costs. Lower cutterhead rpm will promote lower cutter rolling distances and velocities for a given section of tunnel, resulting in significantly higher cutter ring life and a reduction in potential damage to cutters. Moreover, for a given thrust level and fewer revolutions of the main bearing reduce the probability of bearing failure and cutterhead damages, as well as energy consumption.

The loading rate of the cutter rings over a given point of the rock face is proportional to cutterhead rpm. The general rule in rock mechanics testing is that the loading rate influences the deformation and strength properties of a rock sample. A higher loading rate will normally result in higher rock strength.

This loading rate dependence can be explained by the fact that a high loading rate does not permit the development of dislocations, deformations and microcrack growth to the same extent as low loading rates (Bruland, 2000g). When the loading rate is high, microcracks are given insufficient time to close, resulting in a high modulus of elasticity. Changes in deformation properties are explained by the number of induced microcracks. This loading rate effect can be compared to that reported from UCS tests analysed by Fuenkajorn et al. (2012).

The influence of rpm on penetration rate was evaluated by means of full-scale trials of specified cutterhead velocities. Detailed information concerning the procedure for these trials is provided in section 3.4.3 of this thesis.

The trials revealed that in general, a lower cutterhead velocity would result in an increase in penetration rate up to a given value beyond which it decreases dramatically. The values concerned are dependent on cutterhead design, rock mass properties and level of thrust.

The resulting values obtained from the ‘RPM tests’ include values of penetration rate (PR, in mm/rev) and net penetration rate (NPR, in m/h) for each cutterhead rpm at constant level of thrust. These values are used to plot a trend line from which calculations of the initial point of the ‘RPM test’, optimal cutterhead velocity and the corresponding penetration rate for the recommended cutterhead velocity can be made.

The ‘RPM tests’ usually result in a cutterhead velocity value and a maximum net penetration rate for a given machine, geology and level of thrust. For higher and lower cutterhead rpm values, the NPR is reduced. The PR is reduced for higher cutterhead rpm. Lower cutterhead rpm result in an increase in PR up to a given value beyond which it decreases dramatically. This also causes the NPR to be reduced.

An increase in penetration rate (PR), without compromising the net penetration rate (NPR), results in improved tunnelling efficiency. The 'optimal' cutterhead velocity is thus defined as the cutterhead rpm value, which achieves maximum penetration rate while maintaining the

'optimal' level of net penetration rate for the geological conditions and level of thrust in question. Net penetration rate is assumed ‘optimal’ for a 5% from the maximum value.

Cutterhead velocity values were normalised using the recommended cutterhead rpm value (Figure 68). The penetration rate was normalised by the PR value obtained from the recommended rpm values from all the RPM tests. The reader is referred to section 3.4.3 for a detailed description of the procedure and data processing.

The variation between the initial and optimal cutterhead rpm and PR values provides an indication of improvements in boring efficiency achieved during the tests for a given machine, geology and level of thrust. The results indicate that the tendency for all normalised ‘RPM tests’ is similar.

Table 36 provides a summary of the ‘RPM test’ results, including the initial and optimal values of RPM and PR. Rock property values such as DRI, CLI and k_{ekv} are also included in the table.

Table 36. Summary of the ‘RPM tests’ included in this thesis. Rock property values such as DRI, CLI and k_{ekv} are also included, as well as values for thrust, relative cutterhead rpm (initial and optimal) and relative PR (initial and optimal).

RPM Test	DRI	CLI	k_{ekv}	Thrust (kN/c)	PNR (m/h)	Relative rpm		Relative PR		Slope
						Initial	Optimal	Initial	Optimal	
B-1	44	4.9	0.79	286	2.85	1.12	0.80	0.88	1.19	0.95
C-1	65	18.0	0.86	331	5.19	1.31	1.08	0.85	0.98	0.59
C-2	55	18.0	1.78	347	4.22	1.29	1.05	0.83	1.01	0.76
D-1	54	5.8	-	309	2.99	1.32	0.91	0.67	1.06	0.97
D-2	65	9.4	0.47	271	0.61	0.97	0.83	1.10	1.26	1.17
D-3	48	4.5	0.66	342	2.55	1.21	0.95	0.75	1.02	1.01
D-4	41	15.8	0.55	333	1.84	1.43	0.97	0.68	1.02	0.74
D-5	38	24.0	0.49	306	3.40	1.21	0.96	0.75	1.01	1.05
D-6	38	24.0	0.37	339	2.60	1.39	0.97	0.68	1.02	0.78
D-7	66	83.4	0.61	317	3.66	1.48	1.01	0.60	1.00	0.84

The plot in Figure 86 provides a summary of the normalised ‘RPM tests’ included in this thesis. Relative maximum and optimal cutterhead rpm values are included.

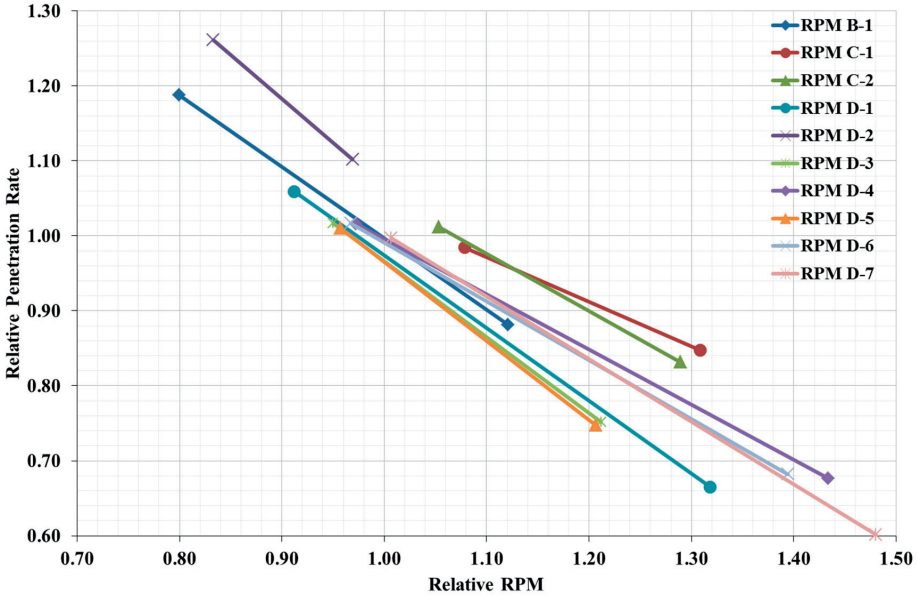

Figure 86. A Summary of the normalised RPM tests conducted as part of this thesis. Maximum and optimal relative rpm and relative penetration rate values are included.

The results of the tests indicate a clear linear relation when relative maximum and optimal cutterhead rpm values are taken into account (Figure 87).

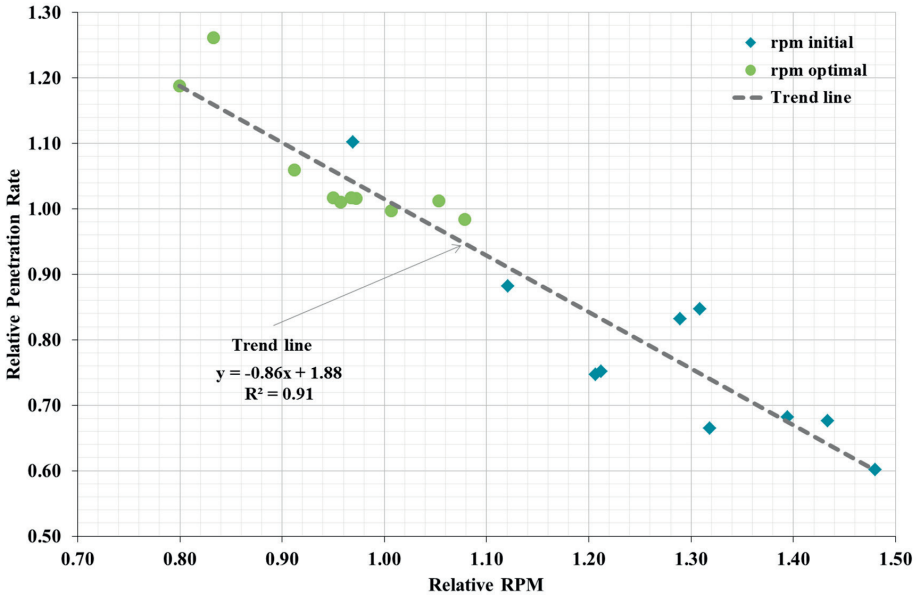

Figure 87. Values obtained from 'RPM tests' conducted as part of this thesis. The trend line shows the relative influence of RPM on relative penetration rates.

As has been established earlier, the relative optimal cutterhead rpm values resulting from the tests were used to evaluate the recommended rpm values introduced in this thesis.

Cutterhead velocity values can be standardised for a given machine diameter. Figure 88 is a histogram showing the relationship between optimal cutterhead rpm and machine diameter values resulting from the 'RPM tests'.

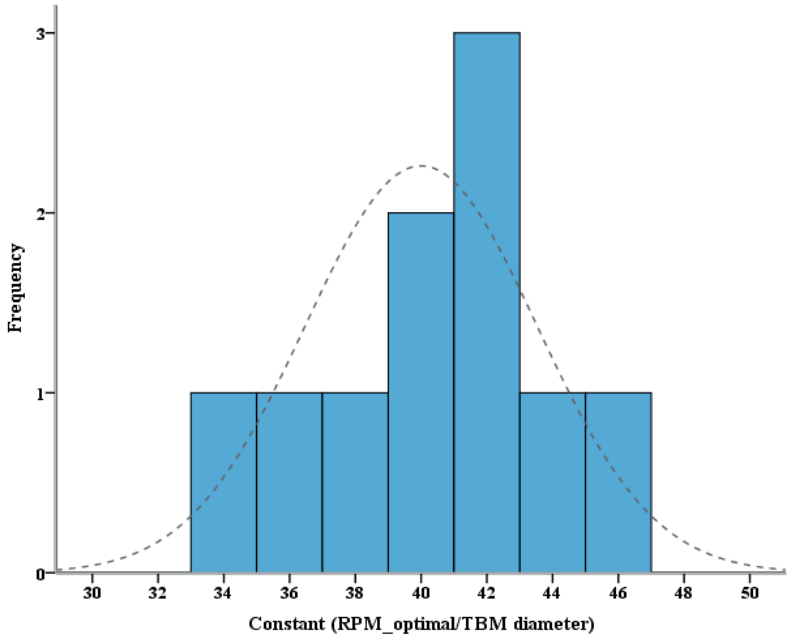

Figure 88. A histogram and normal distribution curve illustrating the relationship between optimal RPM and machine diameter values.

The optimal value for the parameter "rpm_optimal/TBM diameter" shown in Figure 88 is 42. This value is thus selected as the recommended cutterhead rpm value for predictions of performance and cutter life used by the updated NTNU model.

Example of analysis of a 'RPM test'

A complete analysis, including chip examination, of one of the 'RPM tests' included in this thesis ('RPM test' C-2) is used as an example in this section.

Table 37 provides a summary of rpm, gross cutter thrust, penetration rate, net penetration rate and torque values for the RPM test C-2.

Table 37. Summary of the values of rpm, gross cutter thrust, penetration rate, net penetration rate and torque for the 'RPM test' C-2 (Eide, 2014).

Cutterhead rpm	Thrust (kN/cutter)	PR (mm/rev)	NPR (m/h)	Torque (kNm)
10	346.5	7.57	4.54	1 383
9	346.5	8.47	4.57	1 533
8	346.5	9.59	4.60	1 700
7	346.5	8.49	3.57	1 400
10	346.5	7.16	4.30	1 400

Figure 89 shows the penetration rate and net penetration rate values obtained from the 'RPM test' C-2.

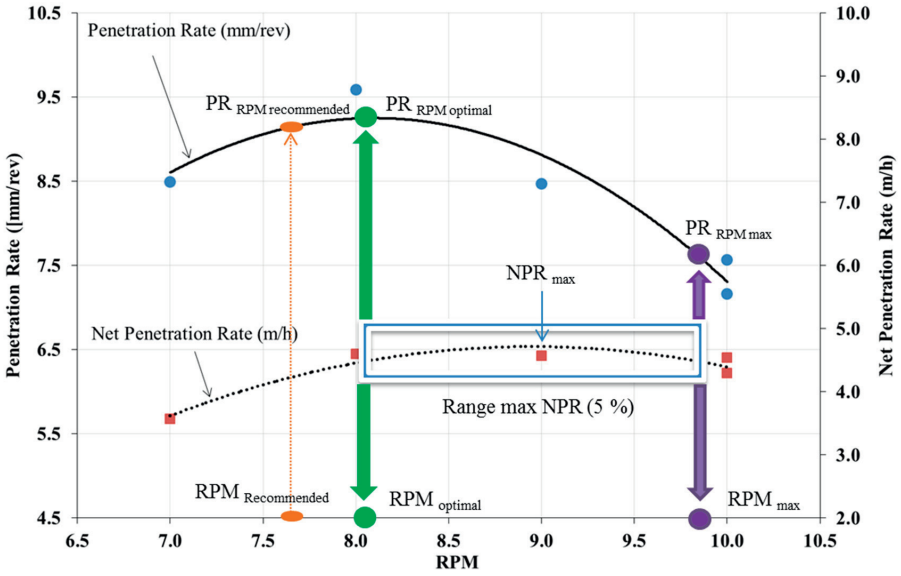

Figure 89. Penetration rate and net penetration rate values obtained from the 'RPM test' C-2.

The 'optimal' cutterhead rpm value is defined as that which achieves maximum penetration rate while maintaining the 'optimal' net penetration rate (maximum net penetration rate value within a margin of variation of 5%).

Table 38 provides a summary of the 'RPM test' outcomes following analysis of the data as described in section 3.4.3 of this thesis.

Table 38. Summary of outcomes for the RPM test C-2.

	rpm	PR (mm/rev)	NPR (m/h)
-5% NPR (after max.)	9.85	7.60	4.48
Max. NPR	9.00	8.81	4.72
rpm optimal (-5% NPR before max.)	8.05	9.25	4.48

Based on the values shown in Table 38, the optimal cutterhead velocity for the given geology during this test was 8.05 rpm. The same maximum velocity was achieved for cutterhead rpm values varying from 8.05 to 9.85. A higher penetration rate results in a more efficient rock breaking process. Lower rpm implies a higher cutter life that will result in an improved machine utilization, which it will be beneficial for the advance rate.

Table 39 is a summary of parameters, including average chip size measurements, chipping frequency, cubic chip shape and chip shape factor for every rpm value applied in the 'RPM test' C-2 included in this thesis. For detailed information of chipping analyses, the reader is referred to Bruland (2000f).

Table 39. Summary of average chip size measurements, chipping frequency, cubic chip size and chip shape factor values applied during the RPM test C-2 (Eide, 2014).

rpm	PR (mm/rev)	Average chip size (mm)			Chipping frequency f_{ch} (rev^{-1})	Cubic chip size (1 000 mm^3)	Chip shape factor	
		h_{ch}	w_{ch}	l_{ch}			f_{hw}	f_{wl}
10	7.57	25.77	83.18	197.48	0.29	423.27	0.31	0.42
9	8.47	27.24	86.59	183.18	0.31	432.05	0.31	0.47
8	9.59	32.13	90.88	193.92	0.30	566.24	0.35	0.47
7	8.49	25.90	83.43	181.95	0.33	393.18	0.31	0.46
10	7.16	28.21	87.57	196.13	0.25	484.47	0.32	0.45

On the basis of the chip analysis data presented in Table 39, it is possible to show that the rock breaking process is most efficient at cutterhead rpm values of about 8 for a given machine and set of geological conditions. The 'optimal' cutterhead rpm value coincides with the largest cubic chip size (and thickness and width values). Moreover, trends in chipping frequency increase at lower cutterhead rpm values, and thus also with rock breaking efficiency.

Figure 90 shows variation in average chip size and cubic chip size as a function of cutterhead velocity.

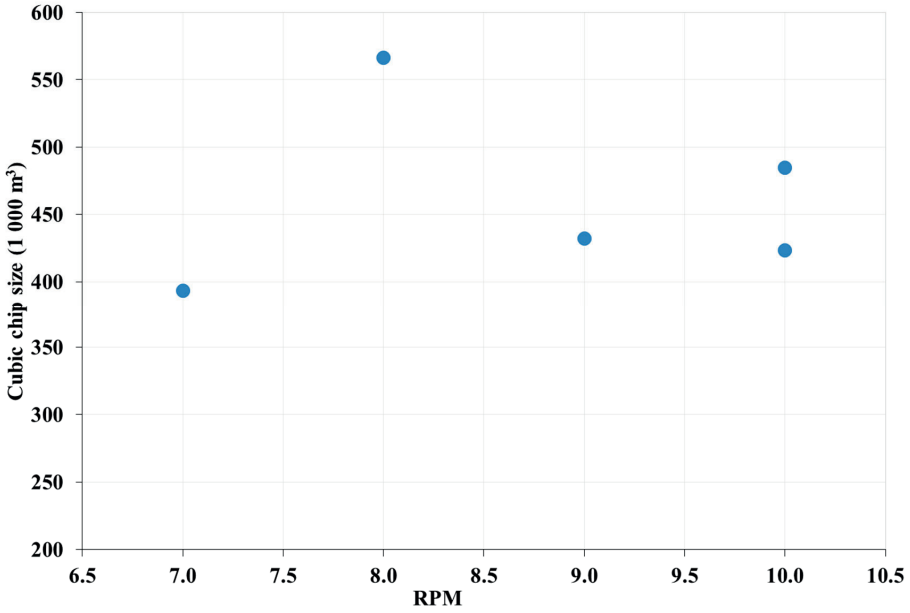

Figure 90. Average values of size of largest chip (left) and cubic chip size (right) obtained from the 'RPM test' C-2 (Eide, 2014).

Relationships and correlations

'RPM test' results are mainly influenced by geology, cutter thrust level and/or cutterhead design.

An analysis has been carried out of the relationships between the various parameters (relative cutterhead rpm 'optimal', gross cutter thrust, rock mass fracturing equivalent factor, and trend slope) presented in Table 36.

The following conclusions can be drawn from the 'RPM tests'. (Reservations are made for the limited number of tests carried out).

- The relative optimal values of cutterhead rpm and PR are influenced by the level of thrust used during testing. The higher the thrust, the lower the influence of cutterhead velocity on the penetration rate.
- The level of thrust does not have a major influence on the slope obtained from the 'RPM tests' (Figure 86).
- The 'optimal' cutterhead rpm value is influenced by geology (drillability and/or rock mass fracturing).

The lower the value of the equivalent fracturing factor (k_{ekv}), the lower the relative rpm value. This can be explained by the fact that a lower loading rate allows the stresses imposed to induce cracks in an otherwise non-fractured rock. As previously discussed, this loading rate effect might be compared to that reported from uniaxial compressive strength tests described by Fuenkajorn et al. (2012).

'RPM tests' demonstrate uncertain behaviour for values below the optimal. It is highly probable that at sufficiently low cutterhead rpm values, relative PR values would also fall dramatically. Extremely low rpm values may result in a loss of the dynamic effect of the breaking process during boring. Due to uncertainties revealed during the trial tests, no influence of cutterhead velocity has been included for values below the relative 'optimal' cutterhead velocity.

Figure 91 and Figure 92 present the relationships between gross cutter thrust and relative 'optimal' cutterhead rpm and PR values, respectively. The trends revealed are considered to be acceptable in that lower relative 'optimal' cutterhead rpm values coincide with reduced gross cutter thrust levels (Figure 91). Figure 92 shows that relative PR values decrease when gross cutter thrust increases.

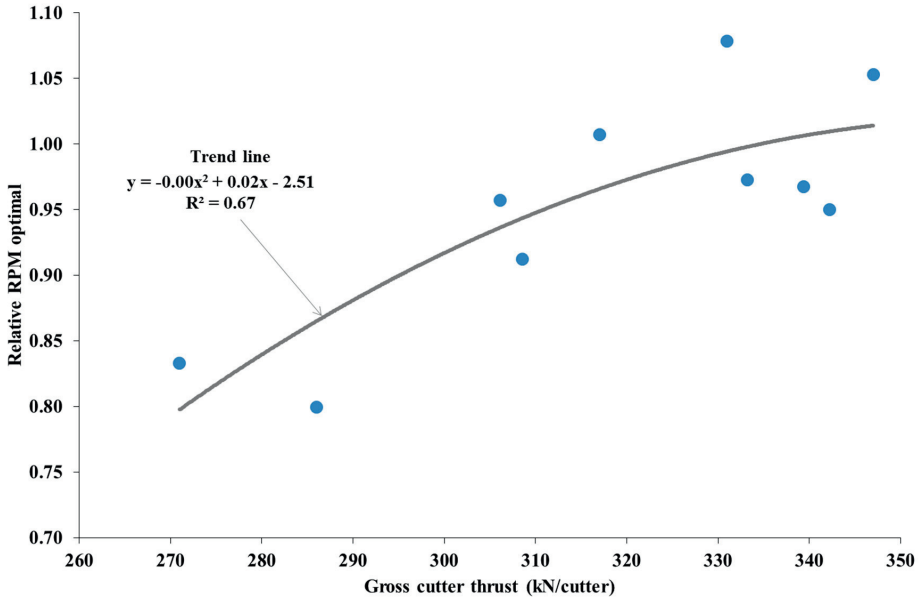

Figure 91. Relationship between gross average cutter thrust and relative 'optimal' cutterhead rpm based on the tests conducted as part of this thesis. A maximum correlation level fit has been selected.

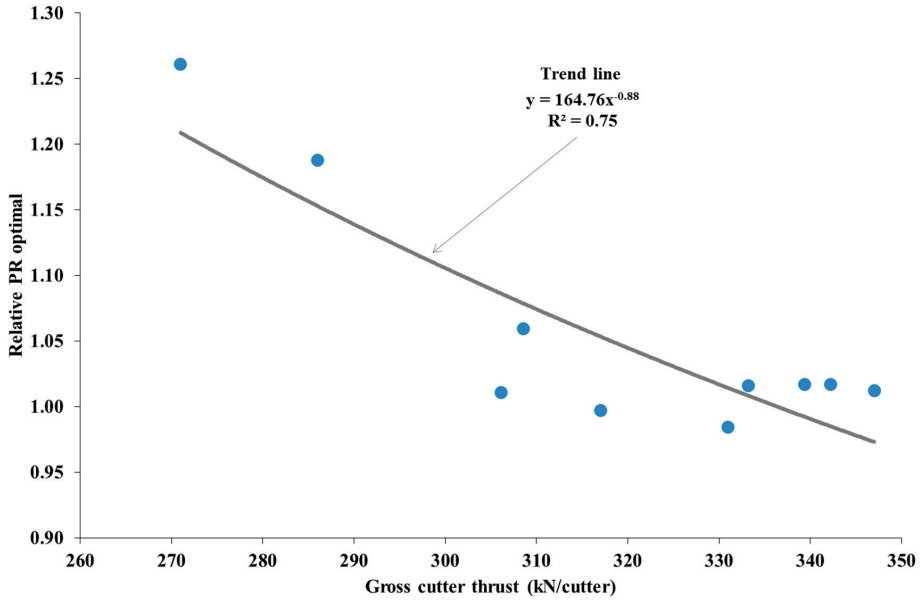

Figure 92. Relationship between gross average cutter thrust and relative optimal PR based on the tests conducted as part of this thesis. A maximum correlation level fit has been selected.

Figure 93 shows the relationship between the equivalent rock mass fracturing factor and relative RPM values.

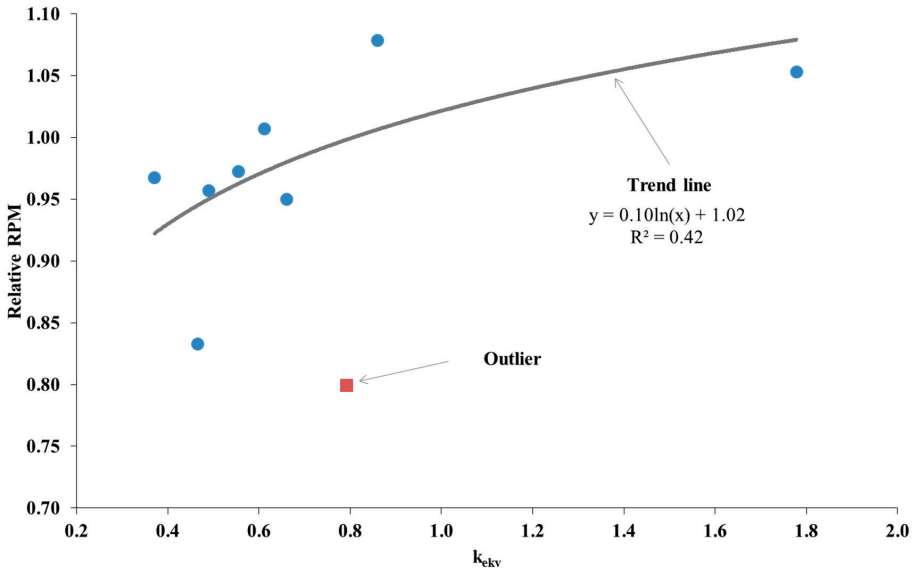

Figure 93. Relationship between the equivalent fracturing factor (k_{ekv}) and relative cutterhead rpm based on the tests conducted as part of this thesis. A maximum correlation level fit has been selected.

Figure 94 shows that the lower the relative 'optimal' cutterhead rpm value (y-axis), the steeper the slope of the 'RPM test' trend.

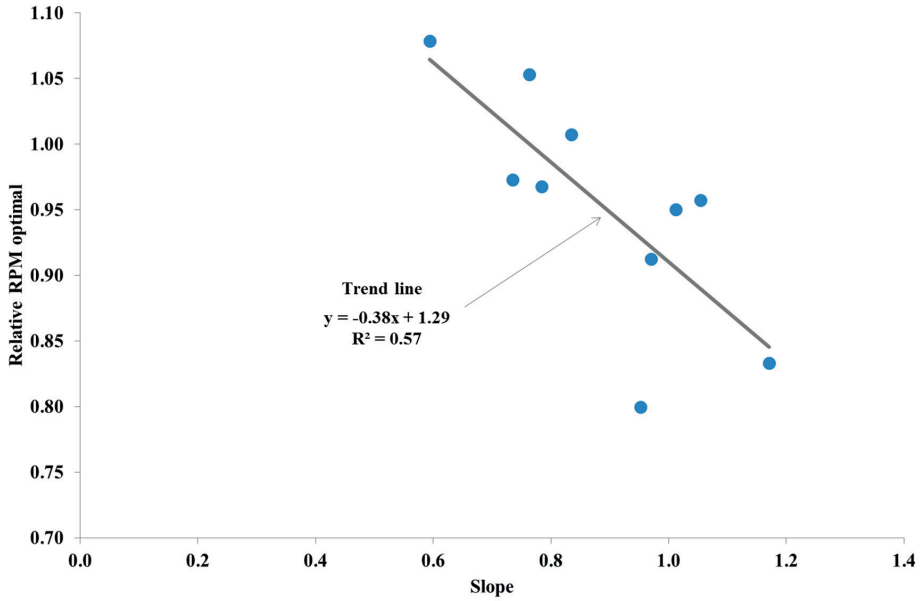

Figure 94. Relationship between the slope generated from all test results and the relative cutterhead rpm value based on the tests conducted as part of this thesis. A maximum correlation level fit has been selected.

The results in Figure 94 indicate a distinguished effect of the 'optimal' cutterhead rpm when this is lower.

Figure 95 shows the variation in relative penetration rate as a function of relative cutterhead rpm values (below optimum) for the tests conducted as part of this thesis. The tests exhibit a practical minimum due to the loss of net penetration rate.

Based on the normalised 'RPM tests' performed during the research work and included in this thesis, a correction factor for cutterhead velocity (k_{rpm}) has been introduced which differs from the recommended value as a function of relative cutterhead rpm (Figure 96).

As previously discussed, penetration rates and other behaviours for values of relative cutterhead velocity below 1 for a given TBM diameter are unpredictable (see also Figure 95).

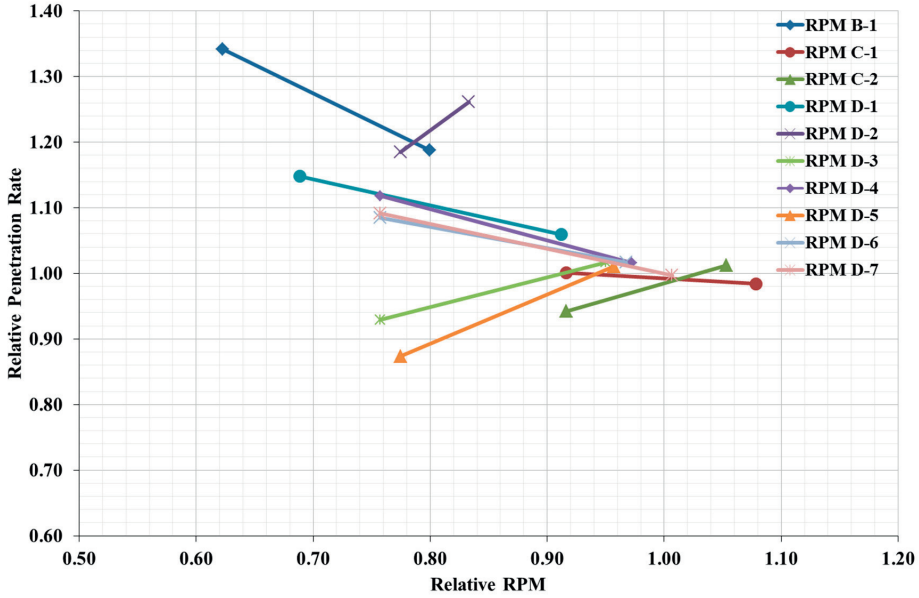

Figure 95. Summary of results of 'RPM tests' carried out at below optimal cutterhead rpm values. The data included are optimal and minimum relative rpm, together with relative penetration rate.

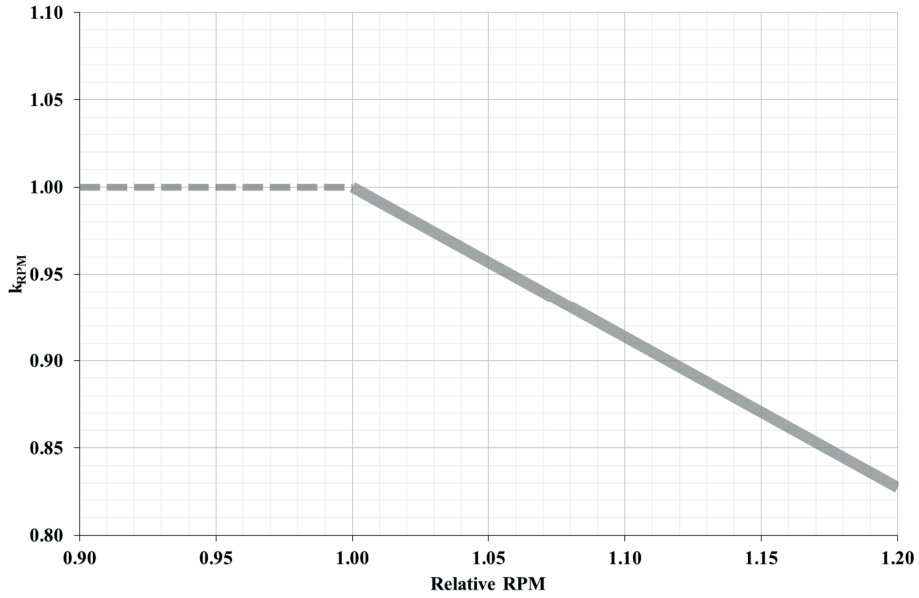

Figure 96. A correction factor for cutterhead velocity that differs from the recommended value as a function of relative rpm.

Thus, for values below the recommended cutterhead velocity (relative rpm with value 1), no influence of cutterhead velocity is considered.

The rpm factor applies to basic net penetration rate behaviour. The basic net penetration rate (I_0) parameter is a function of basic penetration and cutterhead velocity, and can be applied in situations involving systematically fractured rock masses lacking so-called 'Marked Single Joints'.

$$I_0 = i_0 \cdot rpm \cdot \left(\frac{60}{1000}\right) \cdot k_{rpm} \quad \text{(m/h)} \tag{27}$$

Penetration rate analysis: actual versus predicted

Figure 97 shows the comparison between actual and predicted penetration rates of sections analysed in different of the projects included in the thesis.

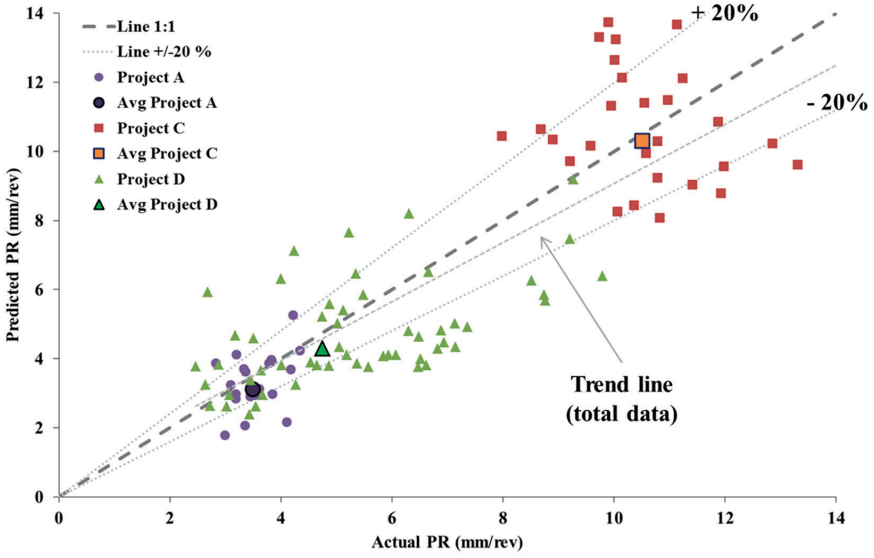

Figure 97. A plot showing penetration rate data obtained from projects A, C and D. The data shows actual versus predicted PR values measured along 50-metre tunnel sections.

The comparison between actual and predicted PR values (Figure 97) shows good correlation along the PR levels, especially when the average of the section is considered. This is due that the prediction model is based on average data from different sections.

4.1.7 Cutter life model

The NTNU cutter life model has been reviewed based on detailed information about geology, rock mass, drillability testing and instantaneous cutter life obtained from selected tunnel sections at projects A, C, D and E included in this thesis.

Basic cutter ring life was back-calculated from the instantaneous cutter life parameter for every tunnel section, taking correction factors for TBM diameter, cutterhead rpm, number of cutters, abrasive minerals content and cutter thrust into consideration. For detailed

information about the calculation approach, the reader is referred to section 3.3.6 which describes the research methodology.

Correction for TBM diameter

Centre and gauge cutters have shorter lifetimes than face cutters. As TBM diameter increases, the ratio of centre and gauge cutters to face cutters decreases, causing the lifetime of the average cutter to increase (Figure 68).

The cutterhead factor is calculated by analysing the cutter ring consumption in each position as a cutterhead of radius = 1 and an average cutter position of 1 (see section 3.3.6).

An analysis has been carried out of the TBM correction factor. More recent cutterheads include a greater proportion of centre cutters with lower relative cutter life. The general trend of the face cutters is similar to, though slightly deviated from, the increment of the centre cutters. For gauge cutters, relative cutter life is somewhat shorter (Figure 98).

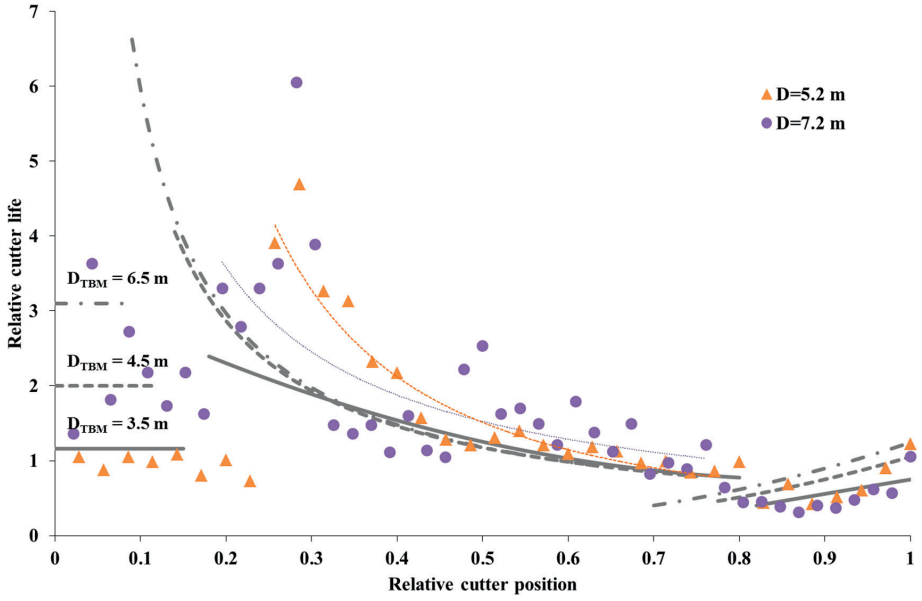

Figure 98. Normalised cutter replacement curves for different TBM diameters (Bruland, 2000e). The plotted points (dots and triangles) represent an example of data from the projects used in this thesis.

Calculations have been made for the correction factors for different TBM diameters (k_D). Comparison with the previous version of the model (Bruland, 2000e) shows good agreement for TBMs with diameters up to about 7 metres. However, for 10m-diameter TBMs, the results are greater than predicted values. Due to the limited number of cutterheads available, no variation has been implemented. It is recommended that the correction factor for large TBMS should be revised in subsequent revisions of the model using a greater volume of data. Figure 99 shows the correction factor resulting from varying the k_D parameter with TBM diameter using the previous version of the model.

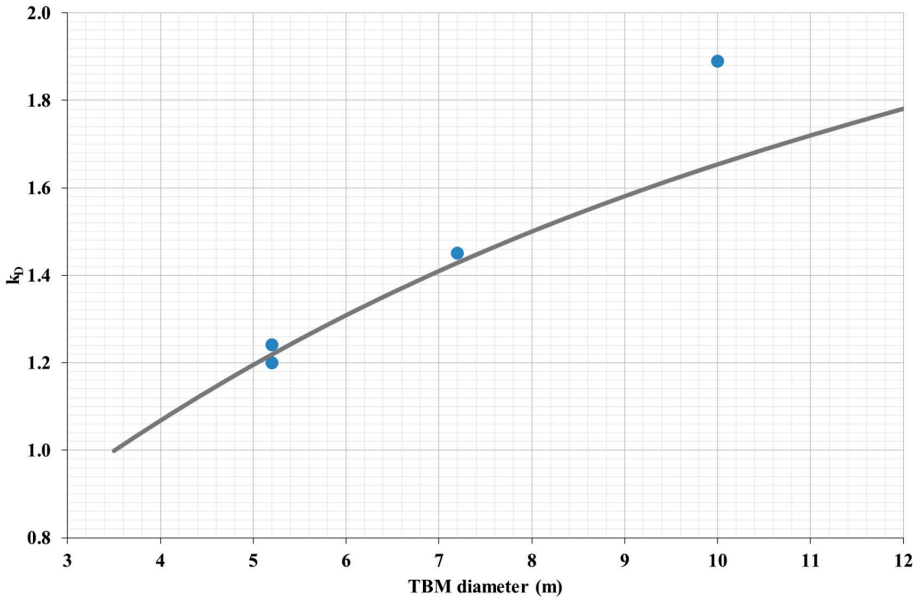

Figure 99. Correction factor for TBM diameter. The plotted points represent data from the projects used in this thesis.

Correction for the standard number of cutters

When the actual number of cutters on a cutterhead differs from the model, the average lifetime of an individual cutter will change. The correction factor is then expressed by:

$$k_N = \frac{N_{tbm}}{N_0} \tag{29}$$

where

N_{tbm} = actual number of cutters
N_0 = standard number of cutters (updated as part of this thesis)

Correction for cutterhead velocity (rpm)

Cutter ring life is inversely proportional to cutterhead velocity (rpm), based on the assumption that for a given set of lithological conditions, lifetime is proportional to rolling distance and independent of rolling velocity.

The recommended cutterhead rpm has been updated, and hence the 'rpm factor' used to calculate basic cutter ring life. The updated correction factor used under conditions of varying cutterhead velocity is shown in equation (28).

$$k_{rpm} = \frac{42 / d_{tbm}}{rpm} \tag{28}$$

where

d_{tbm} = TBM cutterhead diameter (m)
rpm = cutterhead velocity (updated as part of this thesis)

The influence of cutterhead velocity on hard rock tunnelling has been analysed as part of this study, resulting in a new recommendation for applied velocities. This has already been included in the velocity correction factor. The new constant value is 42 (see section 4.1.6, appendix).

Correction for abrasive minerals

Cutter ring life varies with the relative proportions of quartz and other hard and abrasive minerals contained in the rock under excavation. Experience at NTNU has shown that the content of minerals such as garnet, epidote, olivine or pyrite should be incorporated with quartz content when estimating cutter ring life from the plot (Bruland, 2000e). In this study, the influence of these abrasive minerals have been analysed being considered in the calculations.

The results show a good correlation with the correction factor obtained from the previous version of the model (Figure 100).

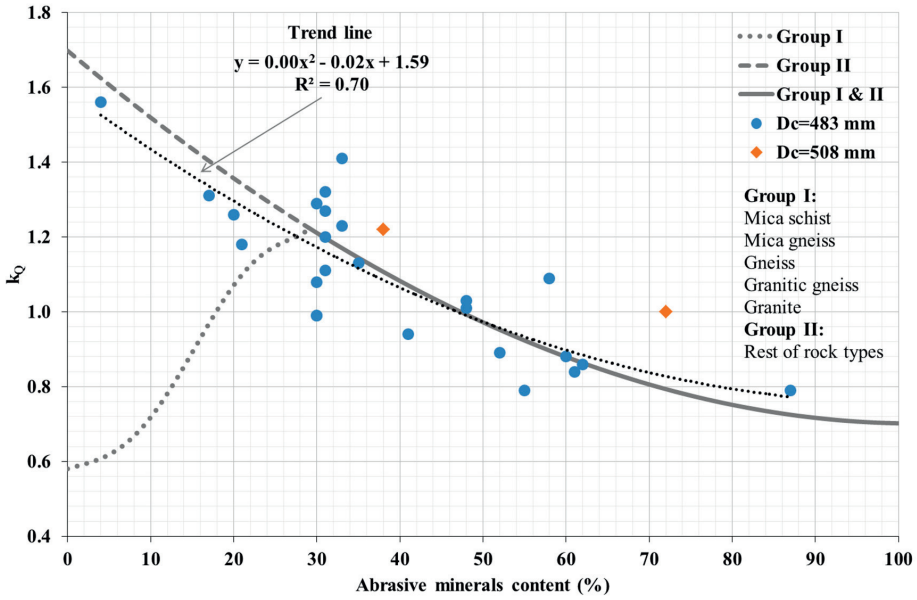

Figure 100. Correction factor for abrasive minerals (k_Q).

The abrasive mineral correction factor is based on normalised field and laboratory data. Rock types were categorised into two groups based on previous versions of the model (Bruland, 2000b): Group I contains mica schists, mica gneisses, gneisses, granitic gneisses and granites,

while Group II encompasses all other rock types. The shape of the curve for Group I rock types (Figure 100) can be explained by the fact that the CLI and rock quartz content parameters are not independent variables and/or that laboratory test procedures used to determine the CLI parameter are influenced by the mineral composition of the rock according to Bruland, (2000b).

During the research work, and confirming previous experiences, it was found that other abrasive minerals (garnet, epidote, olivine or pyrite) have a significant presence when rocks from Group I are analysed and therefore given high values of abrasive minerals content.

Therefore, based on the results and only a limited data for rock types of Group I (Bruland, 2015); distinctions between rock types are not going to be considered. At any event, care should be exercised when quartz contents are between 0 and 27% for Group I rock types.

Influence of thrust levels on cutter consumption

The influence of applied cutter thrust on cutter life has been analysed for tunnel sections exhibiting hard rock conditions (high levels of strength, high abrasivity and slightly fractured rock mass properties). The selected sections are taken from projects B, D and E included in this thesis.

The influence of cutter thrust on cutter consumption under hard rock boring conditions has previously been noted by NTH (1983) and Bruland (2000f).

The results of the analysis reveal the influence of gross cutter thrust levels in highly abrasive rock types where $4.5 < CLI < 5.9$. For comparison, thrust is plotted against basic cutter ring life in Figure 101. The use of basic cutter ring life (hours) allows the comparison between the data from different TBM cutterhead diameters, cutterhead rpm levels or amount of abrasive minerals.

Figure 101 indicates that the increment of the applied cutter thrust will reduce considerably the basic cutter ring life while a more limited increment will result from a reduction of the applied cutter thrust. It is important to consider that, a variation of the thrust will result in variations on the net penetration and therefore in cutter life (expressed in m/c or m^3/c).

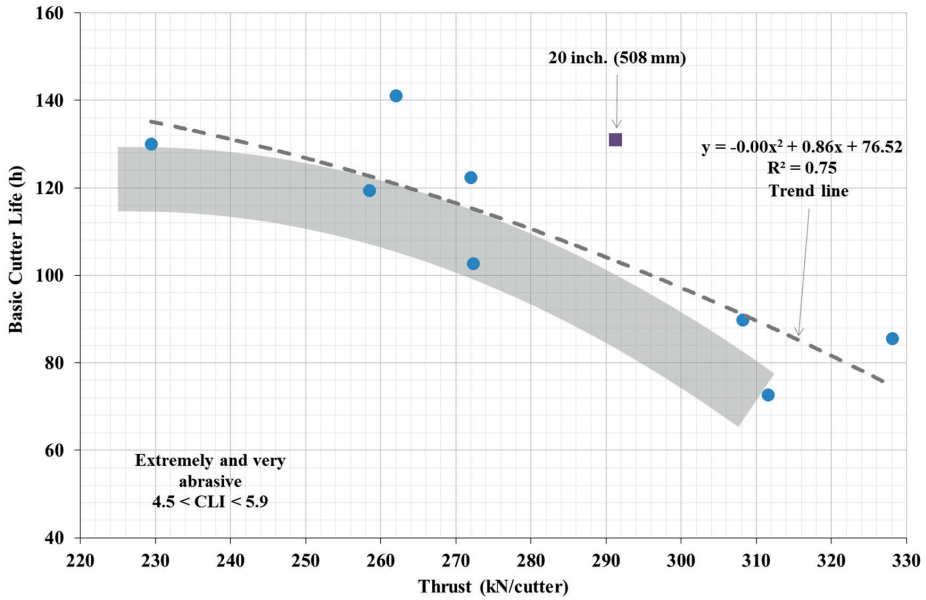

Figure 101. The influence of cutter thrust levels on cutter life for highly abrasive rocks (4.5<CLI<5.9). The 20-in. cutter diameter value is deliberately excluded from the data used to construct the trend line.

In the light of the recommendations for cutter thrust values previously discussed in section 4.1.2, a correction factor has been calculated which normalises the basic cutter ring life parameter (h). The recommended value for gross cutter thrust of 280 kN/cutter is used. Figure 102 shows the correction factor applied to cutter life in the case of highly abrasive rocks (4.5<CLI<5.9).

The factor illustrated in Figure 102 should be used with caution due to the limited amount of data on which it is based and the high levels of variability in the parameters involved in the calculation.

Cutter life (expressed in m/c or m^3/c) will not necessarily exhibit consistent behaviour due to variations in TBM penetration rates and/or TBM diameters.

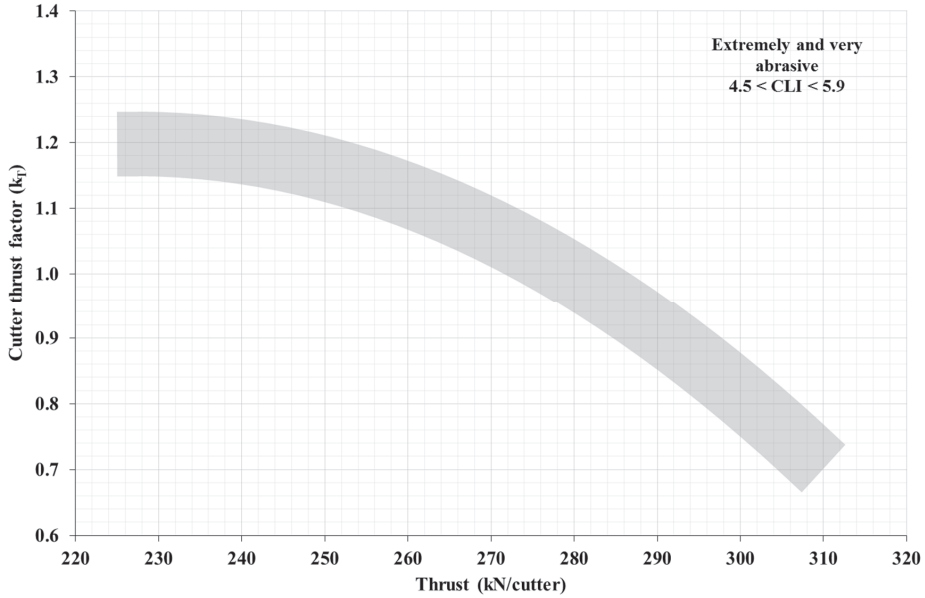

Figure 102. Correction factor applied to the influence of cutter thrust on cutter life for highly abrasive rocks (4.5<CLI<5.9).

The average life of cutter rings is given by equations (30), (31) and (32) below

$$H_h = (H_0 \cdot k_D \cdot k_Q \cdot k_{rpm} \cdot k_N \cdot k_T) / N_{tbm} \quad \text{(h/c)} \tag{30}$$

$$H_m = H_h \cdot I_n \quad \text{(m/c)} \tag{31}$$

$$H_f = H_h \cdot I_n \cdot \pi \cdot d_{tbm}^2 / 4 \quad (\text{sm}^3/\text{c}) \tag{32}$$

where

H_0 = basic average cutter ring life (hours)
H_h = average cutter ring life (hours)
H_m = average cutter ring life (metres)
H_f = average cutter ring life (solid cubic metres)
I_n = net penetration rate (m/h)
d_{tbm} = TBM diameter (m)

A first comparison with the previous version of the model (Bruland, 2000b) is considered relevant.

The instantaneous cutter life (H_h, H_m and H_f) are calculated along the tunnels in question and averaged for each selected section. The basic cutter ring life (H_0) is back-calculated based on measured rock properties and the relevant machine parameters.

A calculation of the basic cutter ring life has been carried out based on an uncertainty analysis. Section 3.3.6 of this thesis includes a more detailed description of the procedure used. A variation factor of 15% of the cumulative distribution of CLI and quartz content (Bruland, 2000i) is applied. In order to account for uncertainties arising from ring steel quality, set bearing capacity and other properties, a variation factor of 10% is used.

The results indicate that the previous version of the model (Bruland, 2000b) provides a marginally conservative result, even taking uncertainties in the input parameters into consideration. This might be due to the effects of changes of cutter tip design and/or improvements in cutter technology.

The updated version has been modified in the light of minimum cutter ring life values and data obtained from previous versions of the model (Figure 103).

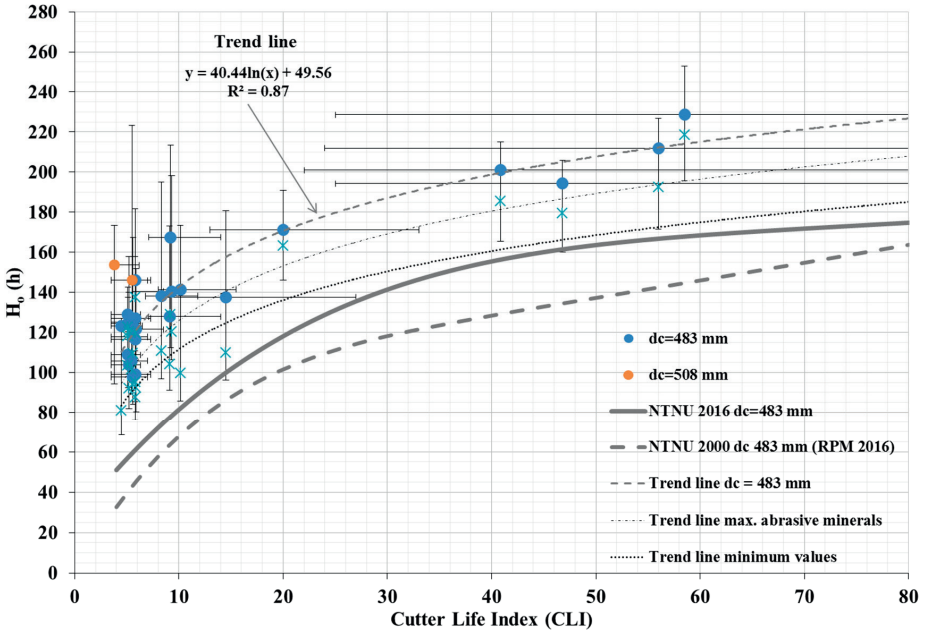

Figure 103. A plot showing basic cutter ring life obtained using the 2016 version of the NTNU model for 483 mm and 508 mm diameter cutters. For comparison, the plot also shows basic cutter ring life of the NTNU 2000 version of the model. Results from the uncertainty analysis are also plotted.

The increment of the predicted basic cutter ring life in the updated version compared with the previous (Bruland, 2000b) has been up to around 20%. A reason for this might an increment of the cutter disc quality over the last two decades.

The same percentage increment in the basic cutter ring life along the CLI values has also been considered for cutter diameters of 432 mm (17 inch) and 483 mm (19 inch).

Figure 104 shows plots of basic cutter ring life (h) for 432 and 483 mm cutter diameters obtained from the updated (2016) version of the NTNU model.

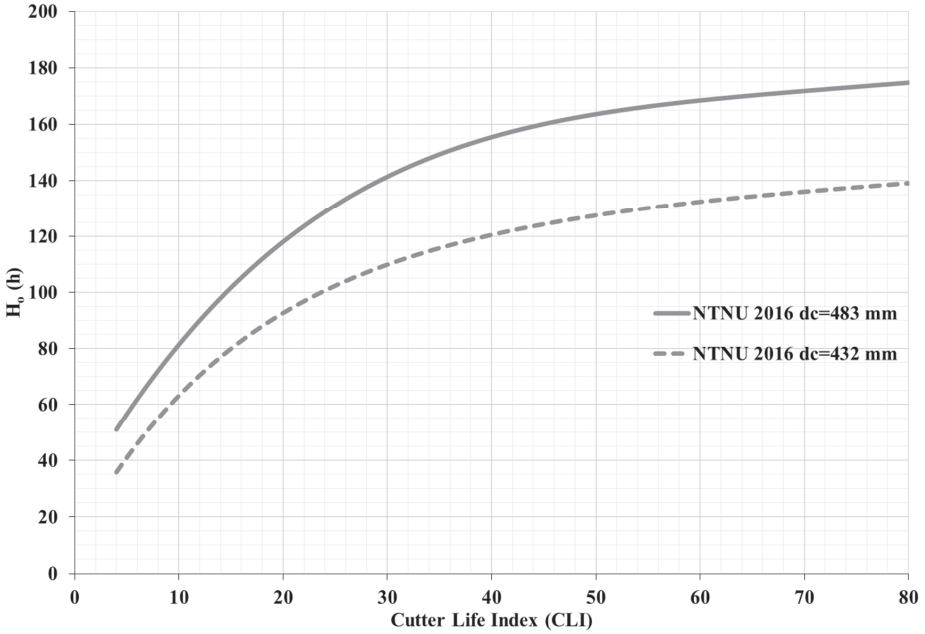

Figure 104. Plots showing basic cutter ring life (h) for 432 and 483 mm cutter diameters obtained from the updated (2016) version of the NTNU model.

Calculations for 508 mm (20 inch) cutter diameters have not been included due to insufficient data, although it can be noted that results indicate a longer basic cutter ring life for highly abrasive rocks (exhibiting extremely and very low CLI values).

Rock surface hardness or resistance to indentation is the rock property that exerts the greatest influence on cutter ring life at low SJ values (equivalent to extremely high, very high and high surface hardness values, $2.0 < SJ < 6.9$). Figure 105 shows basic cutter ring life (H_0) as a function of the Sievers' J value (SJ) corresponding to CLI values between 5.2 and 9.9 (equivalent to very low to medium, according to Dahl et al., 2012). No direct correlation is identified with the AVS value.

Figure 105 indicates a major influence of the rock surface hardness for rocks with low CLI.

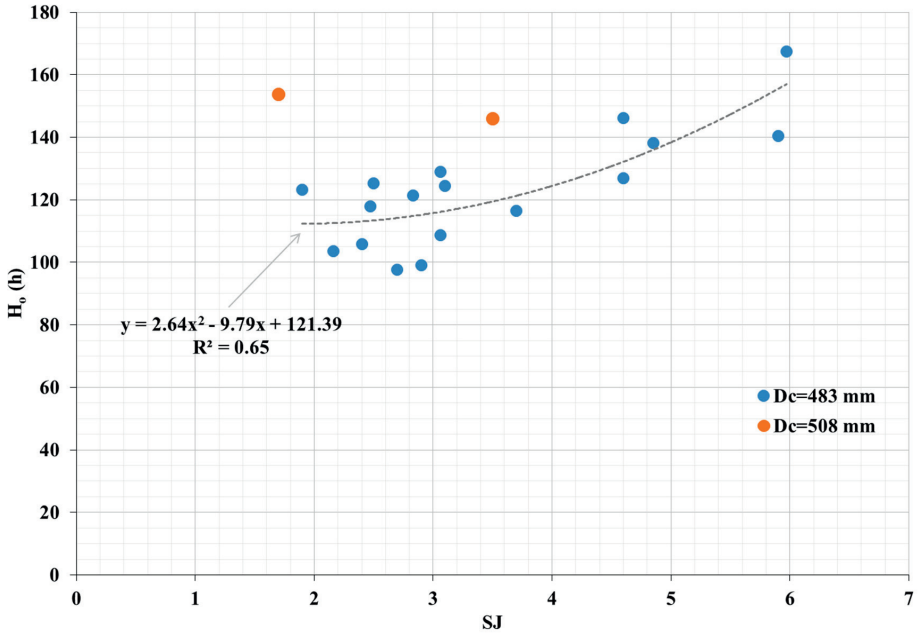

Figure 105. Basic cutter ring life (H_o) as a function of the Sievers' J value (SJ) corresponding to CLI values between 5.2 and 9.9 (from very low to medium, according to Dahl et al., 2012). The minimum SJ value is limited to 1.5.

For rock types where CLI > 30 (very high and extremely high), a high proportion (60-90%) of cutter replacements are due to bearing-related issues. Cutter life is thus influenced most by factors other than the prolonged life of the cutters installed on the cutterhead. The high percentage of cutters change due to set bearing or others is a reason of the almost flat estimated basic cutter ring life in rock masses with high CLI values.

Figure 106 and Figure 107 show the relationship between bearing-related or other reasons for cutter replacement and CLI values, and basic cutter ring life, respectively. The trends indicated in these figures exhibit the same curve shape as for the basic cutter ring life (Figure 104).

The bearing life plays a significant role for rock masses with exhibit low abrasivity and/or high degree of fracturing.

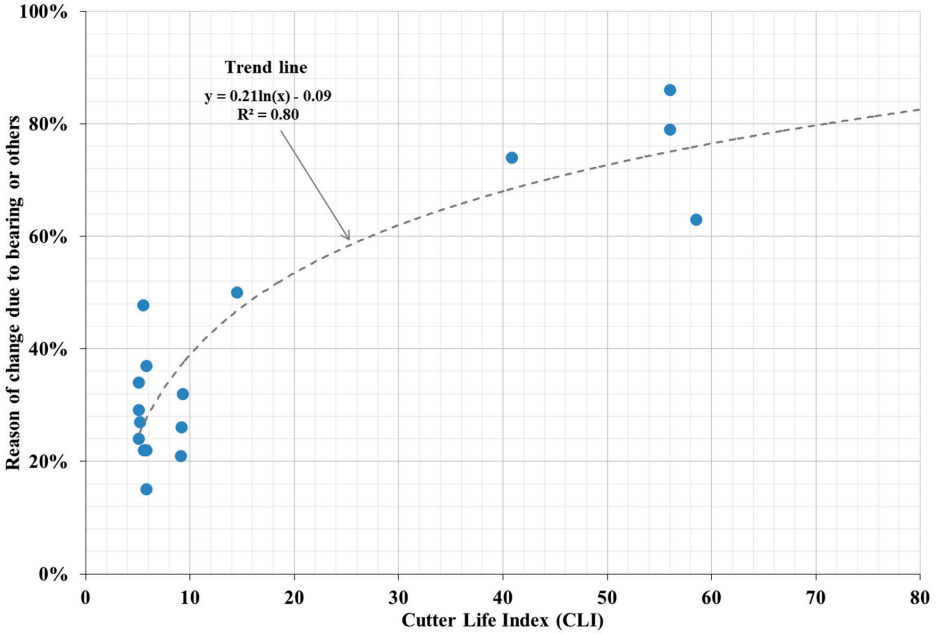

Figure 106. Relationship between CLI and bearing-related or other reasons for cutter replacement.

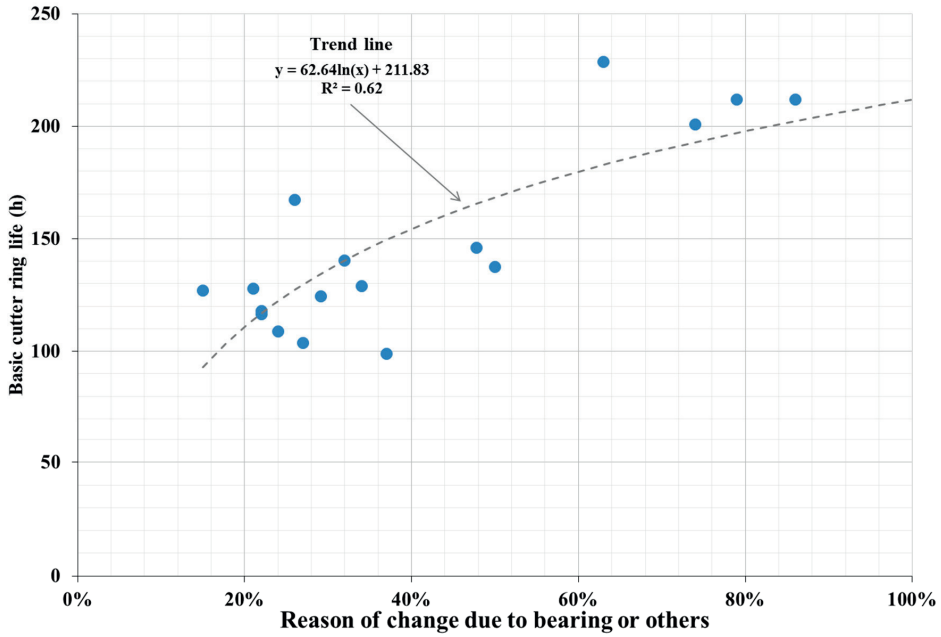

Figure 107. Relationship between basic cutter ring life (h) and bearing-related or other reasons for cutter replacement.

Other factors influencing cutter wear

In fractured rock masses, or in situations where extremely good rock chipping occurs, the cutters will be exposed to large instantaneous loads. Entacher et al. (2013) measured momentary loads in individual cutter discs up to 3.5 times higher than a nominal cutter load and up to 10 times higher than the average load in fractured rock.

Under such conditions, a cutter ring exhibits a tendency to chip along its edge. Extensive ring chipping and high cutter thrust may result in bevel edge wear, loosened rings and blocked bearings.

Additional loads will result in higher abrasion on protruding cutters when the difference in diameter between adjacent cutters is too large as a result of deficient wear height control. Heavy vibration of the cutterhead results in high lateral forces on the cutters, which in turn causes additional abrasion.

Fractured rock masses promote greater penetration rates and thus effectively prolong cutter life (in m/c and sm^3/c). However, due to the aforementioned effect of fractures, higher levels of cutter consumption, measured in hours, will be expected. This effect will be more dominant in rocks exhibiting low drillability and high abrasivity. Figure 108 illustrates the effect of rock fracturing on cutter ring life.

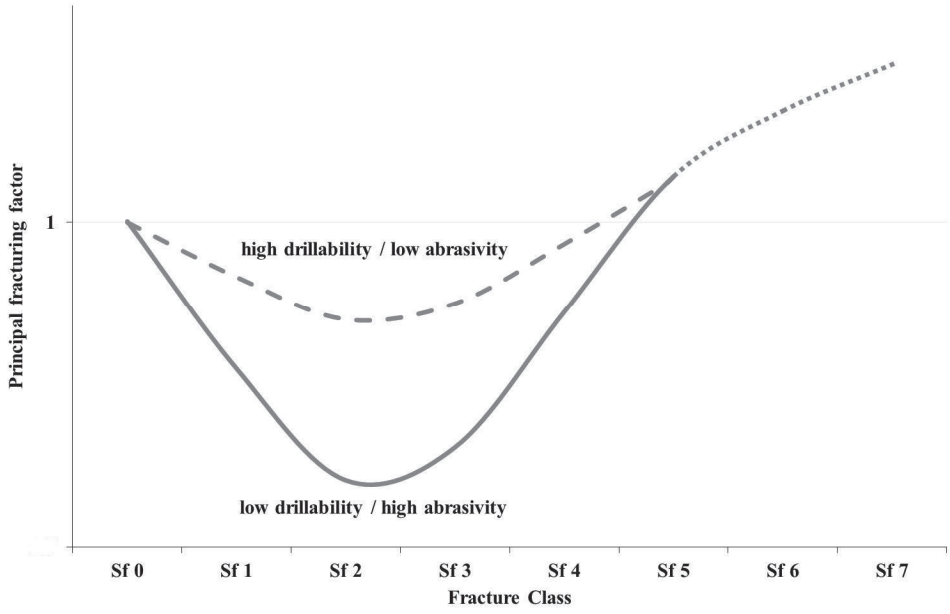

Figure 108. Principal cutter life fracturing factor.

Figure 109 shows cutter life data (sm^3/c) and wear patterns taken from several tunnel sections exhibiting a variety of rock mass conditions.

The contact skarn in Figure 109 is a tunnel section transitioning to a fractured rock type, which produces large instantaneous loads on the cutters resulting in a high rate of cutter replacement due to bearing set problems such as blockage.

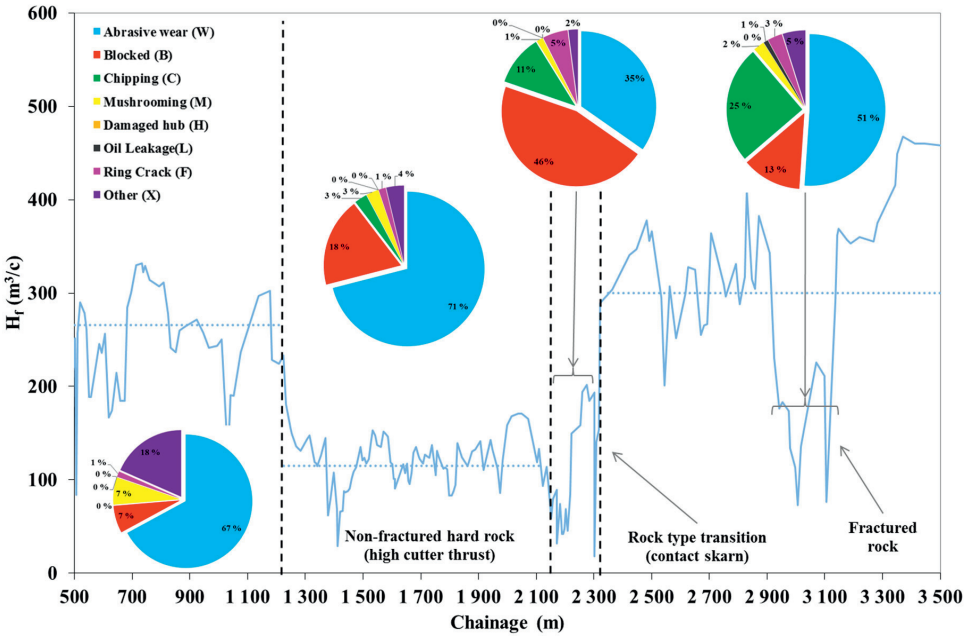

Figure 109. Cutter life data and wear patterns from several tunnel sections.

Higher amount of chipping is related to fractured rock while blocked cutters occur in rock types transition and high cutter thrust.

4.1.8 Machine utilization and gross advance rate

Gross advance rate is measured in metres per week, averaged over a longer period. Gross advance rate depends on net penetration rate, machine utilization and the number of hours worked during the period in question.

The term machine utilization is equivalent to net boring time expressed as a percentage of total tunnelling time. The total tunnelling time term includes:

- Boring, T_b
- Re-gripping, T_r
- Cutter replacement and inspection, T_c
- Repair and service of the TBM, T_{tbm}
- Repair and service of the back-up, T_{back}

- Miscellaneous T_m
- Tunnel length T_l

The time spent in carrying out these activities is expressed in hours per kilometre. The time spent in this case is representative of the vast majority of current tunnelling practice. Machine utilization is given by equation (33):

$$u = \frac{100 \cdot T_b}{T_b + T_r + T_c + T_{tbm} + T_{back} + T_m + T_l} \quad (\%) \tag{33}$$

Boring

The boring time depends on average net penetration rate I_n.

$$T_b = \frac{1000}{I_n} \quad \text{(h/km)} \tag{34}$$

Re-gripping

The time required for re-gripping depends on the stroke length of the thrust cylinders and unit time per re-grip.

$$T_r = \frac{1000 \cdot t_r}{60 \cdot l_s} \quad \text{(h/ km)} \tag{35}$$

l_s = stroke length, typically 1.5 - 2.0 metres
t_r = time per re-grip.

The average re-grip time is 4.5 minutes. The time spent varies with the gripper hold parameter, stroke length, TBM diameter, whether tunnelling is carried out along curved sections and down inclines, and on the capacity of the hydraulic system. Under favourable conditions, the time spent will be relatively short, but may increase substantially under difficult conditions.

Cutter replacement

The timing of cutter replacement and inspection depends on the cutter ring life (H_h), net penetration rate (I_n) and the time used to replace the cutter in question (t_c):

$$T_c = \frac{1000 \cdot t_c}{60 \cdot H_h \cdot I_n} \quad \text{(h/km)} \tag{36}$$

An analysis was performed of the time spent to replace a cutter. Figure 110 shows a histogram of the time spent for cutter replacement, including inspection time (minimum), from Projects D and C.

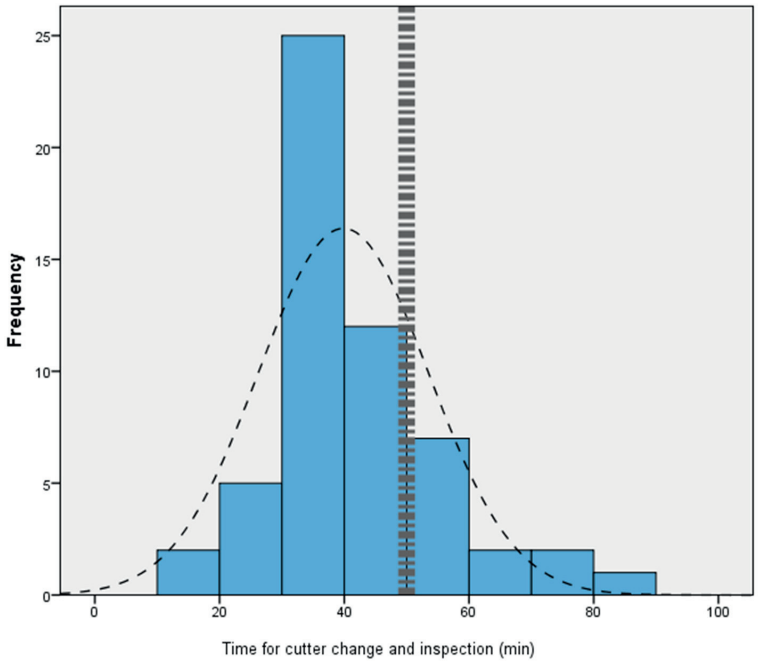

Figure 110. Time spent to replace a cutter, including inspection time (min.). From Projects D and C.

The time taken to replace a cutter varies with cutter size. Typical values are given in Table 40.

Table 40. The time taken to replace a cutter.

Cutter diameter	Front loaded	Back loaded
≤ 432 mm (17 inches)	45 min	40 min
≥ 483 mm (19 inches)	-	50 min

The parameter T_c in equation 34 is based on data acquired under favourable working conditions. However, unfavourable factors such as water ingress, unstable rock conditions, high rock temperatures and other factors, may result in substantial alterations to the time measured.

Inspection time per replaced cutter increases when boring in rocks exhibiting low abrasivity. Inspection time also depends on the number of cutters replaced at any one time. If only a few cutters are replaced during each stop, the unit time (t_c) will be longer, and this may also result in lower cutter life.

Miscellaneous

Miscellaneous includes the following activities:

- Normal rock support in good rock conditions, i.e. the installation of rock support while boring is in progress and without the need for additional crew
- Transport system stops
- Installation and maintenance linked to the transport system
- Surveying, moving of laser
- Installation and maintenance of water and ventilation systems, or electrical cables
- Washing and cleaning of the TBM and back-up
- Other factors such as crew changes, incidental lost time, etc.

In addition to the items listed above, factors including time spent in relation to the tunnelling method and organisation also come under the category of miscellaneous factors.
Time consumption is representative for well-organised tunnelling operations, and the time lost due to possible main bearing failures and other prolonged breaks in operations is not included. The risks related to such events must be evaluated separately for a given project on a case-by-case basis.
An analysis has been carried out of time consumption per kilometre for long tunnel sections. The results indicate that the predictions produced by the model are in good agreement with actual time spent in situations where tunnel operations are well organised and the tunnelling system adequate.
Figure 111 shows a summary of time consumption data (h/km) from long tunnel sections compared with data predicted by the model.

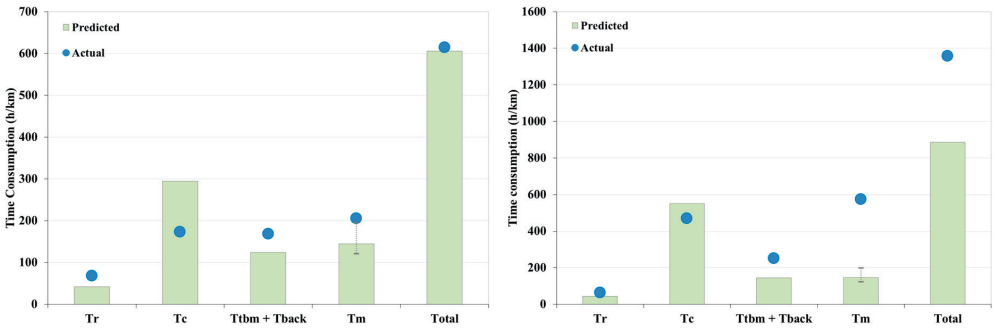

Figure 111. Actual time consumption compared with model predictions for Project D (left) and for a tunnel section from Project E (right).

Figure 112 shows time consumption per kilometre for repair and service of the TBM, for miscellaneous factors, and for repair and service of the back-up.

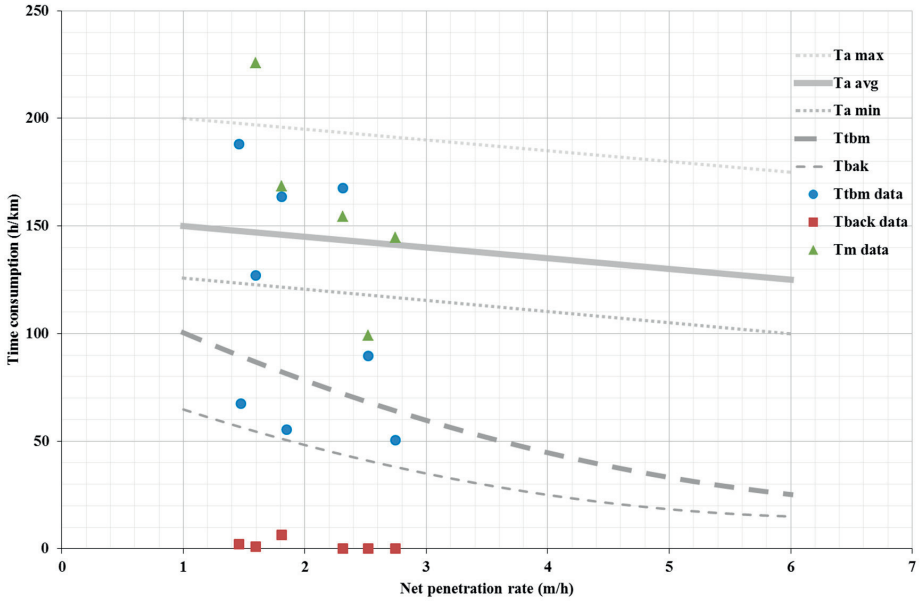

Figure 112. Time consumption per kilometre (h/km) for repair and service of the TBM (T_{TBM}), for miscellaneous factors (T_m), and for repair and service of the backup (T_{back}). Data from Projects D and E.

Most of the data are taken from tunnelling operations based on approximately 100 working hours per week, which is also the figure that forms the basis of the model (Bruland, 2000b). Hence, it is assumed that some time outside standard working hours is made available to address unforeseen and critical work such as major repairs. Some components of such time consumption are not recorded in shift logs and thus cannot be included in the aforementioned 'time consumption per km' parameter.

The effective time (T_e) parameter provides an expression of effective available working hours in situations where the weekly working hour figure deviates from 100. The opportunities flexibly to address unforeseen and critical work become fewer as the weekly working hours (T_u) parameter increases towards 168. Figure 113 shows new data on the effective working hours per week. The new data shows higher working hours per week than standard with good agreement with the curve in the figure. The curve in the figure must be regarded as a conservative representation of effective working hours lost.

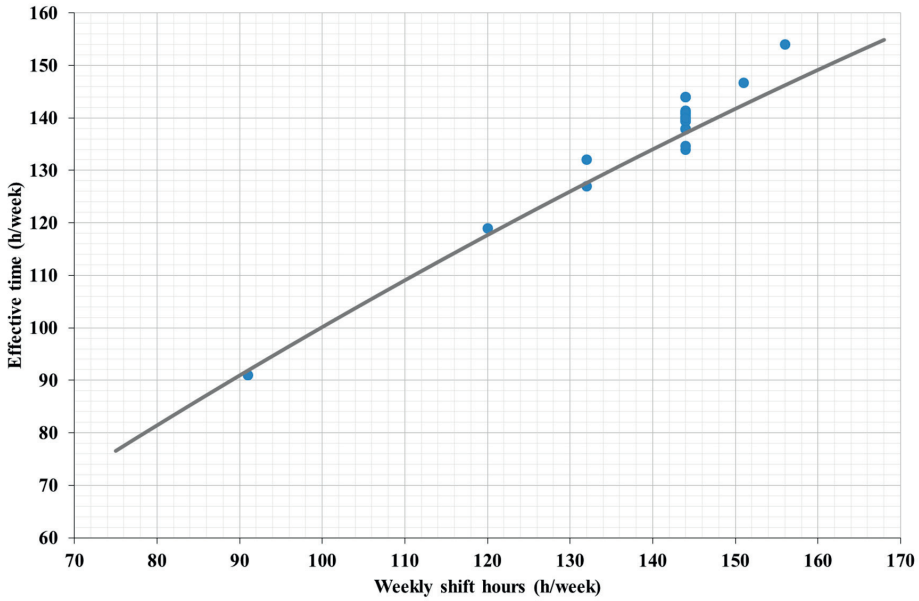

Figure 113. Effective working hours per week. From Projects D and E.

Length Factor

Tunnel length exerts an important influence on the time taken to carry out tunnelling activities (Barton. 2000). During the initial "learning curve" period of a tunnelling project, certain operations take a relatively long time as the crew builds up its skills levels, and the tunnelling quality assurance system evolves. For long headings (>8 km), miscellaneous factors put increasing demands on available tunnelling time (Bruland, 2000b).

The longer the tunnel, the higher the probability of problems arising linked to factors such as muck transport and ventilation, electricity and water supply systems, as well as other supply delays. Waiting times for transport will increase substantially if the capacity of the transport system is inadequate.

Problems linked to ventilation, electricity and water supplies will continue to increase with increasing tunnel length. Moreover, the transport system will be dependent on penetration rate and the amount of material that requires transportation. The higher the penetration rate, the greater the likelihood of downtime and other problems linked to supply delays and other issues with the transport system.

The NTNU model database is based on tunnels up to 10 kilometres in length. Time consumption data used in previous versions of the model were averaged over total tunnel length. Figure 114 shows additional time consumption resulting from "learning curve" factors obtained from so-called 'borderline' cases. Low skills levels among crews (and others), and inadequate tunnel system quality, will result in higher levels of additional time consumption.

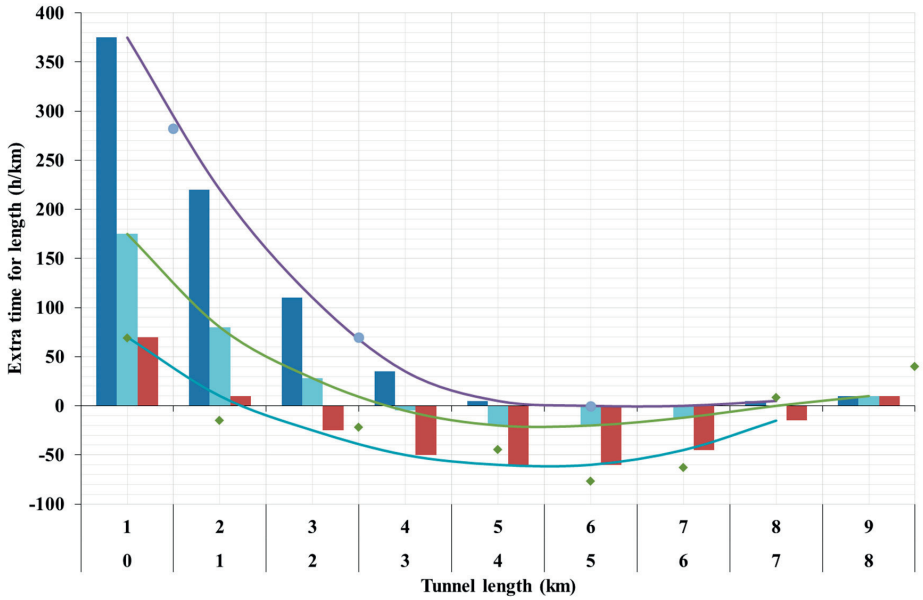

Figure 114. Analysis of the influence of the tunnel length.

A factor for additional time consumption (h/km) related to tunnel length is proposed (Figure 115). Boundary limits have been included for low and high skills levels and tunnel system quality. The values for every kilometre correspond to the extra time during the last km.

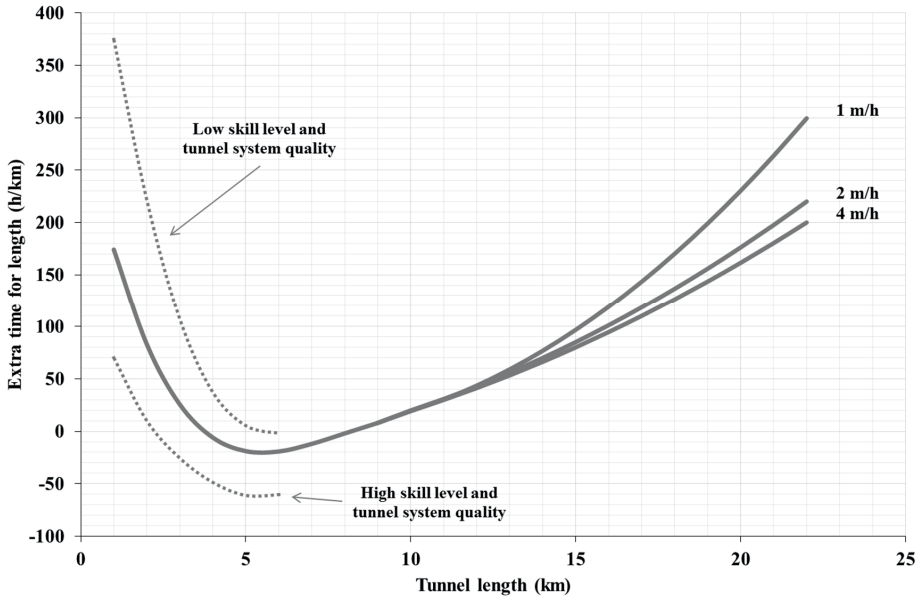

Figure 115. Additional time (h/km) plotted against tunnel length.

The term 'skills levels' refers not only to crew members, but also to equipment manufacturers and others.

Figure 116 shows the cumulative additional time (h/km) for the total tunnel length under consideration. This graph might be used for overall rough estimations.

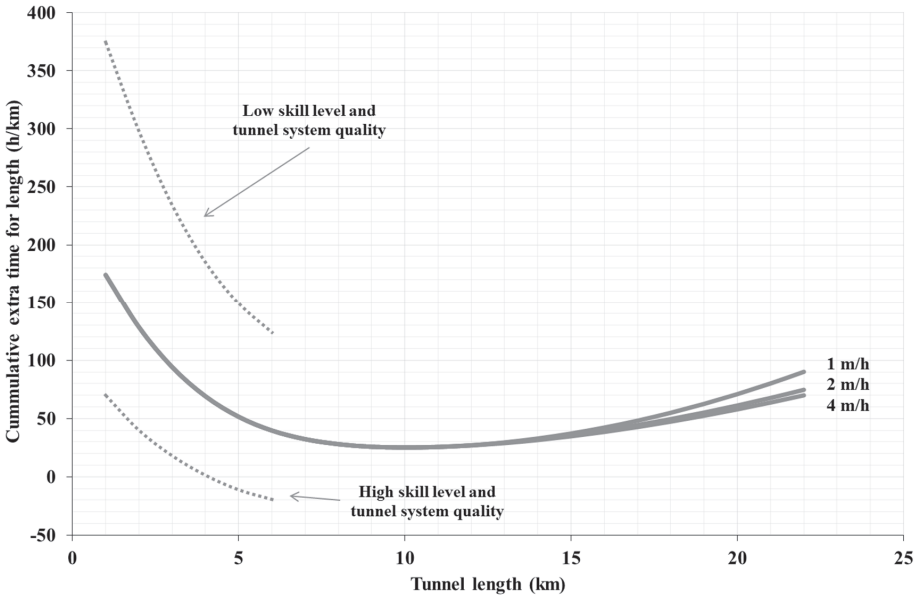

Figure 116. Cumulative additional time for the length of the tunnel (h/km).

Table 41 provides an example of application of the calculation of additional time resulting from tunnel length.

Table 41. Example of application of the calculation of additional time resulting from tunnel length.

Section (m)		h/km	h/section
0	1,000	174	174
1,000	3,000	83 + 26	109
3,000	5,500	(-6) + (-19) + (-19)	-34
5,500	8,000	(-19) + (-12) + (-2)	-23
8,000	11,000	8 + 19 + 30	57
		Total (h)	283
		Average (h/km)	26

4.1.9 Sensitivity analysis of the NTNU model

Many uncertainties are involved in performance prediction and cutter life assessments. An analysis of the influence of selected parameters on the predicted net penetration rate (m/h) and cutter life (h/c; sm^3/c) as produced by the 2016 version of the NTNU model, included in this thesis, was performed. The analysis was conducted using the standard specifications of a 7-metre diameter TBM and medium range of rock parameters. A window of 40% variation was applied for every parameter while the rest parameters were set at their mean values.

The parameters selected for this analysis are related to net penetration rate (DRI, k_s, cutter thrust and cutterhead velocity), and for cutter life (CLI, Q. k_s, cutter thrust and cutterhead velocity).

Table 42 lists the standard values for the input parameters used in the analysis.

Table 42. Standard values used in the sensitivity analysis.

Standard parameter	Value
TBM diameter (m)	7.0
Cutter diameter (mm)	483
Number of cutters	49.0

Table 43 shows the variation in parameter values used in the sensitive analysis.

Table 43. Variation in parameter values used in the sensitive analysis.

Parameter	Parameter variation				
	- 40%	**- 20%**	**Mean**	**+ 20%**	**+ 40%**
Cutterhead velocity (rpm)	3.6	4.8	6	7.2	8.4
Thrust (kN/cutter)	168	224	280	330*	330*
DRI	30	40	50	60	70
CLI	6	8	10	12	14
Q (%)	18	24	30	36	42
Rock mass fracturing factor (k_s)	0.48	0.6	0.7	0.79	0.86

*Maximum limited to 330 kN/cutter

The maximum gross average thrust used to perform the estimates is 330 kN/cutter. The mean value of the rock mass fracturing factor has been obtained based on fracture class 4 (average spacing of 40 cm) and an alpha angle of 20 degrees.

Thrust is seen to be the main parameter influencing net penetration rate. A reduction of 20% in thrust results in a dramatic decrease of 40% in net penetration rate.

The rock mass fracturing factor (k_s) and DRI influence the net penetration rate. Their influence is greater at lower values.

rpm values below the recommended value exert a major influence. They act to reduce the net penetration rate, while rpms above the recommended value exert no influence on net penetration rate due to the rpm factor and on the basis of 'RPM tests'.

Figure 117 shows the variation in predicted net penetration rate based on the 2016 version of the NTNU model plotted for selected input parameters.

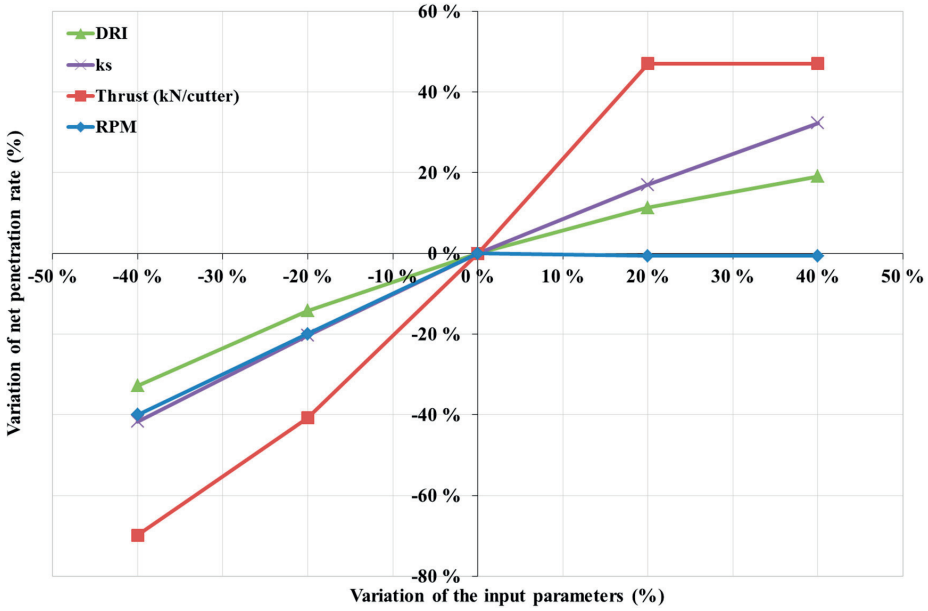

Figure 117. Variation in predicted NPR (m/h) in response to variation in input parameters.

The main machine parameters influencing cutter life (in h/c) are thrust and cutterhead velocity. As previously discussed, the quantitative influence of thrust on cutter life is based on limited data and applies to highly abrasive rocks. The influence of the rpm is related to the cutter rolling distance.

The CLI and abrasive minerals content (Q) are the rock parameters influencing cutter life (in h/c). Both exert influence in opposite directions.

The k_s parameter does not influence cutter life (in h/c) in the NTNU model. During this PhD research work, it has been found that a fractured rock mass results in higher levels of cutter consumption due to bearing-related damage, such as blocked cutters. This may be explained by the occurrence of higher peak loads on the cutter discs during boring. However, the relative lack of data makes it too early to draw any definitive conclusions.

Figure 118 shows the variation in predicted cutter life (in h/c) plotted for selected input parameters.

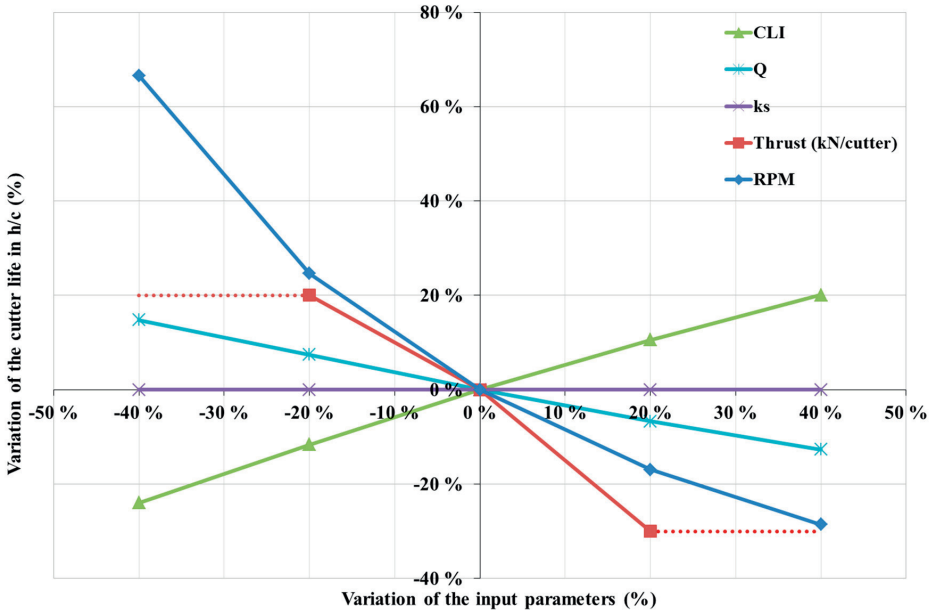

Figure 118. Variation in predicted cutter life (in h/c) in response to variation in input parameters.

Increases in the k_s and rpm parameters have an important influence on cutter life (in sm^3/c).

At lower values, the cutter thrust and k_s parameters exert greater impact due to their influence on net penetration rate.

As in cutter life (in h/c), the CLI and abrasive minerals content (Q) are the rock parameters influencing cutter life (in sm^3/c) and in opposite directions.

Figure 119 shows the variation in predicted cutter life (in sm^3/c) in response to variations in the selected input parameters.

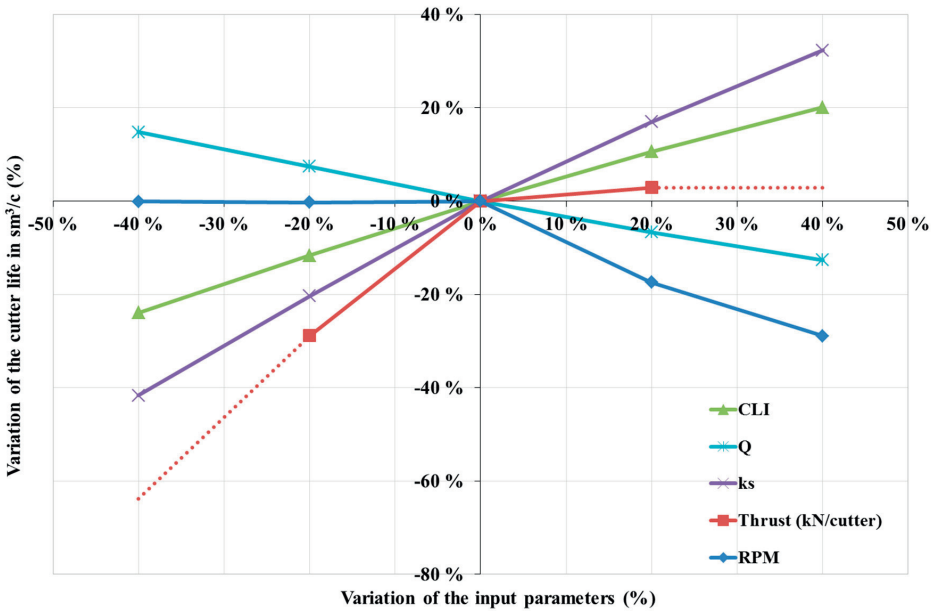

Figure 119. Variation in predicted cutter life (in sm^3/c) in response to variation in input parameters.

It is important to bear in mind that this analysis has considered only variation in individual parameters. It is possible that if several parameters were varied, different outcomes may result.

4.1.10 Limitations of the NTNU model

A model is a simplified description of a given phenomenon, which can be used to make predictions. A good model is both as accurate as possible and as simple as possible, which makes it not only powerful but also easy to understand. However, no matter how good a model is, it will usually have limitations. Since models must be simple enough to enable them to be used to make predictions, they often lack the ability to simulate all the details of the phenomenon in question.

In the case of the NTNU prediction model for hard rock TBMs, the following limitations should be taken into account:

The NTNU model does not cover the entire range of rock masses that occur in nature:

- Rock drillability expressed by the Drilling Rate Index (DRI) parameter should lie within the range 20 to 80, which roughly corresponds to the UCS parameter values 25 to 350 MPa. The strength parameter applied is in accordance with the ISRM classification 'medium to extreme' (see Table 2).
- The rock type in question should exhibit medium to low porosity – less than approximately 10% by volume.

- The rock mass degree of fracturing, expressed by the average spacing between planes of weakness, should be greater than approximately 50 mm.
- The rock-breaking process must be mainly by brittle failure (chipping) between the disc cutters.
- Rock mass quality should be such that the excavated tunnel will generally only require light-duty support mechanisms (rock bolts and/or shotcrete). Exceptions will occur in zones of weakness or as a result of other specific phenomena.
- Rock mass qualities roughly related to Q and RMi values should be somewhere greater than 0.1 and 20 for the RMR.
- Boreability assessments do not include the possible influence of groundwater and/or rock mass stress.

The NTNU/SINTEF drillability test method has gained international recognition. There are few laboratory facilities in the world that are able to reproduce these tests, unlike other test methodologies such as UCS and BTS. There are other laboratories worldwide with the necessary equipment, such as in Australia, South Korea, Spain, South Africa, Turkey and the USA. The trademark acronyms and terms relating to the indices DRI™ (Drilling Rate Index™) and CLI™ (Cutter Life Index™) are unique to these test results and originate from the NTNU/SINTEF laboratory in Trondheim in Norway.

A cutter diameter of 483 mm (19 inches) and 508 mm (20 inches) are currently the most commonly used in hard rock tunnelling. For smaller TBMs, diameters of 432 mm (17 inches) are used. The NTNU model makes no distinction between cutter ring design or quality, and assumes in all cases that cutter ring quality is tailored to the rock conditions.

The machine type assumed by the model is a hard rock TBM (open or shield). However, the model is based on data derived from a large number of open TBM types tunnelling in rock mass conditions summarised in the foregoing. No distinction is made between machine types.

The gross cutter thrust parameter may interfere with the influence of TBM type, diameter, and/or cutter type. TBM cutterhead design is not included in the model as an independent parameter.

The machine utilisation parameter (expressed as a percentage of tunnelling time) used in the model does not include additional time spent on operations such as TBM and back-up assembly and disassembly, excavation work (niches, branching, etc.), tunnelling through zones of poor quality, additional time for unexpected rock mass conditions, permanent rock support and lining operations, and additional TBM downtime. These activities need to be quantified separately.

4.2 Development of a new rock abrasivity test method

This section addresses an analysis of the opportunity for, and need to, develop a new rock abrasivity test method to assess cutter ring wear during hard rock tunnelling.

4.2.1 Introduction

Cutter consumption has a major impact on performance and the costs of tunnelling projects. Reliable assessments of cutter consumption are needed for planning and risk management, especially in hard rock conditions.

Many factors are influencing the number of cutters consumed in during hard rock tunnelling projects. Standard TBM operations result mainly in abrasive wear of the cutter rings, and this consideration has been confirmed as being proportional to cutter rolling distance by various authors (Rostami, 1997; Bruland, 2000; Frenzel et al., 2008).

Rock abrasiveness cannot simply be considered as an intrinsic rock property, and a full description of the phenomenon requires consideration of the complete tribological system, as well as rock properties.

Some accepted and commonly used tests for estimating rock abrasiveness have already been described in section 2.4.1 of this thesis.

Since none of the currently available laboratory test methods were developed for cutter wear assessment, they do not reproduce the wear behaviour encountered during hard rock tunnelling in a realistic manner. Due to the importance of cutter wear, it was thus considered to be of interest to develop a new rock abrasivity test with the aim of assessing cutter wear under more realistic conditions.

Initially, two main goals were defined:

- ✓ To evaluate the ability of the Soft Ground Abrasion Tester using crushed rock (SGAT-CR) to provide an assessment of rock abrasivity.
- ✓ To investigate the need and ability to develop a new rock abrasivity test method.

The Soft Ground Abrasion Tester (SGAT) was developed by Jakobsen et al. (2013) to assess tool wear in soft ground TBM conditions. The SGAT apparatus has previously been described in the chapter addressing research methodology.

In order to study the potential of the SGAT approach (Jakobsen et al., 2014) as a means of assessing rock abrasivity, tests on crushed rock were performed in accordance with the procedure, and using the tool design, described in section 3.5.2.

Table 44 provides a summary of the results of SGAT-CR tests carried out for three fraction sizes of the Iddefjord granite using three selected rotational speeds.

Table 44. The results of SGAT-CR tests using crushed rock for three fraction sizes of Iddefjord granite, carried out at three rotational speeds.

Fraction size (mm)	Rotational speed (rpm)	Weight loss (mg)				
		Test 1	Test 2	Test 3	Average	Standard deviation (%)
0 – 5 mm	30	25	22	21	23	7 %
	50	42	42	66	49	24 %
	70	81	69	70	73	7 %
0 – 10 mm	30	47	53	53	51	6 %
	50	74	56	70	67	12 %
	70	98	93	95	95	2 %
4 – 6 mm	30	66	59	53	59	9 %
	50	94	83	82	86	6 %
	70	130	120	116	122	5 %

The highest weight losses were achieved using the 4-6 mm fraction size. All samples exhibited a relatively low standard deviation for the three rotational speeds. The results show a more consistent standard deviation for the 4-6 mm sample, where all values are lower than 10%.

The highest weight loss and lowest standard deviation were achieved using rotational speeds of 70 rpm due to the longer distance travelled by the tool.

Figure 120 shows the average weight loss resulting from the SGAT tests using crushed Iddefjord granite for the aforementioned fraction sizes and rotational speeds. The figure also displays standard deviation data.

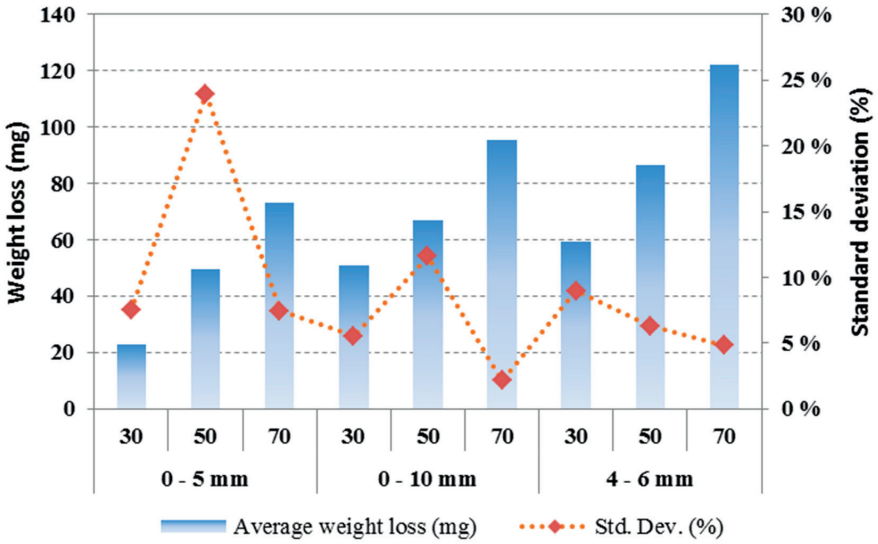

Figure 120. Average weight loss results following SGAT tests using crushed rock for three fraction sizes of the Iddefjord granite (0-5 mm, 0-10 mm and 4-6 mm) and three rotational speeds (30, 50 and 70 rpm). The standard deviation is also shown.

SGAT-CR tests and grain size distribution curves

Table 45 shows the results of fraction size distribution analyses of four Iddefjord granite samples before and after testing using the SGAT-CR method. Weight loss data are also included.

Table 45. Distribution of fraction sizes from four samples (A, B, C and D) of Iddefjord granite before and after testing using the SGAT-CR method. Weight loss data for all the samples are also included.

Size (mm)	Sample A (% pass)		Sample B (% pass)		Sample C (% pass)		Sample D (% pass)	
	Before	After	Before	After	Before	After	Before	After
9.5	100 %	100 %	100 %	100 %	100 %	100 %	100 %	100 %
8.0	98 %	98 %	84 %	86 %	74 %	77 %	50 %	57 %
6.3	90 %	ND	71 %	73 %	50 %	54 %	25 %	ND
4.0	75 %	76 %	53 %	55 %	30 %	36 %	10 %	17 %
2.0	50 %	51 %	34 %	36 %	16 %	21 %	3 %	9 %
0.01	0 %	0 %	0 %	0 %	0 %	0 %	0 %	0 %
Weight loss (mg)	48		72		83		138	

Figure 121 shows the resulting sieve curves for the four samples (A, B, C and D) before and after testing.

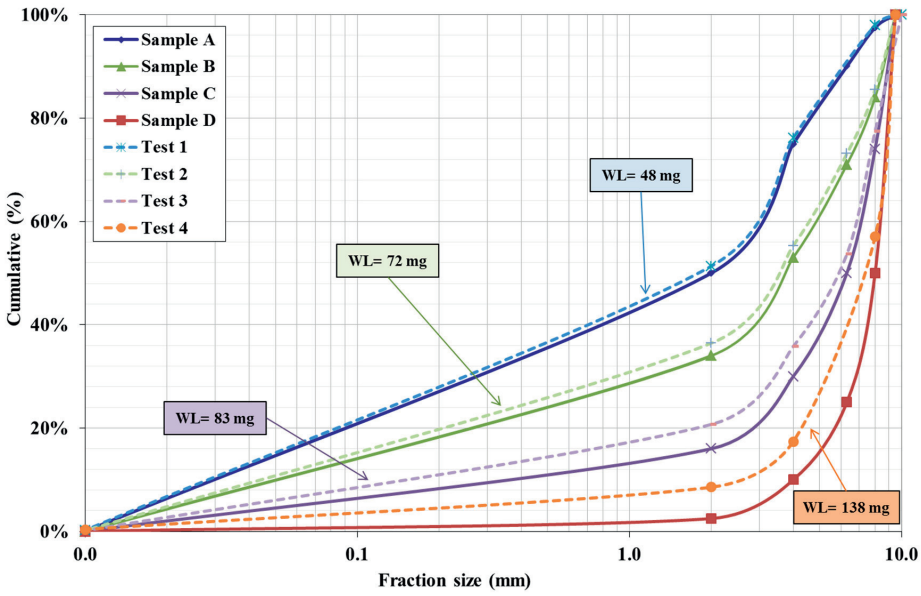

Figure 121. Sieve curves for the samples A, B, C and D before and after testing. Weight loss data obtained from the SGAT-CR tests are also included.

The weight loss data in Figure 121 illustrate the influence of grain size distribution on wear. Samples with higher proportions of larger grain sizes result in higher weight loss and greater size reductions which displaces the sieve curve following testing.

The results indicate that the SGAT with crushed rock is able to assess rock abrasivity. Nevertheless, the proposed test method uses a similar behaviour than the existing methods, crushed material and sliding contact and, so finally, the test method was not developed further for hard rock TBM tunnelling purposes.

4.2.2 Development of the Rolling Indentation Abrasion Test (RIAT)

The design and development of the Rolling Indentation Abrasion Test (RIAT) is a direct result of the research linked to this PhD thesis. The preliminary procedure and results have already been published (see Papers VII and VIII included in this thesis). Moreover, a summary of the procedure has also been included in the chapter addressing research methodology (section 3.5.3). For this reason, only a brief summary of the main results and a discussion are included in this section.

RIAT – initial results and discussion

The Rolling Indentation Abrasion Test method (RIAT) involves the use of miniature rolling discs that penetrate the surface of an intact rock sample. As is shown in Figure 122, the RIAT tool is fitted with two replaceable miniature cutter rings. A suitable drive unit provides the rotation, torque and vertical thrust of the tool.

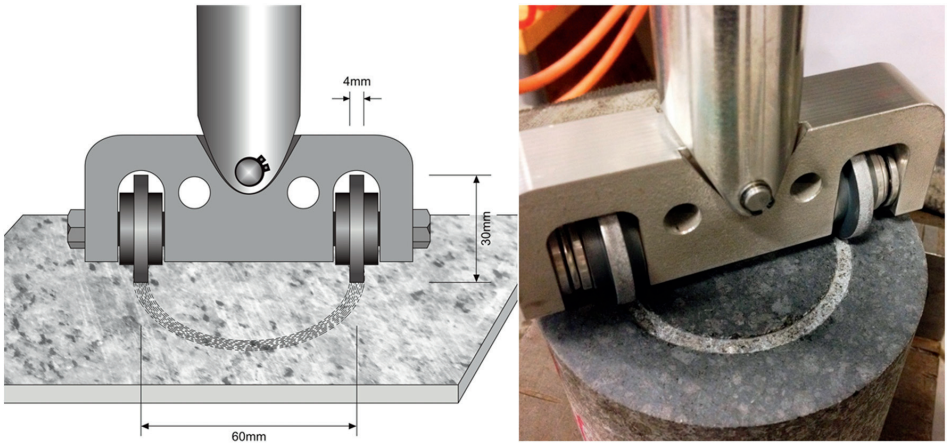

Figure 122. Outline and photograph illustrating the components of the Rolling Indentation Abrasion Test (RIAT) method (reproduced from paper VIII).

The discs consist of miniature cutter rings and a bearing system that are easily disassembled to facilitate the testing procedure.

Initial RIAT tests involved eight different rock types covering a wide range of hard rock abrasivity; limestone, basalt, Basalt Xiamen, Trondhjemite (tonalite), Rosa Porriño (RP) granite, Iddefjord granite, Gris Mondariz (GM) granite and quartzite. Figure 56 in the research methodology chapter (section 3.5.3) shows illustrations of the rock samples after testing.

The rock types were selected on the basis of previous test results (Paper VII) in order to encompass a wide range of hard rock abrasivity properties.

The samples were prepared according to the procedure previously described in section 3.5.3 and paper VIII. A minimum of three parallel tests were carried out for each rock type,

resulting in a total of 29 tests. The results are summarised in Table 46, including mean and standard deviation data.

Table 46. Results of RIAT tests on eight rock types (reproduced from Paper VIII).

Rock types	$RIAT_a$ (mg)			$RIAT_i$ (1/100 mm)		
	Mean	Standard deviation		Mean	Standard deviation	
		Value	%		Value	%
Limestone	3	1.4	47 %	380	55	14 %
Basalt	10	1.7	17 %	116	15	13 %
Basalt Xiamen	25	4.7	19 %	118	3	2 %
Trondhjemite	30	2.4	8 %	68	7	10 %
RP granite	34	5.5	16 %	51	4	7 %
Iddefjord granite	39	2.2	6 %	50	9	18 %
GM granite	45	7.1	16 %	49	3	7 %
Quartzite	104	16.0	15 %	NM*	NA	NA

*For practical reasons 5.

The lowest and the highest mean RIAT abrasivity values ($RIAT_a$) are recorded for limestone (3) and quartzite (104), while for the RIAT indentation parameter ($RIAT_i$), the corresponding values are for quartzite (5) and limestone (380). It was not possible to obtain a measurable indentation value for the quartzite sample.

Figure 123 shows the results for the RIAT, $RIAT_a$ and $RIAT_i$ for the selected rock types.

Initial results obtained using the RIAT procedure as described indicate that the method is highly suitable for assessing abrasive wear on rolling discs for a wide range of rock abrasivity. The RIAT method has an improved ability to distinguish high-end abrasivities.

Rock types such as Basalt Xiamen, RP granite and GM granite, which contain high proportions of coarse-grained hard minerals, display higher standard deviations for the RIAT indices. Coarse-grained hard minerals may also induce a dynamic effect during testing because penetration is inhibited along parts of the roller disc track.

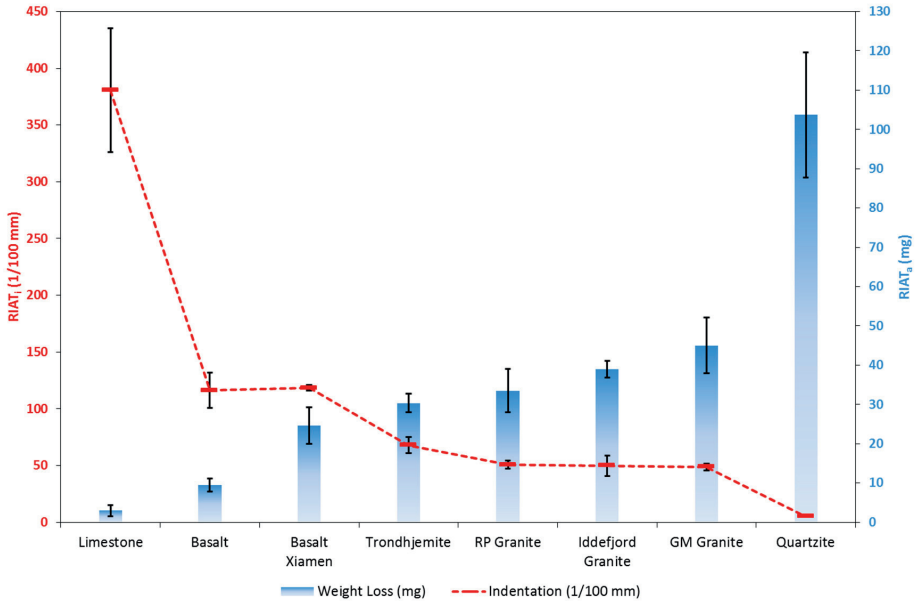

Figure 123. Results from RIAT tests for eight rock types. The RIAT$_i$ parameter is shown on the x-axis left (red stippled line) and the RIAT$_a$ parameter on the x-axis right (blue columns). The error bars indicate the standard deviation (reproduced from Paper VIII).

An analysis was carried out of the relationship between abrasivity and the indentation indices RIAT$_a$ and RIAT$_i$, and the correlation enables the eight rock types to be distinguished from each other (Figure 124). The graph indicates that the RIAT$_i$ parameter decreases with increasing RIAT$_a$. A best-fit regression has been applied to the data (as is the case for all correlation analyses presented in this thesis).

There is no logical reason explanation for the relationship between the RIAT indices displayed in Figure 124. However, it may simply help to confirm that cutter abrasion is dependent on rock surface hardness (resistance to indentation by cutter discs), as is currently understood and applied as part of the NTNU/SINTEF methodology (Dahl et al., 2012).

During the tests, wear behaviour was analysed at 10 minute intervals for a selected Trondhjemite sample (Figure 125). The results indicate that weight loss from the miniature cutters exhibits a clear linear relation with elapsed time. This finding may enable estimations of 'ultimate' weight loss to be made using shorter testing times. This relationship should be investigated for other rock types.

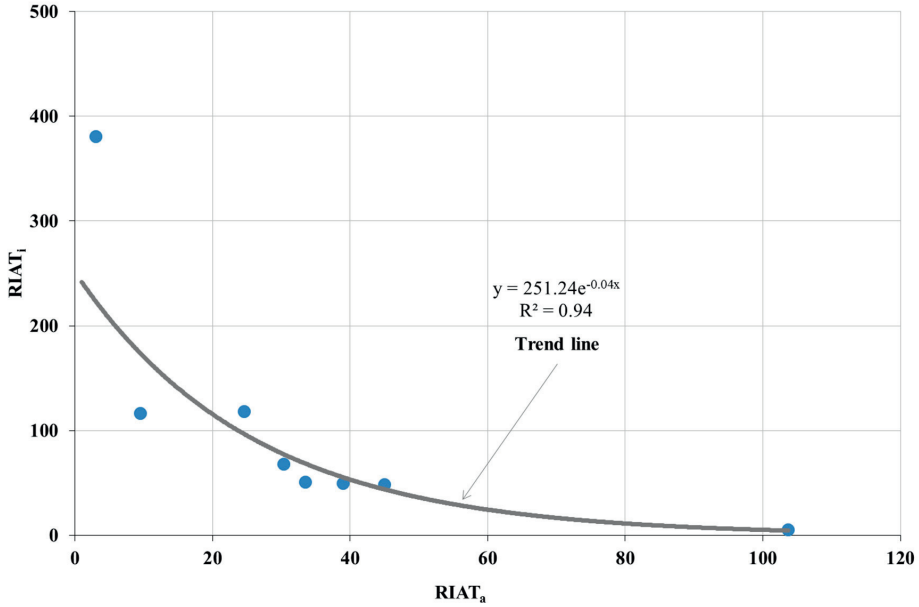

Figure 124. The relationship between the $RIAT_a$ and $RIAT_i$ indices based on data obtained from testing eight rock types. A best-fit maximum correlation level has been selected (reproduced from Paper VIII).

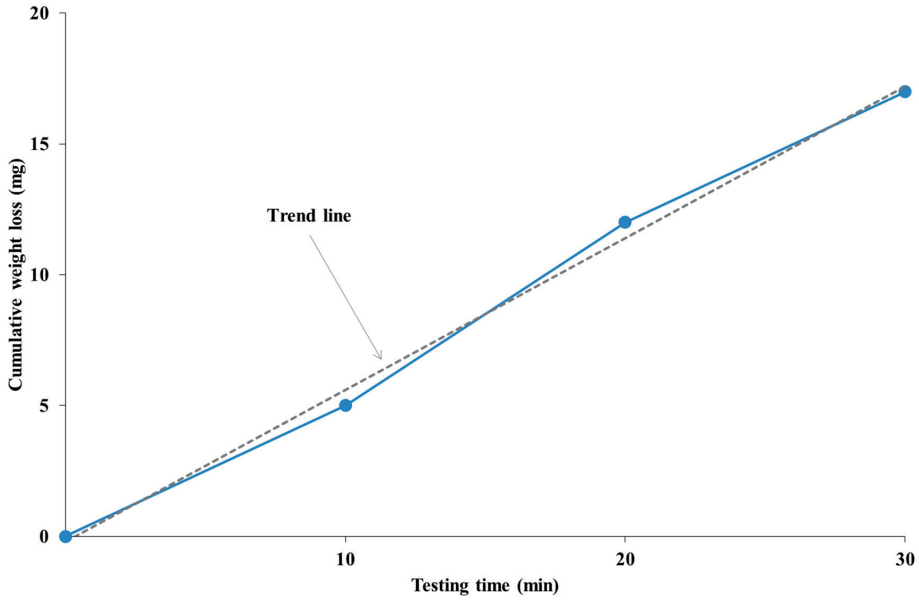

Figure 125. Cumulative weight loss for a miniature cutter as a function of elapsed RIAT test time using a sample of Trondhjemite (reproduced from Paper VIII).

Relationships and correlations with other abrasivity indexes

In order to evaluate the RIAT method, a comprehensive set of laboratory tests, including well-established and widely used approaches, has been performed. Such tests included NTNU drillability tests (S_{20}, SJ, AVS) in order to obtain the DRI and CLI (Bruland, 2000g; Dahl et al, 2012); the Cerchar test (CAI) as described by ASTM (2010); a uniaxial compressive strength test (UCS) as described by ISRM (1978), as well as measurements of density and mineralogical composition using XRD analysis. The Cerchar index for saw cut surfaces (CAI_s) as described by ASTM (2010) has been used to generate rock surface test data comparisons with the RIAT tests. Density has been determined in accordance with methods previously suggested by NTNU/SINTEF and published at Drillability.com (Dahl, F., 2003), and used to calculate the DRI, BWI and CLI parameters. The results of these various tests were analysed and compared with the RIAT results, and a summary is presented in Table 47.

Table 47. Laboratory test results for eight rock types (limestone, basalt, Basalt Xiamen, Trondhjemite, RP granite, Iddefjord granite, GM granite and quartzite). Tests include NTNU drillability tests (S20, SJ, AVS, DRI™ and CLI™), the Cerchar test (CAI_s), uniaxial compressive strength tests (UCS) and density measurements (Reproduced from Paper VIII).

Rock type	S_{20}	SJ	AVS	DRI™	CLI™	CAI_s	UCS (MPa)	Density (g/cm^3)
Limestone	53.2	66.7	0.5	63	90.9	2.0	175	2.60
Basalt	34.7	9.2	8.5	34	14.3	3.0	261	2.95
Basalt Xiamen	39.6	3.0	19.5	34	6.8	2.7	279	3.00
Trondhjemite	56.1	3.6	27.5	51	6.3	4.3	196	2.68
RP granite	67.4	8.8	38.0	67	7.9	4.5	170	2.63
Iddefjord granite	61.9	5.0	31.5	58	6.8	3.4	188	2.60
GM granite	60.4	4.5	35.5	56	6.2	4.0	169	2.65
Quartzite	52.3	1.6	42.2	43	3.9	2.5	359	2.60

It was considered logical to analyse the relationship between the $RIAT_a$ and the AVS and CAI_s parameters because the $RIAT_a$ index is defined as the weight loss incurred by the miniature cutters and as such reflects a given rock type's ability to induce wear in cutter ring steel as a result of rolling contact. Figure 116 illustrates the results of this analysis between $RIAT_a$ and AVS.

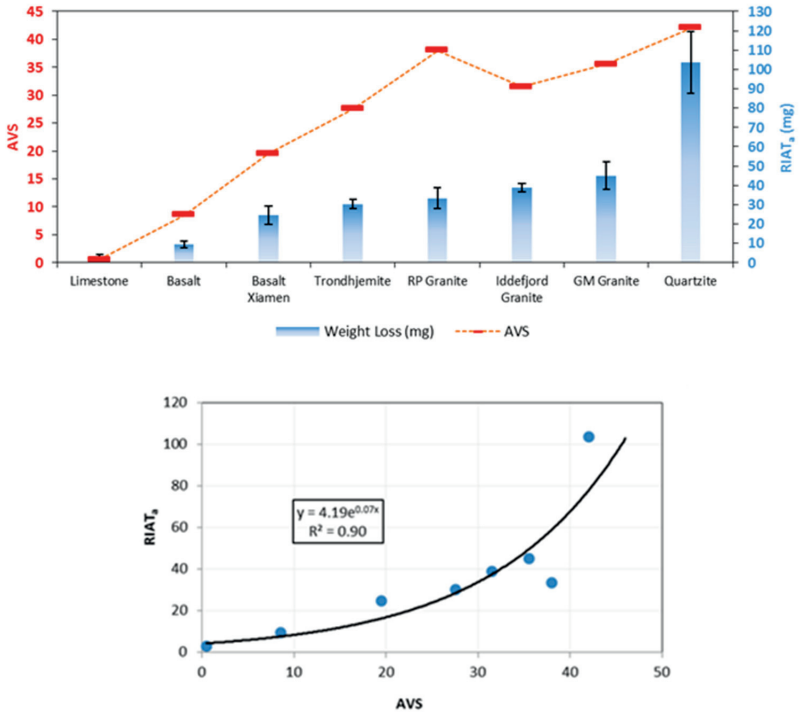

Figure 126. Diagrams showing the relationships between the $RIAT_a$ index and the AVS following the testing of eight rock types (Reproduced from Paper VIII).

Figure 116 shows that there exists a clear correlation between the $RIAT_a$ index and the AVS. The best-fit regression is an exponential due to the improved distinction in the upper rock abrasivity range determined by the RIAT.

The result for the RP granite showed an irregular result in the relation between the $RIAT_a$ and the AVS. This is probably due to the fact that during sample preparation (involving crushing to produce particles less than 1 mm in diameter), rock types which contain relatively large grains of quartz, such as the RP granite, generate quartz fragments with freshly broken and sharpened angles. These angular quartz grains may act as highly abrasive as the AVS steel tool slides across the crushed rock.

There is no clear correlation between the $RIAT_a$ index and the CAI_s. However, a correlation appears if the value for quartzite is excluded from the analysis. The CAI_s result for quartzite can be regarded as lower than that which would be expected for this rock type. This phenomenon is encountered frequently during the measurement of the CAI_s connection with in very hard rock types. The reason is that the tip of the tool stylus is not able to fully penetrate the rock surface, resulting in a "skating effect", which in turn results in an underestimation of wear behaviour (ISRM, 2014; Ellecosta et al., 2015; Paper VII).

In the case of the $RIAT_i$ index, recorded values show the same general trend and a good correlation with data set as a whole. However, this is mostly a result of the limestone value. No correlation exists if data from the limestone test are excluded. This can be explained by differences in rock breaking behaviours induced by the different tests. The Sievers' J test uses drillhole depth to measure rock surface hardness, while the $RIAT_i$ index is derived from a test that measures the depth of a track induced by a rolling disc.

Figure 127 (a and b) show that a correlation exists between the CLI and the $RIAT_a$ index on the basis of results from tests carried out on the eight rock types. The correlation between the CLI and the $RIAT_i$ indexes is somewhat weaker, but is nevertheless regarded as good (Figure 127, c and d). As previously discussed, the CLI determined from the SJ and AVS values. Since there is no correlation between the SJ and the $RIAT_i$ index, a weaker correlation is anticipated between the CLI and the $RIAT_i$ index than between the CLI and the $RIAT_a$ index. Figure 127 (b and d) are plots where the limestone data are excluded.

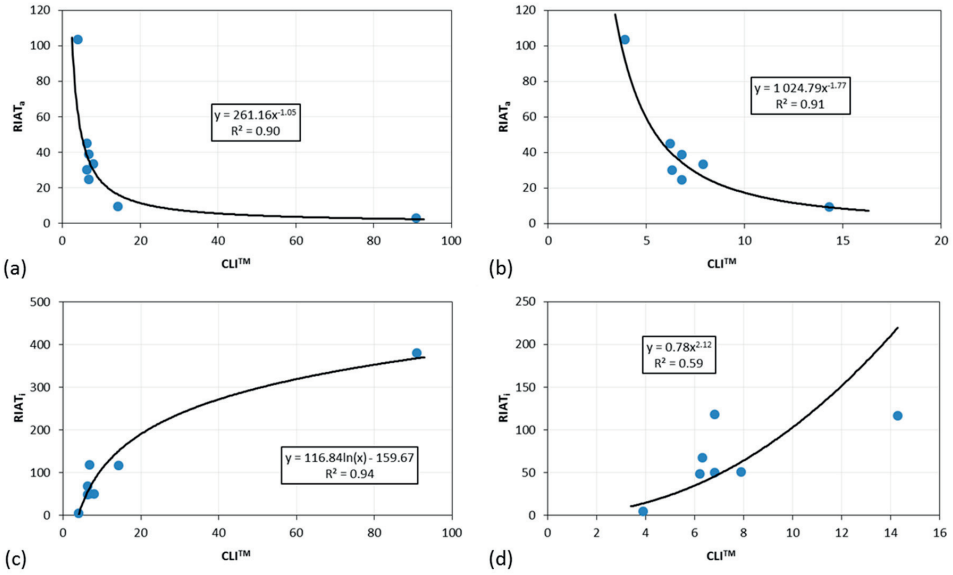

Figure 127. Plots illustrating correlations between the $RIAT_a$ (a) and (b), and $RIAT_i$ (c) and (d) indices and the CLI for the eight rock types tested. Plots (b) and (d) are the corresponding correlations in which the limestone values are excluded (Reproduced from Paper VIII).

Moreover, no clear correlations were found between the RIAT indices and the results obtained from the remaining laboratory tests.

Influence of mineral composition

The mineral composition of a rock type (quartz and other abrasive minerals) may have considerable influence on the ability of a given rock type to induce tool wear. X-ray diffraction analysis results are shown in Table 48.

The term 'equivalent quartz content includes the entire mineral content's influence on the abrasiveness properties relative to quartz. The parameter is calculated by multiplying the proportion of each mineral in a given rock type by its relative Rosiwal abrasiveness to quartz according to Thuro (1997).

Table 48. Essential mineral compositions for limestone, basalt, basalt Xiamen, Trondhjemite, RP granite, Iddefjord granite, GM granite and quartzite (Reproduced from Paper VIII).

Rock type	Quartz	Olivine	Plagioclase	Feldspar	Epidote	Pyroxene	Calcite	Mica
Limestone	2%	-	-	-	-	-	98%	-
Basalt	-	-	57%	4%	-	34%	-	-
Basalt Xiamen	-	15%	27%	18%	-	35%	-	-
Trondhjemite	31%	-	53%	-	4%	2%	-	9%
RP granite	43%	-	25%	27%	-	2%	-	3%
Iddefjord	25%	-	32%	35%	-	-	-	8%
GM granite	34%	-	36%	21%	-	3%	-	4%
Quartzite	100%	-	-	-	-	-	-	-
Rosiwal abrasiveness	100	98	59	59	76	36	2	3
Mineral Vickers hardness (kg/mm^2)*	1060	990	800	730	667	600	125	110

*Derived from several sources including Verhoef (1997) and Bruland (2000)

Table 49 shows the quartz content, quartz content equivalent and Vicker Hardness Number for Rock (VHNR) values for the eight rock types used in the RIAT tests.

Table 49. Quartz content, equivalent quartz content and Vickers hardness number for rock (VHNR) values for the eight rock types used in the RIAT tests (Reproduced from Paper VIII).

Rock type	Quartz	Quartz equivalent	VHNR	VHNR
Limestone	2 %	4 %	144	14 %
Basalt	-	48 %	689	65 %
Basalt Xiamen	-	55 %	704	66 %
Trondhjemite	31 %	66 %	801	76 %
RP granite	43 %	75 %	868	82 %
Iddefjord granite	25 %	65 %	785	74 %
GM granite	34 %	69 %	825	78 %
Quartzite	100 %	100 %	1060	100 %

Figure 128 shows correlations between the RIAT indices and the quartz content and equivalent quartz content.

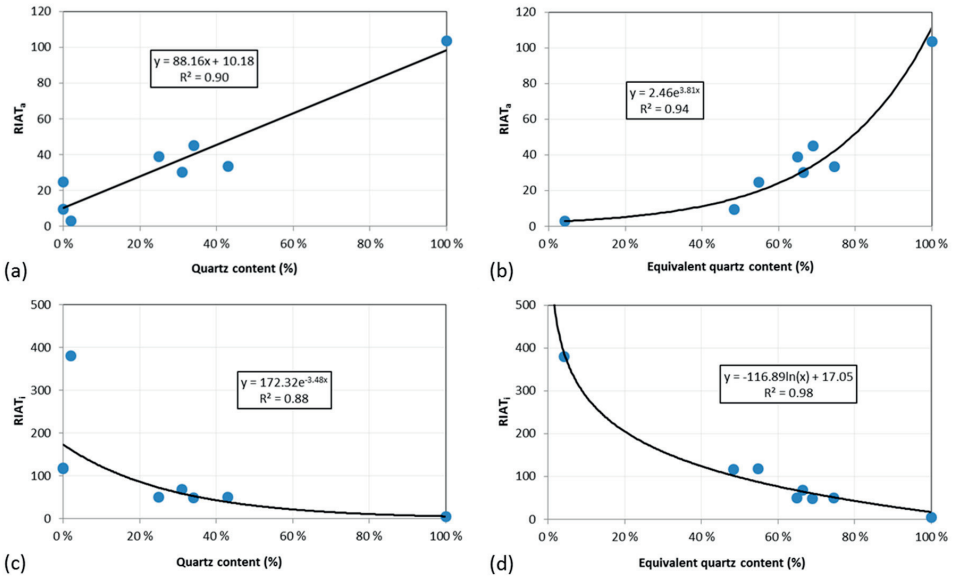

Figure 128. Correlations between the $RIAT_a$ and $RIAT_i$ indices and quartz content (a) and (c) and equivalent quartz content (b) and (d), for the eight rock types used in the RIAT tests (Reproduced from Paper VIII).

Individual Vicker's hardness values, combined with the proportions of the relevant mineral in the rock types used in the RIAT tests (Table 49), were used to calculate a Vicker's Hardness Number Rock (VHNR) for each rock type (Bruland, 2000d). Figure 129 shows the correlations between the VHNR values and the RIAT indices.

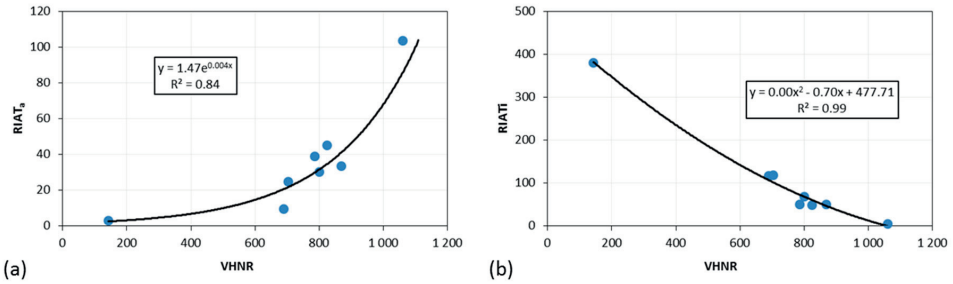

Figure 129. Correlations between VHNR and the (a) $RIAT_a$ and (b) $RIAT_i$ indices for the eight rock types used in the RIAT tests (Reproduced from Paper VIII).

The figure demonstrates the clear correlations between the VHNR parameter and the RIAT indices for the tested rock types. However, due to the spread of the values, more testing is recommended to verify these results.

4.3 Cutter wear mechanisms in hard rock tunnel boring

4.3.1 Introduction

The interaction between cutter rings and the rock mass during hard rock tunnelling entails a complex tribological system, and several different rock properties, machine parameters and others influence cutter ring wear.

During the work leading to this PhD thesis, a comprehensive set of comparative analyses of worn cutter ring samples from three TBM projects (A, C and D), and mini-cutter rings from laboratory testing using the developed Rolling Indentation Abrasion Testing (RIAT) on standard rock samples, was carried out. The analyses have involved making comparisons between field and laboratory scale data, and have been performed in collaboration with the Tribology group at the Department of Engineering Design and Materials at NTNU, headed by Professor Nuria Espallargas and some of her department's Master's degree students.

The main objective is to improve the accuracy of cutter life prediction by means of a better understanding of cutter wear processes and failure mechanisms. A number of goals have been defined in order to achieve this objective:

- To identify TBM cutter ring failure mechanisms arising from tunnel boring (e.g. modes of contact, wear, load effects).
- To assess the influence of temperature on cutter ring wear processes.
- To evaluate the influence of corrosion on TBM cutter rings.
- To evaluate the suitability of the new RIAT test method for assessing cutter ring wear.

Analysis was carried out on two types of steel component: TBM cutter and RIAT mini-cutter rings. Samples of these components were collected from Projects A, C and D. The reader is referred to the section 3.5.4 in this thesis addressing research methodology.

Table 50 shows the probable composition of the TBM cutter and RIAT mini-cutter rings.

Table 50. Composition of a standard TBM cutter ring and RIAT mini-cutter samples.

Composition (wt. %)	TBM cutter ring*	RIAT mini-cutter ring**	AISI Type H13***
C	0.57	0.39	0.32 – 0.40
Mn	0.29	0.40	-
Si	0.98	1.00	1.00
Cr	4.84	5.20	5.13 – 5.25
V	0.92	0.90	1.00
Mo	1.35	1.40	1.33 – 1.40
Ni	0.12	-	-
Cu	0.12	-	-

*Average composition of a typical TBM cutter ring (Krogstad, 2013)
**Original composition (Uddeholm, 2015)
***AISI 2015

The composition of the steel used in the TBM cutter rings is regarded as sensitive information, so a standard composition is included. The AISI H13 tool steel is used as a basic for TBM cutter rings with slightly modified composition.

Hard rock TBM tunnelling requires a cutter ring composition that provides an effective balance between hardness and ductility/toughness. The vanadium and nickel components contribute towards increasing strength, hardness and resistance to impacts. The carbon, silicon and manganese components contribute to hardness, but reduce ductility.

Figure 130 shows the microstructure of cutter disc steel after metallographical preparation. It displays a typical tempered martensite microstructure with some paler areas of retained austenite. The steel has been die-forged and heat-treated to increase its hardness (See Paper IX).

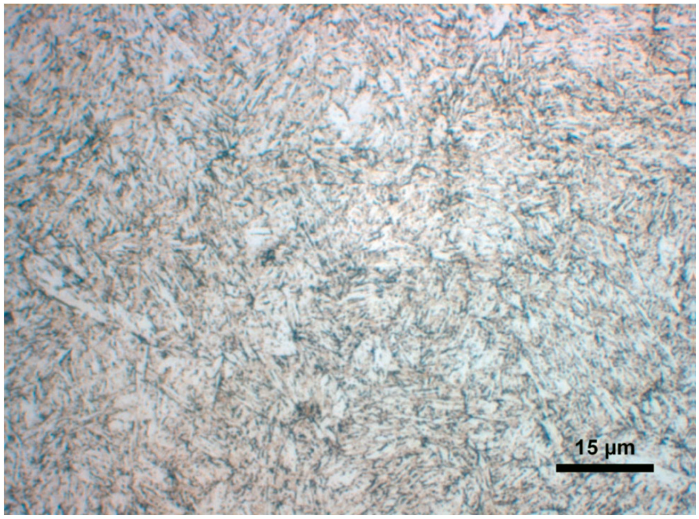

Figure 130. Microstructure of the cutter disc steel (H 13 tool steel) tested as part of this study (Reproduced from Paper IX).

4.3.2 Hardness profiles of worn cutters

Macro and micro hardness measurements were performed on both the TBM cutter and RIAT mini-cutter rings in order to analyse the steel hardness of the samples. The equipment and testing procedures used have previously been described in chapter 3.5.4 of this thesis addressing research methodology.

In order to obtain data representing comparable rolling conditions, indentations were made on cross-sections parallel to the rolling direction. To obtain hardness profiles, three parallel measurements were performed for each selected distance. To obtain hardness data after tempering, ten parallel surface measurements were performed for each sample (Figure 60, section 3.5.4). In both cases, an average value was calculated.

Some of the results from the TBM cutter and RIAT mini-cutter rings indicate work hardening due to an increase in hardness close to the cutter surface. The hardness increments near the surface compared to the hardness in the inner part are about 10%.

However, in some of the cross-sections, hardness decreases close to the steel surface indicating some degree of surface softening. On the basis of a single measurement, a sharper gradient is observed for the RIAT mini-cutter sample.

Figure 131 shows a hardness profile resulted from the hardness measurements on cross-section in the TBM cutter ring sample no. 02 that indicate work hardening on the surface. Figure 132 shows the hardness profiles of TBM cutter ring sample no. 04 that indicates softening on the surface.

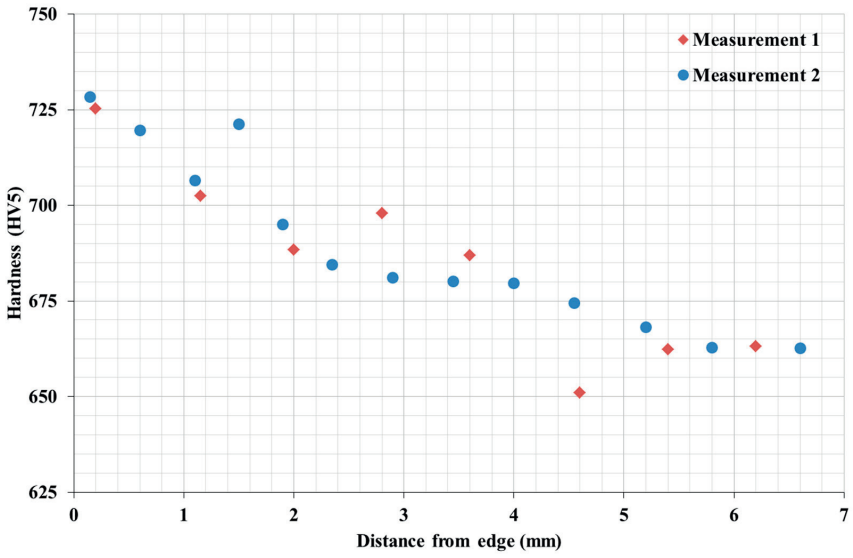

Figure 131. Hardness profiles for TBM cutter ring sample no. 02.

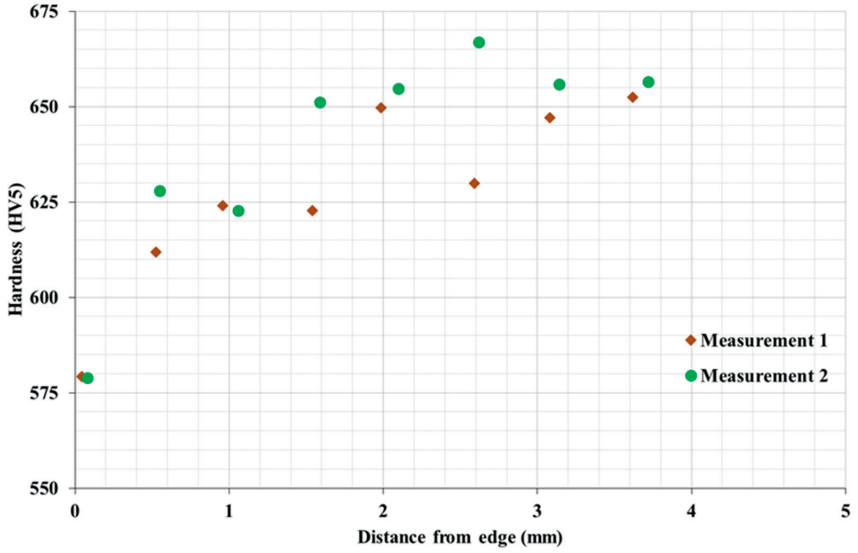

Figure 132. Hardness profiles for TBM cutter ring sample no 04.

4.3.3 Influence of temperature - Tempering experiment

Tempering experiments were performed in order to analyse the possible influence of temperature on cutter wear. The objective here is to study the evolution of hardness as a function of the time and temperature, excluding the deformation effect. A description of the procedure used, as well as more detailed information about the tempering experiments, are included in section 3.5.4 of this thesis.

The effect of tempering was quantified by means of hardness measurements made after each sample was air-cooled. The results for different temperatures and selected tempering times (1, 2 and 4 hours respectively) exhibit similar trends. The maximum temperature was maintained for 1 hour. The hardness decreases from approximately 670 HV5 at 500°C to 300 HV5 at 700°C.

It is assumed that a boring time for one stroke (1.5-2.0 m) of 1 hour, is representative for hard rock tunnel boring. Comparison with surface hardness values of TBM cutter ring samples nos. 01 and 04 in the hardness profile resulting from tempering experiments will indicate the temperature required to obtain the softening level found in the TBM cutter ring samples. The surface temperature is equivalent to around 620°C. The results indicate a clear temperature gradient that decreases with depth below the surface of the sample. Temperatures of 540 and 320°C were measured at depths of 2 and 3 mm, respectively, into the cutter surface.

Figure 133 shows hardness profiles resulting from tempering experiments performed for 1, 2 and 4 hours on TBM cutter ring sample no. 05. Figure 134 presents a hardness profile resulting from a tempering experiment performed for 1 hour on TBM cutter ring sample no. 04.

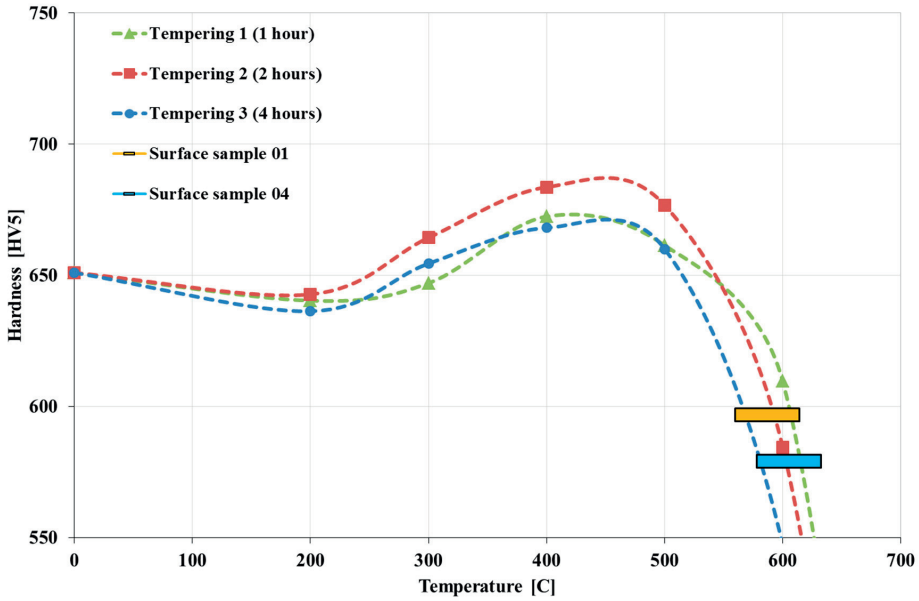

Figure 133. Hardness profiles resulting from tempering experiments performed after 1, 2 and 4 hours on TBM cutter ring sample no. 05 (unused cutter ring). The rectangles represent hardness values at the wear surface of TBM cutter ring samples 01 and 04.

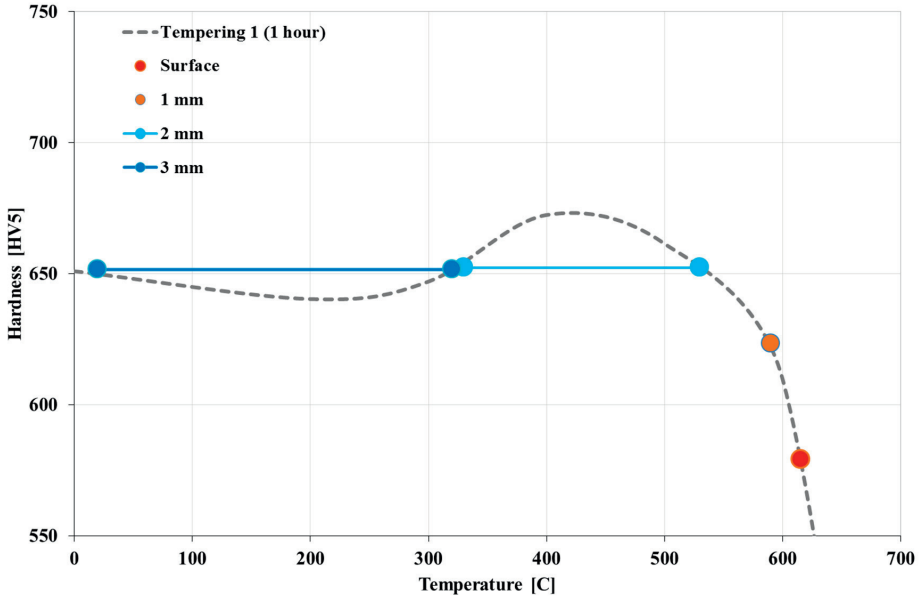

Figure 134. Hardness profile resulting from a tempering experiment performed for 1 hour on TBM cutter ring sample no. 04. Points and horizontal lines indicate hardness values at known distances from the wear surface of the sample.

4.3.4 Influence of corrosion on the abrasion of cutter steels

An evaluation of the potential influence of corrosion on abrasive wear on TBM cutter tool steel has been performed using a variety of laboratory tests (Paper IX). The reason for this evaluation is that cutter tools interact with a variety of excavation fluids (i.e. soil and rock conditioners, anti-abrasion additives and water). These fluids can be aggressive chemicals that might damage the integrity of the cutters, leading to changes in the wear mechanism that accelerate their degradation.

Only a summary of the main results is presented in this chapter. The reader is referred to Paper IX for a detailed presentation and discussion of the experimental results.

The results obtained clearly show that corrosion has an influence on abrasion rates under hard rock conditions. However, the validity of the results is yet to be evaluated under operational conditions (actual TBM projects). This can be carried out when more field data, in the form of worn TBM tools, becomes available. However, on the basis of laboratory tests, the following conclusions can be drawn:

• The use of conditioning additives results in lower abrasion rates in H13 steel (based on tests using two different water media – low and high chloride content).

• Wear was less pronounced in the presence of additives, demonstrating the positive effect of additives in the abrasion process.

• Steel corrosion was observed in the presence of seawater and additives. This was demonstrated by means of chemical analysis of the liquid media and a microstructural analysis of the steel.

• This work demonstrates the potential of using this approach in the study of TBM tools exposed to degradation mechanisms, wear and corrosion. It should also be possible to test other types of tunnel excavation tools such as the drill bits used in drill and blast tunnelling operations.

4.3.5 Failure mechanisms

Microstructural analysis using optical and electron microscopes was performed for all TBM cutter ring samples and RIAT mini-cutter rings in order to identify the different aspects of failure mechanisms that occur during tunnel boring (e.g. modes of contact, wear or load effects).

Modes of contact

An analysis of cross-sections parallel to the direction of rolling was carried out in order to observe the mode of contact. Lamellar structures at the surface, running parallel to the rolling direction, may be caused by a sliding contact mode (see Figure 135). Structures similar in appearance, but running at right angles to the rolling direction, may be caused by plastic deformation during rolling contact (Nærland, 2015).

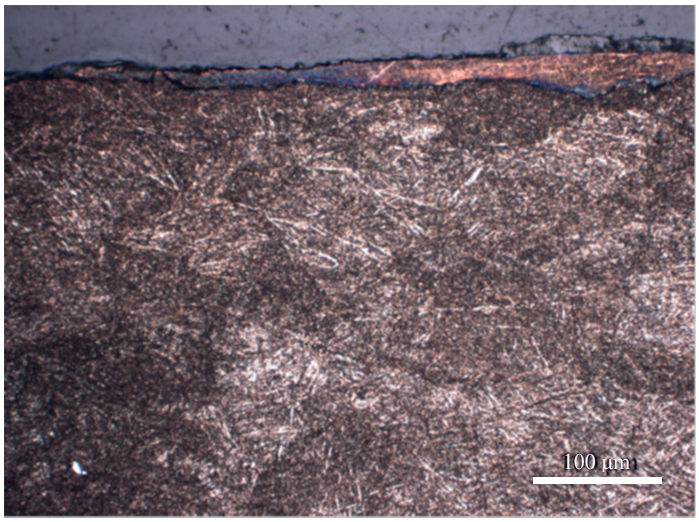

Figure 135. An optical image of a cross-section cut parallel to the rolling direction of a TBM cutter ring (sample no. 03). Reproduced from Nærland (2015).

None of the TBM cutter rings showed signs of sliding contact. This indicates that rolling behaviour is the dominant mechanism, regardless of geological factors.

The results from analyses of the RIAT mini-cutter ring samples revealed lamellar structures for quartzite, granite and basalt.

Figure 136 shows two images of RIAT mini-cutter ring samples used on a sample of quartzite. The presence of a deformed layer indicates the contribution of sliding to the contact mode.

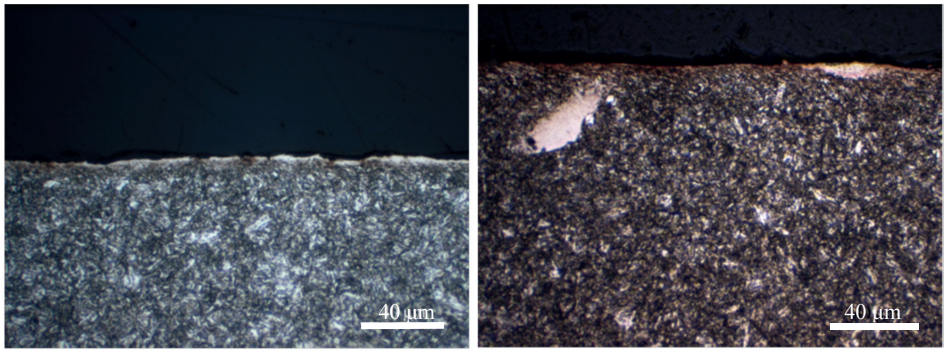

Figure 136. Optical images of cross-sections cut parallel to the rolling direction of RIAT mini-cutter ring sample 15 (left) and 16 (right). Reproduced from Nærland (2015).

The lamellar layer was observed to vary in thickness with values that correlated with rock abrasiveness. The largest thickness value was found for tests using a basalt sample and the lowest for a quartzite sample. The lower the abrasivity, the greater the thickness of the

lamellar layer, indicating that the sliding contact component dominates in the case of the RIAT mini-cutter ring samples. This relation is in good agreement with the research findings of Petrica et al. (2014) for martensitic steels under two-body conditions. A different mode of contact will probably vary the results; less deformation due to rolling than due to sliding contact is expected.

Sliding contact parallel to the rolling direction might indicate the use of excessive thrust or/and limited rotation diameter during the RIAT tests. It is not possible to increase the rotation diameter due to practical reasons such as the laboratory scale of the experiments and difficulties linked to obtaining samples.

Wear mechanisms

Cross-sections cut parallel and at right angles to the rolling orientation were used to identify wear mechanisms in the TBM cutter samples and RIAT mini-cutter rings.

The optical microscope images presented in Figure 137 make it possible to distinguish fatigue from the folding of asperities. SEM images of the worn surface are used to identify abrasive wear.

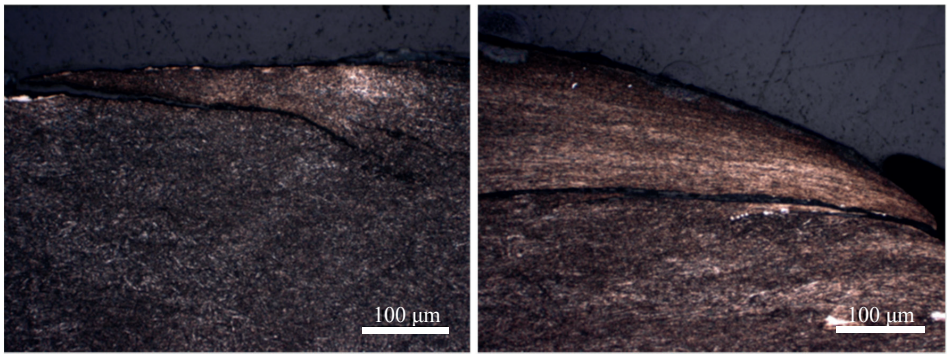

Figure 137. Optical images of cross-sections taken from TBM cutter ring sample no 02. The cross-sections are cut parallel (left) and at right angles (right) to the rolling orientation. Reproduced from Nærland (2015).

Several types of crack have been identified (Figure 137 and Figure 138). Some have a subsurface origin that is not linked to surface wear mechanisms (Figure 138). The formation of such cracks are clear indications of wear caused by fatigue, which is a common result of rolling contacts. The mechanism called “chipping”, which is commonly cited as a reason to replace TBM cutters under hard rock conditions, arises when subsurface cracks reach the surface of the cutter producing a chip of material that detaches from the steel.

Cracks connected to the surface may have a subsurface origin, or may result from the folding of asperities by plastic deformation leading to crack growth caused by fatigue.

Asperity surface wear produces an oxide layer that inhibits potential crack re-adhesion.

Figure 138 provides an example of visible cracks initiated in the subsurface.

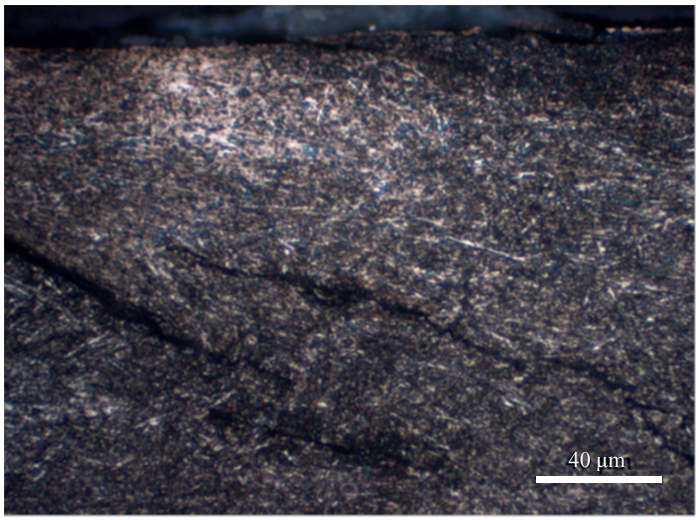

Figure 138. An optical image of a parallel cross-section of TBM cutter ring sample no. 02. Reproduced from Nærland (2015).

Similar wear mechanisms are observed for the RIAT mini-cutter samples. From the tests performed, it is reasonable to assume that fatigue would make a greater contribution to wear if the tests were run for longer periods.

Abrasive wear was analysed using an electron microscope, and was demonstrated by the presence in some samples of several wear lines produced by abrasive ploughing.

The most pronounced wear lines were identified in RIAT mini-cutter ring samples tested using quartzite. This is to be expected since quartzite is the most abrasive rock type tested as part of this research work.

Figure 139 shows the wear surface of RIAT mini-cutter sample 13, tested on granite. The bright areas of the image indicate the presence of embedded rock debris. The largest amounts of debris, but lower densities of ploughing marks, are encountered on samples tested using highly abrasive rocks such as quartzite, granite and basalt (Nærland, 2015).

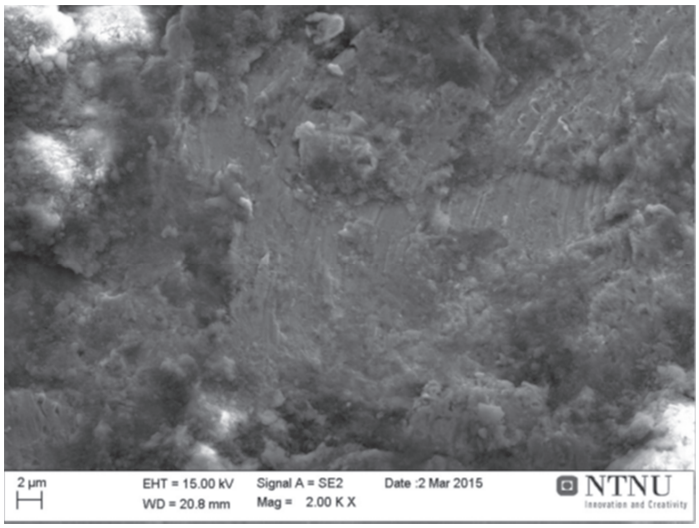

Figure 139. An SEM surface image of the RIAT mini-cutter ring sample no. 13. Reproduced from Nærland (2015).

Load effects

A microstructural analysis was carried out to study the presence of deformation layers in TBM cutter and RIAT mini-cutter ring samples, and to compare load effects.

Figure 140 shows a cross-section from a TBM cutter ring sample illustrating the presence of a martensitic microstructure (Nærland, 2015). The dark layer in the image, observed at the specimen surface, represents a nanocrystalline deformation layer. Below this is a heavily deformed area marking a transition to the undeformed bulk steel of the subsurface. No differences are identified when comparing cross-sections cut parallel and at right angles to the rolling direction.

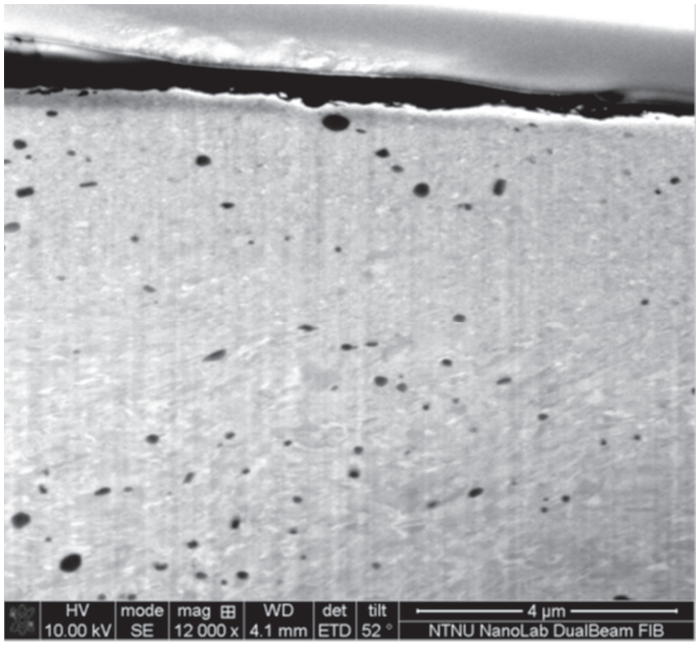

Figure 140. An FIB image of a cross-section (transverse) from TBM cutter ring sample no. 02 (Reproduced from Nærland, 2015).

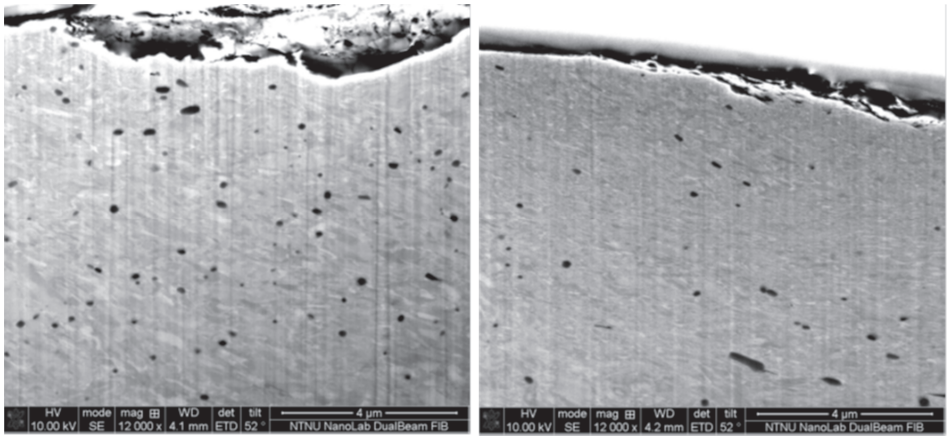

Figure 141. FIB images of cross-sections (transverse) from TBM cutter ring samples no. 01 (left) and no. 04 (right). Reproduced from Nærland (2015).

In the case of RIAT mini-cutter ring samples, both sample no. 7 (Figure 142, left), which was tested using basalt (low abrasivity), and sample no. 16(Figure 142, right), tested using quartzite (high abrasivity), show similar patterns to the TBM cutter ring samples. The RIAT mini-cutter ring worn by basalt does not show a clear deformation layer, while that worn by quartzite exhibits no deformation layer.

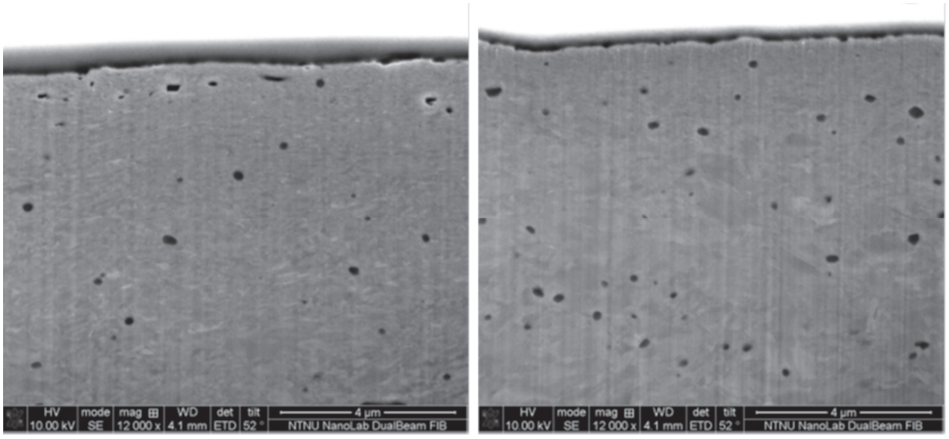

Figure 142. FIB images of cross-sections (transverse) from RIAT mini-cutter ring sample no. 07 (left) and no. 16 (right). Reproduced from Nærland (2015).

4.3.6 Concluding remarks

The main conclusive remarks to the analysis of cutter wear mechanisms in hard rock tunnel boring are listed following.

Test results indicate the presence of work hardening in TBM cutter samples and RIAT mini-cutter rings. The amount of hardening is similar for both, with an increase in hardness of approximately 10%.

Some of the TBM cutter rings exhibited the presence of softening which may be the result of high temperatures induced during boring. In order to quantify the temperatures achieved during cutter ring contact, a tempering experiment was performed. The results indicate that a maximum temperature of 620°C was achieved in the surface layer of several TBM cutter ring samples. Temperatures of between 540 and 320°C are indicated for depths 2 and 3 mm from the cutter surface respectively. This temperature-dependency might play an important role in cutter ring wear.

Laboratory testing has revealed the influence of corrosion on the effects of rock abrasivity. However, more field data from actual tunnelling projects are required to validate these results.

An increase in chipping of cutters is observed to correlate with reduced rock abrasivity and increased cutter life. This can be explained by prolonged exposure to cyclic loads and higher load peaks during boring.

Abrasive wear has been demonstrated to occur in the TBM cutter ring and RIAT mini-cutter ring samples. Rolling is indicated as the primary mode of contact in the case of the TBM cutter ring samples, but represents a less dominant component for the RIAT mini-cutter ring samples. This can be explained by excessive thrust and/or the restricted rolling diameters applied during laboratory scale testing.

Cracks have been identified in the subsurface steel of cutters, and are interpreted to have been produced by fatigue, which is a common result of rolling contacts.

5 Conclusions and recommendations

This research work has resulted in three main contributions:

- ✓ A revision and update of the current version of the NTNU prediction model for TBM tunnelling performance and cutter life assessments. A new version has been published and the relevant report is included as an appendix to this thesis.
- ✓ The development of a new rock abrasivity laboratory test method for tool life assessments in hard rock tunnel boring.
- ✓ An analysis of the wear processes and failure mechanisms that are encountered in cutter rings used for hard rock tunnel boring.

5.1 Research questions

A number of research goals have emerged as a result of this research with the aim of addressing the following proposed objectives:

To revise and extend the NTNU performance and cutter life prediction model for hard rock tunnel boring:

- To decide if a revision of the current version is required and appropriate.
- To revise and amplify TBM specifications and operational parameters.
- To establish a rock mass classification system.
- To find out if it is possible and necessary to address the influence of recently-defined parameters such as:
    - Cutterhead velocity – and its influence on penetration.
    - Cutter thrust – and its influence on cutter consumption.
    - Tunnel length influence on machine utilization.

To develop a new rock abrasivity laboratory test method for tool life assessments in hard rock tunnel boring:

- To establish if a new rock abrasivity test is required.
- To find out if the development of a new rock abrasivity test is appropriate.
- To establish if the results are of interest when compared with existing laboratory test methods.

To analyse the wear processes and failure mechanisms that are encountered in cutter rings used for tunnel boring:

- To establish if the identification of wear mechanisms in TBM cutter rings is appropriate.

- To establish if the identification of the influence of other possible wear factors such as temperature and tribocorrosion are relevant.
- To investigate if the wear process for the new laboratory test method is representative.

The research questions have been answered.

5.2 Main findings

•The publication of a new version of the NTNU performance and cutter life prediction model for hard rock TBMs.

The NTNU model has been revised on the basis of data from five international projects involving TBMs varying from 3.4 to 10 metres in diameter and experience from the last decades. Adequate amounts of laboratory testing, geological back-mapping, TBM data analysis and field trials have been carried out in sufficient detail.

Recommended TBM specifications have been updated and extended to adapt to current technologies.

The recommended cutterhead velocity (rpm) parameter has been modified in response to the results of in-situ trials ('RPM tests'), field data and rock mass assessments.

The penetration coefficient (b) and predicted basic penetration rate have been modified according to research results and the modified recommended cutterhead rpm.

The definition of the rock mass fracturing factor has been updated. The type of fracture term has been unified and a new fracture classification for low degrees of fracturing has been established.

The influence of the cutterhead velocity (rpm) on penetration rate has been discussed and a factor describing the influence has been introduced on the basis of cutterhead velocity testing so-named 'RPM test'. Procedure for 'RPM test' has been proposed

The category intervals for DRI and CLI have been updated.

The correction factor for the DRI has been updated.

The basic cutter ring life has been updated and a methodology stablished.

A factor describing the influence of average cutter thrust on cutter life for extremely and very abrasive rock types has been introduced.

Extra time consumption for tunnel activities regarding to the length of the tunnel has been included.

• The development of a new rock abrasivity test method for tool life assessments on hard rock tunnel boring.

A new test method for tool life assessments in connection with hard rock tunnel boring (the Rolling Indentation Abrasion Test – RIAT) has been developed. The new test uses a rolling disc on intact rock samples reproducing in a more realistic way, analogous to the tribological process involved using TBM cutter discs during actual tunnelling projects.

Initial results obtained from the RIAT test indicate that it has the ability to assess abrasive cutter wear for a wide range of rock abrasivities, capable to evaluate rock abrasivity on TBM cutters. It can also account for indentation results recorded for hard rock types worn by rolling discs.

The RIAT method improves the ability to enlarge the classification of abrasivities for rock types with the greatest capacity to produce cutter wear and the highest resistance to indentation. Both of these factors contribute to high levels of cutter consumption.

A comprehensive set of laboratory tests has been performed to evaluate the RIAT method. An analysis of the relationship between preliminary RIAT tests and currently applied test methods has been carried out. The results reveal that a relationship exists between the AVS and CLI, while weak correlation occurs with SJ test and results from the RIAT. The RIAT and SJ tests exhibit different penetration behaviour. The indentation process involving wear by means of a rolling contact, as exhibited by the RIAT test, appears to be a more realistic mechanism. However, it will be necessary to carry out studies of actual TBM projects in the field in order to confirm the cutter wear results observed in the laboratory. A comparison of the Cerchar Abrasivity Index (CAI_s) with the RIAT fails to reveal a satisfactory correlation, probably as a result of differences in wear behaviour. The limited ability of the tip of the stylus to fully penetrate hard rock types may result in an underestimation of wear (Paper VIII).

The mineral composition of hard rock samples was also analysed and significant relationships between quartz content, equivalent quartz content, VHNR and the RIAT indices ($RIAT_a$ and $RIAT_i$) were found.

• Identification of the wear mechanisms in TBM cutter and RIAT mini-cutter rings.

Abrasive wear has been established in TBM cutter ring and RIAT mini-cutter ring samples. Rolling is indicated as the primary mode of contact for TBM cutter rings, while its contribution has been found to be slightly less in the case of the mini-cutter ring samples. This may be explained by the limited rolling diameter acting on the samples at laboratory scale.

An increase in chipping is correlated with reduced abrasivity and increased cutter life. This can be explained by prolonged exposure to cyclic loads and high load peaks during boring. Cracks have been identified in the subsurface and are anticipated to have been produced by fatigue.

Results have revealed similar levels of work hardening in both TBM cutter and RIAT mini-cutter rings, with an increase of the hardness of approximately 10%.

Results also indicate that temperatures of 620°C have been achieved at contact surfaces of the cutter rings. Temperatures between 540 and 320°C have been demonstrated at depths of 2 and 3 mm from the cutter surface respectively.

The influence of the corrosion on the rock abrasivity rates has been demonstrated at laboratory scale. However, more data from actual tunnelling projects are required in order to verify these results.

5.3 Recommendations and further work

5.3.1 General recommendations

Tunnelling technologies continue to improve, and the TBM sector is no exception. This factor should drive to a continuous updating of the prediction models for performance predictions and cutter life assessments. Furthermore, outcomes from research resulting in a better understanding of the tunnel boring process should be applied to the development and revision of prediction models.

This thesis strongly recommends the inclusion of test procedures both at the commencement of, and during, TBM projects in order to select the optimal operational parameters from among the many options available for a given machine and set of geological conditions. It is believed that by including this requirement in project contracts, many tiresome disputes can be avoided. Continuous trial testing (penetration and 'RPM tests'), combined with descriptions of geology, drillability and rock mass fracturing will enhance our knowledge of the tunnel boring process.

Prediction models are developed on the basis of a variety of fields, types of machines and other particularities. The models have limitations and, in some cases, specific range of applicability resulting in reliable predictions. The use of different models will result in greater reliability of the estimates.

More effort should be invested in improving cutter technology (cutter ring steel quality and bearing systems). An increase in cutter load would result in major improvements in performance and the applicability of the TBM method.

The real-time monitoring of cutter thrust, cutter rolling, cutter wear and temperature parameters for individual TBM cutter discs can form the basis for major improvements in machine efficiency, and provide a better understanding of rock-breaking and cutter wear processes.

The influence of machine designs (i.e. cutterhead layouts and cutter designs) on cutter life and machine performances is not well investigated. It could be achieved a greater efficiency by small adaptations.

5.3.2 Further work

The following proposals are put forward for further research work based on the results of this thesis. Much of the further work is already in progress:

1) The prediction model

   - The inclusion of more data derived from large TBMs and/or shield machines.
   - An investigation of the gross cutter thrust parameter, which may exhibit different characteristics for open gripper and shield TBMs and/or large diameters.
   - A classification of fractures incorporating characteristics such as persistence, aperture and filling. The influence of tunnel diameters should also be included.
   - Continuous 'RPM testing' combined with descriptions of geology, drillability and rock mass fracturing in a greater variety of geologies, cutter thrust and rpm levels as well as TBM types and designs.
   - Research in order to investigate the need and opportunity to further develop the existing drillability testing.
   - An analysis of the influence of additional parameters like groundwater inflow and rock stress.
   - A study of the influence of cutter tip width and steel quality on tool performance and tool consumption. This analysis was not possible during the present research work due to the lack of variability in this parameter among the data available.
   - Analysis of the influence of cutter thrust on cutter consumption should be verified and expanded by first acquiring more data.
   - Study of the influence of cutterhead design and layout on cutter consumption.

2) Develop of a new test method

   - The applicability of the SGAT-CR to assess tool wear in crushing machines or similar should be considered.
   - To date, the results of RIAT tests (Macias et al. 2016) and the comparisons observed with most other commonly used abrasivity test methods in relation to mineral composition are promising. However, the recently developed RIAT method has not been analysed against data from actual TBM operations in order to evaluate the capability for cutter life prediction in hard rock TBMs. A study involving the testing and analysis of rock samples from a TBM tunnel project is currently underway.
   - Extended testing to improve the capability and reproducibility of the RIAT method. Characterisation of abrasivity for a larger selection of rock types.
   - An analysis of the influence of the properties of the test surface (cut, broken or processed).
   - Studies of the influence of rolling velocity and thrust on miniature cutter wear behaviour.

- The performance of tests under wet conditions, using slurries and additives, etc.
- A new device design for the RIAT method should be considered in order to make testing more efficient and to enhance test repeatability. Focus should be directed on important factors such as the rigidity of the frame, the precision of the drive unit and sample attachment approaches. A new design must incorporate a system to remove rock debris and dust. This will ensure that the mini-cutter rings are constantly in contact with the intact rock sample during testing.

3) Cutter wear mechanism:

- A study should be made to characterise and analyse the structure and wear mechanism of a larger number of worn disc cutter samples obtained from boring under different conditions and for a variety of machine designs.
- A characterisation of the worn surfaces and alloy structures of RIAT miniature cutters.
- Further analyses of the influence of temperature on cutter ring wear.

References

AISI Type H13 Hot Work Steel, Mat Web. Available online at http://www.matweb.com/search/datasheet_print.aspx?matguid=e30d1d1038164808a85cf7ba6aa87ef7

ASTM (2010). Standard test method for laboratory determination of abrasiveness of rock using the CERCHAR method. Designation: D7625-10.

Barton, N., Lien, R. and Linde, J. (1974). Engineering Classification of Rock Masses for the Design of Tunnel Support. Rock Mechanics, Springer-Verlag, Vol. 6 (1974), pp 189 – 236.

Barton, N. (1999). TBM performance in rock using Q_{TBM}. Tunnels & Tunnelling International Vol. 31 (1999), pp 41-48.

Barton, N. (2000). TBM tunnelling in jointed and faulted rock. A.A. Balkema, Rotterdam (2000). ISBN 90 5809 341 7.

Barton, N. and Bieniawski, Z.T. (2008). RMR and Q – Setting records straight. Tunnels & Tunnelling. February (2008), pp 26–29.

Barton, N. (2012). Reducing risk in long deep tunnels by using TBM and Drill and Blast methods in the same project-the hybrid solution. Journal of Rock Mechanics and Geotechnical Engineering, Vol. 4, no. 2 (2012), pp 115-126.

Barton, N. (2013a). Hybrid TBM and Drill-and-Blast from the start. Tunnelling Journal, December 2012/January 2013.

Barton, N. (2013b). TBM prognosis for open-gripper and double shield machines: Challenges and solutions for weakness zones and water. Fjellsprengningsteknikk conference (2013), Oslo, Norway.

Bejari, H. and Khademi, J.H. (2013). Simultaneous effects of joints spacing and orientation on TBM cutting efficiency in jointed rock masses. Rock Mechanics and Rock Engineering, Vol 46, no. 4 (2013), pp 897–907.

Bieniawski, Z.T. (1973). Engineering Classification of Jointed Rock Masses. The Civil Engineer in South Africa, Vol. 15 (1973), pp 335-343.

Bieniawski, Z.T. (1989). Engineering Rock Mass Classifications: a Complete Manual. New York: John Wiley and Sons (1989).

Bieniawski, Z.T., Celada, B., Galera, J.M. and Alvarez, M. (2006). Rock mass excavability indicator: new way to selecting the optimum tunnel construction method. Tunnelling and Underground Space Technology Vol. 21, no.3-4 (2006), pp 237.

Bieniawski, Z.T., Celada, C. B., Galera, J. M. and Tardaguila, I. G. (2009). Prediction of Cutter Wear using RME. Proceedings ITA-ITAES World Tunnel Congress, Budapest, Hungary (2009).

Bruland, A. (2015). Personal communication.

Bruland, A. (2000a). Hard Rock Tunnel Boring: Vol 1, Background and Discussion. PhD thesis. Norwegian University of Science and Technology (NTNU), Trondheim, Norway, 2000.

Bruland, A. (2000b). Hard Rock Tunnel Boring: Vol 3, Advance Rate and Cutter Wear. PhD thesis. Norwegian University of Science and Technology (NTNU), Trondheim, Norway, 2000.

Bruland, A. (2000c). Hard Rock Tunnel Boring: Vol 4, Costs. PhD thesis. Norwegian University of Science and Technology (NTNU), Trondheim, Norway, 2000.

Bruland, A. (2000d). Hard Rock Tunnel Boring: Vol 5, Geology and Site Investigations. PhD thesis. Norwegian University of Science and Technology (NTNU), Trondheim, Norway, 2000.

Bruland, A. (2000e). Hard Rock Tunnel Boring: Vol 6, Performance Data and Back-mapping. PhD thesis. Norwegian University of Science and Technology (NTNU), Trondheim, Norway, 2000.

Bruland, A. (2000f). Hard Rock Tunnel Boring: Vol 7, The Boring Process. PhD thesis. Norwegian University of Science and Technology (NTNU), Trondheim, Norway, 2000.

Bruland, A. (2000g). Hard Rock Tunnel Boring: Vol 8, Drillability Test Methods. PhD thesis. Norwegian University of Science and Technology (NTNU), Trondheim, Norway, 2000.

Bruland, A. (2000h). Hard Rock Tunnel Boring: Vol 9, Drillability – Catalogue of Drillability Indices. PhD thesis. Norwegian University of Science and Technology (NTNU), Trondheim, Norway, 2000.

Bruland, A. (2000i). Hard Rock Tunnel Boring: Vol 10, Drillability – Statistics of Drillability Test Results. PhD thesis. Norwegian University of Science and Technology (NTNU), Trondheim, Norway, 2000.

Callister, W.D. and Rethwisch, D.G. (2009). Materials Science and Engineering: an introduction (8th edition). Wiley (2009). ISBN 978-0-470-41997-7.

Chang, S.H., Choi, S.W., Bae G.J. and Jeon, S. (2006). Performance prediction of TBM disc cutting on granitic rock by the linear cutting test. Tunnelling and Underground Space Technology Vol. 21, no.3–4(2006), pp 271.

Cho, J.W., Jeon, S., Yu, S.H. and Chang, S.H. (2010). Optimum spacing of TBM disc cutters: a numerical simulation using the three-dimensional dynamic fracturing method. Tunnelling and Underground Space Technology Vol 25, no. 3 (2010), pp 230–244.

Cho, J.W., Jeon, S., Jeong, H.Y. and Chang, S.H., (2013). Evaluation of cutting efficiency during TBM disc cutter excavation within a Korean granitic rock using linear-cutting-machine testing and photogrammetric measurement. Tunnelling and Underground Space Technology Vol. 35 (2013), pp 37–54.

Dahl, F., Bruland, A., Jakobsen, P.D., Nilsen, B. and Grøv, E. (2012). Classifications of properties influencing the drillability of rocks, based on the NTNU/SINTEF test method. Tunnelling and Underground Space Technology Vol. 28 (2012), pp 150-158.

Davis, G. H. (1984). Structural Geology of Rocks and Regions. John Wiley & sons. New York (1984).

Delisio, A., Zhao, J. and Einstein, H.H. (2013). Analysis and prediction of TBM performance in blocky rock conditions at the Lötschberg Base Tunnel. Tunnelling and Underground Space Technology Vol 33 (2014), pp 131-142.

Delisio, A. and Zhao, J. (2014). A new model for TBM performance prediction in blocky rock conditions. Tunnelling and Underground Space Technology Vol 43 (2014), pp 440-452.

Dollinger, G.L., Handewith, H.J. and Breeds, C.D. (1998). Use of the punch test for estimating TBM performance. Tunnelling and Underground Space Technology Vol 13 (4) (1998), pp. 403–408

Eide, L.N.R. (2014). TBM Tunnelling at the Stillwater Mine. MSc thesis, Norwegian University of Science and Technology (NTNU), Trondheim, Norway (2014).

Ellecosta, P., Schneider, S., Käsling, H. and Thuro, K. (2015). Hardness - a new method for characterising the interaction of TBM disc cutters and rocks? Proceedings of the 13th Congress on Rock Mechanics, ISRM Congress 2015 - In-novation in Applied and Theoretical Rock Mechanics, May 10-13, 2015, Palais des Congrès der Montréal, Canada, Paper 688, 10 p., ISBN: 978-1-926872-25-4.

Entacher, M., Winter, G. and Galler, R. (2013). Cutter force measurement on tunnel boring machines – Implementation at Koralm tunnel. Tunnelling and Underground Space Technology Vol. 38 (2013), pp 487-496.

Entacher, M., Lorenz, S. and Galler, R. (2014). Tunnel boring machine performance prediction with scaled rock cutting test. Rock Mechanics & Mining Sciences Vol. 70 (2014), pp 450-459.

Espallargas, N., Jakobsen, P.D., Langmaack, L. and Macias, F.J. (2015). Influence of corrosion on the abrasion of cutter steels used in TBM tunnelling. Rock Mechanics and Rock Engineering, Vol 48 (2015), pp 261–275.

Farmer, I. and Glossop, N. (1980). Mechanic of disc cutter penetration. Tunnels and Tunnelling International Vol 12 (1980), pp 22-25.

Farrokh, E., Rostami, J. and Laughton, C. (2012). Study of various models for estimation of penetration rate of hard rock TBMs. Tunnelling and Underground Space Technology Vol. 30 (2012), pp 110-123.

Frenzel, C., Käsling, H. and Thuro, K. (2008). Factors influencing Disc Cutter Wear. Geomechanics and Tunnelling Vol 6 (2008), pp 55-60.

Frenzel, C. (2011). Disc Cutter Wear Phenomenology and their Implications on Disc Cutter Consumption for TBM. 45th US Rock Mechanics / Geomechanics Symposium, San Francisco, USA (2011).

Frenzel, C., Galler, R., Käsling, H. and Villeneuve, M. (2012). Penetration tests for TBMs and their practical application. Geomechanics and Tunnelling Vol. 5 (2012), no 5, pp 557-566.

Frostad, H-I. (2013). TBM Kutterslitasje database. MSc Thesis. Norwegian University of Science and Technology (NTNU), Trondheim, Norway (2013), (in Norwegian).

Fuenkajorn, K., Sriapai, T. and Samsri, P. (2012). Effects of loading rate on strength and deformability of Maha Sarakham salt. Engineering Geology Vol. 135-136 (2012), pp 10-23.

Gehring, K. (1995). Leistungs- und Verschleißprognosen im maschinellen Tunnelbau. Felsbau, Vol. 13, no. 6 (1995), pp 439-448 (in German).

Geng, Q., Wei, Z., Meng, H. and Chen, Q. (2016a). Numerical and experimental research on the rock-breaking process of tunnel boring machine normal disc cutters. Journal of Mechanical Science and Technology Vol. 30 (2016), pp 1733-1745.

Geng, Q., Zhengying, W., Hao, M. and Macias, F.J. (2016b). Mechanical performance of TBM cutterhead in mixed ground conditions. Tunnelling and Underground Space Technology Vol. 57 (2016), pp 76-84.

Gertsch, R., Gertsch, L. and Rostami, J., (2007). Disc cutting tests in Colorado Red Granite: Implications for TBM performance prediction. International Journal of Rock Mechanics & Mining Sciences Vol. 44, no.2 (2007), pp 238–246.

Gong, Q.M., Zhao, J. and Jiamg, Y.S. (2007). In situ TBM penetration tests and rock mass boreability analysis in hard rock tunnels. Tunnelling and Underground Space Technology Vol. 22 (2007), pp 303-316.

Gong, Q.M. and Zhao, J. (2009). Development of a rock mass characteristics model for TBM penetration rate prediction. International Journal of Rock Mechanics & Mining Sciences Vol. 46 (2009), pp 8-18.

Gong, Q.M., Zhao, J. and Jiao, Y. (2005). Numerical modelling of the effects of joint orientation on rock fragmentation by TBM cutters. Tunnelling and Underground Space Technology Vol. 20 (2005), pp 183-191.

Gong, Q.M., Jiao, Y. and Zhao, J. (2005). Numerical modelling of the effects of joint spacing on rock fragmentation by TBM cutters. Tunnelling and Underground Space Technology Vol. 21 (2006), pp 46-55.

Grandori, R, Bieniawski, Z.T., Vizzino, D., Lizzadro, L., Romualdi, P. and Busillo, A. (2011). Hard rock extreme conditions in the first 10 km of TBM driven Brenner Exploratory Tunnel. Rapid Excavation Tunneling Conference (RETC, 2011), San Francisco, USA.

Grimstad, E. and Barton, N. (1993). Updating of the Q-system for NMT. In Proceedings of the International Symposium of Sprayed Concrete-Modern Use of Wet Mix Sprayed Concrete for Underground Support, Oslo: Fagernes (1993), Norwegian Concrete Association.

Grøv, E., Jakobsen, P.D., Kane, A-P., Hoang, H., Smading, S. and Sagen, T.B. (2013). TBM cutter steel – a challenge for Norwegian steel suppliers. Tunnelling Journal June/July (2013), pp 40-45.

Handewith, H.J. (1970) Predicting the economic success of continuous tunneling and hard rock. 71st Annual General Meeting of the CIM, vol. 63, pp. 595–599.

Hassanpour, J., Rostami, J. and Zhao, J. (2011). A new hard rock TBM performance prediction model for project planning. Tunnelling and Underground Space Technology Vol. 26 (2011), pp. 595-603.

Hassanpour, J., Rostami, J., Tarigh Azali, S. and Zhao, J. (2014). Introduction of an empirical TBM cutter wear prediction model for pyroclastic and mafic igneous rock; a case history of Karaj water conveyance tunnel, Iran. Tunnelling and Underground Space Technology Vol. 43 (2014), pp 222-231.

Hassanpour, J., Vanani, A.A.G., Rostami, J. and Cheshomi, A. (2016). Evaluation of common TBM performance prediction models based on field data from the second lot of Zagros water conveyance tunnel (ZWCT2). Tunnelling and Underground Space Technology Vol. 52 (2016), pp 147-156.

Hoek, E. and Brown, E.T. (1997). Practical estimates or rock mass strength. International Journal of Rock Mechanics & Mining Science & Geomechanics Abstracts. 34 (8), 1165-1186.

Hoek, E., Wood, D. and Shah, S. (1992). A modified Hoek-Brown criterion for jointed rock masses. In: Hudson J.A. (ed.) Proceedings of the rock mechanics symposium. International Society of Rock Mechanics Eurock' 92, British Geotechnical Society (1992), London, pp 209-214.

Howarth, D.F. (1981). The effect of jointed and fissured rock on performance of tunnel boring machines. In: Proceedings of the International Symposium on Weak Rock, Tokyo, Japan, September 1981, pp. 1069-1074.

Howarth, D.F. and Rowlands, J.C. (1987). Quantitative Assessment of Rock Texture and Correlation with Drillability and Strength Properties. Rock Mechanics and Rock Engineering Vol. 20 (1987) pp 57–85

Innaurato, N, Oggeri, C, Oreste, P.P. and Vinai, R. (2007). Experimental and Numerical Studies on Rock Breaking with TBM tools under high stress confinement. Rock Mechanics and Rock Engineering Vol. 40, no. 5 (2007), pp 429-451.

ISRM International Society for Rock Mechanics. (1978). Suggested methods for the quantitative description of discontinuities in rock masses. – Commission on Standardization of Laboratory and Field Tests, Document No. 4, International Journal of Rock Mechanics & Mining Science, Vol. 15 (1978), pp 319-368.

ISRM International Society for Rock Mechanics. (1979). Suggested method for determining the uniaxial compressive strength and deformability of rock materials. International Journal of Rock Mechanics & Mining Science, Vol. 15 (1979), pp 137-140.

ISRM International Society for Rock Mechanics. (1985). Suggested method for determining point load strength. – Commission on Testing methods, International Journal of Rock Mechanics, Mining Science & Geomechanics, Vol. 22 (1985), no. 2, pp 51-60.

ISRM International Society for Rock Mechanics. (2014). ISRM Suggested Method for Determining the Abrasivity of Rock by the CERCHAR Abrasivity Test. Rock Mechanics and Rock Engineering Vol. 47, no.1 (2014), pp 261-266.

Jakobsen, P.D., Langmaack, L., Dahl, F, and Breivik, T. (2013). Development of the Soft Ground Abrasion Tester (SGAT) to predict TBM tool wear, torque and thrust. Tunnelling and Underground Space Technology Vol. 38 (2013), pp 398-408.

Jakobsen, P.D. (2014). Estimation of Soft Ground Excavation Tool Life in TBM Tunnelling. PhD thesis. Norwegian University of Science and Technology (NTNU), Trondheim, Norway (2014).

Jeong, H-Y., Cho, J-W, Jeon, S. and Rostami, J. (2015). Performance Assessment of Hard Rock TBM and Rock Boreability Using Punch Penetration Test. Rock Mechanics and Rock Engineering Vol. 49, no. 4 (2015), pp 1517-1532.

Klug, H.P., and Alexander, L. (1974) X-ray diffraction procedures. 2nd edition. Wiley, New York (1974), 966 p.

Krogstad, D. (2013). Degradation mechanisms due to wear and corrosion interaction of cutter tools used in Tunnel Boring Machines. M.Sc. thesis, Norwegian University of Science and Technology (NTNU), Trondheim, Norway (2013).

Langnes A.S. (2012). Hard Rock Tunnel Boring and the effect of cutterhead rotation speed on penetration per revolution. Project work, Norwegian University of Science and Technology (NTNU), Trondheim, Norway (2012) (Unpublished).

Lindqvist, P.A. and Lai, H-H. (1983). Behaviour of the crushed zone in rock indentation. Rock Mechanics and Rock Engineering, Vol 16 (1983), pp 199–207.

Lislerud, A. (1997). Principles of Mechanical Excavation. Possiva report 97-12, Helsinki, Finland (1997). ISBN 951-652-037-5.

Log, S. (2010). The effects of using large cutter diameters in hard rock TBM tunneling. MSc thesis, Norwegian University of Science and Technology (NTNU), Trondheim, Norway (2010).

Log, S. (2016). Personal communication.

Løset, F. (1992). Support needs compared at the Svartisen road tunnel. Tunnels & Tunnelling, June 1992. UK: British Tunnelling Society.

Macias F.J. (2013). Project Research: Estimation of TBM Performance and Tool Life. PhD Research Project, NTNU (unpublished).

Macias, F.J., Jakobsen, P.D., Seo, Y, Bruland, A. and Grøv, E. (2014a). Rock Mass influence on Hard Rock TBM Performance Prediction. Proceedings of the World Tunnel Congress 2014 - Tunnels for a better Life, Foz do Iguazu, Brazil (2014).

Macias, F.J., Jakobsen, P.D., Bruland, A., Log, S. and Grøv, E. (2014b). The NTNU Prediction Model: A Tool for Planning and Risk Management in Hard Rock TBM Tunnelling. Proceedings of the World Tunnel Congress 2014 - Tunnels for a better Life, Foz do Iguazu, Brazil (2014).

Macias, F.J. and Bruland, A. (2014c). D&B versus TBM: Review of the parameters for a right choice of the excavation method. The 2014 ISRM European Rock Mechanics Symposium (Eurock 2014), Vigo, Spain (2014).

Macias, F.J., Jakobsen, P.D. and Bruland, A. (2014d). Rock mass variability and TBM prediction. The 2014 ISRM European Rock Mechanics Symposium (Eurock 2014), Vigo, Spain (2014).

Macias, F.J., Jakobsen, P.D., Seo, Y. and Bruland, A. (2014e). Influence of the rock mass fracturing on the net penetration rates of hard rock TBMs. Tunnelling and Underground Space Technology Vol. 44 (2014), pp 108-120.

Macias, F.J., Dahl, F.E. and Bruland, A. (2015a). New rock abrasivity test method by rolling disc. Proceedings of the 13th Congress on Rock Mechanics, ISRM Congress 2015 - In-novation in Applied and Theoretical Rock Mechanics, May 10-13, 2015, Palais des Congrès der Montréal, Canada, Paper 634, 10 p., ISBN: 978-1-926872-25-4 634.

Macias, F.J., Eide, L.N.R., Jakobsen, P.D., Jacobs, C. and Bruland, A. (2015b). Performance prediction of a hard rock TBM used in mining development. Proceedings, Rapid Excavation and Tunnelling Conference (RETC, 2015), New Orleans, USA (2015).

Macias, F.J., Wilfing, L., Andersson, T., Thuro, K. and Bruland, A. (2015c). Performance and cutter life assessments in hard rock tunnelling. EUROCK 2015 & 64th Geomechanics Colloquium. Schubert (ed.). Salzburg, Austria (2015).

Macias, F.J., Dahl, F.E. and Bruland, A. (2016). New rock abrasivity test method for tool life assessments on hard rock tunnel boring: The Rolling Indentation Abrasion Test (RIAT). Rock Mechanics and Rock Engineering, Vol. 49, no. 5 (2016), pp 1679-1693.

Marinos, V., Marinos, P. and Hoek, E. (2005). The geological strength index: applications and limitations. Bulletin of Engineering Geology and Environment, Vol. 64 (2005), pp. 55-65.

Marinos, P. and Hoek, E. (2000). GSI – A geologically friendly tool for rock mass strength estimation. In proceedings of the GeoEngineering 2000 Conference. Melbourne, Australia (2000).

Marinos, P. and Hoek, E. (2001). Estimating the geotechnical properties of heterogeneous rock masses such as flysch. Bulleting of Engineering Geology and the Environment, Vol. 60 (2001), pp 82-92.

Maidl, B., Schmid, L. and Herrenknecht, M. (2008). Hard rock Tunnel Boring Machines. Ernst & Sohn (2008), ISBN 978-3-433-01676-3.

NTH (1976). Hard Rock Tunnel Boring. Project report 1-76. Norwegian Institute Technology, Div. of Construction Engineering and Geology, Trondheim, Norway (1976) (In Norwegian).

NTH (1981). Hard Rock Tunnel Boring. Project report 1-81. Norwegian Institute Technology, Div. of Construction Engineering and Geology, Trondheim, Norway (1981) (In Norwegian).

NTH (1983). Hard Rock Tunnel Boring, Project Report 1-83. Norwegian Institute Technology, Div. of Construction Engineering, Trondheim, Norway (1983).

NTH (1988). Hard Rock Tunnel Boring, Project Report 1-88. Norwegian Institute Technology, Div. of Construction Engineering, Trondheim, Norway (1988).

NTH (1994). Hard Rock Tunnel Boring, Project Report 1-94. Norwegian Institute Technology, Div. of Construction Engineering, Trondheim, Norway (1994).

NTNU (2009). Fullprof software 2009. Norwegian University of Science and Technology (NTNU), Trondheim, Norway (2009).

Nærland, J. (2015). Failure mechanisms in cutter tools for tunnel boring. MSc thesis, Norwegian University of Science and Technology (NTNU), Trondheim, Norway (2005).

Palmström, A. (1995). RMi – a rock characterization system for rock engineering purposes. PhD thesis, University of Oslo (1995).

Paltrinieri, E., Sandrone, F., Zhao, J. (2016). Analysis and estimation of gripper TBM performances in highly fractured and faulted rocks. Tunnelling and Underground Space Technology Vol. 52 (2016), pp 44- 61.

Petrica, M., Badisch, E. and Peinsitt, T. (2013). Abrasive wear and their relation to rock properties. Wear, Vol. 308 (2013), pp 86-94.

Petrica, M., Painsi, M., Badisch, E. and Peinsit, T. (2014). Wear Mechanisms on Martensitic Steels Generated by Different Rock Types in Two-Body Conditions. Tribology Letters, Vol. 53, no. 3 (2014), pp 607-616.

Ratia, V., Heino, V., Valtonen, K., Vippola, M., Kemppainen, A., Siitonen, P. and Kuokkala, V-T. (2014). Effect of abrasive properties on the high-stress three-body abrasion of steels and hard metals. Finnish Journal of Tribology, Vol 32 (2014), pp 3-18.

Ribachi, R. and Lembo-Fazio, A. (2005). Influence of Rock Mass Parameters on the Performance of a TBM in a Gneissic Formation (Varzo Tunnel). Rock Mechanics and Rock Engineering, Vol. 38, no. 2 (2005), pp 105-127.

Roby, J, Sandell, T, Kocab, J and Lindbergh, L (2009). The Current State of Disc Cutter Design and Development Directions. Mining Engineering, Vol. 61, no.3 (2009), pp 36-45.

Rostami, J. and Ozdemir, L. (1993). A new model for performance prediction of hard rock TBMs. Proceedings, rapid Excavation and Tunnelling Conference (RETC 1993), Boston, Massachusetts, USA (1993), pp 793-809.

Rostami, J. (1997). Development of a force estimation model for rock fragmentation with disc cutters through theoretical modelling and physical measurement of crushed zone pressure, PhD Thesis. Colorado School of Mines, Golden, Colorado, USA (1997).

Rostami, J. (2008). Hard Rock TBM Cutterhead Modeling for Design and Performance Prediction. Geomechanics and Tunnelling Vol. 1, no. 1 (2008), pp 18-28.

Salminen, P. and Viitala, R. (1985). Rock Drillability Study. Helsinki University of Technology, Department of Mining and Metallurgy. Laboratory of Mining Engineering. ISBN 951-753-591-0.

Sanio, H.P. (1985). Prediction of the performance of disc cutters in anisotropic rock. International Journal of Rock Mechanics and Mining Sciences & Geomechanics Abstracts, Vol. 22 no. 3 (1985), pp 153-161.

SINTEF (2013). Test Reports, SINTEF, Trondheim, Norway (confidential).

SINTEF (2014). Test Reports, SINTEF, Trondheim, Norway (confidential).

SINTEF (2015). Test Reports, SINTEF, Trondheim, Norway (confidential).

SINTEF (2016). Test Reports, SINTEF, Trondheim, Norway (confidential).

Schneider, E., Thuro, K. and Galler, R. (2012). Forecasting penetration and wear for TBM drives in hard rock – Results from the ABROCK research project. Geomechanics and Tunnelling, Vol. 5 (2012), pp 537-546.

Seo, Y. (2016). Personal communication.

Shanahan, A. (2010). Cutter Instrumentation System for Tunnel Boring Machines. Proceedings of the North American Tunneling Conference (2010), pp 110-115.

Singh, B. and Goel, R.K. (2011). Engineering Rock Mass Classification. Elsevier Inc (2011). ISBN 978-0-12-385878-8.

Smading, S. (2016). Personal communication.

Stachowiak, G.W. and Batchelor, A.W. (2005). Engineering tribology, 3rd edition. Butterworth-Heinemann, Burlington (2005).

Steingrimsson, J.H., Grøv, E. and Nilsen, B. (2002). The significance of mixed-face conditions for TBM performance. World Tunnelling, Vol. 9 (2002), pp 435–441.

Thuro, K. (1997). Prediction of drillability in hard rock tunnelling by drilling and blasting. Tunnels for People, Golser, Hinkel & Schubert eds. (1997), pp 103-108.

Thuro, K., Singer, J., Käsling, H. and Bauer, M. (2007). Determining abrasivity with the LCPC Test. In E. Eberhardt, D. Stead & T. Morrison (eds.). Proceedings of the 1st Canada – U.S. Rock Mechanics Symposium, Vancouver B.C., London: Taylor & Francis (2007).

Thuro, K. and Käsling, H. (2009). Classification of the abrasiveness of soil and rock. Geomechanics and Tunnelling, Vol. 2 (2009), pp 179-188.

Toth, A., Gong, Q. and Zhao, J (2013). Case studies of TBM tunnelling performance in rock-soil interface mixed ground. Tunnelling and Underground Space Technology Vol. 38 (2013), pp. 140-150.

Uddeholm "Uddeholm Orvar Supreme" September 2015 (on line)
http://www.uddeholm.com/files/PB_orvar_supreme_english.pdf

Valantin, A. (1974). Description des tests CERCHAR, "Durete et abrasivite des roches". Travaux Publics 167, N 322, pp 88-92. November 1974 (in French).

Valestrand, A.J. and Langnes, A.S. (2013). Anti Abrasive for Hard Rock TBM Tunnelling. MSc thesis, Norwegian University of Science and Technology (NTNU), Trondheim, Norway (2013).

Vassenden, S. (2016). Personal communication.

Verhoef, P.N.W. (1997). Wear of rock cutting tools. A.A. Balkema, Rotterdam (1997). ISBN 90 5410 434 1.

Wanner, H. and Aeberli, U. (1979). Tunnelling machine performance in jointed rock. In 4th Congress of the International Society for Rock Mechanics, Montreux, Switzerland, September 197, Vol 1, pp 573-580.

West, G. (1989). Rock Abrasiveness Testing for Tunnelling, Technical Note. International Journal of Rock Mechanics, Mining Science & Geomechanics Abstracts Vol. 26, no. 2. (1989), pp. 151-160.

Wilfing, L, Käsling, H, Thuro, K (2015a). Towards a Uniform Definition of Rock Toughness for Penetration Prediction in TBM tunneling. Engineering Geology for Society and Territory – Volume 6: 469 – 473.

Wilfing, L., Käsling, H. and Thuro, K (2015b). Improvement of penetration prediction in TBM-tunneling by performing on-site penetration tests. Proceedings of the 13th Congress on Rock Mechanics, ISRM Congress 2015 - In-novation in Applied and Theoretical Rock Mechanics, May 10-13, 2015, Palais des Congrès der Montréal, Canada, Paper 618, 10 p., ISBN: 978-1-926872-25-4.

Wilfing, L. (2016). The Influence of Geotechnical Parameters on penetration Prediction in TBM Tunneling in Hard Rock. PhD Thesis, Technical University of Munich, Munich, Germany (2016).

Wittke, W. (2014). Rock Mechanics Based on an Anisotropic Jointed Rock Model. Wiley Ernst & Sohn (2014). ISBN: 978-3-433-03079-0.

Yagiz, S. (2002). Development of rock fracture and brittleness indices to quantity the effects of rock mass features and toughness in the CSM model basic penetration for hard rock tunneling machines. PhD thesis, Colorado School of Mines, Golden, USA (2002).

Yagiz, S. (2009). Assessment of brittleness using rock strength and density with punch penetration test. Tunnelling and Underground Space Technology, Vol. 24 (2009), pp 66-74.

Yagiz, S. and Karahan, H. (2011). Prediction of hard rock TBM penetration rate using particle swarm optimization. International Journal of Rock Mechanics & Mining Sciences Vol. 48 (2011), pp 427-433.

Yagiz, S. (2014). Modified CSM model for predicting TBM performance in rock mass. LAP (Lambert Academic Publishing), 2014.

Yin, L.J., Gong, Q.M. and Zhao, J. (2014). Study of rock mass boreability by TBM penetration test under different in situ stress conditions. Tunnelling and Underground Space Technology Vol. 43 (2014), pp 413- 425.

Zhao, Z., Gong, Q.M., Zhang, T. and Zhao, J. (2007). Prediction model of tunnel boring machine performance by ensemble neural networks. Geomechanics and Geoengineering: An International Journal, Vol. 2, no.2 (2007), pp 123–128.

Part II: Published papers

Title:

Influence of the rock mass fracturing on the net penetration rates of hard rock TBMs

Paper I

Authors:

Macias, Francisco Javier

Jakobsen, Pål Drevland

Seo, Yongbeom

Bruland, Amund

Published on:

Tunnelling and Underground Space Technology Vol. 44 (2014), pp 108-120

Tunnelling and Underground Space Technology 44 (2014) 108–120

Contents lists available at ScienceDirect

Tunnelling and Underground Space Technology

journal homepage: www.elsevier.com/locate/tust

Influence of rock mass fracturing on the net penetration rates of hard rock TBMs

F.J. Macias *, P.D. Jakobsen, Y. Seo, A. Bruland

Department of Civil and Transport Engineering, NTNU, Trondheim, Norway

ARTICLE INFO

Article history:
Received 31 January 2014
Received in revised form 10 July 2014
Accepted 17 July 2014

Keywords:
Hard rock TBMs
Net penetration rate
Rock mass boreability
Rock mass fracturing factor (k_s)
NTNU prediction model

ABSTRACT

Penetration rates during excavation using hard rock tunnel boring machines (TBMs) are significantly influenced by the degree of fracturing of the rock mass. In the NTNU prediction model for hard rock TBM performance and costs, the rock mass fracturing factor (k_s) is used to include the influence of rock mass fractures. The rock mass fracturing factor depends on the degree of fracturing, fracture type, fracture spacing, and the angle between fracture systems and the tunnel axis. In order to validate the relationship between the degree of fracturing and the net penetration rate of hard rock TBMs, field work has been carried out, consisting of geological back-mapping and analysis of performance data from a TBM tunnel. The rock mass influence on hard rock TBM performance prediction is taken into account in the NTNU model. Different correlations between net penetration rate and the fracturing factor (k_s) have been identified for a variety of k_s values.

1. Introduction

The prediction of construction time and costs is important in the selection of excavation method and the planning and risk management of tunnelling projects. Good prediction facilitates the control of risk and enables delays and budget overruns to be avoided.

In the case of hard rock TBM projects, net penetration rate (m/h) is an important factor used to estimate advance rates, cutter life and excavation costs. The main influences on net penetration rate are intact rock properties, rock mass properties, and machine parameters.

Many studies have examined the influence of geological parameters on tunnel boring machine (TBM) performances (Wanner and Aeberli (1979), Howarth (1981), Lindqvist and Lai (1983), Sanio (1985), Zhao et al. (2007), Bruland (1998), Barton (2000), Ribacchi and Lembo-Fazio (2005), Gong et al. (2005, 2006), Bieniawski von Preinl et al. (2006) Yagiz (2009), Yagiz et al. (2010), Hassanpour et al. (2009, 2010, 2011), Bejari and Khademi (2012), Farrokh et al. (2012).

Wanner and Aeberli (1979) considered in their studies the joint frequency which is determined by the total joint area per unit volume of excavated rock. It was found by field observation that only joints produced by shear stresses influence significantly the specific TBM penetration. Howarth (1981) performed an experimental work concluding that moderately fractured rock can improve the TBM performances. Lindqvist and Lai (1983) indicated by laboratory experiments the influence of the intact rock properties. Sanio et al. (1985) considered and studied the importance of the anisotropy in addition to the discontinuities. Zhao et al. (2007) developed an ensemble neural network to establish a relationship between the specific rock mass boreability index (SRMBI) and four influential rock mass properties: rock compressive strength, rock brittleness, joint spacing and joint orientation. Ribacchi and Lembo-Fazio (2005) performed an analysis of excavation data from a TBM project in a gneiss formation. It was found out the influence of rock quality on TBM performances. It is indicated that for a given type of rock, fracture spacing has a predominant influence. Gong et al. (2005, 2006) studied numerical modelling of joint spacing and orientation getting good agreement with field investigation in the results.

The influence of both, intact rock properties and rock mass parameters, have a great importance on the TBM prediction models developed by Bruland (1998), Barton (2000), Bieniawski von Preinl et al. (2006) and Delisio et al. (2013). Hassanpour et al. (2010, 2011) and Farrokh et al. (2012) analysed some TBM prediction models in several TBM projects considering the rock geological influence on the performance predictions.

The main purpose of the present research is to find an appropriate tool to enable an assessment of the influence of the rock mass conditions on the penetration rate of hard rock TBMs.

As part of the NTNU prediction model for hard rock TBMs, the rock mass fracturing factor (k_s) has been developed as a means of

* Corresponding author. Tel.: +47 735 94 626.
E-mail address: Javier.macias@ntnu.no (F.J. Macias).

http://dx.doi.org/10.1016/j.tust.2014.07.009
0886-7798/

representing the simultaneous effect of the degree of fracturing (fracture type and spacing) and the angle between the tunnel axis and the rock mass' planes of weakness using a single coefficient. The rock mass fracturing factor is the most important rock mass parameter currently used in tunnel boring (Bruland, 1998).

The rock mass fracturing factor (k_s) represents rock mass boreability. Higher values imply greater boreability during hard rock TBM excavation. Throughout this paper, the term rock mass boreability refers to rock mass resistance to boring, while the term drillability, or intact rock boreability, refers to intact rock resistance to boring (as tested at the laboratory).

In order to assess rock mass fracturing (k_s) as an appropriate tool for the empirical evaluation of the net penetration rate of hard rock TBMs, field work involving geological engineering back-mapping and TBM log data analysis, recorded along selected sections amounting to a total length of 1200 m, was carried out. The EIDI2 Tunnel project in Faroe Islands was chosen for this study, since it provides satisfactory research conditions.

The present research validates the influence of rock mass fracturing, as expressed by the fracturing factor (k_s), on penetration rates for hard rock TBMs. The fracturing factor (k_s) is shown to be an ideal tool for evaluating the influence of rock mass fracturing, and is thus a good indicator of rock mass boreability during hard rock TBM tunnelling.

2. Rock mass boreability

Boreability can be defined as the resistance (in terms of ease or difficulty) encountered by a TBM as it penetrates a rock mass composed of intact rock and planes of weakness (Bruland, 1998).

The penetration rate is influenced by intact rock and the properties of the rock mass. Intact rock properties are typically defined in terms of rock petrography, abrasivity, porosity, schistosity and strength.

The NTNU/SINTEF laboratory method is used extensively in major international TBM projects to determine drillability or intact rock boreability in hard rock (Dahl et al., 2012).

The Drilling Rate Index™ (DRI) has been selected as the drillability parameter of intact rock. It is an indirect measure of the breaking work required, and an effective gauge of the rock-breaking process under a cutter.

The main rock mass boreability parameters are type, degree of fracturing, and orientation of the fracture system(s). In addition, in situ rock stress, groundwater and other factors may influence the net penetration rate.

The planes of weakness or discontinuities in the rock mass contribute considerably to the net penetration rate. Rock mass fracturing is characterised by the degree of fracturing and the angle between the tunnel axis and the plane of weakness.

Rock mass fracturing is found to be the geological factor applying the greatest influence on net penetration rate, and thus it has a major influence on tunnelling costs in hard rock (Bruland, 1998). High rock mass fracturing means greater rock mass boreability during hard rock TBM excavation.

Increases in net penetration rate due to higher degree of fracturing also influence operation of the TBM, e.g., by the operator's control of thrust and cutter head rotation speed. Very high degrees of fracturing should result in a higher net penetration rate. However, in many cases it is necessary to reduce thrust and cutter head rotation on the TBM in order to optimise mucking out, prolong tool life, and avoid damage to the machine. It is important to mention that not all TBMs have RPM control.

In order to characterise the rock mass during tunnelling projects, several rock mass classification systems have been developed. Table 1 illustrates the most commonly used systems.

More recently, Rock Mass Rating (RMR) and the Rock Tunnelling Quality Index (Q) have also been applied to predict net penetration rates. An evaluation of these predictive models is beyond the scope of the present research.

Many of the rock mass classification systems take rock properties (intact rock and rock mass properties) into account. For this reason, they are not regarded as appropriate for an evaluation of the influence of rock mass fracturing on net penetration rates using hard rock TBMs. Only the RQD system and fracturing factor (k_s) were considered for the purposes of the present research.

The RQD (Rock Quality Designation) method is used to determine the percentage of intact rock fragments longer than 100 mm (4 in.) recovered in a core.

The rock mass fracturing factor (k_s), introduced by Bruland (1998), considers the simultaneous influence of the degree of fracturing and the orientation of the plane of weakness.

The RQD may not be appropriate for determining rock mass fracturing because it does not consider factors such as the average discontinuity spacing, fracture orientation, or the number of fracture sets present. Consequently, the rock mass fracturing factor (k_s) was chosen as a more suitable rock mass classification index.

A description of planes of weakness includes:

- *Type:* joints, fissures, or so-called "Marked Single Joints".
- Joint or fissure spacing.
- Orientation in relation to the tunnel axis.

The basic features of the different types of planes of weakness are as follows:

- *Joints:* Continuous fractures that can be followed all around the tunnel profile.
- *Fissures:* Non-continuous joints or fractures that can only partly be followed around the tunnel profile such as (a) filled joints exhibiting low strength, (b) foliation, and (c) bedding plane fissures.
- *Marked Single Joints (MSJ):* Highly distinctive discontinuities. These may be entirely open, may conduct water or may be filled with clay. Minor faults filled with gouge may be classified as single joints.

Joints and fissures occur systematically in a fractured rock mass. For practical purposes, the degree of fracturing is divided into classes which are determined on the basis of the type of planes of weakness encountered, and the spacing between them. Table 2 presents a summary of the fracture class ranges.

Table 2 was modified in order to achieve a higher level of detail and better accuracy for the k_s estimation.

Subdivisions of the classes shown in Table 2 may be added for practical mapping purposes, or as dictated by the characteristics of the rock mass.

In a typical tunnel, the rock mass fracturing factor is rarely constant over long stretches. Spacing between the planes of weakness is measured perpendicularly to the planes, and is expressed as an average over a given distance. In our study, the average distance employed is 5 m.

Table 1
Commonly used rock mass classification systems in tunnelling projects.

Rock mass classification	Author	Year
Rock Quality Designation (RQD)	D.U. Deere	1964
Rock Mass Rating (RMR)	Z.T. Bieniawki	1973
Rock Tunnelling Quality Index (Q)	N. Barton, R. Lien and J. Lunde	1974
Rock Mass Index (RMi)	A. Palmstrom	1995
Geological Strength Index (GSI)	E. Hoek and E.T. Brown	1997
Degree of fracturing (k_s factor)	A. Bruland	1998

Table 2
Fracture class as defined by the spacing between planes of weakness (modified from Bruland (1998)).

Fracture class (joints/fissures)	Average spacing between the planes of weakness a_f (cm)	Range class (cm)
0	∞	240–∞
0+	190	160–240
0–I	140	110–160
I–	90	60–110
I	40	37.5–60
I+	35	32.5–37.5
I–II	30	27.5–32.5
II–	25	22.5–27.5
II	20	17.5–22.5
II–III	15	12.5–17.5
III	10	8.75–12.5
III–IV	7.5	6.25–8.75
IV	5	4–6.25

In situations where it is difficult to distinguish between planes of weakness and the structure of intact rock (e.g., schistosity), it is important not to include the effect twice.

Marked Single Joints are distinctive discontinuities observed in the rock mass, and are thus recorded individually. They occur as isolated phenomena at tunnel level, although on a larger scale they may belong to a systematic set of joints.

Locally, Marked Single Joints may result in very high net penetration rates. However, due to the risk of stability problems and cutter/cutter head damage, their influence should be evaluated with care (Bruland, 1998).

In the NTNU prediction model, the angle between the tunnel axis and the planes of weakness is calculated using the following equation:

$$\alpha = \arcsin(\sin\alpha_f \cdot \sin(\alpha_t - \alpha_s)) \tag{1}$$

where α_s is the strike angle of the planes of weakness, α_f is the dip angle of the planes of weakness, and α_t is the azimuth of the tunnel axis (see Fig. 1).

The fracture factor (k_{si}) for each section is calculated using the plots in Fig. 2.

The curves in Fig. 2 suggest that with increased spacing between the joints or fissures, there will be an optimum angle between the tunnel axis and the planes of weakness. The angle providing the highest fracturing factor (k_s) is about 60°. This is explained by the presence (or absence) of joints or fissures at the rock face as illustrated in Fig. 3.

When the spacing between the planes of weakness is very low, such as in fissure class IV, the maximum fracturing factor occurs at 90°. For this case, the radial cracks from under the cutter will reach a weakness plane (see Fig. 4) and the fracturing factor k_s will increase until an angle of 90°.

It is possible that both joints and fissures will be recorded within the same section being mapped. In such cases, the dominant fracture class should be chosen. In cases where no clear dominance of Joints or fissures is recorded, an interpolation between the two fracture types must be made in the graph of Fig. 2 using the *Y*-axis.

Excavation using TBMs involves a geological risk which requires careful analysis. In high quality rock masses containing few or no fractures, the risk to achieve accurate performance predictions takes on a greater importance. Thus, in the case of low fracture classes (0, I, II), a detailed determination of fracture class is essential. This analysis will enable us to determine if the intact rock or rock mass properties control the boring process. Fig. 5 shows the interpolated curves used for such detailed analysis. The interpolated curves are found by linear interpolation between the given curves.

Once k_{si} has been obtained for each section, a total (weighted) average is calculated using the following equation (Bruland, 1998):

$$k_{s\text{-}avg} = \frac{\sum_{i=1}^{n} l_i}{\sum_{i=1}^{n} \frac{l_i}{k_{s\text{-}i}}} \tag{2}$$

where l_i is the tunnel length for fracturing class "*i*" along the mapped section and $k_{s\text{-}i}$ is the k_s factor for fracturing class "*i*" along the mapped section.

It is essential to obtain $k_{s\text{-}avg}$ in the form of a weighted average in order to provide a realistic average value in relation to section length.

In situations where more than one set of planes of weakness are recorded, the total fracturing factor is calculated using equation below (Bruland, 1998):

$$k_{s\text{-}avg} = \sum_{i=1}^{n} k_{si} - (n-1)\cdot 0.36 \tag{3}$$

where k_{si} is the fracturing factor for a set of planes of weakness number "*i*" and n is the number of fracture sets.

In situations where it is difficult to separate rock mass fracturing into sets, an average spacing and average angle for total rock mass fracturing should be calculated.

3. A practical approach to geological back-mapping for hard rock TBMs

The engineering geological back-mapping of a TBM-bored tunnel consists of the following steps:

- Determination of rock type.
- Identification of the strike and dip of Marked Single Joints.
- Notes on other singular phenomena such as intrusions, mixed face, water, and rock support.
- Determination of the number of fracture systems and type of fracturing (joints or fissures) for each system.
- Measurement of the strike (α_s) and dip (α_f) of the fracture system(s).
- Measurement of the strike (azimuth) of the tunnel (α_t).

Rock sampling should also be carried out to enable the laboratory testing of drillability properties.

Geological back-mapping establishes a geological model of the tunnel that can be used for the evaluation of TBM performance, cutter life, and machine utilisation.

According to Bruland (1998), measurements made should represent the average of the sections in question. If changes in rock type or other factors so dictate, sections may be subdivided for measurement purposes.

Section volume may be evaluated in order to obtain a representative view. However, in order to ensure that the rock mass being measured is representative of the global situation, the degree of fracturing should be measured using a scanline along one of the tunnel walls.

The individual re-mapping of selected subsections (20–30 m in length, at 150–200 m intervals) should be carried out when mapping of the total tunnel section is completed.

Prior to mapping of a new tunnel section it is important to check and evaluate the map of the previous 30–50 m section. This will ensure that individual mapping is adapted to on-site geology.

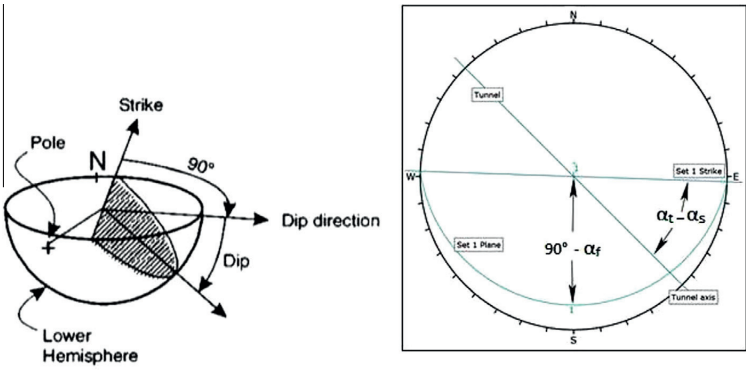

Fig. 1. Basic terms of stereographic projection and stereonet illustrating the angles used in Eq. (1).

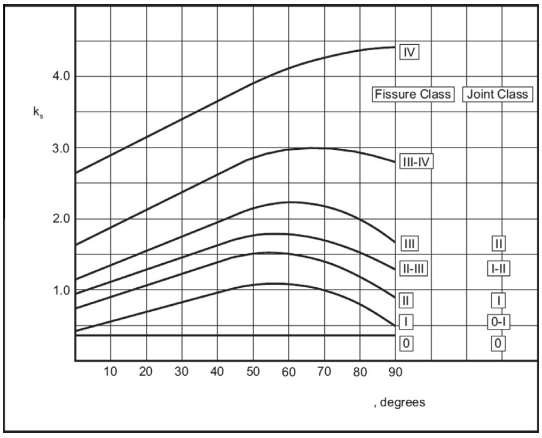

Fig. 2. Graph used to calculate the fracturing factor (k_s) on the basis of fracture class and the angle between the tunnel axis and the plane of weakness. From Bruland (1998).

4. Field data

A major part of the research presented in this paper is TBM performance data analysis, together with geological back-mapping. The geological back-mapping was carried out along 240 sections of the Eidi II Tunnel. The total length of tunnel from which data were obtained is 1200 m.

TBM performance studies have many purposes. These include the improvement of on-site tunnel boring operations, feedback to the planning process and, in some cases, knowledge and expertise enhancement promoting the development of TBM technology.

4.1. EIDI 2 tunnel project

The EIDI 2 tunnel is part of a hydropower project in the Faroe Islands. It was selected for the present research because of its wide range of degree of rock mass fracturing, the homogeneous nature of the lithologies present, and its relative ease of mapping due to the open gripper TBM used for excavation. A view of the tunnel portal is shown in Fig. 6.

The geology along the 8 km tunnel drive consists of basalt and a sill. The sill is an intrusive body that commonly occurs in joints and voids within the basalt. In some sections of the tunnel, the sill encompasses the entire tunnel diameter. It comprises relatively homogenous, coarse-grained and unweathered rock containing no pores. Mapping revealed that the transition between the basalt and the sill was pronounced. The intact rock is defined as hard, with uniaxial compressive strength values in the range 120–250 MPa.

A complete drillability testing was performed in Engineering Geology Laboratory at NTNU/SINTEF according to Dahl et al. (2012).

Table 3 shows the NTNU/SINTEF drillability parameters values, DRI™ and CLI™ values of a total of 11 samples tested along the studied section.

Table 4 shows the rocks' NTNU/SINTEF drillability parameters DRI™ and CLI™.

Table 4 shows that there is a significant difference in the DRI™ values of the sill and basalt. According to Dahl et al. (2012), a sill is classified as a rock exhibiting a "low" drilling rate (meaning low boreability). Basalt is classified as having a "high" drilling rate

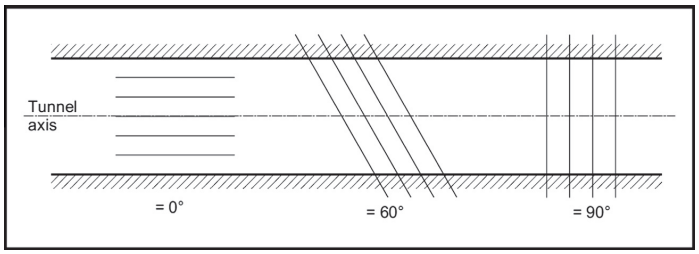

Fig. 3. Influence of systematically occurring fissures or joints at various angles to the tunnel axis, Bruland (1998).

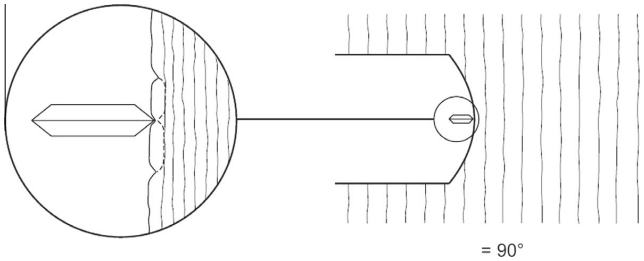

Fig. 4. Chipping pattern for boring in systematically fractured rock with low space between planes of weakness (e.g., class IV) and angle of 90°, Bruland (1998).

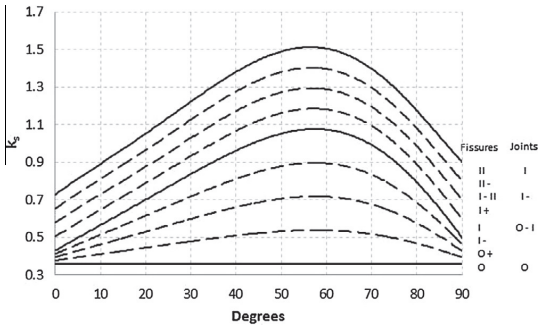

Fig. 5. Detailed graph for calculating low values of the fracturing factor (k_s).

(meaning high boreability – a rock exhibiting relatively little resistance to boring).

The TBM used in this project is a main beam (open gripper) Robbins High Performance TBM (HP) with a cutter head diameter of 3.4 m and a maximum thrust of 6387 kN. The cutter head has not RPM control and it is fixed at a constant rate of 12.8. Table 5 lists the main characteristics of the TBM. The fixed RPM value eliminates this factor as a variable during data collection.

A TBM with constant RPM removes the influence of one variable in subsequent analytical work, and this was an important factor in selecting this particular project for the present research.

4.2. Geological back-mapping

A complete geological back-mapping was performed along a total length of 1200 m, subdivided into 5 m sections. The selection of the sections was carried out with the aim of including the maximum possible range of fracture classes and penetration rates.

Geological mapping is in part a subjective activity and mapping quality is improved using a team of at least two persons. In this study, mapping was carried out by a team of three engineers working individually on pre-defined sections selected on the basis of providing the largest possible range of geological conditions. The average values obtained by the geological back-mapping team will be used in subsequent analyses.

Marked Single Joints are not considered in the present study since none were recorded in the sections studied.

Fig. 7 shows an example of the geological back-mapping carried out for this study.

Fig. 8 shows the fracture spacing (joints and fissures) for the 5 m sections measured along the 1200 m of tunnel.

The range of average fracture spacing values in the mapped section is wide enough to provide data for a complete analysis for research purposes. The total weighted average for the mapped section is 82 cm, and the section is classified as fracture class "I–" (ref. Table 2).

Using the RQD method, a plot along the section would show an almost horizontal line with a value close to or at 100%. Such a plot would provide an inadequate description of the degree of fracturing.

Fig. 9 shows the complete fracture class distribution (in percentages) for the total length of the mapped section.

The angle between the fractures sets and the tunnel axis along the mapped sections is shown in Fig. 10. The weighted average is 42°, with values ranging from 11° to 72°.

The fracture class (defining fracture type), combined with the angle between the tunnel axis and the planes of weakness, determines the fracturing factor (k_s). Fig. 11 shows the fracturing factor calculated at every 5 m along the total number of mapped sections.

Fig. 12 is a histogram showing rock mass fracturing factor frequency along the 1200 m tunnel section.

The total weighted average of the fracturing factor (k_s) along the 1200 m section is 1.04, with values ranging from 0.46 to 4.06.

Fig. 11 demonstrates that there are several outlier values of k_s recorded in the 5 m sections. These are due to a combination of factors both favourable (high k_s) and unfavourable (low k_s) to rock mass boreability.

Fig. 13 shows photographs of tunnel sections exhibiting high and low k_s values.

4.3. TBM field performance data

In the present study, performance data is taken from tunnel boring reports recorded during each shift. The TBM is not equipped with a continuous data logger which means that measured performance and machine parameters represent average values for each stroke length. The data thus relate to the number of metres excavated, which is not constant for every stroke (1550 mm).

Data acquired from these reports includes; (1) boring time, (2) boring length, and (3) cutter head thrust for different working periods. The average net penetration rate (m/h) and average thrust (kN/cutter) are also calculated.

The average penetration rate is calculated as a weighted average of data recorded during the total number of machine hours used to bore the tunnel length in question (Eq. (4)),

$$I_m = \frac{\sum_i^n l_i}{\sum_i^n T_{ni}} = \frac{\sum_{i=1}^n l_i}{\sum_{i=1}^n \frac{l_i}{I_{ni}}} \tag{4}$$

where I_m is the average net penetration rate (m/h), I_{ni} is the net penetration rate for section i (m/h), l_i is the length of the section i (m), and T_{ni} is the machine time used to bore section i (hours).

The net penetration rate and average thrust are calculated as weighted averages. Applied thrust values will vary. For the present study, the parameter "gross thrust" is the gross thrust force from the thrust or propel cylinders, including friction or drag of the

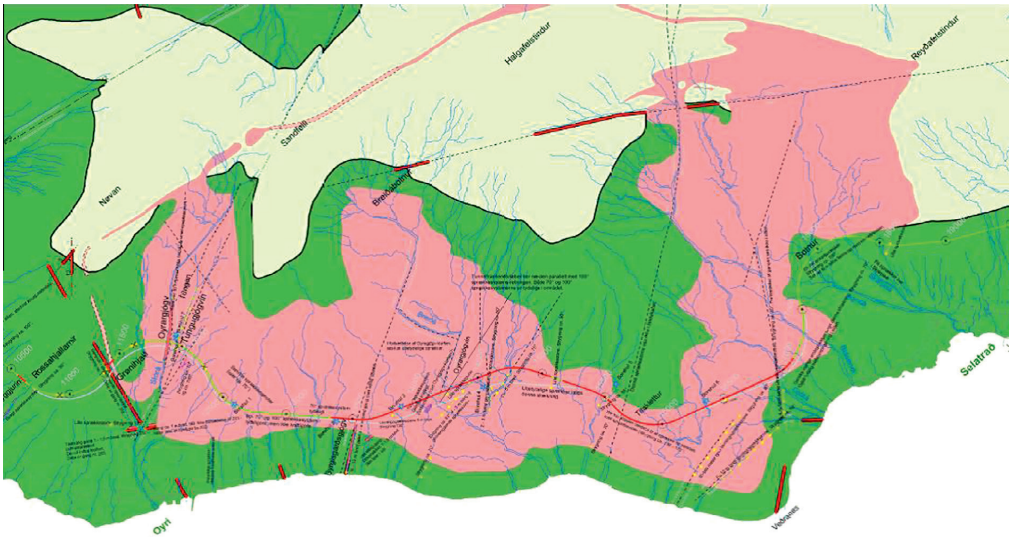

Fig. 6. Geological and tunnel profile of the EIDI 2 hydropower tunnel in the Faroe Islands.

Table 3
Drillability testing results.

Sample	Rock type	DRI™	CLI™	Q (%)
1	Basalt	58	35	0
2	Basalt	69	47	0
3	Sill (fine grained)	43	16	0
4	Hard sill	42	13	2
5	Sill	37	14	1
6	Sill	36	14	0
7	Sill	33	8.8	1
8	Sill	42	18	0
9	Sill (coarse grains)	34	18	0
10	Sill	43	14.4	0
11	Sill (coarse grains)	35	16.4	2

Table 4
Rock type drillability results.

	Sill	Basalt
DRI™	38	64
CLI™	15	41
Quartz content (%)	1	0

cutter head and the cutter head support system and other losses of thrust (Bruland, 1998).

Table 6 shows the key values obtained for net penetration rate and thrust.

The values of net penetration rate and thrust are not directly related to each other, i.e., maximum net penetration values are not the direct result of maximum thrust, but are isolated values achieved during excavation.

4.4. Field penetration test

Penetration tests are commonly used to obtain data on the boring process. The main purpose of such tests is to evaluate machine performance under given geological conditions (Bruland, 1998).

Table 5
Main characteristics of the TBM.

Parameter	Value
TBM diameter	3.4 m
Number of cutters	27
Cutter diameter	432 mm
Maximum cutter head thrust	6387 kN
Cutter head power	671.13 kW
RPM	12.8
Cutter head torque	42,375 N m
Boring stroke	1550 mm
Maximum system pressure	331 bar

The penetration test involves a measurement of penetration over a given time at various thrust levels and constant RPM. The penetration test includes five thrust levels (Palm, 2011).

The penetration is measured in mm over a time given. This time correspond to approximately 30 revolutions of the cutter head at each thrust level.

Table 7 shows the data given from the test performed.

The result is a penetration curve derived from manipulating recorded data as shown in the following equation:

$$i_0 = \left(\frac{M_t}{M_1}\right)^b \tag{5}$$

where i_0 is the basic penetration rate (mm/rev), M_t is the gross average thrust at each thrust level (kN/cutter), M_1 is the critical thrust required to achieve a penetration of 1 mm/rev (kN/cutter), and b is the penetration coefficient.

M_1 and b are found by linear regression of the $\log_{10}$ values of the thrust and penetration (Bruland, 1998).

Fig. 14 plots the $\log_{10}$ values of M_1 and i_0 for the penetration test including the linear regression curve. The test was performed on site with geology defined by a fracturing factor (k_s) equal to 1.2.

A good fitting by linear regression is found as is shown in Fig. 14. This good fitting is in accordance with Bruland (1998).

The equation obtained from the linear regression of the $\log_{10}$ data results obtained in Fig. 14 is theoretically presented following:

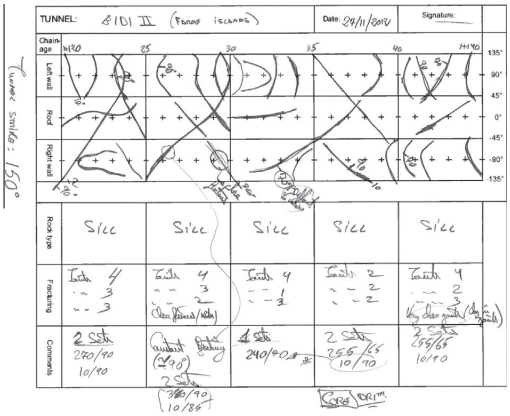

Fig. 7. Example of a geological back-mapping sheet.

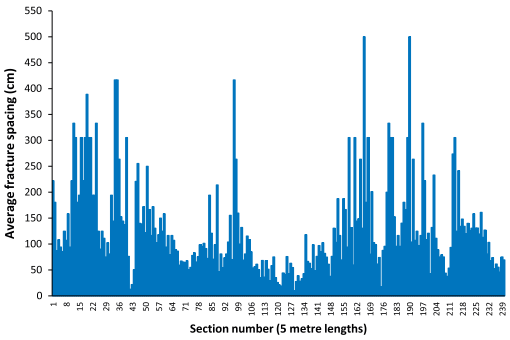

Fig. 8. Spacing of fractures along the mapped sections.

$$\log_{10}(i_0) = A_R \cdot \log_{10}(M_t) + B_R \quad (6)$$

where A_R is a regression constant and B_R is a regression constant.

For the penetration test performed, the regression constants (A_R and B_R) values are 2.63 and −5.42 respectively.

Since M_1 is the critical thrust for a penetration of 1.0 mm/rev, M_1 is found by solving Eq. (6) for $i_0 = 1$ mm/rev ($\log_{10}(1) = 0$). Eq. (7) is the result:

$$M_1 = 10^{-\frac{B_R}{A_R}} \quad (7)$$

Hence, the critical thrust value for the test performed is 114.2 MPa.

B is the slope of the linear regression shown in Fig. 14:

$$b = A_R \quad (8)$$

For the present penetration test the value the parameter b is 2.63.

4.5. Mixed face

The mixed face phenomenon describes a tunnel face exhibiting significant variation in rock boreability properties. Mixed face conditions are very difficult to categorise due to the wide range of lithologies and other factors that may be encountered.

According to Steingrimsson et al. (2002), mixed face conditions influence machine design, tunnelling layout, actual penetration rate, machine utilisation, and cutter life. The same authors also proposed a correction factor for use under mixed face conditions.

In projects where mixed face conditions are anticipated, a detailed study based on case-specific data must be carried out prior to tunnelling in order to pre-empt potential subsequent disputes.

Mixed face conditions were encountered in the first 270 m of the tunnel length mapped during this study. The sill lithology and basalt differ in terms of rock boreability, resulting in complex progression of the boring process. The mixed face consists of basalt intrusions within a confining sill and is illustrated in Fig. 16.

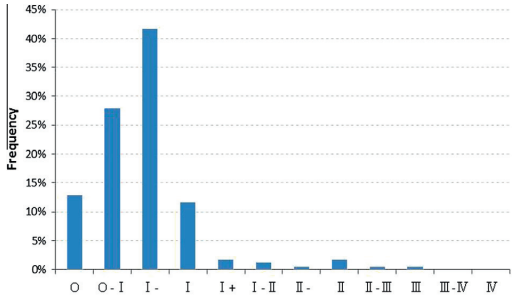

Fig. 9. The distribution of the rock mass fracturing classes along the 1200 m tunnel.

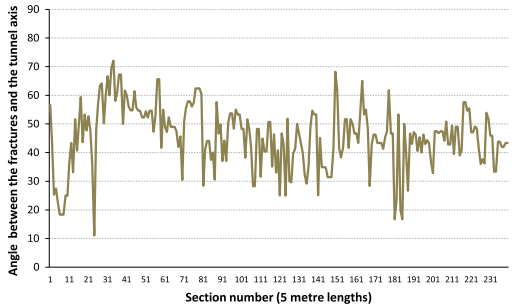

Fig. 10. Angle between the fracture sets and the tunnel axis along the mapped sections.

5. Analysis and discussion of the field data

The present study shows a clear relationship between the fracture factor (k_s) and net penetration rate to the extent that high k_s values indicate a higher penetration rate. It is important here to distinguish the section where mixed face (sill and basalt) conditions were encountered, i.e., along the previously described first 270 m of the tunnel length.

The relationship between the fracture factor (k_s) and net penetration rate is shown in Fig. 17. High fracture factor (k_s) values indicate easier rock mass boreability because fracture spacing and the angle between the fracture systems and tunnel axis are more favourable to boring.

The relationship between the fracturing factor and the net penetration rate is regarded as significant provided for section values with relative low data resolution. In order to obtain a complete description of the degree of fracturing, the k_s should be calculated over longer section lengths.

In the present study, the range in performance data varies greatly, and comparisons are made along sections longer than

those suggested by Bruland (1998). As a result the data have been averaged over sections of about 50 m in length. Weighted average values of performance, k_s and thrust have been used.

Fig. 18 shows the relationship between k_s, net penetration rate and thrust averaged along section lengths of 50 m.

The relationship of k_s with thrust is the opposite of that with net penetration rate, in that here increases in k_s indicate decreases in thrust. Reductions in thrust are carried out by the operator to avoid vibrations and possible damage to the cutters and the machine.

As noted above, mixed face phenomena are observed in the first 270 m of mapped tunnel section. The mixed face consists of basalt intrusions within a confining sill. The proportion of sill lithology and basalt varies along this section, making it difficult to treat the mixed face as a uniform rock mass. Intact rock boreability also varies between the basalt and sill lithology, resulting in differential fragmentation of the tunnel face under the cutter head.

Thus, boring is influenced by the varying boreability properties of the rock face. No clear relationships have been identified in the mixed face area, so data obtained from this section have been removed from the analysis used to find a correlation between the fracturing factor (k_s) and net penetration rate.

Fig. 19 shows a correlation of the fracturing factor and net penetration rate, excluding mixed face data.

The best correlation between the fracturing factor (k_s) and penetration rate is obtained using a second order polynomial.

Fig. 19 suggests that the strength of the correlation between k_s and net penetration rate varies with k_s. The trend is flatter at low k_s values, but as k_s increases the curve becomes steeper. This means that at low k_s values, penetration rate is little influenced by k_s, whereas there is an increasing dependence at higher k_s values.

Fig. 20 shows a data analyses for different k_s ranges.

It is difficult to identify a k_s value at which this apparent change in behaviour occurs. However, for the purposes of this study, we recognise a change in the range of k_s values between 1.1 and 1.3.

Fig. 20 suggests that the correlation is less marked at low k_s values. This is because low degrees of fracturing cease to be the main factor influencing penetration rate. Thus, intact rock properties become more important in influencing rock boreability.

For k_s values greater than 1.3, the steepness of the curve indicates that the correlation between the fracturing factor and net penetration rate is stronger. At high k_s values, rock mass boreability properties are the main influence on TBM performance.

An analysis of the above correlation for the entire range of k_s values means that we can also examine the relationship between the PR/k_s coefficient for this range (Fig. 21).

The curve in Fig. 21 shows that for k_s values above 1.3 or 1.4, the relationship between k_s and net penetration rate is almost constant. This indicates that increments in k_s indicate increments in net penetration values at a constant rate keeping the relation net penetration rate/k_s constant.

The PR/k_s coefficient is higher at low k_s values. This agrees with our previous conclusion, that at low k_s values intact rock or drillability properties have a greater influence over rock boreability than rock mass boreability, integrated using the fracturing factor.

After analysing the variation in penetration rate with k_s, we turned our attention to an analysis of the influence of thrust.

Fig. 22 shows the relationships between k_s and penetration rate (described previously) and thrust. Good correlations are obtained in both cases.

The best correlation of k_s with thrust is obtained with a polynomial regression. At high k_s values, thrust is reduced.

For any given geological conditions, increases in thrust will result in increases in net penetration rate, as shown in Fig. 14. As k_s increases, an operational decision is taken to reduce thrust.

Decisions to reduce thrust in response to increases in degree of fracturing are taken for operational reasons to avoid damage and excessive wear to the cutters resulting from vibrations and machine damage. Reductions in thrust reduce the influence of k_s on net penetration rate. However, net penetration rate still increases with increases in the fracturing factor. This "indirect effect" of thrust reduces the real influence of k_s on net penetration rate.

At low k_s values, thrust is close to the TBM's maximum limit, and becomes the main factor influencing increases in net penetra-

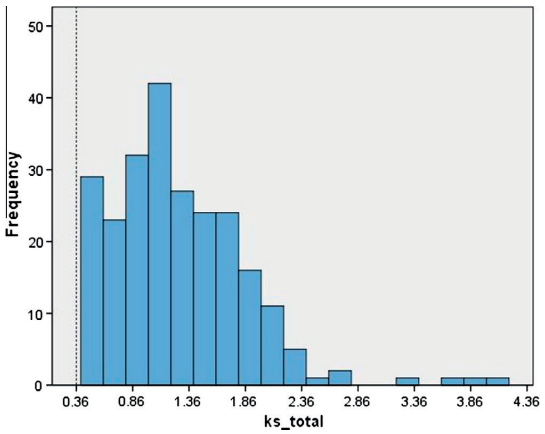

Fig. 12. Histogram showing the frequency of the rock mass fracturing factor (k_s).

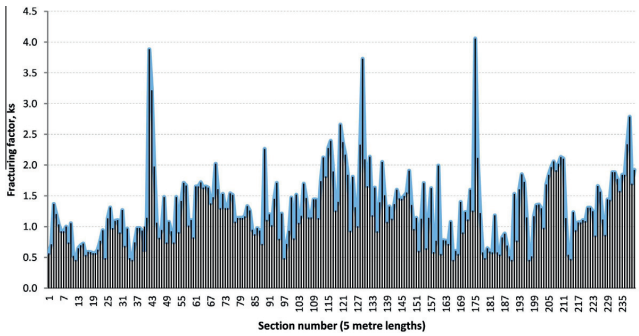

Fig. 11. Distribution of the fracturing factor (k_s) along the mapped sections.

Fig. 13. Examples of high (left) and low (right) k_s tunnel values.

tion rate. This is because at these low values, intact rock properties exert the dominant influence on rock mass boreability.

Fig. 18 shows that when k_s is very low, the penetration rate increases due to the influence of thrust. At high k_s values, rock mass properties exert a greater influence on TBM performance.

The field penetration index (FPI) has been applied in many studies. According to Hassanpour et al. (2010), the relationship between cutter load and penetration per revolution (i) in mm/rev can be calculated using the following formula:

$$FPI = \frac{Cutter\ thrust\left(\frac{kN}{cutter}\right)}{i\left(\frac{mm}{rev}\right)} \quad (9)$$

Fig. 20 shows that the field penetration index (FPI) displays a good correlation with the fracturing factor (k_s). The accuracy of correlation is similar to that observed in relation to thrust penetration rates described earlier. It confirms the observed relationship between performance data and the fracturing factor, and the relevance of k_s in predicting TBM performance during hard rock tunnelling (see Fig. 23).

In order to reveal the real influence of k_s on net penetration rate, by removing the "indirect effect" of thrust, an analysis will be presented of the hypothetical relationship between k_s and net penetration rate as shown in Fig. 14.

Table 6
The key values obtained for net penetration rate and thrust.

	Net penetration rate (m/h)	Thrust (kN/cutter)
Average	2.5	158.4
Maximum	4.4	228.7
Minimum	0.8	85.8

Table 7
Cutter thrust and basic penetration for the penetration test (Palm, 2011).

Gross thrust M_t (kN/cutter)	Basic penetration i_0 (mm/rev)	$\text{Log}_{10}\, M_t$	$\text{Log}_{10}\, i_0$
124	1.06	2.09	0.02
144	2.06	2.16	0.31
164	2.99	2.21	0.48
184	3.84	2.26	0.58
204	3.84	2.31	0.58

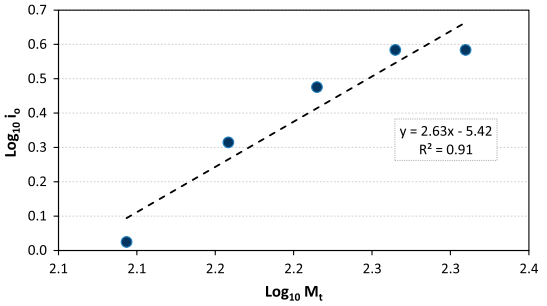

Fig. 14. Plot of $\log_{10}$ values of M_1 and i_0 for the penetration test including linear regression curve.

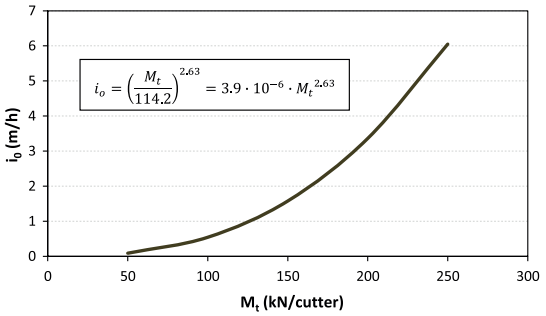

Fig. 15. Penetration curve obtained by treatment of the observed data on the penetration test carried out. The equation of the penetration curve is also presented.

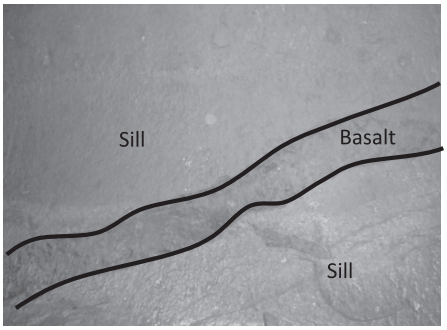

Fig. 16. An example of mixed face conditions encountered in the mapped sections.

Table 8 shows the range and average values of thrust recorded along the 50 m section lengths.

The penetration curve (Fig. 14) was obtained from data recorded in a rock mass with a fracturing factor of 1.25. The average k_s value is 1.14. The variation is considered not significant and it is assumed that the degree of rock mass fracturing is constant.

Using the average, maximum and minimum thrust values, and the penetration curve obtained from the penetration test (Fig. 15), we have estimated the hypothetical net penetration rates (Table 9).

An increase in thrust of 22% results in a 68% increase in net penetration rate, while a decrease in thrust of −29% results in a 60% decrease in net penetration rate.

When the penetration test is performed on rock masses exhibiting different degrees of fracturing, the penetration curve will be steep for low values of fracturing factor, but less so for high values.

Since along the section mapped the net penetration curve is related to a degree of fracturing of the rock mass close to the total

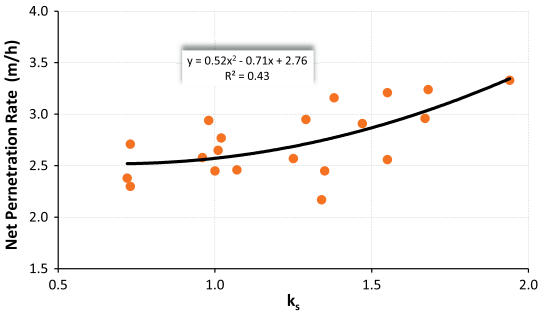

Fig. 19. Correlation of the fracturing factor (k_s) with net penetration rate, excluding mixed face data.

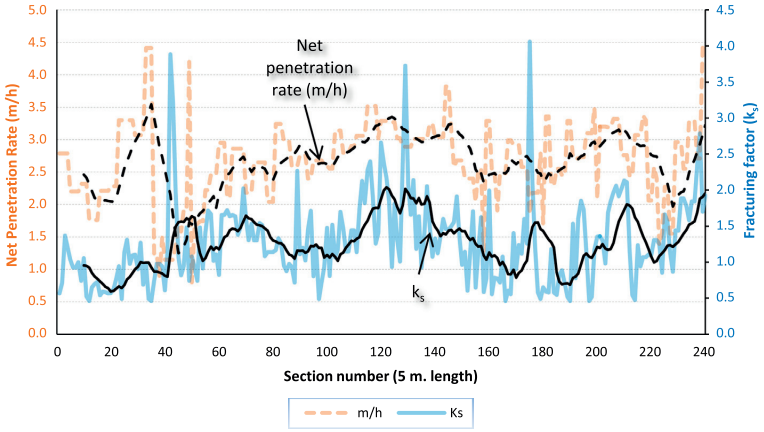

Fig. 17. Variation of penetration rate (m/h) and fracture factor (k_s) along the tunnel, measured along 5 m sections.

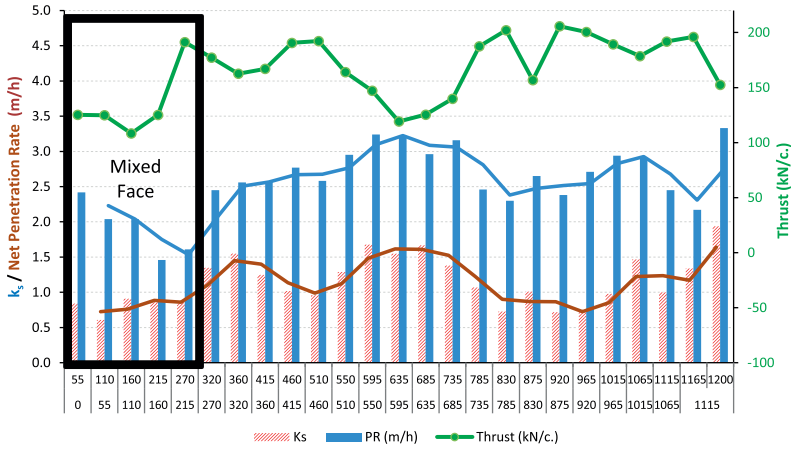

Fig. 18. Variation in net penetration rate (m/h), fracturing factor (k_s) and thrust (kN/cutter) using weighted average values along 50 m section lengths. Black box represents mixed face behaviour.

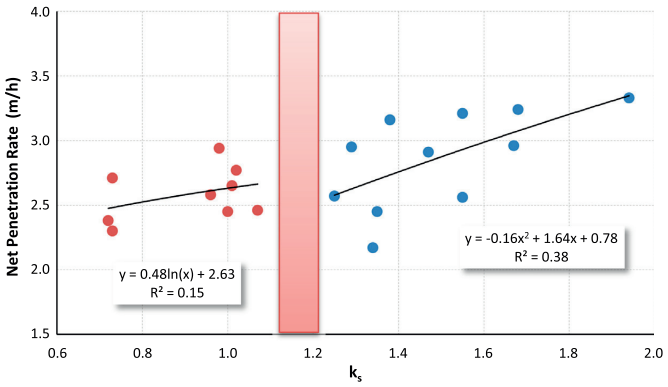

Fig. 20. Correlation of the fracturing factor (k_s) with net penetration rate.

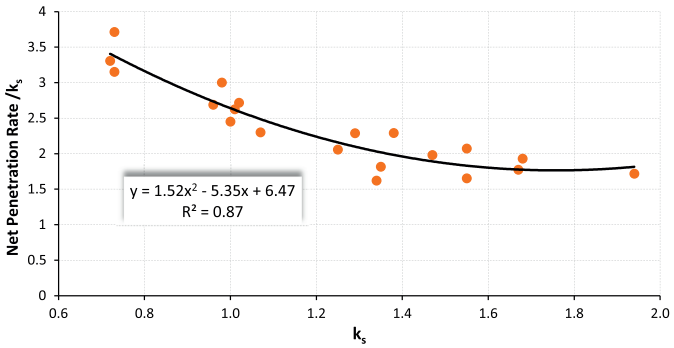

Fig. 21. Correlation of the fracturing factor with the net penetration rate/k_s coefficient.

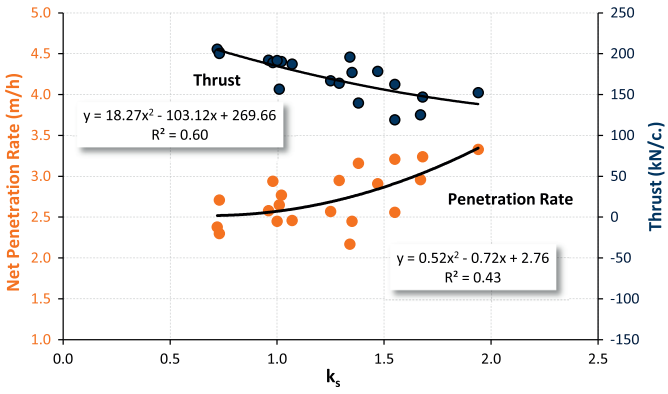

Fig. 22. Correlation of the fracturing factor (k_s) with the net penetration rate and the thrust without mixed face data.

k_s average, no consideration will be given to variations in the curve at different k_s values.

Boring using a constant thrust equal to the average value would result in an increase in the higher net penetration rate obtained for the highest k_s value (68%), and a decrease for the lowest k_s value (60%). Fig. 24 shows a curve estimated by removing the "indirect effect" of thrust, together with a curve showing the relationship between k_s and net penetration rate obtained from this study. The curve is obtained adding the variations of net penetration rate (Table 9) to the actual values.

This "estimated" curve shown in Fig. 24 can be regarded as representative of the maximum possible effect of k_s since the influence of the fracturing factor (k_s) on the penetration curve is not taken into consideration.

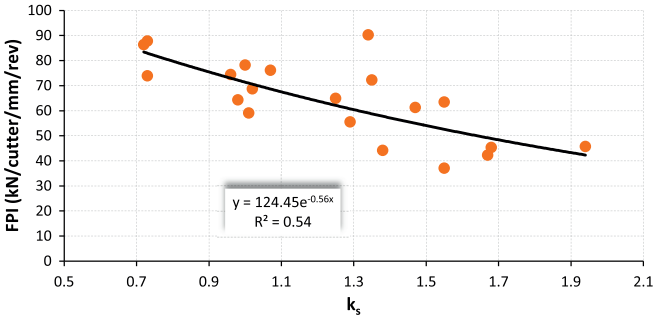

Fig. 23. Correlation of the field penetration index (FPI) with the fracturing factor (k_s).

Table 8
Thrust values recorded along approximately 50 m section lengths. Data from the mixed face section are excluded.

	Thrust average 50 m sections (kN/cutter)	% Variation
Average	168.9	
Maximum	205.7	22
Minimum	119.2	−29

Table 9
Net penetration rate obtained using the penetration curve for the range of thrust values taken from the example in Fig. 15.

	Net penetration rate (m/h)	% Variation
Average	2.18	
Maximum	3.65	68
Minimum	0.87	−60

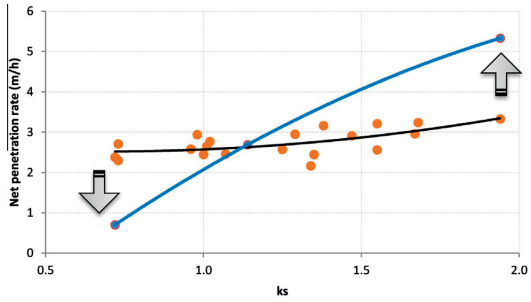

Fig. 24. "Estimated" and correlated curves showing the influence of k_s on penetration rate after removal of the "indirect effect" of thrust.

The graph shows that at low k_s values, the lack of fractures makes it essential to increase thrust in order to maintain penetration rate.

6. Conclusions

This present research has analysed the influence of rock mass fracturing on net penetration rate for hard rock TBMs. Higher degrees of fracturing result in higher net penetration rates.

According to the NTNU prediction model for hard rock TBMs, the fracturing factor (k_s) is shown to be an adequate expression of rock mass fracturing and rock mass boreability. The field penetration index (FPI) also exhibits good correlations with the fracturing factor.

Geological mapping along short sections fails to provide adequate and complete descriptions of the degree of fracturing. Extended geological sections are required to obtain a complete overview of the rock mass.

The fracturing factor is confirmed as a useful indicator of how rock mass fracturing influence TBM performance in terms of rock mass boreability.

At low values of k_s (low degrees of rock mass fracturing), net penetration rates are less influenced by k_s and intact rock properties play the most dominant role. At high values of k_s, rock mass properties dominate the boring process and net penetration rate is influenced to a much greater degree by the fracturing factor. In the present study, the change in behaviour is observed at k_s values between 1.1 and 1.3.

An "indirect effect" of thrust on the influence of the fracturing factor on net penetration rate has been identified and verified.

We have presented an "estimated" curve based on a penetration curve which demonstrates the influence of the fracturing factor on net penetration rates after removing the "indirect effect" of thrust.

It has been shown that geological back-mapping is a subjective process, and can result in data outliers if not carried out by corroborative teams. This subjectivity in relation to hard rock TBM projects will be the topic of discussion in a future research paper.

Future studies will focus on the assumption that the degree of rock mass fracturing is one of the main factors influencing prediction of the degree of penetration of hard rock TBMs. In order to update and improve our prediction models for lined tunnels, it will be necessary to develop indirect measurements of the degree of rock mass fracturing. Geological back-mapping in tunnels lined with concrete elements or shotcrete is very difficult and restricted to specific zones where rock exposures are accessible.

Acknowledgements

The authors would like to thank the research project "Future Advanced Steel Technology for Tunnelling" (FAST-Tunn). This project is managed by SINTEF/NTNU and funded by the Research Council of Norway, the Robbins Company, BASF Construction Chemicals, the Norwegian Railroad Authorities, Scana Steel Stavanger and BMS steel. We also extend our thanks to Jacob Clemmensen at MT Höjgaard in Denmark, and former M.Sc. student Anders Palm for assisting in arranging the field work and sharing data.

References

Barton, N., 2000. TBM Tunnelling in Jointed and Fault Rock. Balkema, Rotterdam.

Bejari, H., Khademi, J.H., 2012. Simultaneous effects of joints spacing and orientation on TBM cutting efficiency in jointed rock masses. Rock Mech. Rock Eng..

Bieniawski von Preinl, Z.T., Celada Tamames, B., Galera Fernandez, J.M., Alvarez Hernandez, M., 2006. Rock mass excavability indicator: new way to selecting the optimum tunnel construction method. Tunn. Undergr. Space Technol. 21 (3–4), 237.

Bruland, A., 1998. Hard Rock Tunnel Boring: vol. 1–10. Ph.D. Thesis. Norwegian University of Science and Technology (NTNU), Trondheim, Norway.

Dahl, F., Bruland, A., Jakobsen, P.D., Nilsen, B., Grøv, E., 2012. Classifications of properties influencing the drillability of rocks, based on the NTNU/SINTEF test method. Tunn. Undergr. Space Technol. 28, 150–158.

Delisio, A., Zhao, J., Einstein, H.H., 2013. Analysis and prediction of TBM performance in blocky rock conditions at the Lötschberg Base Tunnel. Tunn. Undergr. Space Technol. 33 (2013), 131–142.

Farrokh, E., Rostami, J., Laughton, C., 2012. Study of various models for estimation of penetration rate of hard rock TBMs. Tunn. Undergr. Space Technol. 30 (2012), 110–123.

Gong, Q.M., Zhao, J., Jiao, Y.Y., 2005. Numerical modelling of the effects of joint orientation on rock fragmentation by TBM cutters. Tunn. Undergr. Space Technol. 20 (2005), 183–191.

Gong, Q.M., Jiao, Y.Y., Zhao, J., 2006. Numerical modelling of the effects of joint spacing on rock fragmentation by TBM cutters. Tunn. Undergr. Space Technol. 21 (2006), 46–55.

Hassanpour, J., Rostami, J., Khamehchiyan, M., Bruland, A., 2009. Developing new equations for TBM performance prediction in carbonate-argillaceous rocks: a case history of Nowsood water conveyance tunnel. Geomec. Geoeng. 4 (4), 287–297.

Hassanpour, J., Rostami, J., Khamehchiyan, M., Bruland, A., Tavakoli, H.R., 2010. TBM performance analysis in pyroclastic rocks: a case history of Karaj water conveyance tunnel. Rock Mech. Rock Eng. 43, 427–445.

Hassanpour, J., Rostami, J., Zhao, J., 2011. A new hard rock TBM performance prediction model for project planning. Tunn. Undergr. Space Technol. 26 (2011), 595–603.

Howarth, D.F., 1981. The effect of jointed and fissured rock on the performance of tunnel boing machines. In: Proceedings of the International Symposium on Weak Rock, Tokyo, Japan, September 1981, pp. 1069–1074.

Lindqvist, P.-A., Lai, H.-H., 1983. Behaviour of the crushed zone in rock indentation. Rock Mech. Rock Eng. 16, 199–207.

Palm, A., 2011. Driftsoppfølging av TBM-prosjektet Eidi 2 Sudur (Monitoring of operations at the Eidi 2 Sudur TBM project). Master's Thesis. Norwegian University of Science and Technology (NTNU), Trondheim, Norway.

Ribacchi, R., Lembo-Fazio, A.L., 2005. Influence of rock mass parameters on the performance of a TBM in a gneissic formation (Varzo Tunnel). Rock Mech. Rock Eng. 38 (2), 105–127.

Sanio, H.P., 1985. Prediction of the performance of disc cutters in anisotropic rock. Int. J. Rock Mech. Min. Sci. Geomech. Abstr. 22 (3), 153–161.

Steingrimsson, J.H., Grøv, E., Nilsen, B., 2002. The significance of mixed-face conditions for TBM performance. World Tunn. 9, 435–441.

Wanner, H., Aeberli, U., 1979. Tunnelling machine performance in jointed rock. In: 4th Congress of the International Society for Rock Mechanics, Montreux, Switzerland, September 1979, vol. 1, pp. 573–580.

Yagiz, S., 2009. Geotechnical considerations on TBM tunnelling in rock mass. In: 2nd International Conference on New Developments in Soil Mechanics and Geotechnical Engineering, Nicosia, North Cyprus.

Yagiz, S., Rostami, J., Kim, T., Ozdemir, L., Merguerian, C., 2010. Factors influencing performance of hard rock tunnel boring machines. In: Vrkljan (Ed.), Rock Engineering in Difficult Ground Conditions – Soft Rocks and Karst. Taylor & Francis Group, London, pp. 691–700. ISBN:978-0-415-80481-3.

Zhao, Z., Gong, Q.M., Zhang, T., Zhao, J., 2007. Prediction model of tunnel boring machine performance by ensemble neural networks. Geomech. Geoeng. Int. J. 2 (2), 123–128.

Title:

The NTNU Prediction Model: A Tool for Planning and Risk Management in Hard Rock TBM Tunnelling

Paper II

Authors:

Macias, Francisco Javier

Jakobsen, Pål Drevland

Bruland, Amund

Log, Sindre

Grøv, Eivind

Published on:

Proceedings of the World Tunnel Congress 2014 – Tunnels for a better life, Foz de Iguazu, Brazil (2014)

Is not included due to copyright

Title:

Rock mass variability and TBM prediction

Authors:

Macias, Francisco Javier

Jakobsen, Pål Drevland

Bruland, Amund

Paper III

Published on:

Proceedings of the 2014 ISRM European Rock Mechanics Symposium (Eurock 2014), Vigo, Spain (2014).

Is not included due to copyright

Title:

Performance prediction of a hard rock TBM used in mining development

Authors:

Macias, Francisco Javier

Eide, Leon Nikolay Røren

Jakobsen, Pål Drevland

Bruland, Amund

Published on:

Proceedings of Rapid Excavation Tunneling Conference (RETC 2015), New Orleans, USA (2015).

Paper IV

Is not included due to copyright

Title:

Influence of subjectivity in geological mapping on the prediction of hard rock TBM performance

Authors:

Seo, Yongbeom

Macias, Francisco Javier

Jakobsen, Pål Drevland

Bruland, Amund

Submitted on:

Rock Mechanics and Rock Engineering (Under review)

Paper V

Is not included due to copyright

Title:

Performance and cutter life assessments in hard rock tunnelling

Authors:

Macias, Francisco Javier

Wilfing, Lisa

Andersson, Tobias

Thuro, kurosch

Bruland, Amund

Published on:

Eurock 2015 & 64th Geomechanics Colloquium, Salzburg, Austria (2015).

Paper VI

Is not included due to copyright

Title:

New rock abrasivity test method by rolling disc

Authors:

Macias, Francisco Javier

Dahl, Filip E.

Bruland, Amund

Published on:

International Congress of Rock Mechanics 2015, Montreal, Quebec, Canada. Paper 634 (2015).

Paper VII

Is not included due to copyright

Title:

New rock abrasivity test method for tool life assessments on hard rock tunnel boring: The Rolling Indentation Abrasion Test (RIAT)

Authors:

Macias, Francisco Javier

Dahl, Filip E.

Bruland, Amund

Published on:

Rock Mechanics and Rock Engineering, Vol. 49, no. 5 (2016), pp 1679-1693.

Paper VIII

Is not included due to copyright

Title:

Influence of Corrosion on the Abrasion of Cutter Steels Used in TBM Tunnelling

Authors:

Espallargas, Nuria

Jakobsen, Pål Drevland

Langmaack, Lars

Macias, Francisco Javier

Published on:

Rock Mechanics and Rock Engineering, Vol. 48, no. 1 (2015), pp 261-275.

Paper IX

Is not included due to copyright

Appendix:

The NTNU prediction model for hard rock TBMs: Advance rate and cutter wear

Table of contents

1. Introduction 349
2. The NTNU prediction model 351
2.1. General remarks 351
2.2. Model parameters 352
2.2.1. Rock parameters 353
2.2.2. Machine parameters 357
3. The Net Penetration Rate Model 362
3.1. Introduction 362
3.2. Rock mass fracturing 364
3.3. Rock porosity 367
3.4. Basic penetration 368
3.5. Basic net penetration rate 370
3.6. Marked Single Joints 371
3.7. Torque demand 373
3.8. Limitations on net penetration rate 375
4. The Cutter Life Model 376
4.1. Introduction 376
4.2. Cutter ring life 376
4.2.1. Correction for TBM diameter 377
4.2.2. Correction for cutterhead velocity 377
4.2.3. Correction for the standard number of cutters 378
4.2.4. Correction for abrasive minerals 378
4.2.5. Correction for gross cutter thrust: 379
4.3. Considerations for cutter life assessments 380
5. Gross advance rate 381
5.1. Introduction 381
5.2. Machine utilization 381
5.3. Additional time consumption 387
6. Limitations of the NTNU model 388
7. References 390

1. Introduction

This appendix presents the most recent edition of the NTNU prediction model for hard rock TBMs (Macias, 2016). In recent years, a review of the model has been carried out by means of several ongoing and recently completed TBM projects, combined with revisions of the model in response to developments in TBM technology. The review has led to an extension of the range of application of the model in the light of the influence of recently defined parameters (Macias, 2016).

The report includes the complete methodology and necessary data required for the prediction of performance, time consumption and cutter wear for hard rock tunnel boring projects.

A brief presentation is given of the relevant rock mass properties and TBM parameters to determine the main factors influencing predictions of penetration rate and cutter wear.

The report presents the following data and models:

- Section 2: The rock mass and machine parameters required as input to the estimation models
- Section 3: An estimation of net penetration rate
- Section 4: Estimations of cutter wear and cutter life
- Section 5: Estimations of machine utilisation and weekly advance rate

For a given tunnelling project, performance predictions and costs estimates are often decisive in the selection of TBM excavation methods and as inputs to planning and risk management. Reliable prediction enables the control of risk and the avoidance of delays and budget overruns.

The main factor used as input for predictions of advance rate, cutter consumption and excavation costs hard rock TBM projects is net penetration rate. Penetration rate represents the interaction of rock mass properties with machine parameters.

Predictions of excavation costs for hard rock TBM projects involve the consideration of geological risk. The level of risk increases in importance as the degree of rock mass fracturing decreases.

Figure 1 shows relative excavation costs as a function of rock mass fracturing (the reference excavation cost value is set as that corresponding to Fracture Class 4) for a 7-metre diameter

TBM with standard machine specifications in a tunnel exhibiting standard rock properties of medium drillability and abrasivity.

The figure shows that low values of fracturing (e.g. S_f 0, 1 and 2) result in dramatic increases in excavation costs. However, at high degrees of fracturing, changes in fracture class have relatively little effect on costs.

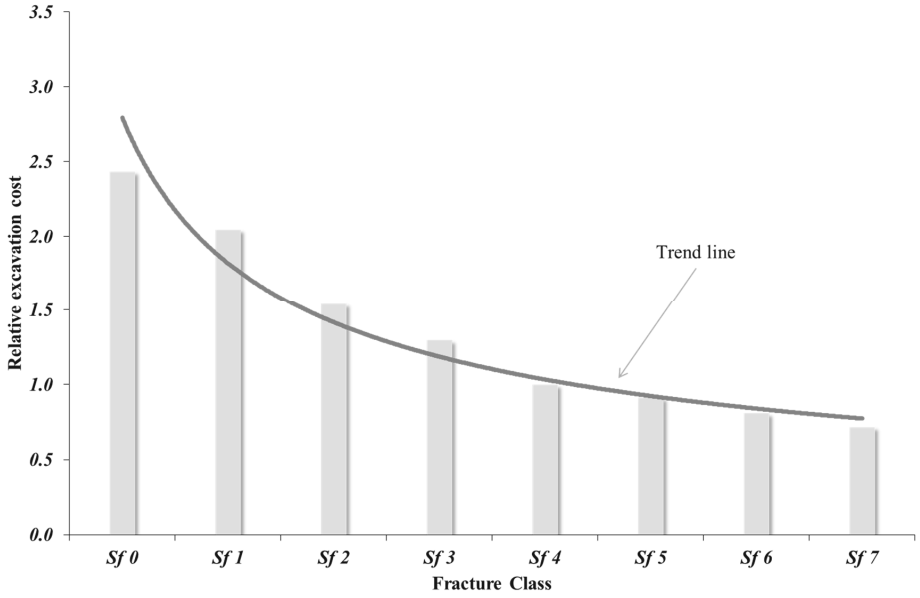

Figure 1. Relative excavation costs as a function of rock mass fracturing (fracture classes).

At lower degrees of fracturing, results indicate increments in predicted excavation costs of 20 to 70 per cent between individual classes, amounting to an increase in approx. 150 per cent relative to the reference standard, class St I. However, variation within highly fractured rock masses results in a reduction of the predicted excavation cost of 10 to 30 per cent between individual classes (amounting to a reduction of approx. 40 per cent relative to the reference). Important to bear in mind that additional time and cost associated with ground stability in highly fractured and faulted zones is not included.

It is also important to bear in mind that the fracture classes St 0, St I and St IV shown in Figure 13 represent fracture factors (k_s) of 0.36, approx. 1.0 and over 4.0 respectively. This emphasises the degree of risk involved when moving from class St 0 to St I.

Special care should thus be taken when predicting TBM performance and excavation costs in rock masses exhibiting low levels of fracturing.

2. The NTNU prediction model

2.1. General remarks

The philosophy of the NTNU model is to achieve reliable predictions by combining relevant rock properties and machine parameters. The model involves several steps are involved in the NTNU prediction model for hard rock TBMs in order to estimate time and costs involved in tunnel excavation using factors such as : net penetration rate, cutter life as well as advance rate and excavation costs. The model has been the subject of progressive development since the first version was used in 1976 by the NTNU (formerly NTH).

Estimation models for hard rock tunnel boring should be applied with care. In combination with other models published in the Project Report Series issued by the NTNU Department of Civil and Transport Engineering, the Hard Rock Tunnel Boring reports provide reliable and practical tools for the following processes:

- estimating net penetration rate and cutter wear
- estimating time consumption and excavation costs, including risk
- assessing risk linked to variation in rock mass boreability and machine parameters
- establishing and managing contract price regulation
- verifying machine performance
- verifying variation in geological conditions

The estimation models are designed for use during several stages of a given project:

- ✓ Preliminary and feasibility studies
- ✓ Evaluation of the excavation method
- ✓ Project design and optimisation
- ✓ During tendering and contract processes
- ✓ Documentation during construction
- ✓ Possible disputes and claims

The estimation models are based on on-site project studies, combined with analysis and statistics from tunnelling projects carried out in both Norway and abroad, involving more than 40 sites and more than 300 kilometres of tunnel. The data have been systematised and normalised, and the results are regarded as representative for well-organised tunnelling projects (Macias, 2016).

The model has had been the subject of continuous development a successive development since the first version was published in 1976 by the NTNU (formerly NTH).

Table 1 shows the successive editions of the NTNU prediction model to date.

Table 1: History of the NTNU prediction model for hard rock TBMs

EDITION	YEAR
1st edition	1976
2nd edition	1979 (published in 1981)
3rd edition	1983
4th edition	1988
5th edition	1994
6th edition	2000
7th edition	2016

2.2. Model parameters

The values of net penetration rate and cutter life depend on rock properties and machine parameters. Rock properties consist of intact rock and rock mass parameters. These are combined to generate a single rock mass boreability parameter, called the equivalent fracturing factor (k_{ekv}), while the machine parameters are combined into a single parameter, the equivalent thrust (M_{ekv}).

Cutter life, measured in hours, is equivalent to the cutter life in rolled distance at a given cutterhead velocity, measured in rpm. Cutter life in hours is combined with the penetration rate (m/h) and the TBM diameter to calculate cutter life in terms of tunnel metres excavated per cutter (m/cutter) and solid cubic metres excavated per cutter (sm^3/cutter). Table 51 lists the machine and rock parameters that influence net penetration rate.

Table 2. Machine and rock parameters that influence net penetration rate.

ROCK PROPERTIES		MACHINE
Intact Rock	**Rock Mass**	**PARAMETERS**
Drilling Rate Index, DRI	Rock Mass Fracturing Factor (k_s)	TBM diameter
		Cutter diameter
Porosity		Number of cutters
		Gross average cutter thrust
		Average cutter spacing
		Cutterhead rpm

Cutter wear depends on the rock properties and machine parameters listed in Table 52 below.

Table 3. Machine and rock parameters that influence cutter wear.

ROCK PROPERTIES	MACHINE PARAMETERS
Cutter Life Index, CLI	TBM diameter
	Cutter diameter
Content of abrasive minerals	Number of cutters
	Cutterhead rpm
	Gross average cutter thrust

The gross advance rate is estimated on the basis of three input parameters:

- Net penetration rate
- Machine utilisation
- Number of working hours in a given period (e.g. a week).

The machine utilisation is in turn based on time consumption for the various operations involved in the tunnel excavation process.

2.2.1. Rock parameters

This section provides a brief description of the geological parameters required as input to the prediction model. It also provides geological information which may be of help during a project's early planning phase. Estimates of time consumption and costs require an engineering geological pre-investigation, adapted to hard rock TBM tunnelling.

Rock Drillability

The rock drillability is evaluated on the basis of the Drilling Rate Index (DRI) and the Cutter Life Index (CLI).

The DRI is assessed on the basis of two laboratory tests, the Brittleness Value S_{20}' and 'Sievers' J-value'. The DRI is an indirect measure of the work required to break the rock and is thus an effective measure of the rock-breaking process under a cutter.

The CLI is assessed on the basic of the 'Sievers' J-value' and the 'Abrasion Value Steel' (AVS). The CLI is an expression of cutter disc ring life in terms of boring hours.

Recorded variations in the DRI and CLI for some rock types are shown in Figure 2 and Figure 3. The influence of rock porosity is discussed in Section 3.3.

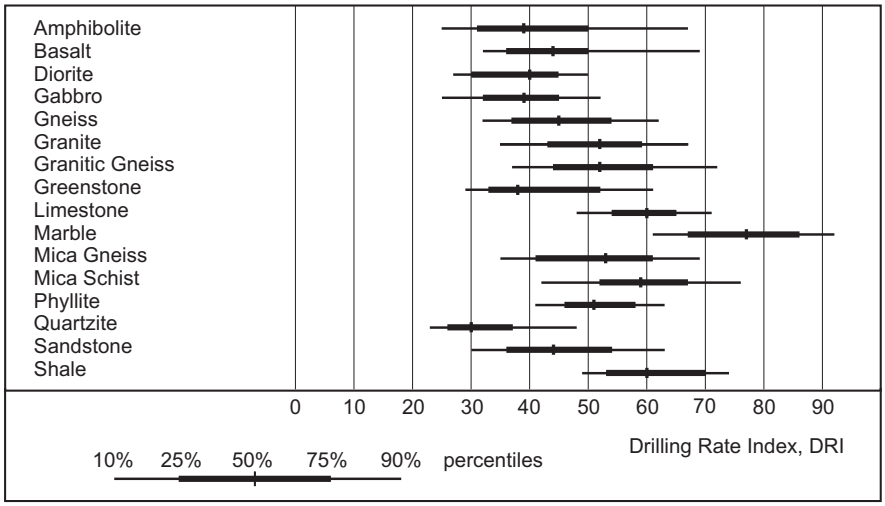

Figure 2. Recorded Drilling Rate Index values for some rock types (Bruland, 2000).

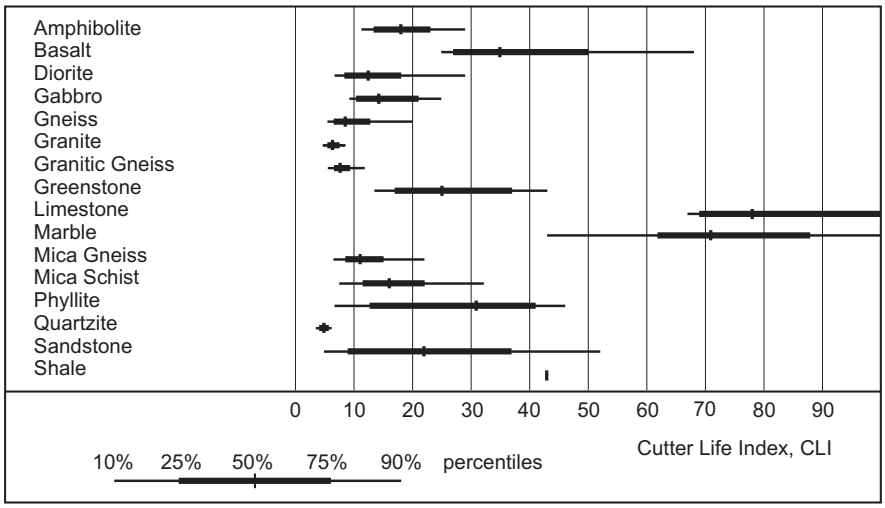

Figure 3. Recorded Cutter Life Index values for some rock types (Bruland, 2000).

Degree of Fracturing

Rock mass fracturing is identified as the geological factor that has the greatest influence on net penetration rate, and thus also on project costs during hard rock tunnelling. In this context, the term 'fracturing' refers to planes of weakness or fractures with limited or no shear strength. The less the distance between the fractures, the greater the influence on penetration rate.

The rock mass fracturing parameter is described in terms of degree of fracturing and the angle between the tunnel axis and the planes of weakness in systematic fractured rock mass.

Fractures

The term 'fractures' incorporates all continuous and non-continuous fractures that are capable of representing relatively weak areas of rock under a cutter disc, and which can thus influence performances.

Fractures may be open, such as joints in granite, or filled with clay or low shear strength minerals, such as calcite, chlorite or similar minerals. In metamorphic rocks, such as schists and gneisses, schistose fabrics can also represent planes of weakness exhibiting low shear strength.

Non fractured Rock Mass (Class 0): This class includes massive rock without fractures, such as may be the case for intrusive dykes, sills or batholiths, etc. Rock masses with joints that are filled or healed with minerals exhibiting high shear strength properties, such as quartz or epidote, may also approach Class 0.

Marked Single Joints (MSJ): MSJ includes highly distinctive discontinuities. These may be entirely open, may conduct water or may be filled with clay. Minor faults filled with gouge may be classified as MSJ.

Single joints are recorded individually. They are marked discontinuities in the rock mass. As the name indicates, they will appear as a singular phenomenon at the tunnel level, even if they belong to a systematically occurring joint set on a larger scale. Marked Single Joints may result in very high net penetration rates locally. Due to the risk of stability problems and damage to the cutters and the cutterhead, one should evaluate the effect carefully and consider possible delays if the Marked Single Joints may result in mixed face conditions, heavy rock support, water inflows, etc.

For detailed descriptions, the reader is referred to Bruland (2000) and Macias (2016).

Figure 4 presents a proposed length-based classification of the main types of discontinuities from an engineering geological perspective according to the NTNU back-mapping methodology.

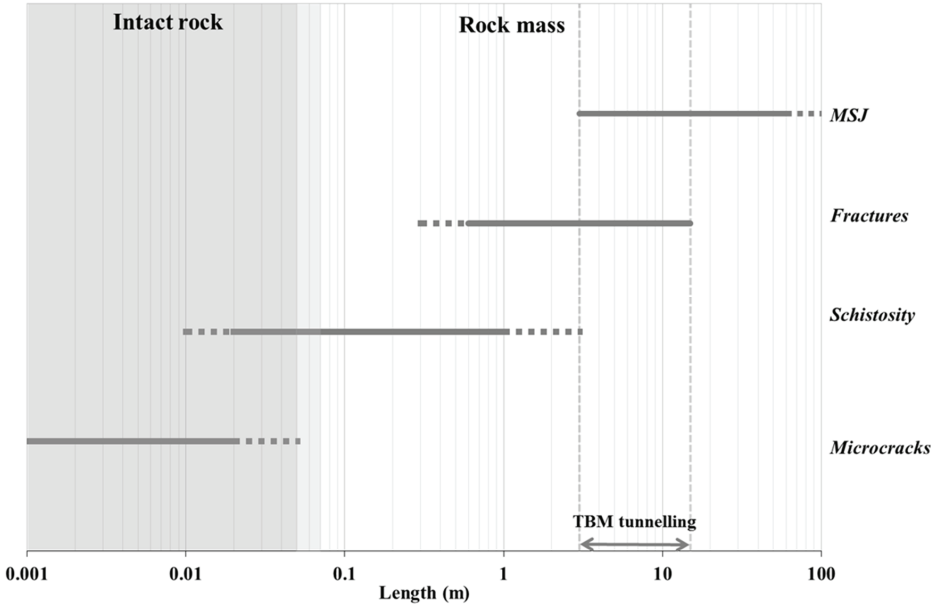

Figure 4. The main types of intact rock and rock mass discontinuities encountered during back-mapping in hard rock TBM tunnelling. Types are categorised according to length based on the NTNU methodology. The shaded area indicates where data have been derived from laboratory tests carried out on intact rock.

For practical mapping purposes in connection with TBM tunnelling projects, the degree of fracturing in a systematically fractured rock mass is divided into classes, shown in Table 4. The definition of classes also includes the average distance between the plane of weakness.

Table 4. Fracture class as defined by the spacing between planes of weakness in systematically fractured rock mass.

Fissure class (St) (Bruland, 2000)	Fracture Class (Sf)	Average spacing between fractures a_f (cm)	Range class (cm)	Degree of fracturing
0	0	∞	480 – ∞	Non-fractured
0	1	320	240 – 480	Extremely low
0 - I	2	160	120 – 240	Very low
I -	3	80	60 – 120	Low
I	4	40	30 – 60	Medium
II	5	20	15 – 30	High
III	6	10	7.5 – 15	Very high
IV	7	5	4 – 7.5	Extremely high

Figure 4 shows recorded degrees of fracturing for some rock types.

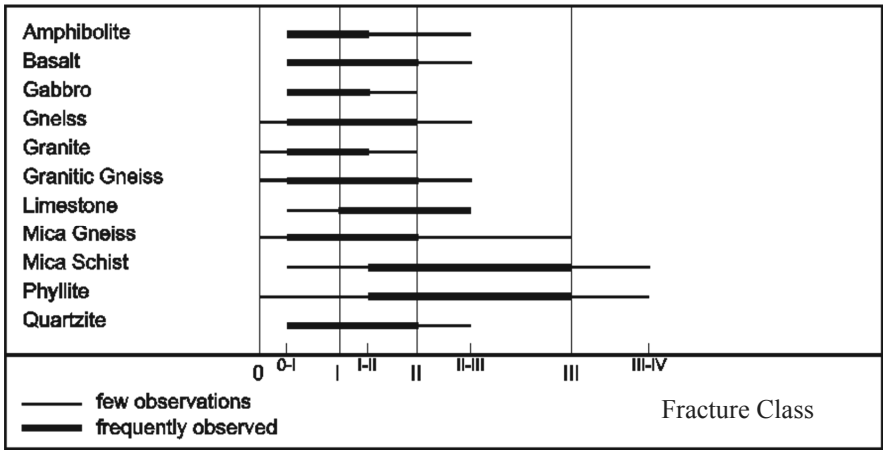

Figure 5. Recorded degrees of fracturing for some rock types (Bruland, 2000).

Geological mapping in connection with tunnelling projects is limited by tunnel size. Fractures also vary in length.

2.2.2. Machine parameters

Several machine parameters have been selected to estimate penetration rate and cutter life. Machine parameters are subdivided into two groups; 'machine specifications', such as machine and cutter diameters, the number of cutters or cutterhead power, and 'machine operation' parameters such as gross cutter thrust and applied rpm.

Machine specifications

During the early stages of project planning, some parameters must be assumed based on general machine specifications.

TBM diameter

TBMs developed for tunnelling in hard rock vary in diameter from 1.2 to 15 metres. Our database indicates that the estimation models currently in use are applicable for TBM diameters ranging from 3 to 12 metres.

Cutter diameter

Currently, cutter diameters of 483 millimetres (19 inches) are the most commonly used in hard rock tunnel projects, although diameters of 432 mm (17 inches) are standard for smaller TBMs. Cutter discs with diameters of 508 mm (20 inches) have recently been introduced, involving the use of 483 mm cutters with enlarged cutter rings.

Standard number of cutters on the cutterhead

Figure 6 shows the standard number of cutters on a cutterhead as a function of TBM and cutter diameter. For smaller TBM cutterhead diameters, the space available on the cutterhead is limited and the number of cutters indicated is the maximum.

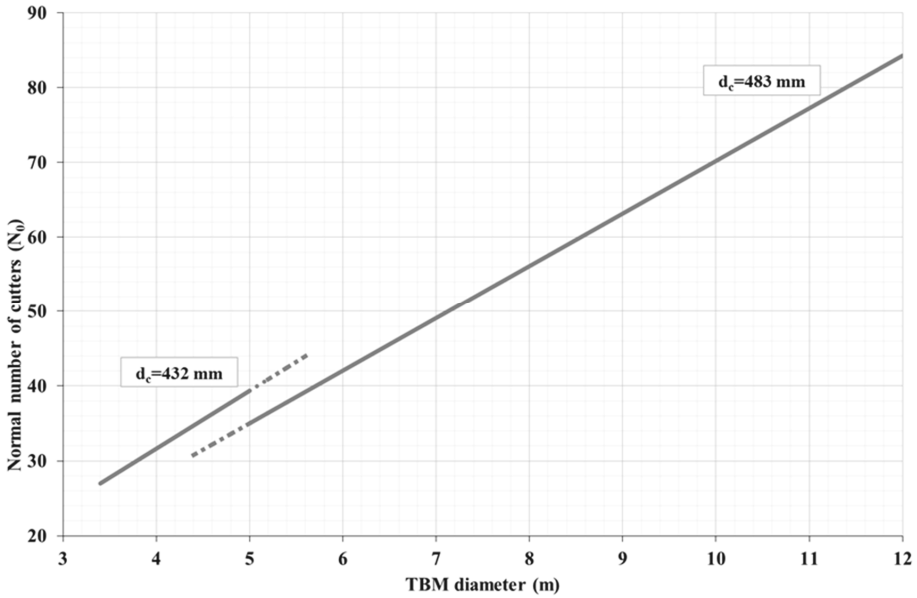

Figure 6. Standard number of cutters on a cutterhead (N_0) as a function of TBM cutterhead diameter.

Installed cutterhead power

Installed cutterhead power is not considered to be a limiting factor for modern TBMs, assuming that they are adequately designed. However, since insufficient cutterhead power may result in limitations, Figure 7 shows the installed power for cutterhead rotation as a function of TBM and cutter diameter.

The installed power indicated should provide sufficient torque to produce a penetration rate of approximately 14 mm/rev.

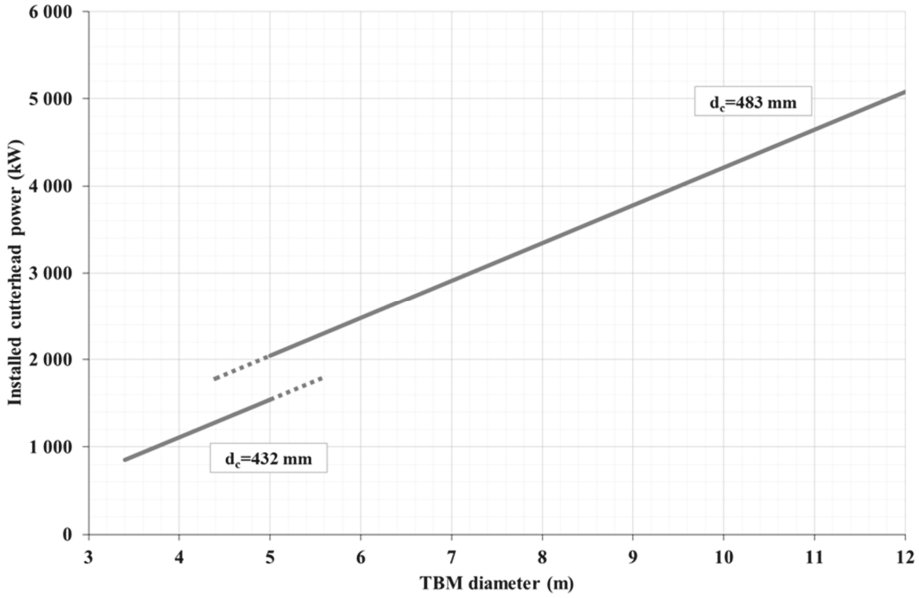

Figure 7. Installed cutterhead power (P_{tbm}) as a function of TBM cutterhead diameter.

Machine operation parameters

Cutter thrust

Figure 8 is a plot showing recommended applied gross average thrust per cutter disc as a function of cutter diameter and TBM diameter.

The 'gross average thrust' term refers to the thrust that cutters are able to utilise over an extended period of time. It does not incorporate peak loads that occur over short time intervals. At present, the quality of the steel in the cutter ring remains the limiting factor on cutter thrust. Estimations of penetration rates and related factors require that the thrust capacity of the cutter rings be taken into account, together with the capacity of the cutter bearings and the cutterhead main bearing.

The upper limit applies to boring operations in a non-fractured rock mass, while the lower limit applies to moderately to very fracture rock masses. Tunnelling operations along curved tunnels or on downward slopes may require lower thrust values.

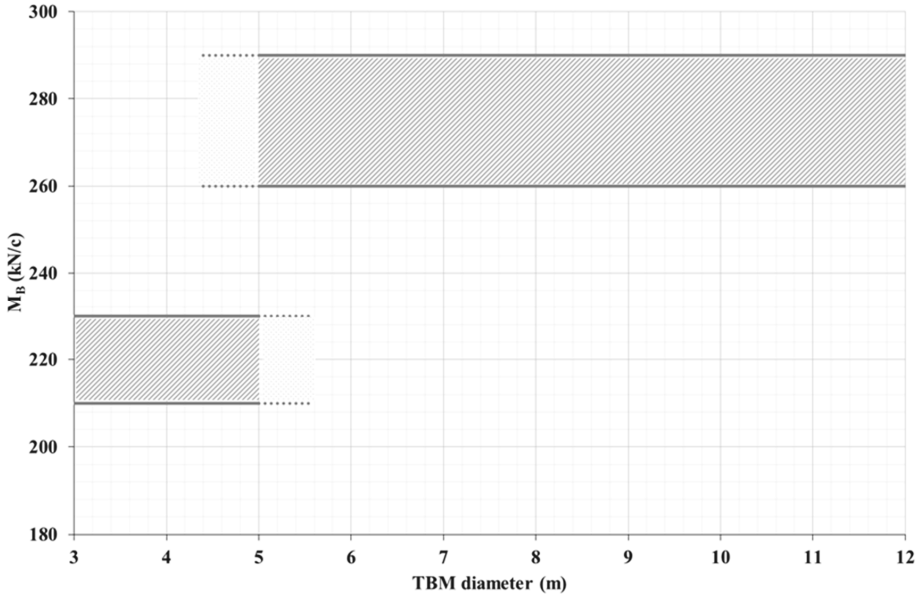

Figure 8. Recommended gross average thrust per cutter disc. The upper limit applies to boring operations in a non-fractured rock mass, while the lower limit applies to moderately to very fracture rock masses.

Cutterhead velocity

Cutterhead velocity (rpm) is inversely proportional to cutterhead diameter. This is because the rolling velocity of the peripheral cutter has to be limited. Figure 9 shows maximum and recommended cutterhead rpm as a function of TBM diameter and cutter diameter. The figure shows a range of available applied rpm. A low optimal velocity in indicated in situations involving low degrees of rock mass fracturing and/or low thrust.

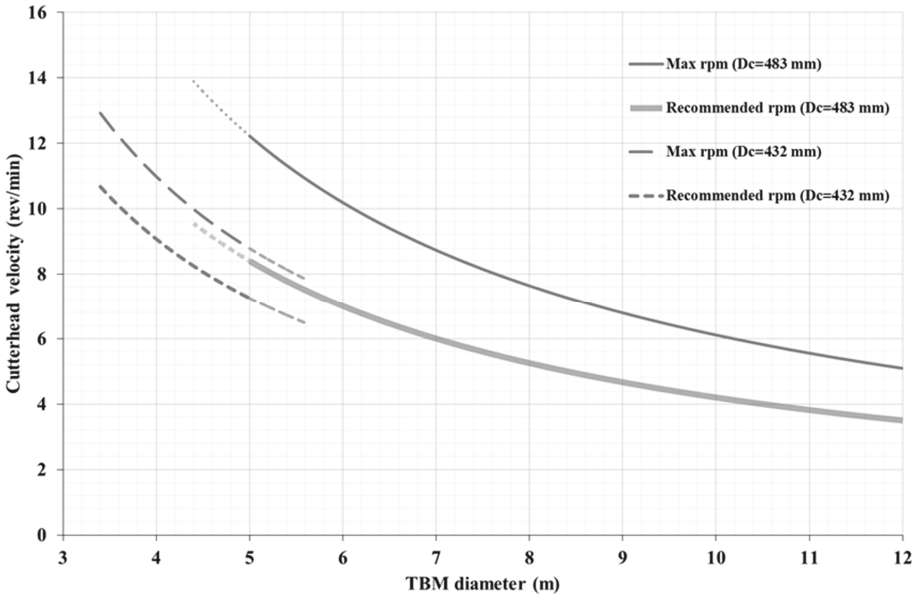

Figure 9. Maximum and recommended cutterhead velocities (rpm) as a function of TBM and cutter diameter.

3. The Net Penetration Rate Model

3.1. Introduction

Net penetration rate is defined as the length of tunnel bored (in metres per hour) during cutterhead rotation against the rock face.

Figure 10 is a flowchart showing the components of performance prediction in the latest version of the NTNU model.

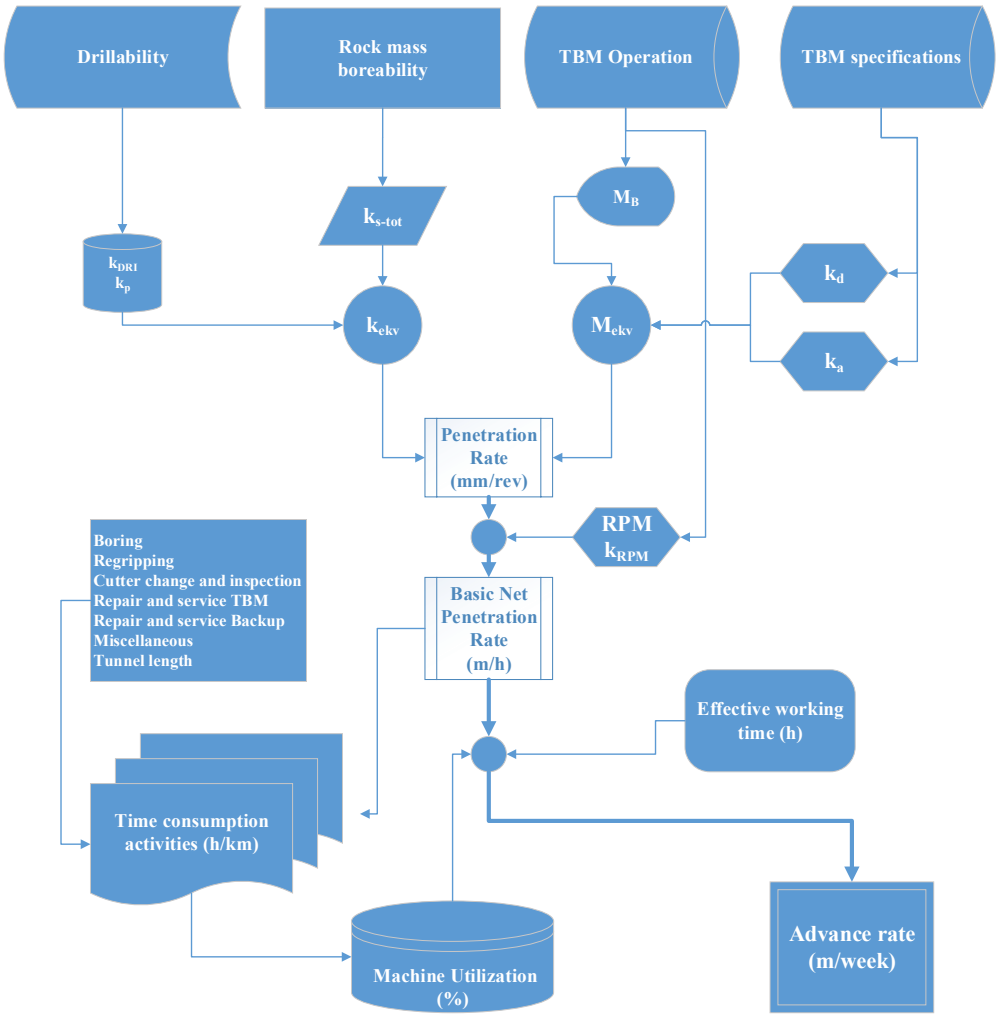

Figure 10. Flowchart for performance prediction by the latest version of the NTNU model

The penetration rate estimation model is based on normalised penetration curves obtained from penetration tests under different rock mass conditions. The best fit is found to be a power function. The following equation (1) is the formula for expressing basic net penetration rate:

$$i_0 = \left(\frac{M_{ekv}}{M_1} \right)^b \quad \text{(mm/rev)} \tag{1}$$

where

i_0 = basic penetration rate (mm/rev)
M_t = gross average cutter thrust at each thrust level (kN/cutter)
M_1 = critical cutter thrust (kN/cutter) required to achieve 1 mm/rev
b = penetration coefficient

Figure 11 and Figure 12 show the relationships between the equivalent fracturing factor (k_{ekv}) and critical thrust (M_1), and the penetration coefficient (b), respectively.

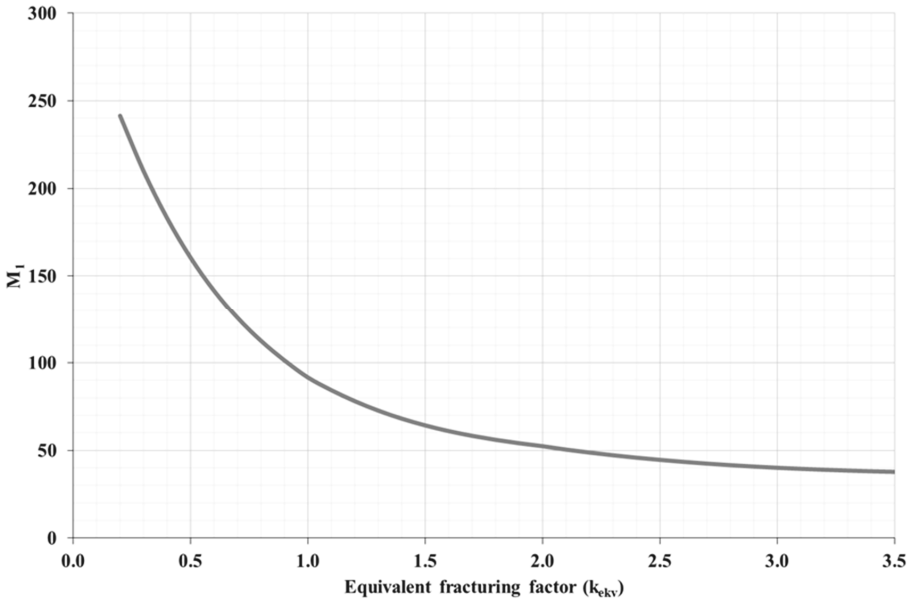

Figure 11. Critical thrust (M_1) as a function of the equivalent fracturing factor.

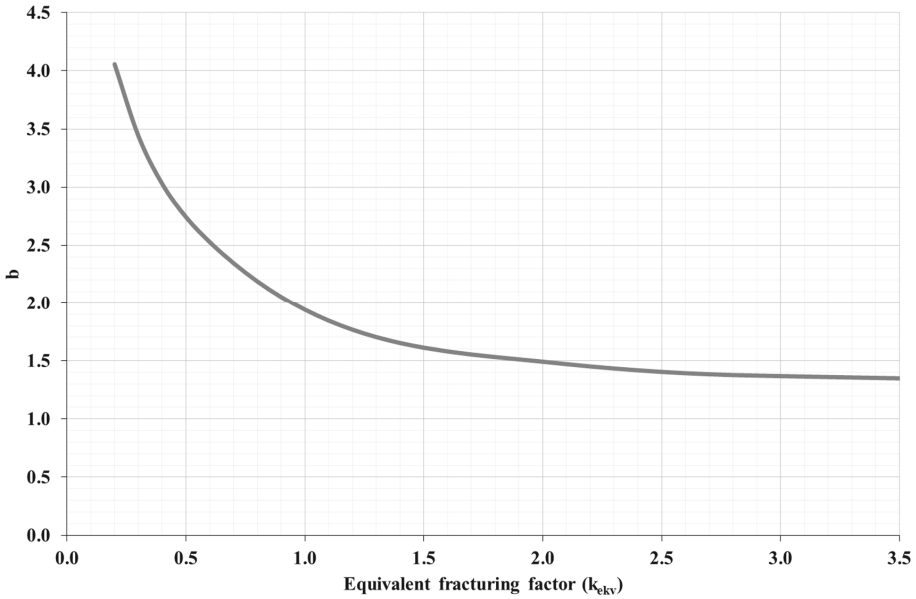

Figure 12. Penetration coefficient (b) as a function of the equivalent fracturing factor.

3.2. Rock mass fracturing

The rock mass fracturing parameter is expressed by the fracturing factor (k_s), which is dependent on the degree of fracturing and the angle between the tunnel axis and the planes of weakness (α).

For practical mapping purposes in connection with TBM tunnelling projects, the degree of fracturing in a systematically fractured rock mass is divided into classes, shown in Table 5.

Table 5. Fracture class as defined by the spacing between planes of weakness.

Fracture Class (Sf)	Average spacing between fractures a_f (cm)	Range class (cm)	Degree of fracturing
0	∞	480 – ∞	Non-fractured
1	320	240 – 480	Extremely low
2	160	120 – 240	Very low
3	80	60 – 120	Low
4	40	30 – 60	Medium
5	20	15 – 30	High
6	10	7.5 – 15	Very high
7	5	4 – 7.5	Extremely high

The orientation of the fractures is determined from measurements of strike and dip and expressed in the following equation:

$$\alpha = \arcsin \cdot (\sin \alpha_f \cdot \sin (\alpha_t - \alpha_s)) \quad (°) \tag{2}$$

where

α_s = strike angle of the planes of weakness
α_f = dip angle of the planes of weakness
α_t = azimuth of the tunnel axis

The fracturing factor is shown in Figure 13 as a function of Fracture Class and the angle between the tunnel axis and the fractures. Figure 14 shows the fracturing factor for detailed calculations of rock masses with low degrees of fracturing.

For more than one set of fractures, the total fracturing factor is as follows:

$$k_{s-tot} = \sum_{i=1}^{n} k_{si} - (n-1) \cdot 0.36 \tag{3}$$

where

$k_{s\text{-}tot}$ = total fracturing factor
k_{si} = fracturing factor for set no. i
n = number of fracture sets

A maximum of three fracture sets (n=3) is recommended, possibly with one or two main sets and one set including the random fractures. It is important to include all the fractures in the rock mass interpretation, i.e. random fractures (except marked single joints, MSJ).The $k_{s\text{-}tot}$ should not exceed a value of 4 since this will be outside the model range.

The rock mass properties that apply to TBM boring are expressed by the equivalent fracturing factor, which is determined from the following:

$$k_{ekv} = k_{s-tot} \cdot k_{DRI} \cdot k_{por} \tag{4}$$

where

k_{ekv} = equivalent fracturing factor
$k_{s\text{-}tot}$ = total fracturing factor
k_{DRI} = correction factor for the DRI of the rock
k_{por} = correction factor for the porosity of the rock

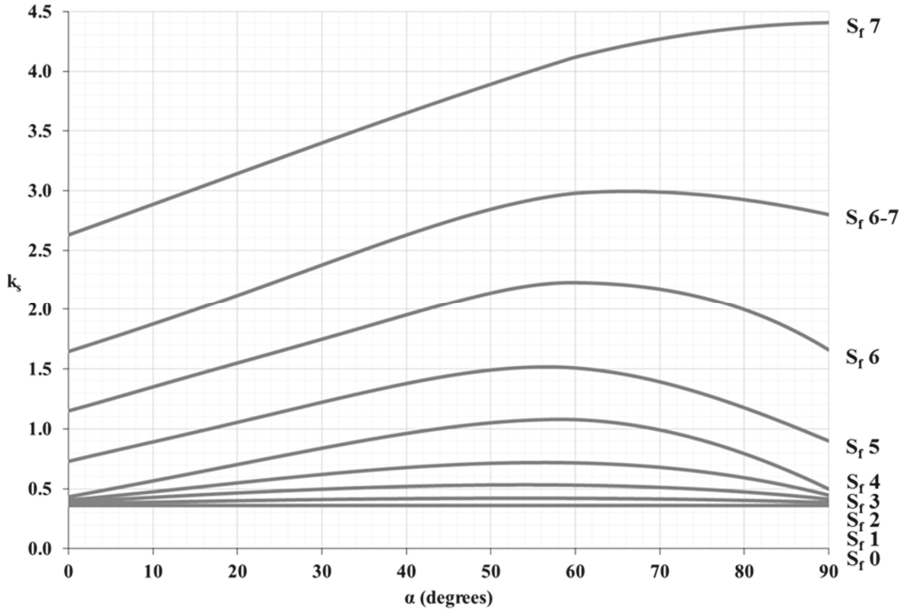

Figure 13. Rock mass fracturing factor (k_s) as a function of the angle between the tunnel axis and the fractures.

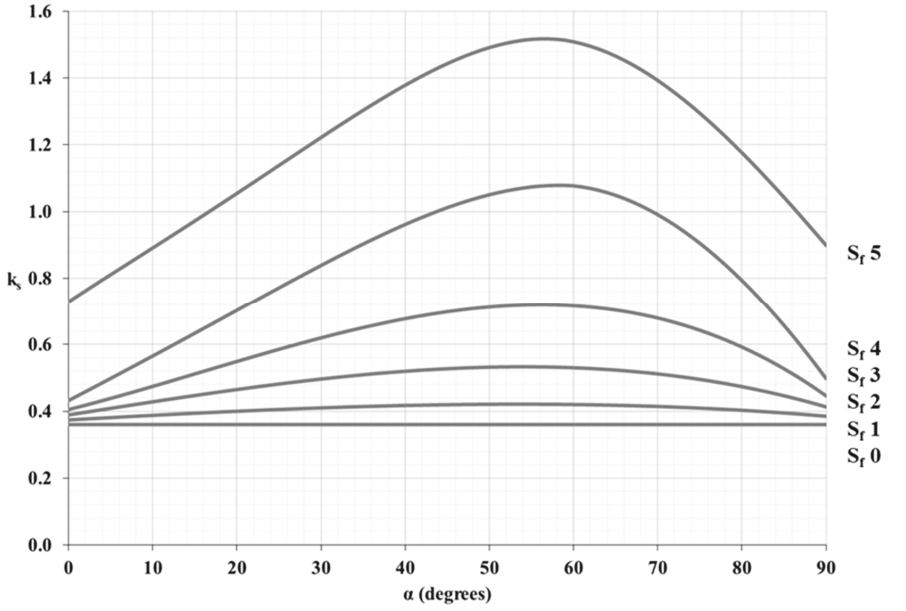

Figure 14. Rock mass fracturing factor (k_s) as a function of the angle between the tunnel axis and the fractures (for detailed calculations of rock masses with low degrees of fracturing).

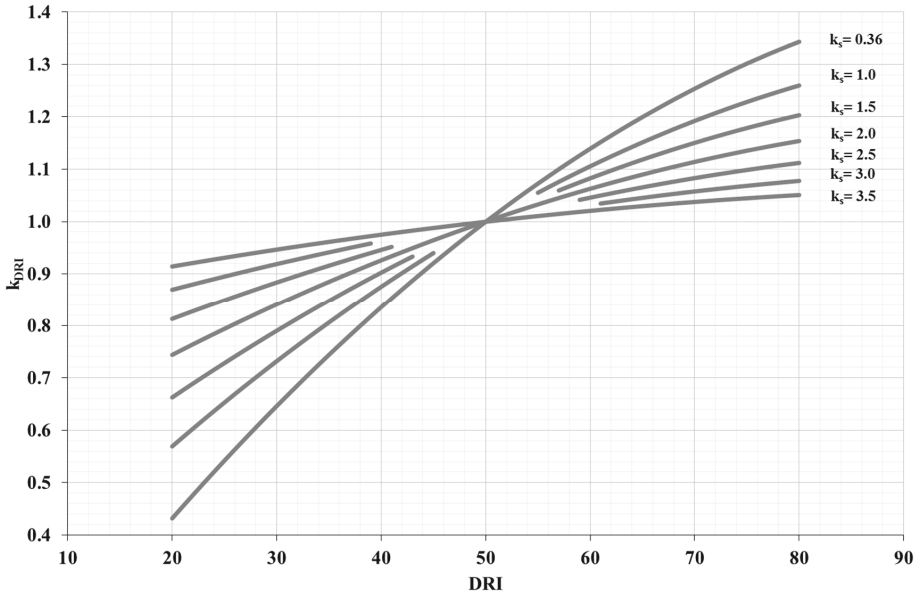

Figure 15 Correction factor for DRI values ≠ 50.

3.3. Rock porosity

The model requires that porosity be measured for rock types with porosities higher than approximately 2%. The influence of porosity on the DRI is negligible for porosities less than about 10-12%. For this reason, porosity must be incorporated in the penetration rate model as an independent parameter.

TBM projects in North Atlantic basalts in the Faeroe Islands have shown that porosity has a significant influence on net penetration rate (Bruland, 2000). The experience data are limited to approximately 15% porosity.

A rough estimate of the influence of porosity on penetration rate (Correction factor for porosity of the rock, k_{por}) is shown in Figure 16.

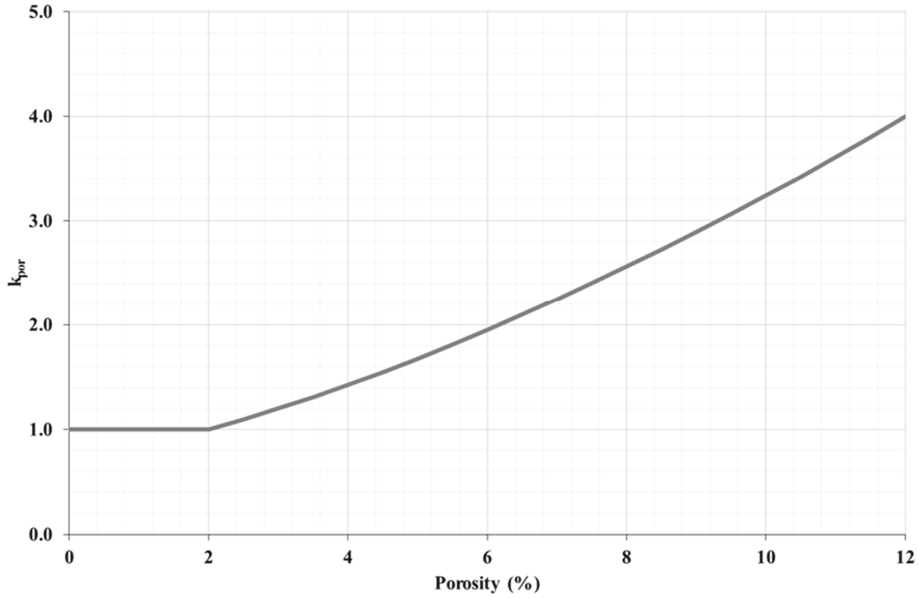

Figure 16 Correction factor for porosity of the rock (k_{por}).

3.4. Basic penetration

Basic penetration (i_0) is a function of the equivalent thrust and equivalent fracturing factor parameters. Equivalent thrust is given by Equation 5.

$$M_{ekv} = M_B \cdot k_d \cdot k_a \quad (\text{kN/ cutter}) \tag{5}$$

where

M_B = applied cutter thrust (kN/cutter)
k_d = correction factor for cutter diameter (Figure 18)
k_a = correction factor for average cutter spacing (Figure 19)

Figure 17 shows the basic penetration rate (i_0) as a function of the equivalent thrust and equivalent fracturing factor parameters when cutter diameter (d_c) is 483 mm, average cutter spacing (a_c) is 70 mm and applied recommended rpm

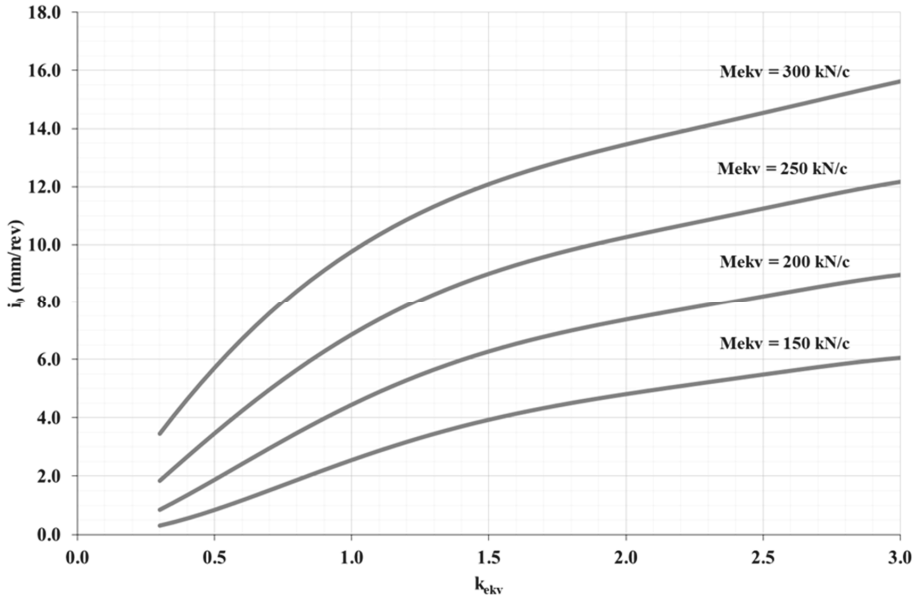

Figure 17. Basic net penetration rate d_c = 483 mm, a_c = 70 mm and recommended cutterhead rpm.

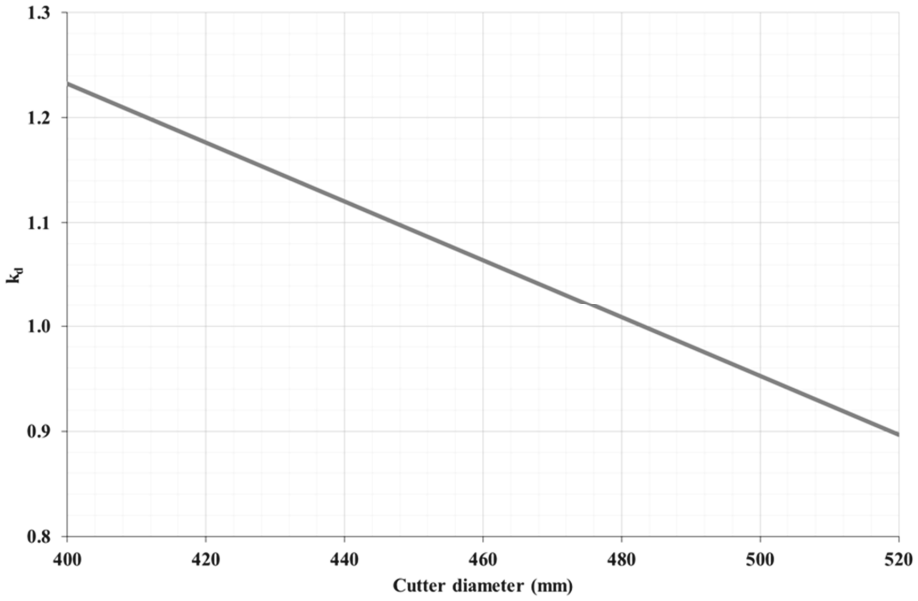

Figure 18. Correction factor for cutter diameter where $d_c \neq 483$ mm. (k_d).

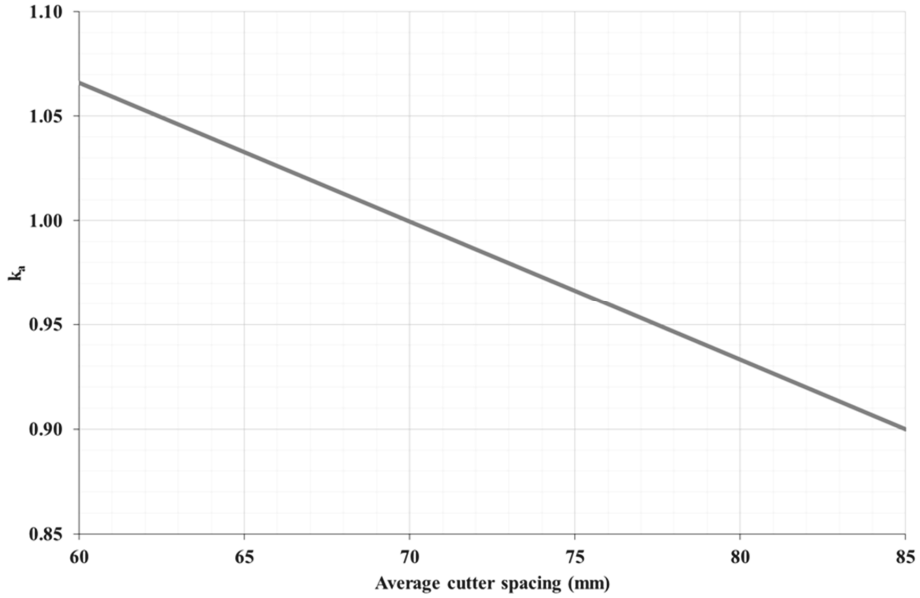

Figure 19 Correction factor for average cutter spacing where $a_c \neq 70$ mm. (k_a).

3.5. Basic net penetration rate

The basic net penetration rate (I_0) is a function of the basic penetration and cutterhead rpm (Equation 6).

$$I_0 = i_0 \cdot rpm \cdot \left(\frac{60}{1000} \right) \cdot k_{rpm} \quad \text{(m/h)} \tag{6}$$

i_0 = basic penetration rate (mm/rev)
rpm = applied cutterhead rpm
k_{rpm} = correction factor for applied cutterhead rpm (Figure 20)

The basic net penetration rate is applicable for systematically fractured rock mass without Marked Single Joints (MSJ). Influence of MSJ on the basic penetration rate is included in the following section.

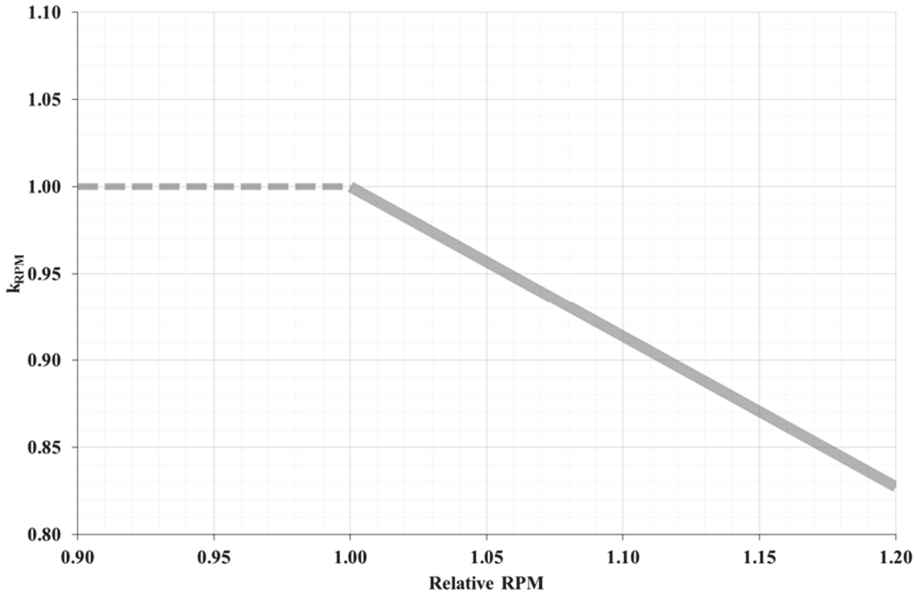

Figure 20 Correction factor for cutterhead velocity (rpm) illustrating where it differs from the recommended value.

The cutterhead velocity correction factor is based on limited information and must be applied with caution. The optimal cutterhead velocity appears to be influenced by rock drillability, rock mass fracturing and/or thrust level. Low values of and applied cutter thrust indicate a lower optimal cutterhead velocity.

3.6. Marked Single Joints

An interpretation of the influence of Marked Single Joints (MSJ) is based on a relatively small number of observations. MSJ are marked discontinuities in the rock mass which may be completely open, lead water or be filled with clay (Bruland, 2000).

The theoretical penetration addition is shown in Figure 21, and the normalised correction factor in Figure 22.

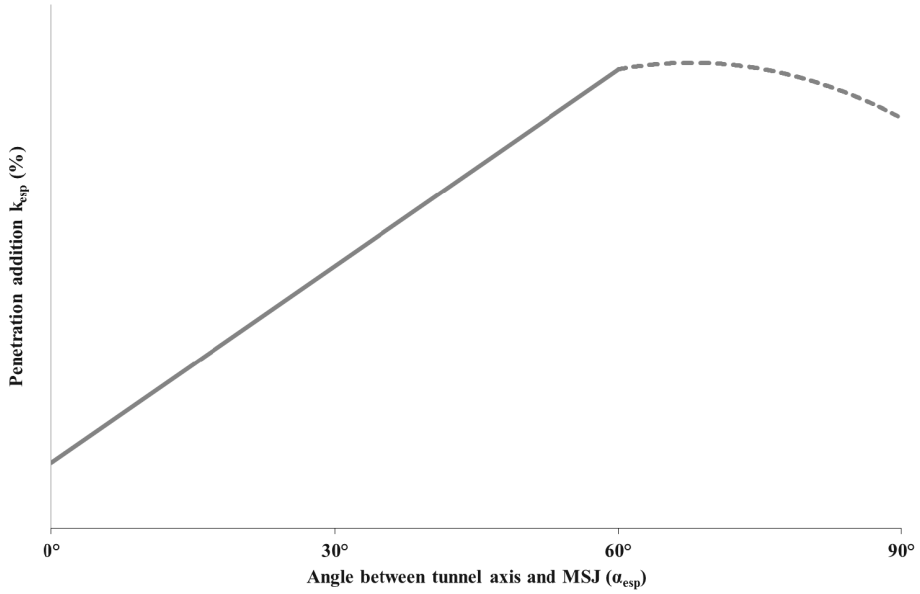

Figure 21. Theoretical averaged penetration addition for Marked Single Joints.

In equation 7 below, the length (l_{esp}) of tunnel that is influenced by Marked Single Joints is estimated from the tunnel diameter (d_{tbm}), the angle between the Marked Single Joints and the tunnel axis (α_{esp}), and the number (n) of similar Marked Single Joints occurring in the geological zone in question. The angle (α_{esp}) can be found by manipulating equation 7.

$$l_{esp} = n \cdot d_{tbm} / \tan\alpha_{esp} \quad \text{(m)} \tag{7}$$

The net penetration rate achieved when boring through zones characterised by Marked Single Joints (I_{esp}) is found by:

$$I_{esp} = I_0 \cdot k_{esp} \quad \text{(m/h)} \tag{8}$$

where

k_{esp} = correction factor for Marked Single Joints (Figure 22)

The correction factor (k_{esp}) is dependent of the angle between the Marked Single Joints and the tunnel axis (α_{esp}) and the DRI of the rock. k_{esp} should not be assigned a value greater than 1.4. At a penetration increase of this size, the vibration level of the cutterhead and the peak forces on the cutters are very high, requiring a reduction in the level of thrust.

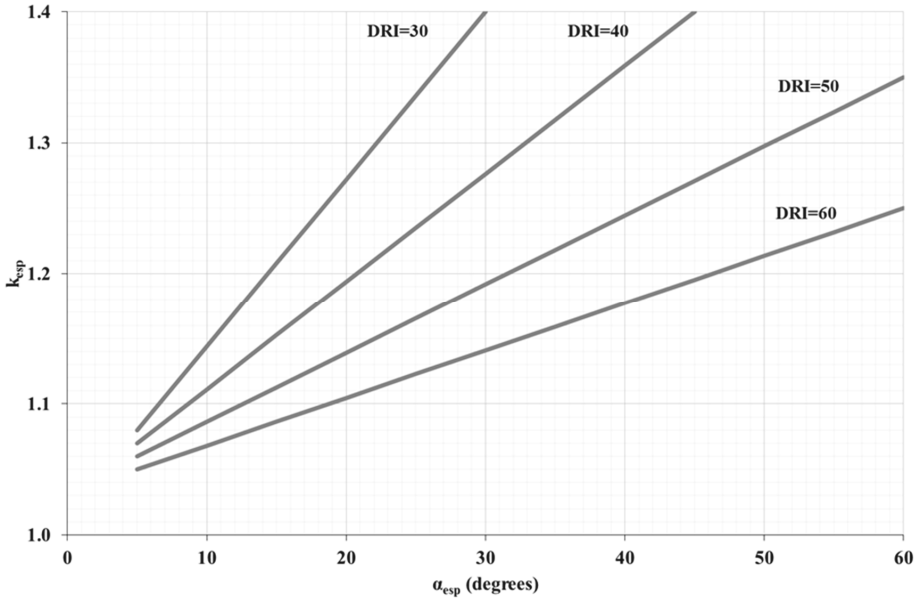

Figure 22. Correction factor for Marked Single Joints (k_{esp}).

The average net penetration rate (I_n) within a rock mass zone of a total length (l_j) is given by

$$I_n = \frac{l_j}{\frac{l_j - l_{esp}}{I_0} + \frac{l_{esp}}{I_{esp}}} \quad \text{(m/h)} \tag{9}$$

In rock mass with low boreability (e.g. DRI = 30 and a low degree of fracturing) the practical limit of penetration addition will be reached at an angle as low as 20° - 30°. When the angle between the tunnel axis and the plane of the Marked Single Joint is 80° - 90°, the influence of the joint will most likely be negative due to heavy vibrations and damage of the cutter rings. In any case, a Marked Single Joint at an angle of 80° - 90° will have influence over a very short distance and should therefore not be included in the penetration rate estimations.

3.7. Torque demand

At high net penetration rates, or when boring in fractured rock, it is important to check that there is sufficient cutterhead power installed to utilise the estimated thrust. In situations where installed power is too low, the TBM torque is limited and will be unable to rotate the cutterhead to provide the required penetration. In such cases, the thrust must be reduced, and also the torque so that it becomes less than the torque capacity of the cutterhead drive. The required torque is given by:

$$T_n = r_{mc} \cdot d_{tbm} \cdot N_{tbm} \cdot M_B \cdot k_c / 2 \quad \text{(kNm)} \tag{10}$$

where

r_{mc} = the relative position of the average cutter on the cutterhead.

This factor can be calculated once the cutterhead design is known (see equation 11 below). Normally, the value of r_{mc} is approximately 0.59.

d_{tbm} =cutterhead diameter (m)

N_{tbm} =number of cutters on the cutterhead

M_B =gross average cutter thrust (kN/c)

k_c =cutter coefficient (rolling resistance, see equation 11 below)

$$r_{mc} = \frac{\sum_{i=1}^{N_{tbm}} r_i}{N_{tbm}} \Big/ 0.5 \cdot d_{tbm} \qquad (11)$$

where

r_i = radius to position of cutter no. i (m)

Referring again to equation 10,

$$k_c = c_c \cdot \sqrt{i_0} \qquad (12)$$

Figure 23 shows the cutter constant (C_c) as a function of cutter diameter. The required torque determines the required level of installed power (P_n) which is given by equation 13 below.

$$P_n = \frac{T_n \cdot 2 \cdot \pi \cdot rpm}{60} \quad \text{(kW)} \qquad (13)$$

If the installed cutterhead power is less than P_n, the estimation of penetration rate must be recalculated using a lower cutter load value (M_B).

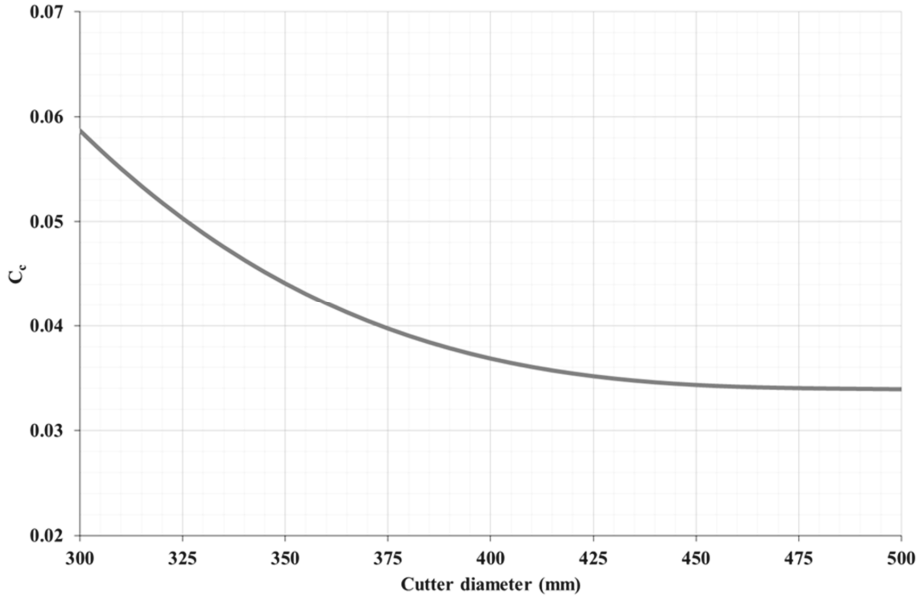

Figure 23. Plot showing the variation in the cutter constant (C_c) with cutter diameter.

3.8. Limitations on net penetration rate

At high penetration rates, or when boring in fractured rock, installed cutterhead power may represent a limitation on net penetration. Such limitations should be considered during the machine design phase.

The capacity of the system (the TBM, back-up for muck removal and the tunnel muck transport systems) may limit the net penetration rate. This is especially true in the case of muck removal systems linked to large diameter machines.

When boring through Marked Single Joints or heavily fractured rocks, it may be necessary to reduce thrust due to too high machine vibration level and very high instantaneous cutter loads are experienced.

Tunnels exhibiting sharp curves and/or steep gradients may also place limits on applied thrust levels and cutterhead velocity, especially in hard rock conditions.

4. The Cutter Life Model

4.1. Introduction

The NTNU prediction model presupposes that a given TBM is operated at a thrust level that results predominantly in abrasive wear of the cutter rings.

The number of cutters replaced due to cutter ring wear (abrasive, mushrooming and chipping) should represent more than approximately 70% of total replacements. Cutter rings worn by ring chipping and/or mushrooming should account for less than 5-10% of the total number of replacements.

Cutters replacements due to bearing damage (blockage, leakage, damaged hubs, etc.) should also account for less than 20- 30% of the total number of replaced cutters.

4.2. Cutter ring life

Basic cutter ring life, in boring hours, is proportional to the Cutter Life Index (CLI). Figure 24 shows basic cutter ring life (H_o) as a function of the CLI and cutter diameter.

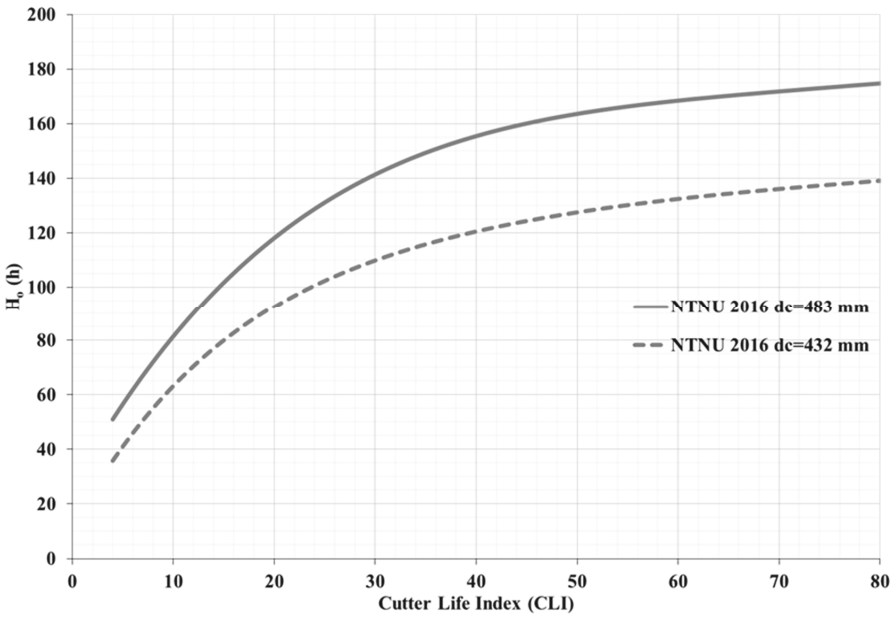

Figure 24. Basic cutter ring life (H_0) as a function of the CLI and cutter diameter.

4.2.1. Correction for TBM diameter

Figure 25 illustrates the correction factor for TBM diameter. Centre and gage cutters have shorter lifetimes than face cutters. With increasing TBM diameter, the ratio of centre and gage cutters to face cutters decreases, so the average cutter will have a longer lifetime.

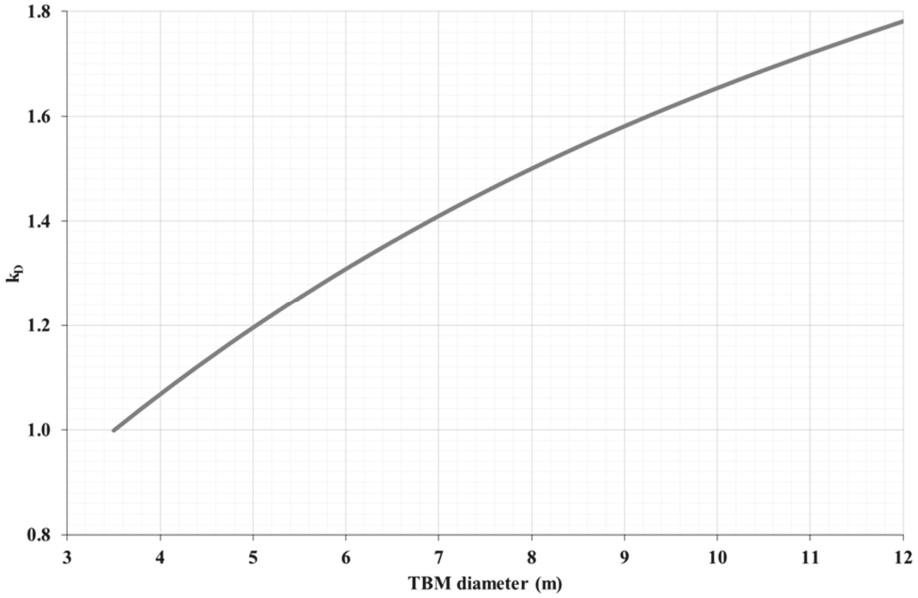

Figure 25. Correction factor for TBM diameter.

4.2.2. Correction for cutterhead velocity

Cutter ring life is inversely proportional to cutterhead velocity (rpm) based on the assumption that cutter ring life, for a given set of rock mass conditions, is proportional to rolling distance but independent of rolling velocity. The correction factor applied under varying cutterhead RPM is shown in equation 14.

$$k_{rpm} = \frac{42 / d_{tbm}}{rpm} \tag{14}$$

where

d_{tbm} = TBM cutterhead diameter (m)
rpm = cutterhead velocity

4.2.3. Correction for the standard number of cutters

In cases where the actual number of cutters on a cutterhead differs from the model, the average cutter life parameter will change. The correction factor applied for the actual number of cutters used is:

$$k_N = \frac{N_{tbm}}{N_0} \tag{15}$$

where

N_{tbm} = actual number of cutters
N_0 = standard number of cutters (updated as part of this thesis, Figure 6)

4.2.4. Correction for abrasive minerals

Cutter ring life varies with the content in the rock mass of quartz and other hard and abrasive minerals such as garnet, epidote, olivine, pyrite and others. Figure 26 shows a correction factor that is applied as a function of abrasive minerals content, including quartz, garnet, epidote, pyrite and olivine; others similar abrasive minerals may be included in the abrasive mineral content parameter when estimating cutter ring life using the plot in.

The correction factor shown in Figure 26 is based on normalised field and laboratory data.

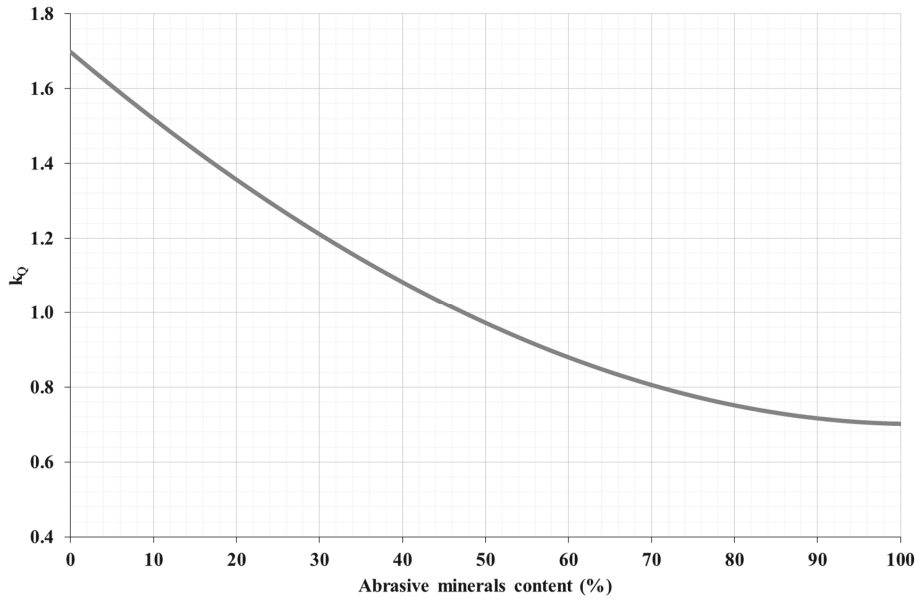

Figure 26. Correction factor (k_Q) for abrasive minerals.

4.2.5. Correction for gross cutter thrust:

The influence of cutter thrust on cutter life has been recently recognised. It is also anticipated that cutter life will be lower when boring in non-fractured rock masses with extremely and very abrasive properties (4.5 < CLI < 6.0).

A correction factor (Figure 160) has been introduced based on observations of the relationship between cutter life and gross cutter thrust data (Macias, 2016). Cutter life, expressed in cubic metres per cutter, may vary in response to variations in penetration rate.

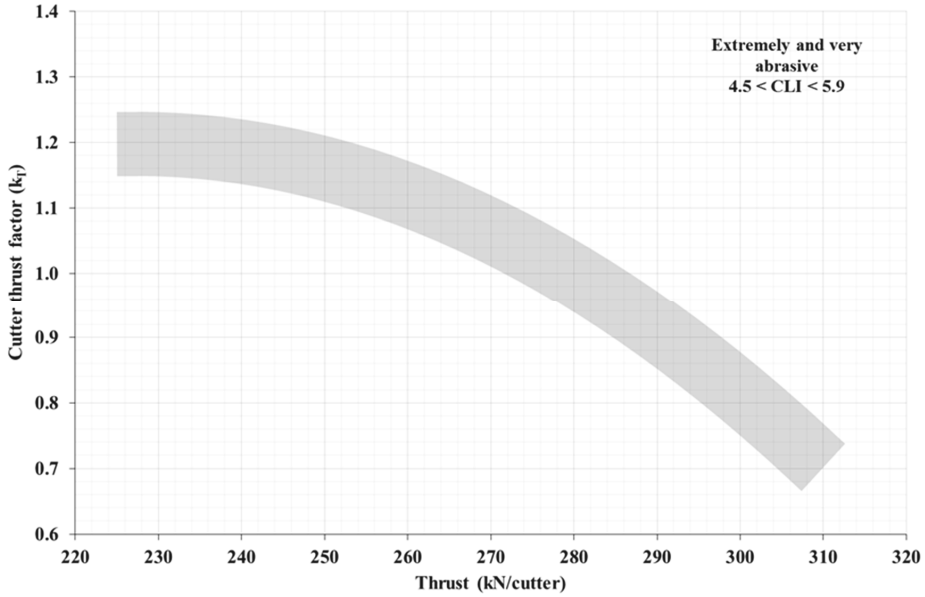

Figure 27. Correction factor (k_T) for cutter thrust level.

The average life of a cutter ring is given by the following equations (16, 17 and 18).

$$H_h = (H_0 \cdot k_D \cdot k_Q \cdot k_{rpm} \cdot k_N \cdot k_T) / N_{tbm} \quad \text{(h/ c)} \tag{16}$$

$$H_m = H_h \cdot I_n \quad \text{(m/c)} \tag{17}$$

$$H_f = H_h \cdot I_n \cdot \pi \cdot d_{tbm}^2 / 4 \quad \text{(sm}^3\text{/c)} \tag{18}$$

where

H_0 = basic average cutter ring life (hours)
H_h = average cutter ring life (hours)
H_m = average cutter ring life (metres)
H_f = average cutter ring life (solid cubic metres)
I_n = net penetration rate (m/h)

d_{tbm} = TBM diameter (m)

The H_0 is an expression of the lifetime, in machine hours, of one individual cutter ring located in the average cutter position ($\approx 0.59 \cdot r_{tbm}$). For example, for a CLI value of 8 and a quartz content of 35%, a single 483 mm diameter cutter ring in position 29, on a 7-metre diameter TBM with standard machine parameters, will have a lifetime of approximately 116 hours.

The H_h, H_m and H_f parameters are expressions of averaged cutter life for a given machine or tunnel. For example, if H_m = 10 m/c, this means that for each 10 metres of tunnel bored, the total wear on all cutters on the cutterhead corresponds to one complete cutter ring. It also means that, on average, a cutter has to be replaced for every 10 metres of tunnel bored.

4.3. Considerations for cutter life assessments

Rock surface hardness or resistance to indentation is the rock property that exerts the greatest influence on cutter ring life at low SJ values (equivalent to extremely high, very high and high surface hardness values, 2.0 < SJ < 6.9).

For rock types where CLI > 30 (very high and extremely high), a high proportion (60-90%) of cutter replacements are due to bearing-related issues. Cutter life is thus influenced most by factors other than the prolonged life of the cutters installed on the cutterhead. The high percentage of cutters change due to set bearing or others is a reason of the almost flat estimated basic cutter ring life in rock masses with high CLI values. Therefore, the bearing life plays a significant role for rock masses with exhibit low abrasivity and/or high degree of fracturing.

In fractured rock masses, or in situations where extremely good rock chipping occurs, the cutters will be exposed to large instantaneous loads. Under such conditions, a cutter ring exhibits a tendency to chip along its edge. Extensive ring chipping and high cutter thrust may result in bevel edge wear, loosened rings and blocked bearings. Additional loads will result in higher abrasion on protruding cutters when the difference in diameter between adjacent cutters is too large as a result of deficient wear height control. Heavy vibration of the cutterhead results in high lateral forces on the cutters, which in turn causes additional abrasion.

5. Gross advance rate

5.1. Introduction

The gross advance rate is expressed in metres per week, representing an average calculated over a longer period. Gross advance rate depends on net penetration rate, machine utilisation and the number of working hours during the period in question.

To a large extent, the NTNU model is based on data derived from a shift system that totals approximately between 100 and 160 working hours per week.

The machine utilisation parameter includes only a limited amount of rock support work. For this reason, the model cannot be applied directly to tunnels that require substantial amounts of rock support and must be evaluated separately. The possibilities of changing cutters, performing maintenance and carrying out repairs on the TBM and the back-up systems, etc. while rock support is being installed, should be evaluated.

5.2. Machine utilization

The machine utilisation parameter is expressed in terms of net boring time as a percentage of total tunnelling time. Total tunnelling time includes time consumed performing the following activities:

- Boring – T_b
- Re-gripping – T_r
- Cutter replacement and inspection – T_c
- Repair and service of the TBM – T_{tbm}
- Repair and service of the back-up systems – T_{back}
- Miscellaneous – Tm
- Tunnel length – T_l

The time consumed in performing these activities is expressed in hours per kilometre. The time consumption used here is representative of the methodologies practised in the majority of modern tunnelling projects. The machine utilisation parameter is expressed as follows:

$$u = \frac{100 \cdot T_b}{T_b + T_r + T_c + T_{tbm} + T_{back} + T_m + T_l} \quad (\%) \tag{19}$$

Boring

Boring time depends on the average net penetration rate (I_n), and is calculated using the following equation:

$$T_b = \frac{1000}{I_n} \quad \text{(h/km)} \tag{20}$$

Re-gripping

The time taken for re-gripping depends on the stroke length of the thrust cylinders and unit time per re-grip. It is calculated using the following equation:

$$T_r = \frac{1000 \cdot t_r}{60 \cdot l_s} \quad \text{(h/ km)} \tag{21}$$

where

l_s = stroke length, typically 1.5 - 2.0 metres
t_r = time per re-grip.

On average, time per re-grip t_r is 4.5 minutes. Time consumption varies with gripper hold, the stroke length, the TBM diameter, boring along curved sections and declines, and the capacity of the hydraulic system. Under favourable conditions, time consumption will be somewhat lower, but may increase substantially under difficult conditions.

Cutter replacement

The time taken to carry out cutter replacements and inspections (T_c) depends on the cutter ring life (H_h), net penetration rate (I_n) and the time used to replace each individual cutter (t_c). It is calculated using the following equation:

$$T_c = \frac{1000 \cdot t_c}{60 \cdot H_h \cdot I_n} \quad \text{(h/km)} \tag{22}$$

The time taken to replace a cutter (t_c) will vary with cutter size. Typically, time consumption per replaced cutter is listed in Table 6

Table 6. Time per changed cutter.

Cutter diameter	Front loaded	Back loaded
≤ 432 mm (17 inches)	45 min	40 min
≥ 483 mm (19 inches)	-	50 min

t_c is based on data under favourable working conditions. Water ingress, unstable rock conditions, high rock temperature and other factors may contribute towards major changes of the time consumed.

The inspection time per changed cutter increases when boring in rock types with low abrasivity. This results in an increase in the total time per changed cutter. This parameter also depends on the number of cutters replaced at any given time. If only a few cutters are changed during a break in operations, the unit time (t_c) increases. This may also result in shorter cutter life.

Other activities

The time consumption for repair, maintenance and service on the TBM and the back-up systems, as well as other miscellaneous activities, is shown in Figure 28. These data are regarded as being representative for well-organised tunnelling operations. The downtime involved in the event of possible main bearing failure and other extended breaks in operations is not included. Such risks must be evaluated separately.

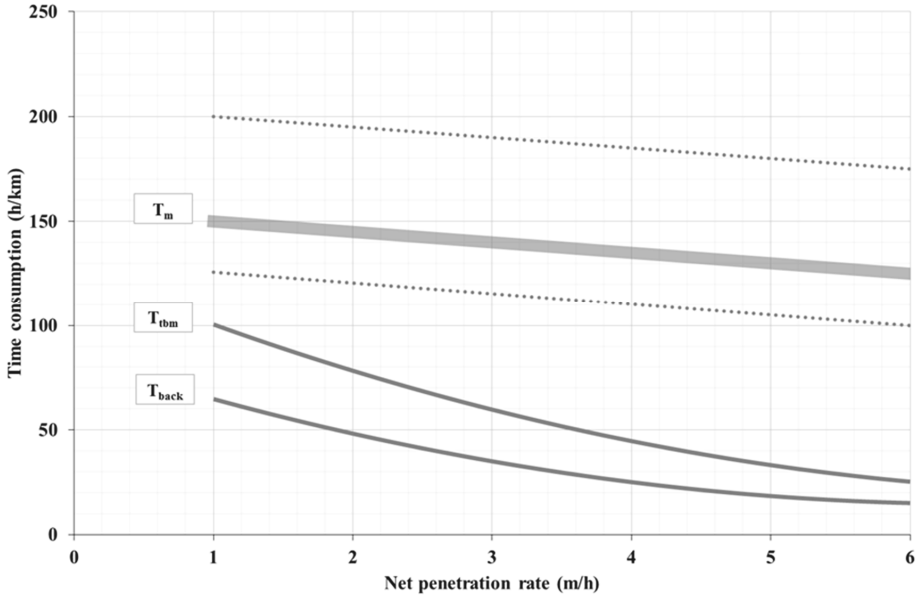

Figure 28. Time consumption for various activities

Miscellaneous activities may include the following:

- Normal rock support work in good rock conditions, such as the installation of support while boring is in progress without having to increase the number of tunnelling personnel
- Transport system downtime
- Installation and maintenance linked to the transport system
- Surveying, moving of laser

- Installation and maintenance linked to water, ventilation and electrical cables
- Washing and cleaning of the TBM and back-up system components
- Other (crew changes, incidental lost time, etc.)

In addition to the activities listed above, time will be consumed in connection with application of the tunnelling method and project organisation.

Length factor

Tunnel length exerts a relevant influence on time consumption during tunnelling operations. During the initial "learning curve" period of a tunnelling project, more time is spent on any given activity as the crew's skills levels are built up, and the quality assurance system adapts to the project in question.

The longer the tunnel (> 8 km), the more likely it will be that problems will be encountered with muck transport, the ventilation, electricity and water systems, and delays linked to supplies. If the capacity of the transport system is inadequate, waiting times for transport services will increase substantially.

Problems with the ventilation, electricity and water systems will continue to increase with tunnel length. The transport system remains dependent on TBM penetration rate and factors such as the volume of material that requires removal. The higher the penetration rate, the greater these problems linked to downtime and delays in connection with the transport system and supply logistics will be.

The data in the NTNU model database is derived from tunnels of up to 10 kilometres in length. Expressions of time consumption in previous versions of the model represent the average of the total tunnel lengths. Low skills levels among the crew, and an inadequate tunnel quality assurance system, will result in additional losses in time. The term 'skills levels' used here refers not only the crew, but also to system manufacturing competence.

This updated version of the model proposes the introduction of an additional time consumption (h/km) related to the tunnel length. The 'additional time consumption' is illustrated in Figure 29, and includes boundary limits for low and high skills levels, and the quality assurance system. The values for every kilometre correspond to the extra time during the last km.

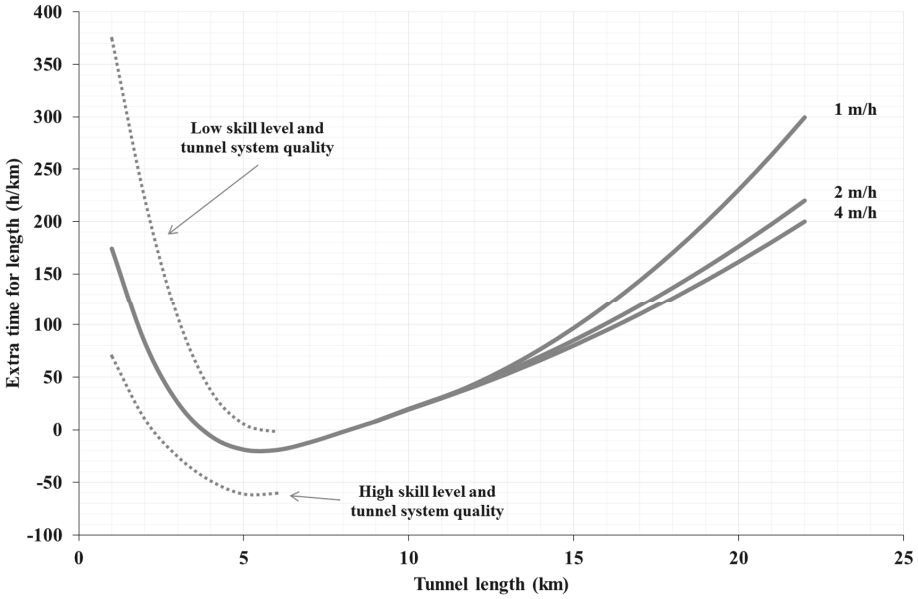

Figure 29. The 'additional time consumption' factor, based on tunnel length T_l.

Figure 30 illustrates the cumulative additional time involved for the total tunnel length under consideration. This graph might be used for overall rough estimations.

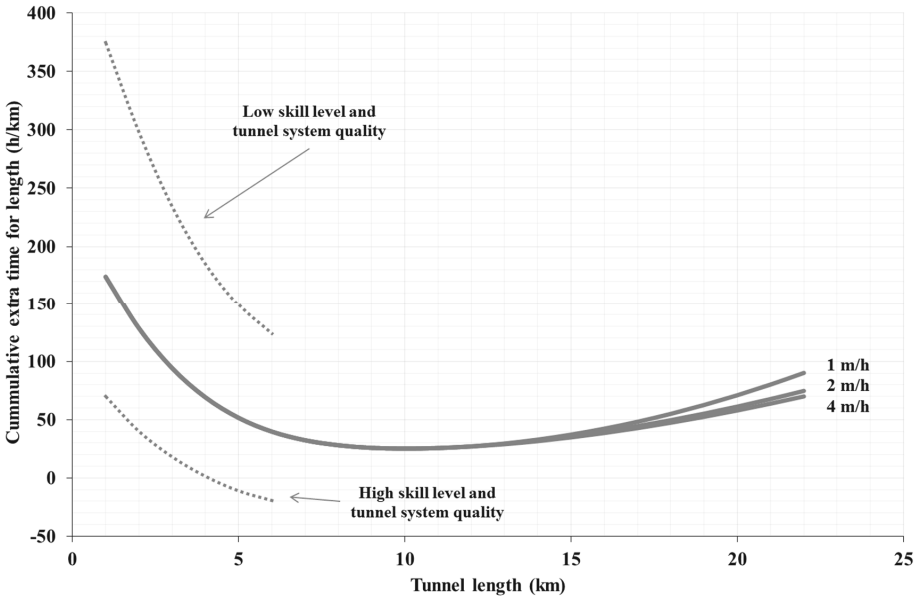

Figure 30. Cumulative additional time involved for the total tunnel length under consideration.

Weekly working hours

Most of the data used as a basis for the model are derived from tunnelling operations involving approximately 100 working hours per week. Thus it is assumed that there exists some time available outside standard working hours to address unforeseen and critical incidents such as major repair work. Some aspects of downtime of this type are not recorded in shift logs and are therefore not included in Figure 28.

The plot in Figure 31 indicates that opportunities to address unforeseen and critical incidents in a flexible manner become fewer as the number of hours worked per week (T_u) increases towards 168 hours. The parameter 'effective time' (T_e) provides an expression of working hours that are effectively available when the number of hours deviates from 100, which forms the basis for the model. The curve in the figure is believed to represent a conservative estimate of losses in effective working hours.

The weekly advance rate (I_u) will be:

$$I_u = u \cdot T_e \cdot I_m / 100 \quad \text{(m/week)} \tag{23}$$

where

u = machine utilisation
T_e = effective working hours per week
I_m = average net penetration rate over the tunnel

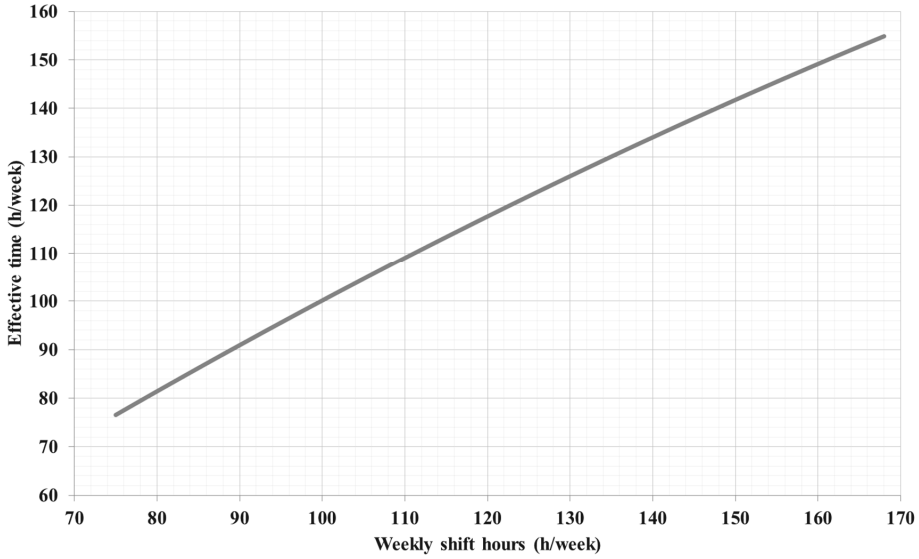

Figure 31. Plot showing effective working hours per week.

5.3. Additional time consumption

Estimates of time consumption for a given tunnel are derived from the weekly advance rate parameter, which is in turn based on net penetration rate and machine utilisation. Furthermore, additional time must be allowed the following factors:

- The excavation of the underground assembly and start-up area, tip station, etc., if necessary
- The assembly and disassembly in the tunnel of the TBM and the back-up systems. This normally takes from 4 to 8 weeks, depending mainly on the TBM diameter
- The excavation of cross passages, niches, branching, etc.
- Boring through and stabilising zones of poor rock quality
- Encounters with unexpected rock mass conditions
- Permanent rock support and lining work
- TBM downtime (due to possible major breakdowns)
- The dismantling of tracks, the ventilation system, invert clean-up, etc.

Furthermore, the time spent to manufacture and/or refurbish the TBM and the back-up systems may exert an influence on overall project schedules, depending on the duration of necessary activities that precede actual excavation operations. The refurbishment of a previously used TBM may take from 3 to 6 months. The manufacture of a completely new TBM may take from 6 months to one year, depending mainly on the TBM diameter.

Transport of the TBM and the back-up systems to the site may also influence the overall project schedule, for the same reasons as above. Transport of a TBM is a demanding operation because the largest component may weigh as much as 20 tons or more, even for a 3.5-metre diameter machine.

6. Limitations of the NTNU model

A model is a simplified description of a given phenomenon, which can be used to make predictions. A good model is both as accurate as possible and as simple as possible, which makes it not only powerful but also easy to understand. However, no matter how good a model is, it will usually have limitations. Since models must be simple enough to enable them to be used to make predictions, they often lack the ability to simulate all the details of the phenomenon in question.

In the case of the NTNU prediction model for hard rock TBMs, the following limitations should be taken into account:

The NTNU model does not cover the entire range of rock masses that occur in nature:

- Rock drillability expressed by the Drilling Rate Index (DRI) parameter should lie within the range 20 to 80, which roughly corresponds to the UCS parameter values 25 to 350 MPa. The strength parameter applied is in accordance with the ISRM classification 'medium to extreme'.
- The rock type in question should exhibit medium to low porosity – less than approximately 10% by volume.
- The rock mass degree of fracturing, expressed by the average spacing between planes of weakness, should be greater than approximately 50 mm.
- The rock-breaking process must be mainly by brittle failure (chipping) between the disc cutters.
- Rock mass quality should be such that the excavated tunnel will generally only require light-duty support mechanisms (rock bolts and/or shotcrete). Exceptions will occur in zones of weakness or as a result of other specific phenomena.
- Rock mass qualities roughly related to Q and RMi values should be somewhere greater than 0.1 and 20 for the RMR.
- Boreability assessments do not include the possible influence of groundwater and/or rock mass stress.

The NTNU/SINTEF drillability test method has gained international recognition. There are few laboratory facilities in the world that are able to reproduce these tests, unlike other test methodologies such as UCS and BTS. There are other laboratories worldwide with the necessary equipment, such as in Australia, South Korea, Spain, South Africa, Turkey and the USA. The trademark acronyms and terms relating to the indices DRI™ (Drilling Rate

Index™) and CLI™ (Cutter Life Index™) are unique to these test results and originate from the NTNU/SINTEF laboratory in Trondheim in Norway.

A cutter diameter of 483 mm (19 inches) and 508 mm (20 inches) are currently the most commonly used in hard rock tunnelling. For smaller TBMs, diameters of 432 mm (17 inches) are used. The NTNU model makes no distinction between cutter ring design or quality, and assumes in all cases that cutter ring quality is tailored to the rock conditions.

The machine type assumed by the model is a hard rock TBM (open or shield). However, the model is based on data derived from a large number of open TBM types tunnelling in rock mass conditions summarised in the foregoing. No distinction is made between machine types.

The gross cutter thrust parameter may interfere with the influence of TBM type, diameter, and/or cutter type. TBM cutterhead design is not included in the model as an independent parameter.

The machine utilisation parameter (expressed as a percentage of tunnelling time) used in the model does not include additional time spent on operations such as TBM and back-up assembly and disassembly, excavation work (niches, branching, etc.), tunnelling through zones of poor quality, additional time for unexpected rock mass conditions, permanent rock support and lining operations, and additional TBM downtime. These activities need to be quantified separately.

7. References

Bruland A. (2000). Hard Rock Tunnel Boring: Vol 1 - 10. PhD thesis. Norwegian University of Science and Technology (NTNU), Trondheim, Norway (2000).

Macias, F.J. (2016). Hard Rock Tunnel Boring: Performance Predictions and Cutter Life Assessments. PhD Thesis, Norwegian University of Science and Technology (NTNU), Trondheim, Norway (2016).

NTH (1983). Hard Rock Tunnel Boring, Project Report 1-83. Norwegian Institute Technology, Div. of Construction Engineering, Trondheim, Norway (1983).